De Montfort University

Faculty of Health and Life Sciences

The School of Pharmacy

Modelling and elucidation of photoreaction kinetics – Applications and actinometry using nifedipine, nisoldipine, montelukast, fluvoxamine and riboflavin.

1st April 2016

PhD Thesis

Wassila Maafi-Damerdji

Contents

Acknowledgements

I would first wish to thank my Lord, Allah, for having given me the strength, patience, health, knowledge and so many more blessings to be able to carry out and complete this work besides many other commitments.

I wish to express my deep gratitude to my beloved parents and sister who have always cherished and given me so much love, care, attention, encouragement and support, that have all deeply contributed to the realisation of my inner self, my love for knowledge, work, family, people and life.

I would sincerely like to express my profound gratitude to my husband and supervisor, Dr Mounir Maafi, who not only taught me a great deal about life but who also taught me invaluable thinking skills and knowledge that I have acquired on a daily basis. I wish to also thank him for his continued support through life and for always seeking to bring out the best in me. He endeavoured to teach me how to nurture intelligence through thinking, reading, researching, exploring various possibilities, selecting best options, experimenting and analysing, but also applying such skills in every step of life. I would also like to thank my second, Dr. Michael Goodman, and third, Prof. Richard Jenkins, supervisors for their support.

I would also like to thank everyone who helped me at DMU including Lokyan, Leonie with whom I shared interesting scientific discussions and friendly relationships and Nazmin and Unmesh who helped considerably through their kind assistance with laboratory equipment and scientific discussions. I also wish to thank everyone at the Graduate School Office who always helped promptly with all my administrative queries.

Last but not least, I would like to dedicate this work to my beloved son Kenzy, whom I love profoundly...

List of publications

Maafi M. and Maafi W., 2016. Modelling and elucidation of the kinetics of multiple consecutive photoreactions $AB_4(4\Phi)$ with Φ-order kinetics - Application to the photoreaction of riboflavin. Submitted.

Maafi M. and Maafi W., 2015a. Quantitative assessment of photostability and photostabilisation of Fluvoxamine and its design for actinometry. Photochemical Photobiological Sciences.14(5),982-94

Maafi M. and Maafi W., 2015b. Quantification of Unimolecular Photoreaction Kinetics: Determination of Quantum Yields and Development of Actinometers—The Photodegradation Case of Cardiovascular Drug Nisoldipine. International Journal of Photoenergy, 2015.

Maafi M., Maafi W., 2014a. Φ-order kinetics of photoreversible drug reactions. Int. J. of Pharm. 471, 536-543.

Maafi M., Maafi W., 2014b. Montelukast photodegradation: Elucidation of Φ-order kinetics, determination of quantum yields and application to actinometry. Int. J. Pharm. 471, 544-552.

Maafi W., Maafi M., 2013. Modelling Nifedipine Photodegradation, Photostability and Actinometric Properties. Int. J. Pharm. 456(1), 153-164.

Symbols and abbreviations

Symbols

A ; absorbance

$\beta_{\lambda_{irr}}$; pseudo rate-constant

$\delta_{\lambda_{irr}}$; pseudo initial velocity

C; concentration

Δ; thermal

ε ; absorption coefficient

E_a, activation energy

F ; photokinetic factor

k ; rate-constant

K; equilibrium constant

l ; path-length

λ; wavelength

υ; velocity

$P_{\lambda_{irr}}$; radiant power

R; gas constant

S_n; singlet state

T; temperature

t; time

T_n ; Triplet state

Φ; quantum yield

Abbreviations

DE; differential equation

EMEA; European Agency for the Evaluation of Medicinal Products

Exp.; experimental

FDA; Food and Drug Administration

FMF; formylmethylflavin

Fluvo; fluvoxamine

HPLC ; High performance liquid chromatography

ICH; International conference on harmonisation

LC; lumichrome

Monte; montelukast

NIF; nifedipine

NIM; numerical integration method

NIS; nisoldipine

PCI; photochemical internalisation

PDT ; photodynamic therapy.

PP; photoproduct

pss; photo-stationary state

QY; quinoline yellow

Ribo; riboflavin

RK; Runge Kutta

SSY; sunset yellow

TRZ; tartrazine

Unk.; unknown

UV; ultraviolet

USP ; United States Pharmacopeoia

Vis; visible

Abstract

The kinetics of drugs photodegradation have traditionally been treated using thermal kinetic analysis methods consisting most commonly in zero and first order kinetics. These treatment strategies were shown to lack specificity and present a number of limitations when applied to photoreactions kinetics. Nevertheless, these methods have widely been used due to a lack of integrated rate-laws for the majority of photoreactions types, in turn, due to the presence of a variable time-dependent factor in most photoreactions rate-laws that prevents their mathematical integration.

To address these limitations, a new methodology for the development and validation of semi-empirical integrated rate-laws that faithfully describe photoreactions kinetics and photoreactions simulated cases generated by numerical integration methods (NIMs), is hereby presented.

Using this methodology, a new kinetic order was ascribed to photoreactions namely the Φ-order kinetics. Semi-empirical integrated rate-laws were, thus, developed for three photoreaction types namely, unimolecular, AB(1Φ), photoreversible ,AB(2Φ), and consecutive, AB_4(4Φ), photoreactions. The proposed models were further tested experimentally on drugs following these photodegradation mechanisms using; nifedipine and nisoldipine for unimolecular photoreactions; montelukast and fluvoxamine for photoreversible reactions; and riboflavin for consecutive photoreactions. The developed

models not only accurately described the photoreaction kinetics of these drugs but also allowed the determination of all the kinetic parameters that characterise them.

Furthermore, the above studied drugs were shown to act as precise and simple actinometers when analytically treated with the Φ-order kinetic methods, hereby presented. A universal standard method for the precise and worldwide reproducible study of drugs stability and compounds photoreactions, based on monochromatic irradiation and Φ-kinetics data analysis, is also detailed and adopted throughout the thesis.

Finally, two new kinetic parameters namely, the pseudo-rate-constant and pseudo-initial velocity have been identified and shown to be more reliable and accurate in the description and universal comparison of photoreactions kinetics.

Chapter I: Introduction, problematic & objectives

I.I. Litterature review

1. Introduction

Nature is abundant with harmonious interactions between light and matter. These phenomena are generously and ubiquitously embedded around us as well as within ourselves. The process of photosynthesis, for instance, involves the interaction between plants and sunlight leading to the formation of vital organic matter and oxygen. Living organisms ranging from unicellular bacteria to man, possess light-sensitive components in cells and organs that interact with light to allow the normal functioning of vital processes including vision and strengthening of the bones. In humans, vitamin D can only be obtained in sufficient amounts to prevent diseases, through the absorption of ultraviolet (UV) radiation through the skin and subsequent interaction with precursor molecules.

Whether designed to sustain and enhance life and/or intrigue and engage the inquisitive mind, these phenomena are not only fascinating but have also inspired the mind and led to crucial scientific advances and developments in a number of fields such as chemistry, biology, medicine, physics and technology. These advances have only been possible with a more profound understanding of the photochemistry, or the mechanistic nature, of the interactions between light irradiation and molecules in matter.

2. The mechanistic nature of light-matter interaction

Electromagnetic radiation is uniquely characterised by a wave-like nature that allow its propagation, as well as particle-like properties whereby a stream of discrete packets of energy, known as photons, characterise each wavelength of the spectrum. This particle-like

property with quantifiable energy confers to light its ability to photoactivate the photoabsorbing molecule with which it interacts, a process known as photoexcitation.

2.1. Photoexcitation

Each chemical species can only absorb and emit specific energies, at the corresponding specific frequencies (and therefore wavelengths), of radiation. As a result, each species is characterised by a unique line and band spectrum (Beijersberge Van Henegouwen, 1997). When a molecule absorbs a quantum of radiation, it is known to become photo-activated or photo-excited as it gains a specific amount of energy (Beijersberge Van Henegouwen, 1997). This additional energy can be assimilated in rotational, vibrational or electronic modes, depending on the wavelength of the incident radiation (Beijersberge Van Henegouwen, 1997). Longer wavelengths are associated with lower energies and therefore, absorption of lower energy infra-red radiation only leads to transitions between rotational or vibrational states as the latter molecular energy levels are closer together in energy than the electronic levels (Beijersberge Van Henegouwen, 1997). On the other hand, the energies associated with ultraviolet (UV, 200-400 nm) and visible (Vis, 400-800 nm) radiation are of the right magnitude to induce transitions between the electronic energy levels of a species (Beijersberge Van Henegouwen, 1997).

Therefore, when a molecule absorbs a photon of UV-Visible light, the difference in energy between the ground and the excited electronic state reached corresponds exactly to the quantum of energy of the absorbed photon (Beijersberge Van Henegouwen, 1997). Having

gained the right amount of energy for an electronic transition to occur, an electron within the photochromic, or photoabsorbing, part of the molecule gets promoted to a higher electronic energy level. This, then, causes a change in the distribution of electrons around the nuclei and in the forces between the atomic nuclei of a molecule (Beijersberge Van Henegouwen, 1997).

In contrast, the more widely known thermal reactions occur by molecular absorption of heat energy in order to overcome the activation energy barrier and proceed to products formation. Following sufficient energy absorption, thermal reactions, most often, take place with organic molecules being in their ground lowest-energy electronic state where the orbitals are normally occupied by a pair of spin-coupled electrons and are as close as possible to the positively-charged nuclei.

Photochemical reactions, on the other hand, take place from the excited electronic state of the molecule, where an outer electron is promoted to a higher energy orbital further away from the nuclei following absorption of UV or visible radiation. Thus, excited-state chemistry was shown to be inarguably different from ground state chemistry in many aspects despite the resemblance of the nuclear skeleton of a molecule in its exited and ground states (Beijersberge Van Henegouwen, 1997).

The promotion of an electron to a different orbital has a number of implications (Beijersberge Van Henegouwen, 1997). First, a new electronic configuration different from

the ground state configuration of the molecule ensues (Beijersberge Van Henegouwen, 1997). This leads to a new and different charge distribution (dipole moment) in the molecule in its excited electronic state, which, in turn, leads to a change in vibrations and rotations of groups of atoms of the molecule (Beijersberge Van Henegouwen, 1997). Therefore, chemical reactivity of molecules in their excited electronic states that follow photoabsorption differ both quantitatively and qualitatively from the chemistry at ground state (Beijersberge Van Henegouwen, 1997). This is due to the dependence of chemical reactivity on a molecule's electronic configuration, charge distribution, vibrations and rotations, all of which differ between the ground and excited electronic states and thus thermo- and photo- chemistry (Beijersberge Van Henegouwen, 1997).

Photoexcitation may lead to two types of excited states, the singlet state following energy absorption or the triplet state following intersystem crossing from the excited singlet state. The latter differ in the spin-state of the promoted electron. The spin of an electron reflects its intrinsic magnetic field relative to an external magnetic field and which results from the combined effect of the electron's rotation around its own axis and its surface electric charge (Beijersberge Van Henegouwen, 1997). The spin of an unpaired excited electron is determined relative to an external magnetic field. This is in contrast to paired electrons within an orbital having opposite spins that neutralise each other's magnetism in most ground state molecules (Beijersberge Van Henegouwen, 1997).

Following photoabsorption and the promotion of an electron to a singlet unoccupied orbital that is further away from the nucleus, the electron remains magnetically coupled to the one that remained in the original orbital. In a triplet state, however, the change in electron spin leads to a loss of magnetic attraction between the promoted and unpromoted electrons and thus the two electrons magnetically repel each other. As a result, in a singlet excited state, there is a smaller distance between the two electrons yet a higher repulsive force between their respective negative charges and higher energy content compared the triplet (Tn) state where the two electrons are no longer magnetically coupled and thus repel each other leading to a lower repulsive force between the corresponding electric charges (Beijersberge Van Henegouwen, 1997). Consequently, the triplet Tn state has a somewhat lower energy content than the corresponding singlet Sn state (Beijersberge Van Henegouwen, 1997).

2.2. Deactivation processes

Photon absorption and the ensuing electronic transition occur in only about 10^{-15}s, which renders spin inversion of the promoted electron a highly improbable process during such a short length of time (Beijersberge Van Henegouwen, 1997). Therefore, light absorption produces exclusively singlet states (S_n) from ground (S_o) singlet states (Beijersberge Van Henegouwen, 1997). The life-times of excited singlet states above the S_1 are in the order of 10^{-11}s being too short for the occurrence of any type of chemical reaction from any S_n above the S_1 electronic level (Beijersberge Van Henegouwen, 1997). However, within this time, molecules may loose some of the gained energy in the form of heat in rotations and vibrations and rapidly tumble down to the lowest vibrational levels of the S_1 state as the energy gap between the S_1 state and higher excited states is lower than that between the S_1 state and the ground S_0 state (Beijersberge Van Henegouwen, 1997). However, the high

energy gap between S_1 and S_0 means that the molecule has a longer lifetime of 10^{-9}-10^{-6}s in its S_1 state (Beijersberge Van Henegouwen, 1997). This implies that the nature of photochemical reactions is independent of the irradiation wavelength used since reactions will usually take place from the longer-lived S_1 state (Beijersberge Van Henegouwen, 1997). As a result, unless monochromatic irradiation experiments using individual wavelengths are conducted, it is not possible to determine which wavelengths are more detrimental to a given molecule. It is also a misconception to believe that shorter wavelengths are more harmful to chemicals than longer ones since photoreactions may only take place from the S_1 or T_1 level (Beijersberge Van Henegouwen, 1997).

Apart from chemical reactivity, the excitation energy of a photoactivated molecule after reaching the S_1 state may be dissipated in the form of radiative and non-radiative processes, ultimately regaining the ground energy state. This can be achieved in a number of ways as detailed below and in figure 1;

(a) Internal conversion is a process which initially proceeds without loss of energy where the electron changes orbital from S_1 to a high vibrational energy level of the S_0 state, while still maintaining the same spin (Beijersberge Van Henegouwen, 1997). This can then be followed by;

(b) a non-radiative process consisting in the rapid loss of heat energy in the form of rotational and vibrational relaxations to the lowest vibrational level of the ground, S_0, state (Beijersberge Van Henegouwen, 1997); or

(c) a radiative process consisting in the emission of a lower energy photon than the one absorbed through fluorescence thus regaining the S_0 (Beijersberge Van Henegouwen, 1997).

(d) From the S_1 state, a non-radiative process known as intersystem crossing may also occur, initially proceeding without loss of energy and whereby the electron remains in the same orbital but undergoes spin inversion and reaches the triplet (T_1) state (Beijersberge Van Henegouwen, 1997). This can then be followed by

(e) phosphorescence, a radiative decay whereby a lower energy photon is emitted from the T_1 state allowing the molecule to regain its S_0 state (Beijersberge Van Henegouwen, 1997). This process is less likely to occur compared to other radiative and non-radiative processes due to the need for a simultaneous change in both electron spin as well as orbital (Beijersberge Van Henegouwen, 1997).

(f) Another non-radiative decay may also occur from the T_1 state, whereby the electron changes both spin and orbital to a high vibrational energy level of the S_0 state followed by a heat energy loss to reach a lower more stable vibrational level of the S_0 state (Beijersberge Van Henegouwen, 1997).

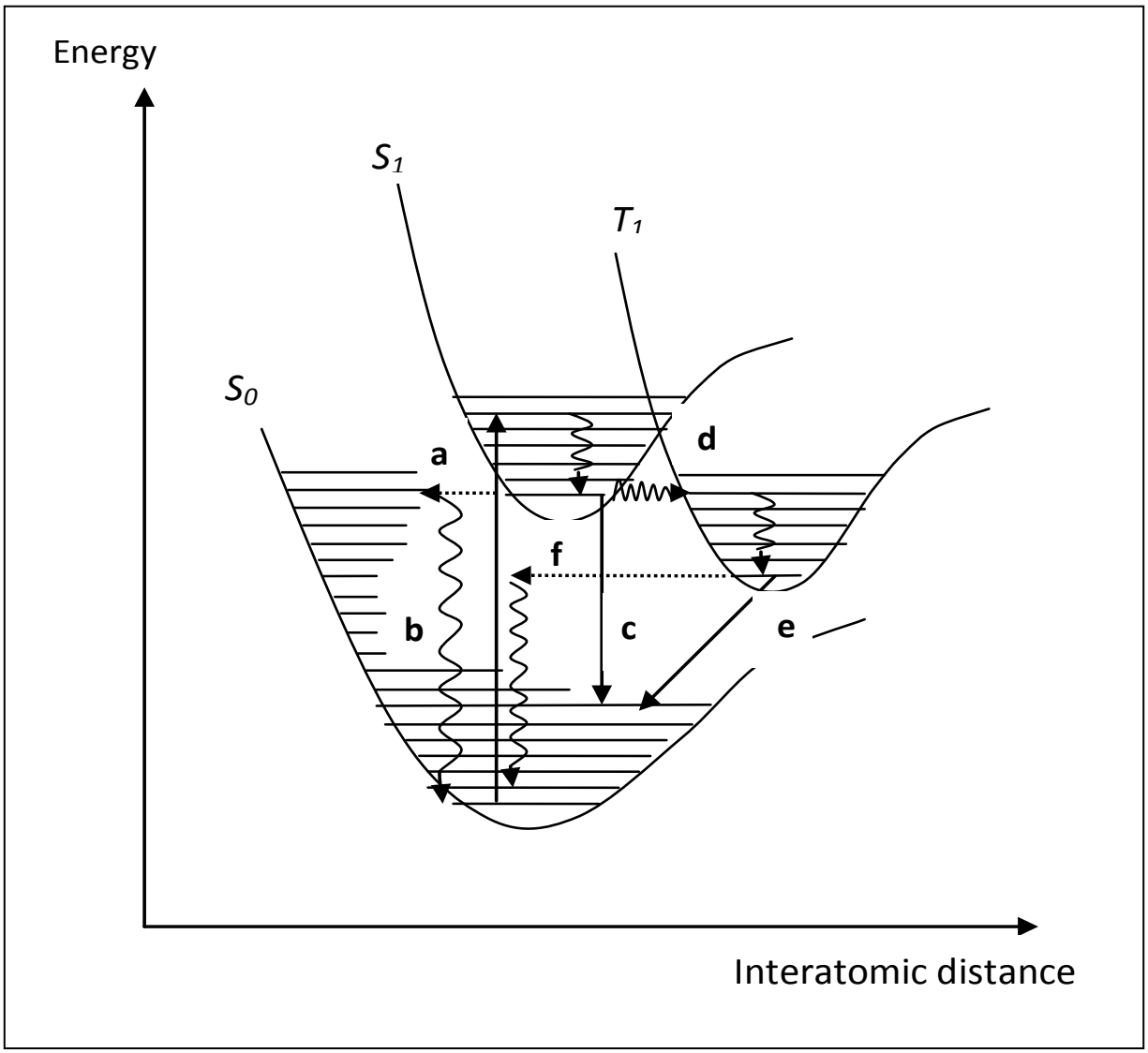

Figure 1: Potential energy diagrams showing the primary deactivation processes following photochemical electronic excitation, as explained above (Adapted from: Pine, 1987)

Processes requiring both spin inversion and change in orbital such as processes (e) and (f) are less likely to occur yet have longer lifetimes than processes requiring either spin or orbital change (Beijersberge Van Henegouwen, 1997). This results in a longer intrinsic lifetime of molecules in their triplet (T_1) state approximating 10^{-3}-10 s compared to 10^{-9}-10^{-6} s in the S_1 state (Beijersberge Van Henegouwen, 1997). The longer T_1 lifetime increases a

molecule's chances of undergoing chemical reactions from that state (Beijersberge Van Henegouwen, 1997).

Photochemical reactions may occur from T_1 or S_1 electronic states whenever reactivity is quicker than other competing deactivation processes. Furthermore, a secondary deactivation pathway whereby an excited molecule can transfer its energy to another surrounding molecule, which may either quench the excess energy and dissipate it without reacting or may in turn participate in chemical reactions through photosensitisation (Wayne & Wayne, 1996).

Therefore, from the S_1 or T_1 states, chemical reactivity may compete with various physical relaxation processes. Colliding reaction partners may not always be involved in photoreactivity and unimolecular reactions such as isomerisation and rearrangement may also take place from either the S_1 or T_1 states. Since unimolecular reactions are usually very fast, the likelihood of their occurrence from the relatively shorter-lived S_1 state becomes higher (Beijersberge Van Henegouwen, 1997).

3. Photochemistry used to our advantage

A vast number of research studies within the scientific community have been devoted to the field of photochemistry. This has led to a better understanding of the topic together with

pertinent advances and achievements in the area. Furthermore, applications of photochemistry have recently encompassed the arenas of pharmaceutics and photo-medicine through the developments of light-responsive drug delivery devices and phototherapy (Fomina et al, 2012; Wohl and Engebersen, 2012; Tomatsu et al, 2011; Feliciano et al, 2010) besides other important technological applications such as solar energy harvesting. Nevertheless, one of the frontiers of photochemistry resides in the determination of the kinetic order of photoreactions and the integrated rate-law models governing these reactions.

Over the past decades, remarkable advances have been made in the field of photochemistry. Novel applications within the field have encompassed the arenas of pharmaceutics and photomedicine through developments in phototherapy and light-responsive targeted drug delivery devices besides other important technological applications such as solar energy harvesting (Fomina et al, 2012; Wohl and Engebersen, 2012; Tomatsu et al, 2011; Feliciano et al, 2010). Nevertheless, one of the unravelled boundaries of photochemistry resides in the determination of the kinetic order of photoreactions and the integrated rate-law models that specifically govern these reactions.

The photoreactivity of many pharmaceuticals *in vivo* have been used to advantage in the treatment of a number of diseases. Regularly, UVA radiation in combination with psoralens, known as PUVA therapy, has been used in the treatment of psoriasis (Moan & Juzenas, 2004). Psoriasis is a common skin disease characterised by high skin cells proliferation. Light

exposure within the absorption spectrum of psoralens (300 to 400 nm) causes the psoralen to covalently bind the pyrimidine bases in DNA. This intercalation within DNA strands slows down the rate of cell division in psoriatic skin (Moan & Juzenas, 2004).

Another area of photochemotherapy is the use photodynamic therapy (PDT) in various cancers, a major area of application being skin tumours. This treatment method consists in administering the patient a photosensitising agent, usually a heamatoporphyrin derivative, which is retained in tumours with some selectivity compared to normal tissues. Subsequently, the patient is irradiated at the site of lesion. The therapeutic effect is brought about by the subsequent formation of singlet oxygen species that produce a number of effects in cells and tissues such as destruction of plasma membrane, lysosomes and tubuli, induction of apoptosis by oxidative stress and tumour suffocation through destruction of tumour blood vessels (Tonnesen, 2008). PDT is now regarded as a promising tool in the treatment of oesophageal carcinoma, barretts oesophagus, age-related macular degeneration and atherosclerotic plaques (Moan & Juzenas, 2004).

In light of the current widespread antibiotic resistances, the use of PDT in the treatment of microbial infections has also revealed to be a promising research avenue. Singlet oxygen generated through PDT can act on a wide range of targets within the bacterial cell and therefore, PDT can have a broad spectrum of activity thereby rendering bacterial resistance unlikely (Moan & Juzenas, 2004).

Novel drug delivery devices represent another area where photoreactivity of molecules has proven to be beneficial. Currently, photoactivation represents an attractive option for triggering and/or controlling drug delivery from carrier systems such as photosensitive hydrogels, microcapsules and liposomes as well as activating inactive drug molecules, such as photosensitisers and prodrugs, when present at the site of action (Moan & Juzenas, 2004).

Furthermore, a recently developed technique, known as photochemical internalisation (PCI) has advanced the field of macromolecular therapeutics such as the delivery of genes, proteins and other macromolecular therapeutic agents with intracellular actions. Macromolecules are normally taken up by endocytic vesicles in cells. However, degradation of macromolecules occurs soon after endocytosis, thereby preventing their action (Moan & Juzenas, 2004). PCI circumvents this barrier through light activation of a photosensitiser localised in the endocytic vesicle membrane and inducing rupture of this membrane. As a result endocytosed molecules are released and can reach their target of action prior to lysosomal degradation (Moan & Juzenas, 2004).

However, despite the various advantages that drug photoreactivity presents, there are a variety of unwanted reactions adversely affecting patients following drug administration as a result of drug (or drug products)-light interactions.

4. Photostability of medicines

The stability of medicines is of major concern to the pharmaceutical industry as well as the hospital and community sectors. This is particularly relevant when a drug or drug formulation is susceptible to heat, moisture, microbiological or light degradation. In order to ensure the quality and integrity of medicinal products, a number of drug-stability tests and protocols have been devised and presented at the International Conference on Harmonisation (ICH) on drug stability testing in the form of standard testing guidelines and recommendations to the pharmaceutical industry in the European Union, US, Japan and Canada.

While most recommended tests have long been established and constitute routine practices, photostability testing guidelines have been introduced in 1998 and only concern drugs introduced to the market following the advent of the ICH Q1b document relating to the photostability testing of medicines. Nonetheless, the number of drugs, new as well as established, found to be unstable to light exposure continues to increase. The European pharmacopoeia prescribes light protection for over 250 medical drugs in addition to a number of adjuvants with new compounds frequently being added to the list (Tonnesen, 2004).

5. Drugs exposure to light and its implications

From its development to its systemic absorption and distribution, a drug molecule may interact with light irradiation, potentially resulting in a wide array of deleterious effects. The

various instances whereby a drug substance may come into contact with light can be categorised into exposure prior the administration of a drug to the patient and/or following drug intake.

5.1. Photoreactivity of drugs prior administration

Solar extraterrestrial radiation comprises visible (Vis, 400-800 nm) and ultraviolet (UV) electromagnetic radiation. UV radiation spans the UVC (200-280 nm), UVB (280-320 nm) and UVA (320-400 nm) wavelength ranges. The ozone layer in the Earth's atmosphere absorbs much of the UVC radiation and allows other wavelengths as well as a certain portion of UVC to reach Earth's surface (Beijersbergen & Henegouwen, 1997). Furthermore, much of today's artificial lighting emits both in the visible as well as the UVA, UVB and sometimes even in the UVC regions such as discharge, germicidal lamps and welding arcs (Moore, 2004).

A large number of drugs have been shown to interact with UV/Vis radiation, following which, a change in their physicochemical properties may result, ultimately leading to deleterious effects on patients' health (Drucker and Rosen, 2011; Ferguson, 2006; Moore, 2002; Gould et al., 1995).

As early as the discovery stage, a drug molecule is already likely to be exposed to ambient laboratory lighting such as window-filtered daylight and artificial lamp lighting of various

spectral outputs and intensities. The subsequent formulation and mass production stages represent further steps whereby a drug in its liquid and/or solid powder forms may further encounter and interact with light radiation before the packaging and distribution stages (Tonnesen, 2008, 2004). When a new drug molecule has been identified as light-sensitive, often light-proof packaging is used to protect the final drug product. Nevertheless, this does not eliminate the risk of further light exposure as the medicine follows its journey to drug distribution centres, community pharmacies, hospital wards, and finally patients or nursing homes.

It is common practice in hospital settings to store a drug product in unit-dose containers, on open shelves directly exposed to artificial lighting or window-filtered daylight, in refrigerators with constant lighting and even on window sills, and this for prolonged periods of time (Tonnesen, 2008). Furthermore, in many instances, the outer protective packaging is removed often leaving only primary transparent plastic or glass containers that may offer little or no protection against UV or visible radiation (Tonnesen, 2008). Another commonly encountered situation whereby a medicinal product may be exposed to light radiation is during the extemporaneous preparation of medicines in hospitals (Tonnesen, 2008). This may involve a reformulation of a dosage form into patient-suited formulations such as reconstitution from solid into liquid forms, dilutions, or the preparation of a medicinal product with particular specifications to meet the patient's medical needs and whereby no suitable licensed alternative exists on the market. The cathecolamines adrenaline, dopamine and isoprenaline, for instance, were shown to photodegrade to different extents when dissolved in various isotonic aqueous media (Tonnesen, 2004).

A third of injectable products have been identified as light-sensitive as specified in the United States Pharmacopoeia (USP) (Baertshi, 2013). On the other hand, the European Pharmacopoeia recommends the use of sufficiently transparent containers for parenterals to allow visual inspection of the contents (Kristensen, 2004). As such, the use of paraenterals especially in the form of long-term infusion bags poses a major photo-instability risk. This is because parenteral infusions are usually contained in clear unprotected bags and administered through plastic tubing over many hours, during which photochemical reactions may occur. Infusion bags kept at patients' bedside were found to contain less than 10% of the active substance near the end of infusion time (Tonnesen, 2008). Furthermore, injectables are often administered in settings where intense lighting is needed to aid visibility during surgical or medical procedures (Baertshi, 2013). Premature babies are also at risk of being administered potentially photodegraded medication intravenously for the treatment of hyperbilirubinemia (Tonnesen, 2008). It has also been reported that ambulatory patients are likely to take their infusion bags and tubings unprotected outdoors thereby exposing them to direct sunlight (Baertshi, 2013). Furthermore, light-exposure of morphine solutions dispensed in plastic syringes and used in patient controlled analgesia devices was shown to reduce the drug shelf-life from 6 to only 1 week (Kristensen, 2004).

Patients use of medication in non-clinical settings has also considerably increased and various drug storage practices have been adopted such as removal of outer packaging, the transfer of solid as well as liquid medicines into different containers or compliance aids and

storage under direct lighting conditions, all of which may be compromising to the photostability of the drug (Baertshi, 2013; Tonnesen, 2008, Church and Smith, 2006).

Such *in situ* interactions between drugs and UV/Vis light have, in many instances, been shown to result in a photodecomposition of the active ingredient (Tonnesen, 2004; Beijersbergen & Henegouwen, 1997). The antibiotic, chloramphenicol, for example, although thermally stable in aqueous solution, with a shelf-life over 2 years (25°C, pH 7), was found to decompose by more than 80% of its original concentration (10 $mg.L^{-1}$ in 0.05M phosphate buffer, pH 7) for a 45 minute-exposure to sunlight of moderate intensity (14 W m^{-2} at 360 nm) (Beijersbergen & Henegouwen, 1997). The degradation of an active ingredient leads to a loss of potency and thus therapeutic effect. This may ultimately lead to a worsening of the medical condition and/or an unnecessary and potentially hazardous dose increase (Tonnesesn, 2008, 2004).

Another potentially hazardous aspect of drug photoreactivity is the formation of toxic photoproducts (Tonnesesn, 2004; Beijersbergen & Henegouwen, 1997). The photodecomposition products of chloramphenicol, for instance, were shown to bind irreversibly to plasma proteins and cell constituents in the blood and cause oxidative stress and phototoxicity to bone marrow cells (Beijersbergen & Henegouwen, 1997).

5.2. Photoreactivity of drugs following administration

Following systemic absorption, a drug molecule is often distributed through the circulatory system to various parts of the body. This molecule or sometimes its metabolites may absorb light radiation penetrating through light-exposed sites such as the eyes and skin. Light absorption may then trigger a wide array of drug-induced phototoxic reactions in the skin, eyes and/or other organs irrigated by blood vessels where the phototoxic agent may be present. The cornea of the eye is capable of absorbing wavelengths below 295 nm while the lens absorbs radiation in the 295-400 nm region and wavelengths above 400 nm are transmitted to the retina (Beijersbergen & Henegouwen, 1997).

It has been recognised that not only natural day light but also our artificial lighting increasingly emit wavelengths capable of inducing phototoxic skin reactions (Ferguson, 2006). Both UV and visible radiation are able, to different extents, to pass through different skin layers and reach the network of capillary blood vessels in the deeper dermis layer. For white skin types, the proportions of incident light radiation reaching the dermis were reported to be; 1% at 250 nm, 5% at 290 nm, 20% at 300 nm, 35% at 320 nm and 50-60% from 350 nm and above. Due to skin pigmentation differences, these values are lower for darker skins. Such fractions of UVA and UVB radiation reaching the dermis are sufficient to cause phototoxic reactions (Beijersbergen & Henegouwen, 1997). UVA radiation, which penetrates deep into the dermis has been most commonly associated with drug photosensitivity, although UVB and visible light have also been implicated (Drucker and Rosen, 2011). Furthermore, it is estimated that approximately half of all existing drugs absorb in the UVA and UVB regions of the spectrum (Ferguson, 2006).

Phototoxicity occurs following an interaction between a chemical and non-ionising radiation (UV and Vis) and results in an alteration of cell function. In the skin, drug-induced phototoxicity manifests as an exaggerated sunburn. Drug-induced photosensitivity dermal reactions represent 8% of only reported cutaneous adverse drug reactions. However, the true incidence of these drug-induced reactions amongst the population and for individual drugs remains unknown given the widespread use of drugs with phototoxic potential, the scant reporting in addition to the fact that adverse drug reporting databases largely underreport the incidence of these reactions especially for drugs that have been marketed for some time and are already known as photosensitisers (Drucker and Rosen, 2011).

Phototoxicity may be provoked by a range of mechanisms following photo-activation of the drug/drug-metabolite molecule in the body by light radiation. The photoactivated molecule may engage in photochemical reactions yielding toxic products. *In vivo* studies on chloramphenicol were found to correlate with *in vitro* findings in terms of photoproducts formed upon UVA exposure. These photoproducts were shown to generate oxidative stress in blood cells (Beijersbergen & Henegouwen, 1997).

Another phototoxicity mechanism involves a reaction between the photoactivated agent and endogenous molecules such as DNA and proteins. The metabolite of the tranquilliser chlordiazepoxide, which can also form as a photoproduct of chlordiazepoxide photoreaction, was found to bind irreversibly to plasma proteins following its exposure to

UVA. Irreversible binding to biomacromolecules in the liver were also observed. This is an illustration that phototoxicity is not necessarily confined to light exposed sites but may also affect inner organs (Beijersbergen & Henegouwen, 1997).

The photoactivated molecule may also transfer its excitation energy to endogenous compounds that become activated and may, in turn, cause phototoxicity through the above mechanisms. Energy transfer to oxygen molecules with the subsequent formation of reactive singlet oxygen has been reported for tetracyclines and phenylpropionic acid derivatives used as anti-inflammatory agents (Beijersbergen & Henegouwen, 1997).

Photoactivation of a drug/metabolite molecule can also be brought about by an endogenous or exogenous photosensitiser that absorb radiation of a certain wavelength and transfers energy corresponding to a different wavelength that the drug/metabolite molecule is capable of absorbing. This indirectly activates the latter which can then lead to phototoxicity. Many oral contraceptives have been shown to undergo direct as well as indirect photoactivation by photosensitisation leading to protein binding with antigen-properties, which then elicits allergic side effects often experienced as erythema (Beijersbergen & Henegouwen, 1997).

These examples illustrate the importance of photostability studies as early as possible in the drug development process and continued monitoring and reporting of photosafety concerns. When conducted appropriately, a substantial amount of information can be

derived from photostability studies. This data can be used to enhance stability through formulation, appropriate packaging, labelling and storage, shelf-life prediction and health professional and patients' education. To this end, and in an ultimate aim to safeguard patients' health, the ICH photostability and photosafety testing guidelines have been introduced and implemented in the three regions of US and Canada, the EU and Japan.

6. Photostability and Photosafety testing of pharmaceuticals

As the number of photoactive drugs is becoming increasingly important, the value of testing drugs for photoactivity and phototoxicity both *in vitro* and *in vivo* is significant. Therefore, in 1996, the International Conference on harmonisation of photostability testing of new active substances and medicinal products (ICH Q1B) issued guidelines on how these tests ought to be conducted.

6.1. ICH Q1b photostability testing

In 1998, it became mandatory to evaluate the photostability of all new drug licenses applications. The ICH Q1b document provides a basic protocol and some guidelines on how to conduct photostability testing on the active drug substance and final drug product. The tests are conducted by exposing the drug substance/product to irradiation experiments and evaluating the drug's photostability according to a pass/fail assessment of acceptable/unacceptable change within limits justified by the applicant (ICH, 1998). The tests consist of two parts; forced degradation testing and confirmatory testing. Forced degradation testing consists of exposing the drug substance/product to stress irradiation

conditions in order to identify the intrinsic stability characteristics of the drug, the degradation products, reaction mechanism and to develop adequate methodology for detection and quantification (ICH, 1998). Confirmatory studies on the other hand, are performed under ambient lighting conditions to inform of any packaging, labelling or handling requirements during formulation, manufacturing and storage. The guidelines also recommend the use of an overall illumination of not less than 1.2 million lux hours and an integrated UV energy of not less than 200 watt hours/m^2 during confirmatory studies on the drug substance and product (ICH, 1998).

With regards to irradiation conditions used, two options have been proposed. Option 1 relies on a single lamp light source with an output similar to outdoor daylight or window-glass filtered indirect daylight with a suggestion for a spectral cut-off of radiation below 320 nm (ICH, 1998). Option 2, on the other hand, recommends a simultaneous or sequential exposure of the sample to a cool white fluorescent lamp emitting mainly in the visible and a near UV fluorescent lamp with an output range of 320-400 nm with a maximum energy emission between 350 and 370 nm (ICH, 1998).

The document also presents guidelines on sample selection and presentation. It is also recommended that sample analysis following irradiation is based on a qualitative examination for any changes in physical properties such as appearance, clarity, and colour of the solution besides an assay of degradation products using a validated method.

Although photostability testing may suggest the potential for *in vivo* photoreactivity, it is not sufficiently predictive of phototoxicity since a number of biological (e.g. tissue distribution, pharmacokinetics, skin type, ...etc) and environmental factors (body exposure to irradiation, latitude, altitude, season, weather, time of the day, exposure length,...etc) participate in the photoreaction (ICH S10, 2013).

6.2. Photosafety testing

Besides photosatability testing of pharmaceuticals, the photosafety of medicines *in vivo* began to be addressed in 2002 with the issue of guidelines on phototoxicity and photosafety testing by the European Agency for the Evaluation of Medicinal Products (EMEA, 2002). In 2009, the M3(R2) document was issued by the ICH, with guidelines on non-clinical safety studies for the conduct of human clinical trials and marketing authorisation for pharmaceuticals. The document highlighted the need for an initial assessment of phototoxic potential based on a drug's photochemical properties and pharmacological/chemical class which should inform of subsequent non-clinical drug distribution studies and experimental evaluation on phototoxic potential before Phase III trials. Further guidance on photosafety testing was provided in 2003 by the Food and Drug Administration (FDA) and the EMEA on photosafety testing (CDER, 2003). It was proposed that phototoxicity testing should be performed for new chemical entities and biotechnology-derived pharmaceuticals for human use which absorb UVB, UVA or visible radiation and can be applied to or partition into the skin or eyes; or are known to affect the condition of the skin or eyes (CDER, 2003).

In 2013, more in-depth recommendations on when and how to conduct photosafety studies were provided in the ICH Harmonised Tripartite Guideline document (S10) on the photosafety Evaluation of Pharmaceuticals (ICH S10, 2013). It is, thereby, recommended that an initial assessment of phototoxicity potential ought to be conducted on new active pharmaceutical ingredients, new excipients, clinical formulations for dermal application, and photodynamic therapy products in order to evaluate the likelihood of an acute light-induced tissue response occurring at light-exposed body sites (ICH S10, 2013). The studies apply to chemicals that (i) absorb radiation within the 290-700 nm range, (ii) have molar absorption coefficients greater than 1000 $L.mol^{-1}.cm^{-1}$, (iii) that generate a reactive species following absorption of UV/Visible light and (iv) distribute sufficiently to light-exposed tissues such as the skin and eyes. It is recommended that UVA irradiation doses in the range of 5 to 20 J/cm^2 are used to conduct *in vitro* and *in vivo* phototoxicity assays, thereby mimicking UVA doses comparable to those obtained during prolonged outdoor activities on summer days around noon time, in temperate zones and at sea levels (ICH S10, 2013). The most widely used *in vitro* test is the 3T3 Neutral Red Uptake Phototoxicity Test (3T3 NRU-PT) that is based on a comparison of the cytotoxicity of a chemical on Balb/c 3T3 cells (OECD/OCDE, 2004). Cytotoxicity is expressed as a concentration-dependent reduction of the uptake of the dye Neutral Red, when tested in the presence and in the absence of exposure to a non-cytotoxic dose of 5 J/cm^2 (in the UVA range) of simulated solar light over approximately 50 minutes (OECD/OCDE, 2004). The maximum test substance concentration used was set at 100 ug/ml and 8 geometric dilutions series should also be used thereby mimicking the low drug concentrations in human cells and tissues (ICH S10, 2013). For *In vivo* phototoxicity testing, on the other hand, no standardised study design has been established and relies on the use of a variety of species including guinea pigs, mice and rats.

Photostability and photosafety studies have provided more or less detailed standard testing protocols in order to provide critical data that should inform the pharmaceutical industry as well as health regulatory bodies of potential photo-instability and/or photo-toxicity hazards as well as precautionary and remedial strategies. Nevertheless, a number of inconsistencies have been identified and criticisms made regarding the core content of the ICH Q1b guidelines (Baertshi et al., 2013, 2010; Filho et al., 2011; Hung, 2004).

6.3. Limitations of the guidelines

It has been argued that photostability testing regulations suffer from a lack of clarity in many parts and a need for improvements and practical interpretations of the guidelines was repeatedly sought (Baertshi et al., 2013, 2010; Filho et al., 2011; Baertshi et al., 2010; Hung, 2004). These issues concerned the experimental as well as the analytical and interpretation parts of the tests.

6.3.1. Irradiation sources and spectral output

A choice of irradiation conditions has been provided in the ICH Q1b document yet providing illumination conditions that are not equivalent (Baertschi, 2010). It has been argued that the use of D65 outdoor equivalent light source does not equate the spectral output of light sources for an ID65 window filtered daylight exposure, either of which may be used according to option 1 (Baertschi, 2010). Furthermore, the spectral output of the irradiation

sources proposed in option 2, designed to simulate indoor lighting conditions is also different from any of option 1 sources (Baertschi, 2010). This is because the maximal wavelength outputs are different between different lamps and the extent of photoreaction is likely to vary between different lamp exposures. This also raises concerns about the significance of the results and their reproducibility.

In addition, it is recommended that the emission energy maximum of the near UV fluorescent lamp in option 2 should be between 350 and 370 nm with a significant portion of UV in the 320-360 nm and 360-400 nm range. Nevertheless, the reasons for this preferential distribution are not clear since various drugs absorb in different regions of the spectrum including the latter regions. It is, therefore, possible to underestimate the photodegradation extent of a drug molecule that absorbs outside the proposed emission maximum.

Although UVA radiation penetrates deep into the dermis to a greater extent than UVB and UVC radiation, UVB and visible light have also been associated with phototoxicity (Drucker & Rosen, 2011) Furthermore, it is estimated that approximately half of all existing drugs absorb in the UVA and UVB regions of the spectrum (Ferguson, 2006). However, the ICH Q1b guidelines recommend that radiation below 320 nm may be eliminated. Thus, compounds absorbing in the UVB region may erroneously appear to be photostable. Furthermore, comparisons between the identified spectral regions of concerns in the ICH Q1b and M3(R2) guidelines suggest a lack of concordance between the documents since the

290-320 nm UVB radiation range is included in photosafety testing yet not photostability tests.

Furthermore, a high discrepancy can be noted between the UVA doses proposed in confirmatory photostability and photosafety testing. In the latter a UVA dose of not less than 200 watt hours/m^2 (i.e. 72 J/cm^2) is recommended for confirmatory tests, which is 3.6-14.4 times higher than the 5-20 J/cm^2 UVA dose recommended for photosafety testing. While the use of such a high dose may be time-saving, it is often desirable to understand a drug's behaviour under more moderate ambient lighting conditions. Moreover, a lack of details on the length or extent to which an irradiation experiment should be performed has also been debated (Baertschi et al. 2010).

6.3.2. Actinometry

When performing photostability testing, it remains essential to know the spectral range and determine the number of photons absorbed by the sample under test as these parameters influence photoreactions rates (ICH, 1996). The experimental determination of the photon flux or light dose to which a photoreactive sample is exposed during a photoreaction is known as actinometry (Khun et al., 2004). This may be performed using either chemical or physical methods.

Chemical actinometry consists of a chemical entity that undergoes a light-induced reaction at a specific wavelength and for which the quantum yield (Φ) is already known and the reaction products can easily be analysed. The reaction rate is measured and used to calculate the incident photon flux using a defined equation (eq.I.1) (Piechocki & Thoma, 2007; Tonnesen, 2004; Khun et al., 2004)

$$Number\ of\ photons\ absorbed\ per\ unit\ time\ per\ unit\ area = Rate/\Phi \quad \text{(eq. I.1)}$$

The chemical actinometer is put in similar experimental conditions as the photoreacting system under investigation and the irradiation and measurements steps are usually performed seperately through indirect actinometry (Tonnesen, 2004). This consists in monitoring the concentration of a secondary species that forms after irradiation has stopped by reaction between the photoproduct of the actinometer and a specific chemical substance added to the reaction medium (Khun et al., 2004).

Physical actinometry, on the other hand, relies on physical devices that convert the energy or the number of the incident photons into a quantifiable electrical signal translated into a direct readout . They tend to be preferred to chemical actinometers due to their simple, fast and precise performance (Tonnesen, 2010). Nevertheless, they represent a more expensive option and their sensitivity may decrease with use, or may be altered by aging and occasional recalibration is recommended. Furthermore, visually unnoticeable damage on the photodiodes may also occur during exposure to high irradiation levels leading to

irreversible reduction in sensitivity and severe inhomogeneities on the surface (Tonnesen, 2010).

For the photostability testing of new active substances and medicinal products, the ICH recommend the use of quinine chemical actinometry to monitor the exposure to a near UV (300-400 nm) fluorescent lamp (ICH, 1996). Nevertheless, this actinometric system has been widely criticised due to a number of associated limitations (De Azevedo Filho et al., 2011; Kester et al, 2010; Baertschi et al., 2010, Baertschi et al. 1997). It was found, for instance, that the timing of the absorbance measurement affects the results as the quinine absorbance at 400 nm continues to increase despite stopping irradiation for more than 60 hours at approximately one fifth the rate of increase in absorbance observed during exposure to the lamp (Baertschi et al., 2010). Therefore, depending on whether the quinine solution absorbance is measured immediately after exposure to the lamp or after a delay, significantly different results are obtained (Kester et al., 2010).

Furthermore, despite the ICH recommendations on the use of quinine actinometry, this system was shown to be incompatible with option 1 sources (Baertschi et al., 2010). It was also found that quinine is sensitive to oxygen content and temperature when using a xenon lamp (Baertschi et al., 1997). Furthermore, the quinine calibration curve was also found to be dependent on concentration and sample location in the irradiation chamber (De Azevedo Filho et al., 2011). It has, thus, widely been recognised that quinine actinometry is not suitable for Option 1 sources (Brower et al., 1998).

In view of the nature and number of drawbacks associated with quinine actinometry, it remains clear that more adequate actinometers are required for the photostability testing of drugs and drug products.

6.3.3. Photostability data collection and analysis

It has been recognised that the ICH Q1b tests are mainly qualitative in nature (Baertshi, 2013). Evaluation of the tests is based on a subjective inspection of changes in the physical aspects of the sample such as appearance, clarity and colour, in addition to an assay of degradation products (ICH, 1996). It also remains up to the applicant's discretion to decide on what might represent an acceptable or unacceptable change (ICH, 1996). However, it is likely that photodegradation may occur without any noticeable physical changes as many drugs are colourless in solution and only absorb UV radiation. In addition, it remains unclear how the tests results may be related to a photostability shelf-life prediction. Thus, the proposal of a more quantitative data assessment and interpretation methodology would benefit photostability studies.

Moreover, the document does not provide any analytical methods for the study and comparison of the effect of variables such as stability enhancing excipients. This lack of standard analytical methods of photostability results has hampered effective evaluations and comparisons to be made between different studies. In the academic sector, kinetic treatment methods based on 0^{th}, 1^{st} and second order kinetics have widely been employed

for the analysis and interpretation of photoreactions data despite their limitations when applied to photochemistry.

7. Photoreactions kinetics

7.1. Relevance of kinetic studies in the photostability testing of pharmaceuticals

The aim of photostability studies is to generate data that, following precise treatment and analysis, should inform on the quality and stability of the medicines under various conditions and allow us to predict shelf-life and any potential toxicity issues. This should also indicate any handling, packaging, labelling and advisory requirements in order to ensure and maintain product's quality and efficacy and ultimately patient's safety. Therefore, a careful design of stability tests combined with the use of specific and accurate analytical data treatment methods constitute essential pre-requisites.

7.2. Reactions kinetics and the nature of photochemical reactions

Kinetic studies represent a crucial means for the understanding and determination of the rates at which a change occurs. The rate of a chemical reaction is defined as the rate of decrease in reactants' or increase in products' concentration. It can, thus, be expressed as the rate of reactants disappearance or that of products formation (eq. I.2).

$$rate = -\frac{d[reactants]}{dt} = \frac{d[products]}{dt} (eq. I. 2)$$

The rate of a reaction can be determined by measuring the reactants' or products' concentrations as a function of time and measuring the gradient of a concentration-time graph at the time of interest.

The rate of a reaction usually decreases as the reaction proceeds. It was also found that the rate of a reaction depends on the concentration of reactants. This variation of reaction rate with reactants concentration is defined by a rate equation of the form;

$$rate = k \times {C_A}^{n_1} \times {C_B}^{n_2} \times {C_C}^{n_3} \ldots (eq.I.3)$$

Where; *k* is a constant known as the rate-constant and provides a useful measure of the rate of a reaction. C_A, C_B, C_C,...are the reactants' concentration and $n_1, n_2, n_3, \ldots$ are constants known as the order of the reaction with respect to A, B, C,..., respectively. The order of a reaction depicts the chemical behaviour of the reaction with respect to reactant(s) species. The overall order of the reaction is the sum of the exponents $n_1 + n_2 + n_3 + \cdots$ with 0^{th}, 1^{st} and 2^{nd} order reactions corresponding to exponents sums of 0, 1 and 2, respectively. Determination of a reaction order can only be achieved using experimental data, often involving species concentrations at different times. This requires the use of adequate analytical methods that allow the determination of the reaction medium species' concentrations at different times of the reaction. This is most often achieved by spectrophotometry or chromatography. Subsequently, concentration-time equations corresponding to different orders are usually fitted against experimental kinetic traces. The reaction is then ascribed the order corresponding to the concentration vs. time equation, or integrated rate-law, that best fits the kinetic traces.

The importance of integrated kinetic rate-laws and related kinetic studies resides in their ability to deliver information on the rates and mechanism of reactions. They represent a necessary tool for an accurate quantitative description of the evolution of reaction species over time. Accurate kinetic studies also take into account all the reaction variables affecting a reaction rate.

Practically, data derived from kinetic model equations are of paramount importance on a drug research and development level where it is essential to predict how the drug will interact with its environment, the mechanistic degradation pathways it will follow as well as its shelf-life and behaviour in alternative conditions.

Therefore, knowledge of the integrated rate-laws that describe the kinetic behaviour of drugs degradation is important for a fundamental understanding of photoreactions kinetics as well as for pharmaceutical applications. For thermal studies, shelf-life anticipation and decisions on stability requirements rely predominantly on established kinetic treatment methods whereas photostability testing is mainly undertaken for the development of analytical methods and the determination of protective requirements based on less well defined analytical protocols (Anderson and Byard, 2004 in Tonnesen 2004).

7.3. The kinetics of thermal and photochemical reactions

Intrinsic differences in the nature of thermal and photochemical reactions imply that different kinetic rate-laws underly each reaction type. For a simple unimolecular reaction whereby species A thermally reacts to produce product B, the rate law is found to depend on temperature (*T*) and has the general form;

$$\frac{dC_A}{dt} = -A \times e^{-\frac{E_a}{RT}} \times C_A(t) = -k_\Delta \times C_A(t)^n \qquad (eq.I.4)$$

Where A is a pre-exponential factor, $E_a$is the activation energy and *R* is the universal gas constant. The exponent, *n*, reflects the kinetic order of the reaction with, *n* = 0 for zero-order, *n* = 1 for first-order, *n* = 2 for second-order kinetics.

An analogous unimolecular photochemical reaction, on the other hand, is governed by a kinetic rate-law of the form;

$$\frac{dC_A}{dt} = -\Phi_{\mathrm{AB}}^{\lambda\mathrm{irr}} \times P^{\lambda\mathrm{irr}} \times \varepsilon_A^{\lambda\mathrm{irr}} \times l_{\lambda\mathrm{irr}} \times \frac{1 - 10^{-A_{tot}^{\lambda_{irr}}(t)}}{A_{tot}^{\lambda_{irr}}(t)} \times C_A(t) \quad (eq.I.5)$$

where $\Phi_{A\to B}^{\lambda_{irr}}$ is the quantum yield of the photoreaction realised at the irradiation wavelength (λ_{irr}); $P_{\lambda_{irr}}$ is the radiant power; $l_{\lambda_{irr}}$ is the optical path length of the irradiation beam inside the sample, $\varepsilon_A^{\lambda\mathrm{irr}}$is the molar extinction coefficient of species A, $A_{tot}^{\lambda_{irr}}(t)$ is the medium's total absorbance at time t, and $C_A(t)$ is the concentration of reactant *A* at time t.

The parameters $\Phi_{\mathrm{AB}}^{\lambda\mathrm{irr}}$, $P^{\lambda\mathrm{irr}}$, $\varepsilon_A^{\lambda\mathrm{irr}}$, and $l_{\lambda\mathrm{irr}}$ have constant values for a given experimental setting. As such, the product of these terms is constant and eq.I.5 can be re-written as;

$$\frac{dC_A}{dt} = -\,Constant \times \frac{1 - 10^{-A_{tot}^{\lambda_{irr}}(t)}}{A_{tot}^{\lambda_{irr}}(t)} \times C_A(t) \;\; (eq.I.5)$$

Despite having the same general chemical form, these reactions show clear differences in the terms of their rate-laws, which can also be explained by a different mechanistic nature of the two reaction types. Therefore, photo- and thermo- chemistry represent two distinct branches of chemistry that display a number of critical differences, as described above. As a consequence, the field of photoreactions kinetics requires the development of kinetic models that accurately and specifically depict the evolution of photoreactions. It has, so far, not been possible to achieve this purpose due to a number of limiting steps, as described in the following section of this chapter.

I.II. The problematic

1. Introduction

Having benefited from standard kinetic elucidation protocols as well as universally applicable kinetic models, thermal reactions studies have now become routine procedures providing consistent and replicable results in various research settings. On the other hand, a lack of uniformity and reproducibility has long characterised photostability studies and a number of limitations have been identified and are hereby described.

2. The problematic

2.1. The use of polychromatic light

The study of drugs degradation with light has mainly been conducted using polychromatic light sources with or without filters for the selection of spectral regions of interest. The spectral ranges and intensities achieved using such irradiation methods varied significantly from one study to another (Moore, 2004). This variation has resulted in the generation of data that cannot be reproduced nor compared between different studies.

The use of polychromatic irradiation light induces a combined kinetic effect due to various wavelengths impacting to a different extent on the molecule. This has, in turn, halted the fundamental understanding and modelling of photoreactions kinetics. It has thus been proposed that the most accurate way for the study of photoreactions kinetics is through the use of monochromatic irradiation experiments where the effect of each wavelength may be delineated (Moore, 2004).

2.2. Data analysis methods

Although it is mandatory to determine the rate and kinetics of degradation during thermal stability testing and accordingly the predicted thermal shelf-life, photodegradation testing is predominantly undertaken for the development of analytical methods and to determine whether a product is sufficiently photostable to avoid unnecessary protective packaging and warning labels (Anderson and Byard, 2004).

Determination of the kinetic order of a reaction is based on the collection and analysis of experimental data reflecting the change in species concentrations with time. For thermal reactions, zero, first and second order kinetic models represent integrated kinetic rate laws that have been developed through closed-form integration of their reaction rate-laws. Most photoreactions, on the other hand, have not benefitted from kinetic models derived from their respective rate-laws whose integration could not be achieved mathematically through closed-form. This is due to the presence of a variable time-dependent factor in photoreactions differential rate-law equations.

In the literature, the kinetic analysis of photostability data has predominantly been undertaken using zero, first and less frequently second-order kinetics (Tonnesen, 2004; Piechocki and Thoma, 2010). However, this analytical method has led to much confusion about which reaction order a given photochemical reaction follows since various interpretations and conclusions could often be reached about the kinetics of a particular

photoreaction. There were some cases, for instance, where the photokinetic traces could equally be fitted with two or more thermal kinetic orders as was shown for benzydamine hydrochloride and ketorolac thromethamine whose photodegradation kinetic traces could be fitted with zero as well as first order kinetics (Piechokcki and Thoma, 2010). Furthermore, poor or only partial fitting was also observed when using thermal kinetics to fit photo-reactions kinetic traces (Maafi and Brown, 2007, Piechokcki and Thoma, 2010). One approach that has been extensively used in an attempt to palliate the poor data fitting is a two-stage treatment approach whereby an initial section of a kinetic trace is fitted with a particular thermal kinetic order while the rest of the trace is fitted with another model (Piechocki and Thoma, 2010; Tonnesen, 2004; Shamsipur et al., 2003; Albini and Fasani, 1998). Nevertheless, this approach has raised questions about the reasons why a photoreaction order would change during the progress of the same reaction. Furthermore, it was also noted that photoreactions are dependent on initial concentration while the widely applied first order kinetics are known to be independent of this parameter (Moore, 2004).

The only exception where first-order treatment of photoreactions kinetics was deemed suitable is when a reaction is performed under monochromatic isosbestic irradiation, where both the reactant and photoproduct have the same extinction coefficients. This is because, in this case, a closed-form integration of the rate-law has been established as a monoexponential model analogous to the first-order thermal equation (Maafi and Brown, 2005). However, the majority of photoreactions are conducted under non-isosbestic conditions and/or often use filters instead of monochromators to select a particular

irradiation wavelength range (Piechocki and Thoma, 2010; Tonnesen, 2004; Gorner, 2010; Souza et al., 2010; Glass et al, 2004; Shamsipur et al., 2003; Thoma and Klimek, 1991; Majeed et al, 1987).

Furthermore, it has been demonstrated that for unimolecular photoreactions occurring under monochromatic irradiation wavelengths where only the initial species absorb the incident radiation but not the photoproduct, the integrated rate-law could be determined mathematically through closed-form by variable separation method since, in this case, the photokinetic factor remains constant (Maafi and Brown, 2007). The integrated rate-law determined for this case was found to have a log-exponential form that is different from the first-order integrated rate-law equation. Despite representing one of the simplest photoreaction mechanisms, the integrated rate-law for this photoreaction type had a log-exponential form that reflects a reaction evolution that is inherently different to that of first-order exponential kinetics. Nevertheless, a lack of alternative kinetic treatment methods meant that valuable photoreactions data and kinetic parameters could not otherwise be characterised.

In contrast, thermal stability testing relies on standard quantitative kinetic parameters derived from universally applicable equations that were developed to analytically describe thermal reactions kinetics. Thus, the lack of specificity of thermal reactions kinetics to describe photoreactions kinetics is principally due to the inherent differences in the terms of the rate-laws describing the two reaction types. As a result, the integrated rate-laws for

photoreactions and thermal reactions cannot be expected to be the same. However, integration of photoreactions rate-laws could not be achieved for most cases, even for the simplest photoreaction mechanisms due to the presence of a time-dependent photokinetic factor that renders the mathematical integration of these equations through closed-form unachievable.

2.3. Rate-constant determination

The lack of integrated rate-laws for the study of photoreactions kinetics has meant that thermal kinetics have been widely used for this purpose. However, it was also observed that the rate-constants determined using this method were neither reproducible nor comparable between different studies (Piechocki & Thoma, 2010). The rate-constant values thus determined may only serve in the study of the effect of a given variable on photoreaction rates within the same set of experiments and experimental settings such as the effect of an additive or pH on a sample's photodegradation rate (Piechocki & Thoma, 2010). This has also meant that, in the field of drug photostability, accelerated photostability data could not be extrapolated to determine the photochemical shelf-life nor to reach any practical conclusions (Moore, 2004).

This is due to the rate-constant determined in this way corresponding to a thermal rate-constant defined by the Arrhenius equation, where the reaction is, by definition, dependent on temperature. However, it is widely known that most photoreactions do not depend on temperature yet on parameters such as wavelength, light intensity and the molecule's

absorptivity. The utility of thermal rate-constants in comparing the effect of one variable in photoreactions experiments conducted within the same settings stems from the fact that these values represent a means of quantifying the change in photoreaction rate whenever the irradiation conditions remain unaltered. However, the values determined in this manner do not represent the true photochemical rate-constant values. Furthermore, the parameters that affect photoreactions kinetics such irradiation wavelength and intensity are not reflected in the Arrhenius equation. This also implies that the rate-constant determined by fitting thermal kinetic equations to photoreactions data do not represent the true photochemical rate-constant and, thus, the analytical expression for photoreactions rate-constants remains to be defined.

2.4. Actinometry

Actinometry is conducted in order to determine the number of photons absorbed by the sample per unit time and volume; and forms an integral part of photodegradation kinetic studies. This is because the intensity of radiation plays a major role in the determination of photoreactions rates and is also likely to vary from one study to another. It is, thus, more accurate to determine the photoreaction quantum yield, as a measure of photoreaction efficiency. Photochemical quantum yield is less frequently determined than overall rate-constants despite being more informative on the inherent photoreactivity of a molecule (Moore, 2004). Quantum yield calculation is often performed using chemical actinometry to determine the number of photons absorbed per unit time in conjunction with a chromatography separation technique to determine the number of photo-reacted molecules per unit time. For drug photostability studies, the ICH guidelines recommend the

use of quinine hydrochloride as an actinometer. However, this actinometer has rarely been used for this purpose as it was shown to present many drawbacks that render it inadequate for these purposes (Baertschi et al., 2010; Baertschi, 1997; De Azevedo Filho et al., 2011). The most widely used ferrioxalate actinometer has also been attributed major drawbacks due to its cumbersome experimental usage and a rapid reaction completion compared to most photoreactions (Moore, 2004) which have rendered accurate quantum yield determination a challenging task. There is thus a clear need for simple, accurate and specific actinometric tools for the study of photoreaction kinetics.

I.III.Objectives

Although it has been acknowledged that the use of thermal kinetics for the study of photoreactions may not represent a correct interpretation for the treatment of photokinetic data, this approach has been widely adopted due to the lack of integrated photoreactions rate-laws and a concomitant need to find some way of analysing photokinetic data. Therefore, a prime aim of this thesis was to develop and validate kinetic laws that are accurate and specific to photoreactions. To this end, a new methodology that circumvents the mathematical integration hurdle was required. Thus, another prime aim was to develop this methodology, as described in Chapter III and which would then allow the generation of photokinetic models. This step was necessary for the subsequent model development stage.

Three abundant photoreactions types were selected for kinetic model development and validation purposes namely unimolecular, photoreversible and consecutive photoreactions as described in chapters four, five and six. Another aim of the thesis consisted in testing the validity of these models experimentally using drug molecules as will be described in these chapters.

The experimental settings used throughout this work clearly addresses the important objective of providing a standard, universally applicable and comparable experimental photostability and kinetic study means that overcome the reproducibility and lack of experimental consensus problem.

The developed models also responded to the valuable aim of performing a full kinetic elucidation of the parameters characterising the photoreactions under study and which can be widely applied and extended to other drug molecules as described in chapters four, five and six.

Palliating the lack of rate-constant analytical expression for photoreactions represents another objective of the thesis that was addressed in the early chapters. This parameter could then be used and compared for the study of the effects of variable factors such as additives and initial concentration on photoreaction kinetics, which formed another integral objective of the thesis.

Finally, these studies were also conducted with the additional aim of evaluating the studied drugs potential to act as actinometers thereby overcoming the limitations identified with currently recommended/used actinometers, as will be described in the penultimate chapter of the thesis.

References

Albini A.; Fasani E., 1998. Drugs Photochemistry and Photostability. The Royal Society of Chemistry: Cambridge.

Anderson N.H. & Byard S.J., 2004. Photostability testing: Design and interpretation of tests on new drug substances and dosage forms. In Tonnesen H. H., 2004 Photostability of drugs and drug formulations. Second edition. London: CRC Press.

Baertschi S.W., Clapham D., Foti C., Jansen P., Kristensen S., Reed R.A., Templeton A.C., Tonnesen H.H., 2013. Implications of In-use photostability: proposed guidance for photostability testing and labelling to support the administration of photosensitive pharmaceutical products, part 1: drug products administered by injection. Journal of Pharmaceutical Sciences. 102: 3888-3899.

Baertschi S. W., Alsante K. M., Tonnesen H. H. A Critical Assessment of the ICH Guideline on Photostability Testing of New Drug Substances and Products (Q1B): Recommendation for Revision. Journal of Pharmaceutical Sciences. 2010; 99: 2934-2940.

Baertschi S.W., 1997. Commentary on the quinine actinometry system described in the ICH draft guideline on photostability testing of new drug substances and products.Drug Stability. 1, 193-195.

Beijersberge Van Henegouwen G.M.J., 1997. Medicinal Photochemistry: Phototoxic and Phototherapeutics Aspects of Drugs. In Tests B and Meyer U.A. Advances in Drug Research. 29, 81-169.

Brower J.F., Drew H.D, Juhl W.E., Thornton L.K. Quinine photochemistry: A proposed chemical actinometer to monitor UV-A exposure in photostability studies of pharmaceutical drug substances and drug products. Pharm Forum. 1998; 24:6334-6346.

CDER, US Department of Health and Human Services Food and Drug Administration Center for Drug Evaluation and Research (CDER), 2003. Guidance for Industry: Photosafety Testing. Accessed online on 19/11/2014; http://www.fda.gov/cder/guidance/index.htm

De Azevedo Filho C.A., De Filgueiras Gomes D., De Melo Guedes J.P., Batista R. M. F., Santos B.S. Considerations on the quinine actinometry calibration method used in photostability testing of pharmaceuticals. Journal of Pharmaceutical and Biomedical Analysis. 2011; 54: 886-888.

Drucker A.M., Rosen C.F., 2011. Drug-induced Photosensitivity: Culprit Drugs, Management and Prevention. Drug Safety. 34(10):821-837.

European Medicines Agency (EMA), 2009. ICH Guideline M3(R2) on non-clinical safety studies for the conduct of human clinical trials and marketing authorisation for pharmaceuticals. Step 5. Accessed online on: 22/11/2014; www.ema.europa.eu

Feliciano M., Vytla D., Medeiros K.A., Chambers J.J., 2010. The $GABA_A$ receptor as a target for photochromic molecules. Bioorg. & Med. Chem. 18, 7731-7738.

Ferguson J., 2006. Investigation of drug-induced photosensitivity in man. Abstracts/Toxicology. 226, 12-77.

Fomina N., Sankaranarayanan J., Almutairi A., 2012. Photochemical mechasnisms of light-triggered release from nanocarriers. Advanced Drug Delivery Reviews. 64, 1005-1020.

Glass B.D., Novak C, Brown M. E., 2004. The thermal and photostability of solid pharmaceuticals - A review. Journal of Thermal Analysis and Calorimetry.77: 1-24.

Gorner H., 2010. Photocyclization of 2,6-dichlorodiphenylamines in solution. Journal of Photochemistry and Photobiology A: Chemistry, 211, 1–6.

Gould J.W., Mercurio M.G., Elmets G.A., 1995. Cutaneous photosensitivity diseases induced by exogenous agents. Journal of the American Academy of Dermatology. 33 (4); 551-573.

Hung J.C., 2004. Inconsistencies and deficiencies in current official regulations concerning photolytic degradation of drugs. In Tonnesen H. H., 2004 Photostability of drugs and drug formulations. Second edition. London: CRC Press.

ICH (S10), 2013. ICH Harminised Tripartite Guideline Photosafety Evaluation of Pharmaceuticals S10. Accessed online on 22/11/2014; http://www.ich.org/fileadmin/Public_Web_Site/ICH_Products/Guidelines/Safety/S10/S10_Step_4.pdf

ICH, 1996. Guidance for industry Q1B photostability testing of new drug substances and products, Fed. Regist. 62, 27115-27112.

IOWA State University. Nature of Radiation. NDT Education Resource Centre; 2001 [Accessed: 01/03/2010]. Available from: http://www.ndt-ed.org/EducationResources/CommunityCollege/RadiationSafety/Graphics/elec_mag_field.gif

Kester T.C., Zhan Z., Bergstrom D.H., 2010. Quinine actinometry studies under two light sources specified by the ICH guideline on photostability testing. Seattle, Washington: 1998. Presented at the AAPS National Meeting. In Baertschi S.W., Alsante K.M., Tonnesen H.H. A critical assessment of the ICH guideline on photostability testing of new drug substances and products (Q1B): recommendation for revision. Journal of Pharmaceutical Sciences, 99 (7): 2934-2940.

Kristensen, 2004. Photostability of Prenteral products. In Tonnesen H. H., 2004 Photostability of drugs and drug formulations. Second edition. London: CRC Press.

Kuhn H. J., Braslavsky S.E., Schmidt R. Chemical Actinometry (IUPAC Technical Report). Pure Applied Chemistry, 2004; 76 (12): 2105-2146.

Maafi M, Brown RG. The kinetic model for AB(1 s. A Closed-form integration of the differential equation with a variable photokinetic factor. J. Photochem. Photobiol. A: Chem. 2007; 187: 319-324.

Moan J. Juzenas P., 2004. Biological effects of combinations of drugs and light. In Tonnesen H. H. Photostability of drugs and drug formulations. Second edition. London: CRC Press. p. 189-212.

Moore D.E., 2004. Photophysical and Photochemical Aspects of Drug Stability. In Tonnesen H. H. Photostability of drugs and drug formulations. Second edition. London: CRC Press.

Moore D.E., 2002. Drug-Induced Cutaneous Photosensitivity Incidence, Mechanism, Prevention and Management. Drug Safety.25 (5): 345-372.

Moore, D.E., 1990. Kinetic treatment of photochemical reactions. International Journal of Pharmaceutics. 63: R5-R7.

OECD/OCDE 432, 2004. OECD Guideline for Testing of Chemicals: In vitro 3T3 NRU phototoxicity test. Accessed online on 22/11/2014: http://ntp.niehs.nih.gov/iccvam/suppdocs/feddocs/oecd/oecdtg432-508.pdf

Piechocki JT, Thoma K. Pharmaceutical Photostability and Photostabilisation Technology. Informa Healthcare: London; 2010.

Piechocki J.T., Thoma K. Pharmaceutical photostability and photostabilisation technology. New York: Informa Healthcare; 2007. p. 79-86.

Pine, 1987. Organic chemistry. McGraw-Hill international editions. 5th edition; London.

Shamsipur M., Hemmateenejad B., Akhond M., Javidnia K., Miri R., 2003. A study of the photodegradation kinetics of nifedipine by multivariate curve resolution analysis. J. Pharm. and Biomed. Anal. 31, 1013-1019.

The European Agency for the Evaluation of Medicinal Products (EMEA), Evaluation of Medicines for Human Use, Committee for Proprietary Medicinal Products (CPMP), 2002. Note for guidance on photosafety testing. CPMP/SWP/398/01. Accessed online on 19/11/2014; http://www.emea.eu.int/

Thoma K., Klimek R., 1991. Photostabilization of drugs in dosage forms without protection from packaging. Int. J. Pharm. 67, 169-175.

Tomatsu I., Peng K., Kros A., 2011. Photoresponsive hydrogels for biomedical applications. Advanced Drug Delivery Reviews. 63, 1257-1266.

Tonnesen H. H., 2008. Photoreactivity of Drugs. In Solar Radiation and Human Health. Oslo: The Norwegian Academy of Science and Letters, 102-113.

Tonnesen H. H., 2004 Photostability of drugs and drug formulations. Second edition. London: CRC Press.

Tonnesen H.H. and Moore D.E., 1993. Photochemical degradation of components in drug formulations. Pharmaceutical Technology International. February, 1993: 27-33.

Wayne C. E., Wayne R. P., 1996. Oxford Chemistry Primers: Photochemistry. Oxford: Oxford University Press.

Wohl B.M., Engebersen J.F.J., 2012. Responsive layer-by-layer materials for drug delivery. Journal of Controlled Release. 158, 2-14.

Chapter II: Materials & Methods

1. Chemicals and solvents

The following chemicals and solvents were purchased for Sigma-Aldrich and used without further purification:

Nifedipine (NIF), dimethyl-1,4-dihydro-2,6-dimethyl-4-(2-nitrophenyl)-pyridine-3,5-dicarboxylate, ≥ 98% TLC grade.

Nisoldipine (*NIS*), ((±)3-isobutyl-5-methyl-1,4-dihydro-2,6-dimethyl-4-(2-nitrophenyl)-pyridine-3,5-dicarboxylate).

Montelukast sodium (Monte), 2-[1-(R)-[3-[2(*E*)-(7-chloroquinolin-2-yl)vinyl]phenyl]-3-[2-(1-hydroxy-1-methylethyl)phenyl]propyl-sulfanylmethyl] cyclopropyl] acetic acid sodium salt.

Fluvoxamine maleate, 2–{[(E)–{5–Methoxy–1–[4–(trifluoromethyl)phenyl]pentylidene} amino]oxy}ethanamine (*E–Fluvo*).

Riboflavin, 10-(2,3,4,5-tetrahydroxypentyl)-7,8-dimethylbenzo[*g*]pteridine-2,4(3*H*,10*H*)-dione), and

Tartrazine (TRZ) with a dye content of ≥ 85%.

Sunset yellow (SSY) with a dye content of 90%.

Quinoline Yellow (QY) with a dye content of 95%.

Spectroscopic grade ethanol, glacial acetic acid and Spectrophotometric grade acetonitrile. Double distilled water was also used as a solvent.

2. Instruments

2.1. The irradiation lamp

For irradiation experiments, a Ushio 1000 W xenon arc-lamp light source (Moore, 2004) housed in a housing shell model A6000 and powered by a power supply model LPS-1200 was used. This setting was equipped with water pipes connected to a water tap in order to prevent excessive warming of the lamp. The equipment was manufactured by Photon Technology International Corporation. The lamp housing was connected to a monochromator model 101 that allows the selection of specific irradiation wavelenghths since it consists of a special f/2.5 monochromator (Loewen and Popov, 1997) with a 1200 groove/mm and a 300nm blaze grating. The excitation beam was guided through an optical fibre joined to the top of the sample cuvette i.e. the excitation and analysis light beams were perpendicular to each other. This set up provided a complete shield to the sample from ambient light. The lamp was connected to a diode array spectrophotometer as shown in figure 1.

2.2. The spectrophotometer

A diode array spectrophotometer (Agilent 8453) was used to measure the various absorption spectra and kinetic profiles for the irradiation and calibration experiments (Agilent Technologies, 2008). This spectrophotometer was equipped with a sample holder that can fit a 1cm cell and which is linked to a temperature control Peltier system model Agilent 8453. Thus, the sample was always kept at 22°C and was also stirred continuously during the experiment. The Spectrophotometer was, in turn linked to a computer system

that recorded the various parameters measured. The whole apparatus set up is illustrated in figure 1.

A Radiant Power/Energy meter model 70260 was used to measure the radiant power of the incident excitation beams.

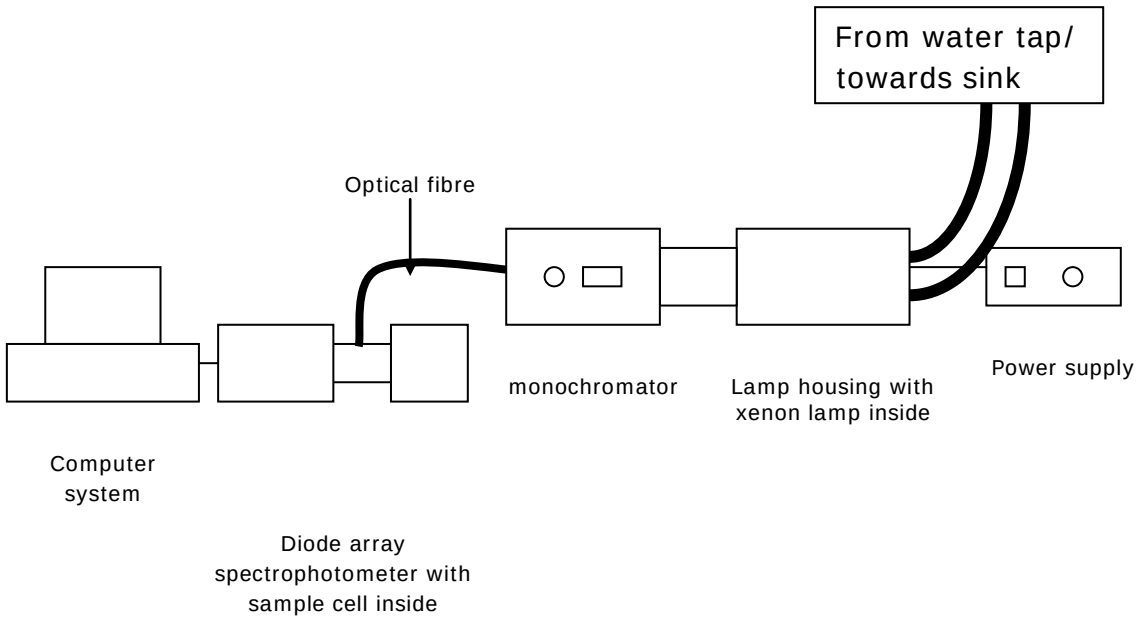

Figure 1: The irradiation and diode array spectrophotometer systems.

2.3. The Radiant Power/Energy meter

A Radiant Power/Energy meter model 70260 was used to measure the radiant power of the incident and/ or transmitted irradiation (Newport, 2000).

The reading cell of the Radiant Power/ Energy meter is positioned perpendicularly to the incident or transmitted light beam. The reading (in Watts) is then divided by the energy associated with a mole of photons for the selected irradiation wavelength ($E_{\lambda irr}$). In order to do this, $E_{\lambda irr}$ must first be calculated using the following equation:

$$E_{\lambda irr} = Nhc/\ \lambda_{irr} \qquad \text{eq.2.4}$$

Where,

N is the Avogadro number (*N* = 6.02214 x 10^{23} mol^{-1})

h is the Planck constant (*h* = 6.62608 x 10^{-34} J.s)

c is the velocity of light (c = 299792458 $m.s^{-1}$)

λ_{irr} is the irradiation wavelength (nm)

$E_{\lambda irr}$ is expressed in J mol^{-1} or J Einstein.

Thus, eq.2.4 can be written as:

$$\mathrm{E}_{\lambda \mathrm{irr}} = \frac{119626728.4}{\lambda} \qquad \text{eq.2.5}$$

Let P_w be the power measured at the irradiation wavelength on the radiant photometer (in mW or $mJ.s^{-1}$). The intensity of the beam or the radiant power (P) at this wavelength is determined by:

$$P = \frac{P_w}{E} \qquad \text{eq.2.6}$$

P is in Einstein s^{-1}.

To express the incident radiant power per volume units, eq.2.6 must be divided by the volume of the irradiated sample (V) as follows:

$$P = \frac{\lambda_{irr} P_w}{119626728.4\ .V} \qquad \text{eq. 2.7}$$

V is in ml whenever P_w is in mW.

P is in Einstein s^{-1} dm^{-3}

2.4. Software

Theoretical numerical integration was constructed based on the Fourth–order Runge-Kutta method using a home-made program.

2.5. High Performance Liquid Chromatography (HPLC)

The HPLC system consisted of a reversed–phase Jupiter 5µ C–18 300A Phenomenex (250 x 4.60 mm) column (Phenomenex, 2013) equipped with Perkin Elmer Series 200 pump, UV/Vis detector, vacuum degasser and a Perkin Elmer type Chromatography Interface 600 series Link linked to a computer system.

For montelukast, the mobile phase consisted of 15 % water adjusted to pH 3.18 with glacial acetic acid and 85 % methanol. A flow rate of 1 ml/min and an injection loop of 20 µl were used. The detector wavelength was set at 254 nm.

For fluvoxamine experiments, the mobile phase consisted of 60 % double distilled water adjusted to pH 4.8 with glacial acetic acid and 40 % acetonitrile. A flow rate of 1.5 ml/min and an injection loop of 20 ul were used. The detector wavelength was set at 245 nm.

3. Solutions preparation

It is worth mentioning that most solutions were prepared in ethanol to avoid hydrolysis reactions which may complicate the photodegradation mechanism.

A stock solution of NIF of 8.6 x 10^{-4} M in ethanol, maintained at low temperatures in the dark, was used to prepare fresh analytical solutions of lower concentrations for irradiation.

A 4.9 x 10^{-4} M stock solution of *NIS* in ethanol was prepared by weighing the solid.. The stock solution was diluted to prepare fresh analytical solutions (*ca*. 7.8 x 10^{-6} M) for irradiation experiments performed at various wavelengths.

A 7.4 x 10^{-4} M stock solution of Monte in ethanol was prepared by weighing the solid. The stock solution was diluted to prepare fresh analytical solutions (*ca.* 2 x 10^{-6} M) for all irradiation experiments performed at various wavelengths.

A 2.88 x 10^{-4} M stock solution of *Fluvo* in water was prepared by weighing the solid. The stock solution was diluted to prepare fresh analytical solutions (*ca.* 2 x 10^{-6} M) for analysis of irradiation experiments performed at various wavelengths.

A 1.20 x 10^{-4} M stock solution of *Ribo* in ethanol was prepared by weighing the solid. The flask was protected from light by aluminium foil wrapping and was kept in the fridge. The stock solution was diluted to prepare fresh analytical solutions (*ca.* 1.5 x 10^{-6} M) for analysis of irradiation experiments performed at various wavelengths.

Stock solutions of *TRZ* (9.14 x 10^{-5} M) and *QY* (6.17 x 10^{-5} M) were prepared in ethanol from their respective powders. All solutions flasks were wrapped in aluminium foil paper and kept in the fridge while not in use.

4. Solutions for actinometry studies

For actinometric studies, NIS and NIF ethanolic solutions of the same concentrations (*ca*. 7 x 10^{-6} M and 5.14 x 10^{-6} M, respectively) were exposed to specific wavelengths irradiations using a series of different intensities for each wavelength. The kinetic traces were observed at a unique irradiation wavelength of 390 nm and subsequently fitted with the Φ–order equations.

Monte solutions of the same concentrations (*ca.* 2 x 10^{-6} M) were exposed to specific irradiation wavelengths (258, 328, 345 and 360 nm) using a series of different intensities for each wavelength. The kinetic traces were observed at the irradiation wavelength and subsequently fitted with the Φ-order equations.

Fluvo solutions of the same concentrations (*ca.* 2.9 x 10^{-6} M) were exposed to specific irradiation wavelengths (260, 270, 280, 285 and 290 nm) using a series of different intensities for each wavelength. The kinetic traces were observed at the observation wavelength $l_{\lambda_{obs}}$= 245 nm and subsequently fitted with the Φ–order equations.

Ribo solutions of approximately the same concentrations (*ca.* 1.8 x 10^{-6} M) were exposed to specific irradiation wavelengths (420, 445, 460 and 480 nm) using a series of different intensities for each wavelength. The kinetic traces were observed at the observation wavelength $l_{\lambda_{obs}}$= 445 nm and subsequently fitted with the Φ–order equations

5. Irradiation under different monochromatic wavelengths

These experiments were conducted using monochromatic continuous irradiation. For each experiment, a different wavelength was used for irradiating a fresh solution of the drug sample being studied. A set of wavelengths spanning the whole absorption spectrum of the studied molecule were selected. All other variables such as sample concentration, sample volume and solvent were kept the same. The kinetic traces of the sample's absorbance versus time could then be observed at the desired wavelength.

6. Studies on the effect of initial drug concentrations

Monochromatic irradiation at the required wavelength was carried out with a different concentration of the drug solution being analysed in each experiment. All other variables were kept unchanged.

7. Studies on the effect of additives

Monochromatic irradiation was conducted on drug samples where specific amounts of dyes were added. For each experiment, a different concentration of the dye was used. The dye solution was considered as the blank solution before adding a known volume of the drug solution and then irradiating it.

References

Agilent Technologies, 2008. Agilent 8453 UV-visible Spectroscopy System. Accessed online from; http://www.agilent.com/cs/library/usermanuals/public/G1115-90042_OperatorManual.pdf

Loewen E.G., Popov E.,1997. Diffraction gratings and applications. Marcel Dekker, inc, New York

Moore D.E., 2004. Standardisation of kinetic studies of photodegradation reactions. In Tonnesen H. H., 2004 Photostability of drugs and drug formulations. Second edition. London: CRC Press.

Newport, 2000. Radiant power meter and probe. Accessed online from; http://assets.newport.com/webDocuments-EN/images/Radiant_Power_Meter_And_Probe_5408.PDF

Phenomenex, 2013. The ultimate guide to HPLC/UHPLC reversed phase selectivity. Accessed online from; https://www.phenomenex.com/Info/WebDocumentServe/reversedguide.pdf

Chapter III: A new methodology for the elaboration of photoreactions semi-empirical integrated rate-laws.

1. Introduction

The growing need for an accurate understanding, description and prediction of photoreactions kinetics (Tonnesen, 2004) in addition to the lack of specific photokinetic integrated rate-laws has prompted us to devise a new methodology to generate and validate semi-empirical integrated rate-laws for different photoreactions mechanisms. This method is based on synthetic data generated by Runge-Kutta numerical integration methods (NIM).

NIMs are mathematical techniques that deliver the values of a given integral at specific time intervals. NIMs generated results are very precise and are mostly useful when the mathematical integration of a differential equation is not possible (Kalagiratu et al., 2013; Crano and Guglielmetti , 1999). A number of NIM methods have been developed, with the Runge-Kutta (RK) method being one of the most widely used. The algorithm of RK can include a number of orders with the precision increasing with the order. In this study, two of the highest orders were employed namely, the fourth and fifth-order RK algorithm (RK-4 and -5), in order to generate synthetic RK data through a homemade programme. The method is based on feeding the programme with plausible photoreactions input values for the system parameters (e.g. initial concentration, absorption coefficient, quantum yield, radiant power and irradiation path-length), after which integral values at regular time intervals are generated for the photoreaction system.

The generated data represent calculated values of concentration versus time, whose kinetic trace can be calculated as total absorbance versus time. The traces obtained in this manner are known as synthetic data. These data can be considered as truthfully representing the kinetic behaviour of the photoreaction system. Varying the input data such as initial concentration, reactants' and products' absorption coefficients, quantum yields and radiant power values, allows the studying of the effect of experimental conditions on a selected system, or comparing the behaviour of different systems. This chapter is concerned with the detailed description of this methodology as used to develop semi-empirical integrated rate-laws for photoreactions.

2. Advantages of the photokinetic model elaboration method

The development of this methodology circumvents the hurdles encountered when attempting to integrate photoreactions rate-laws that cannot be mathematically integrated and offers a number of advantages;

(i) The RK calculated traces are defined with high precision and can, therefore, be considered as truthful representations of photoreactions kinetics for the set of input reaction parameters.

(ii) The validity of the proposed model cannot be confirmed through the sole use of some experimental data as hundreds of experiments would need to be conducted, rendering the model development task very time-consuming requiring several months/years for the development of a single

photoreaction mechanism model. Even if a good fitting is observed between experimental and theoretical model data, the validity of the model cannot be concluded with certitude against only a few experimental kinetic traces.

(iii) Since the RK results are precise and accurate, they represent a good tool to verify the precision of the proposed model equation.

(iv) It offers the possibility of performing quantitative evaluations based on quantitative parameters, such as the rate-constant and initial velocity.

(v) There is a scope for extending the applicability of a given developed model to all photoreactions obeying the same mechanism since the number of simulated cases can be infinite. Hence, if the model is found to accurately describe a vast number of plausible and varied simulation kinetic traces, this would indicate that it is valid for any system reacting via the photoreaction mechanism under study.

(vi) Because the RK approach is mathematically precise, it is possible to indentify any limitations related to the applicability of the proposed model.

3. The methodology

This methodology consists of two stages.

3.1. Stage 1: Development procedure

In order to accurately describe a photoreaction rate-law, a number of conditions must first be met;

(a) The reaction solution must be homogeneous, continuously stirred and kept at a constant temperature.

(b) The concentration of the short-lived excited-state species is assumed to be negligible.

(c) The irradiation is carried out using a monochromatic light beam of a known irradiation (λ_{irr}) wavelength.

(d) If the reaction medium is irradiated at λ_{irr} and the evolution of the photochemical reactions of reactant (A) is simultaneously monitored by spectrophotometry, then the data making up the experimental kinetic trace, should be collected at an observation wavelength, λ_{obs}.which may or may not be the same as λ_{irr}.

(e) Irradiation may be conducted at a wavelength (λ_{irr}) that is equal to that of an isosbestic point (λ_{isos}), i.e. $\lambda_{irr} = \lambda_{isos}$, which represents a wavelength where the absorbance remains unchanged throughout the photoreaction since the reactant and photoproduct(s) have the same absorption coefficient at that particular wavelength.

(f) If the irradiation is carried out at irradiations other than the isosbestic point, i.e. $\lambda_{irr} \neq \lambda_{isos}$, then it is labelled as a non-isosbestic irradiation.

A wide range of photoreactions kinetic traces are generated by feeding RK-4/5 NIMs with plausible photoreactions parameters. For each simulated reaction, a set of parameters are randomly but realistically attributed to represent plausible photoreaction parameters, namely;

(1) the absorption coefficients of the reactant and photoproduct(s).

(2) the reaction quantum yield(s) (Φ_{AB});

(3) the optical path-lengths of irradiation (l_{irr}) and observation (l_{obs});

(4) the radiant power ($P_{\lambda_{irr}}$);

(5) The simulation traces must encompass as wide a range of possible photoreactions scenarios, within a photoreaction type, as possible.

An initial template equation is provided for the description of the photokinetics of the simulation traces, based on previously developed or integrated equations for similar or close photoreaction mechanisms. As a starting point and working on the simplest unimolecular photoreaction mechanism whereby a reactant A phototransforms into a photoabsorbing product B, the template equation was defined based on an existing closed-form integrated photokinetic model where the photoproduct does not absorb the incident irradiation. Subsequently, the equation terms are then altered and or optimised in order to account for the effect of any additional contributing parameters in the reaction and so as to fit the simulated kinetic traces. The model is, then, fitted to synthetic kinetic traces and its limits of applicability are defined by testing its fitting against sets of synthetic traces where only one parameter is systematically changed at a time.

The proposed model is then subjected to a validation process to further confirm its accuracy and reliability in describing specific photoreaction systems.

3.2. Stage 2: Validation procedure

This step consists in generating further kinetic traces (over 100) for the studied photoreaction type following the same procedure used for the development stage. These traces must be different from the ones used in the latter stage and must also cover as wide a range of plausible scenarios as possible within the defined limits of applicability. The validity of the model is confirmed by further testing its ability to accurately describe all the kinetic traces. This is performed in two steps;

(i) The developed model equation is fitted to the NIM kinetic traces by varying the model rate-constant ($k_{AB,Mod.}^{\lambda_{irr}}$) value until the model and NIM traces fit perfectly. An accurate fitting must be obtained in all cases.

(ii) The theoretical value of the rate-constant ($k_{AB,Cal.}^{\lambda_{irr}}$), as calculated from the rate-constant analytical expression, is also compared to the fitted model rate-constant ($k_{AB,Mod.}^{\lambda_{irr}}$) value. The model is deemed accurate if these values differ by no more than 10% in each case.

(iii) The validity of the model equation may further be confirmed by calculating its derivative at the initial photoreaction time t_0, which represents the inititial velocity ($\upsilon_{0\ (Mod.)}^{\lambda_{irr}/\lambda_{obs}}$) and comparing this value to the theoretical initial velocity ($\upsilon_{0\ (Cal.)}^{\lambda_{irr}/\lambda_{obs}}$), calculated using the rate-law equation at t_0. Again, these values should differ by no more than 10% in each case.

4. Conclusion

This two-step photokinetic model development strategy based on theoretical numerical integration simulated cases represents a rather fast and efficient method for the development of integrated rate-laws where mathematical integration of the rate law is not possible. The next stage, however consists in the testing and applying the models to experimental data to further establish a model's validity and accuracy.

References

Crano J.C., Guglielmetti R.J., 1999. Topics in applied chemistry: organic photochromic and thermochromic compounds, vol 2. Pleneum Press; New York.

Kalogiratou Z., Monovasilis T., Psihoyios G., Simos T.E., 2013. Runge-Kutta type methods with special properties for the numerical integration of ordinary differential equations. Physics reports; 536, 75-146.

Tonnesen H. H., 2004 Photostability of drugs and drug formulations. Second edition. London: CRC Press.

Chapter IV: Modelling and elucidation of unimolecular, AB(1Φ), photoreactions kinetics - Application to nifedipine and nisoldipine photodegradation.

IV.I. AB(1Φ) model development and validation

1. Introduction

Unlike thermal reactions, photoreactions have met limited success in being ascribed integrated rate-laws that specifically describe their evolution. Thus far, there are no known general model equations that describe the various types of photoreactions, including the simplest systems involving two species (A and B) interchanging through one or two photochemical (Φ) and/or thermal (Δ) reaction steps. Thus, the NIM based methodology for photokinetic model development methodology was used to propose semi-empirical integrated rate-laws that are accurately describe the kinetics of different photoreactions types. In this chapter, the development of a photokinetic model for unimolecular, AB(1Φ), photoreactions using this methodology will be described. The model will then be applied to the photoreaction kinetics of two drugs, nifedipine (NIF) and nisoldipine (NIS) that photodegrade by unimolecular reaction.

2. AB(1Φ) photoreactions

A vast number of drugs have been shown to react with light leading to the formation of unwanted photoproducts. Amongst the simplest and most common photoreaction types triggered by light are reactions whereby a reactant (A) absorbs light irradiation and generates a photoproduct (B) (Scheme 1).

$$\mathbf{A} \xrightarrow{\phi_{AB}} \mathbf{B}$$

Scheme 1: Generic photoreaction system of the AB(1Φ) type.

However, despite their simple mechanistic nature and widespread applications, no integrated rate-law has been found for these photoreactions due to the presence of a time-dependent photokinetic factor in their rate-law equation. Therefore, the above NIM-based methodology was employed to determine the model equation that underlies these photoreactions types.

3.1. Stage 1: AB(1Φ) Model development

In an AB(1Φ) photoreaction system, the differential equation (DE) expressing the time variation of the concentrations of species A and B (C_A(t) and C_B(t), respectively); considering that the solution is subjected to a monochromatic and continuous irradiation, is homogeneously and continuously stirred, the concentration of the excited state is assumed negligible, the medium temperature is constant, and at the (non-isosbestic) irradiation wavelength (λ_{irr}) species A and B absorb different amounts of light (P), i.e., the absorption coefficients (ε) of the species are different and have non-zero values ($\varepsilon_A^{\lambda_{irr}} \neq \varepsilon_B^{\lambda_{irr}} \neq 0$); is

$$\frac{dC_A}{dt} = -k_{\lambda_{irr}} \times F_{\lambda irr}(t)\, C_A(t) \qquad \text{(eq.1)}$$

Where,

$$k_{\lambda_{irr}} = \Phi_{AB}^{\lambda irr} P_{\lambda irr} \varepsilon_A^{\lambda irr} l_{\lambda irr} \quad \text{(eq.2)}$$

Where, $\Phi_{AB}^{\lambda irr}$ is the quantum yield of the photoreaction, $l_{\lambda irr}$ is the optical path-length of the excitation light, $P_{\lambda irr}$ is the incident light intensity received by the sample, $\varepsilon_A^{\lambda irr}$ is the

extinction coefficient of A, and $F_{\lambda irr}(t)$ is the photokinetic factor at the irradiation wavelength (λ_{irr})

However, despite the simplicity of this reaction scheme, the rate-equation of this reaction type cannot be integrated in a closed-form due to the presence of a varying time – dependent factor in its analytical expression. This factor, known as the photokinetic factor ($F_{\lambda irr}(t)$), involves in its formula a power 10 terms (eq.3)

$$F_{\lambda \mathrm{irr}}(t) = \frac{1 - 10^{-A_{tot}^{\lambda_{irr}}(t)}}{A_{tot}^{\lambda_{irr}}(t)} \ (eq.3)$$

With $A_{tot}^{\lambda_{irr}}$ being the total absorbance of the reaction medium at the irradiation wavelength. $A_{tot}^{\lambda_{irr}}$ represents the sum of the individual absorbances of all the species present in the medium at time t (i.e. absorbances of species A and any generated products in the medium from the photodegradation of A and/or the thermal and photochemical transformations of the photoproducts of A). Therefore, $A_{tot}^{\lambda_{irr}}$ is time-dependent for non-isosbestic irradiations. For AB(1Φ) photoreactions, $A_{Tot}^{\lambda irr}$ is expressed as:

$$A_{Tot}^{\lambda irr}(t) = \varepsilon_A^{\lambda irr} C_A(t)\, l_{\lambda irr} + \varepsilon_B^{\lambda irr} C_B(t)\, l_{\lambda irr} \qquad \text{(eq.4)}$$

Where $\varepsilon_B^{\lambda irr}$is the extinction coefficient of the photoproduct B, and $[B]_t$is the concentration of B at time t.

Using equations 2 and 3, equation 1 can be re-written as:

$$\frac{dC_A}{dt} = -\Phi_{AB}^{\lambda irr} P_{\lambda irr} \varepsilon_A^{\lambda irr} l_{\lambda irr} C_A(t) \frac{1-10^{-A_{tot}^{\lambda_{irr}}(t)}}{A_{tot}^{\lambda_{irr}}(t)} \quad \text{(eq.5)}$$

The only exception where the photokinetic factor remains constant, and thus closed-form integration of the rate-law becomes possible, is when irradiation is performed at isosbestic wavelengths ($i.e.\lambda_{irr} = \lambda_{isos}$), and therefore the absorbance remains constant as A phototransforms into B since both species have the same absorption coefficient. The integrated rate-law equation for this case provided a solid platform for the development of the semi-empirical rate-law describing the non-isosbestic irradiations kinetics of AB(1Φ) reactions. Irradiations performed under non-isosbestic wavelengths where A and B have different absorbtivities, which represents the most common irradiation scenario due to the presence of only a few isosbestic points per photoreaction spectra (usually between one and four). The kinetic models describing these photoreaction types are hereby described.

(i) Irradiations performed at isosbestic wavelengths **($\boldsymbol{\lambda_{irr} = \lambda_{isos} \neq \lambda_{obs}}$ and $\boldsymbol{\varepsilon_A^{\lambda_{irr}} = \varepsilon_B^{\lambda_{isos}} = constant}$)**

In the case where the monochromatic irradiation of the solution is realised at an isosbetic point, $\lambda_{irr} = \lambda_{isos}$, the general integrated rate–law of AB(1Φ) reaction systems has been obtained through closed–form integration (Maafi and Brown, 2005a), as

$$A_{tot}^{\lambda_{isos}/\lambda_{obs}}(t) = A_{tot}^{\lambda_{isos}/\lambda_{obs}}(\infty) + \left(A_{tot}^{\lambda_{isos}/\lambda_{obs}}(0) - A_{tot}^{\lambda_{isos}/\lambda_{obs}}(\infty)\right) \times e^{-k_{AB}^{\lambda_{isos}} \times t} \quad \text{(eq.6)}$$

or;

$$C_A(t) = C_A(\infty) + \left(C_A(0) - C_A(\infty)\right) \times e^{-k_{AB}^{\lambda_{isos}} \times t} \qquad (eq.7)$$

$$C_B(t) = C_B(\infty) - C_B(\infty) \times e^{-k_{AB}^{\lambda_{isos}} \times t} \qquad (eq.8)$$

with $C_A(\infty)$ and $C_B(\infty)$ being the concentrations of the species at the end of the reaction and $k_{AB}^{\lambda_{isos}}$, the overall rate–constant of the reaction performed at an isosbetic irradiation.

The monoexponential form of the equation indicates that isosbestic irradiations induce first–order kinetics. This is primarily due to the fact that when $\lambda_{irr} = \lambda_{isos}$, the photokinetic factor does not vary with reaction time (as the medium absorbance at the irradiation wavelength, λ_{isos}, is time–independent).

$k_{AB}^{\lambda_{isos}}$, has the analytical expression;

$$k_{AB}^{\lambda_{isos}} = \Phi_{A\to B}^{\lambda_{isos}} \times \varepsilon_A^{\lambda_{isos}} \times l_{\lambda_{isos}} \times P_{\lambda_{isos}} \times F_{\infty}^{\lambda_{isos}} \qquad (eq.9)$$

With,

$$F_{\infty}^{\lambda_{isos}} = \frac{1 - 10^{-\left(A_{tot}^{\lambda_{isos}/\lambda_{isos}}(\infty) \times \frac{l_{\lambda_{isos}}}{l_{\lambda_{obs}}}\right)}}{A_{tot}^{\lambda_{isos}/\lambda_{isos}}(\infty) \times \frac{l_{\lambda_{isos}}}{l_{\lambda_{obs}}}} \qquad (eq.10)$$

The reaction initial velocity ($v_0^{\lambda_{isos}}$) can then be determined from the derivative of eq.7 at t_0 as (eq.11);

$$v_{0.Mod}^{\lambda_{isos}} = -k_{AB}^{\lambda_{isos}} \times \big(A(0) - A(\infty)\big) \qquad (eq.11)$$

The value of the initial velocity can be obtained graphically (the tangeant of the initial stages of the kinetic trace) and compared to its theoretical expression (eq.11).

$$v_{0.Cal}^{\lambda_{isos}/\lambda_{obs}} = -(\varepsilon_A^{\lambda_{obs}} - \varepsilon_B^{\lambda_{obs}}) \times l_{\lambda_{obs}} \times \Phi_{A\to B}^{\lambda_{isos}} \times C_A(0) \times \varepsilon_A^{\lambda_{isos}} \times l_{\lambda_{isos}} \times P_{\lambda_{isos}} \times F_{\lambda_{isos}} \quad (eq.12)$$

Despite the simple kinetic laws describing AB(1Φ) kinetic data for isosbestic irradiations, these irradiation conditions are not commonly encountered since only a few isosbestic points are usually present on the electronic spectra. It is, therefore, worth considering the most predominant non-isosbestic irradiation case.

(ii) Irradiations performed under non-isosbestic wavelengths where only A absorbs ($\boldsymbol{\varepsilon_A^{\lambda_{irr}} \neq 0, \varepsilon_B^{\lambda_{irr}} = 0}$ $\boldsymbol{and}$ $\boldsymbol{\lambda_{irr} \neq \lambda_{isos}}$)

Under non-isosbestic irradiation conditions, the photokinetic factor changes with time and integration of eq.1 cannot be achieved through closed-form except for one specific AB(1Φ) photoreaction case where irradiation is performed at a non-isosbestic monochromatic irradiation wavelength where only the initial species A absorbs the incident radiation *(i.e.* $\varepsilon_A^{\lambda_{irr}} \neq 0, \varepsilon_B^{\lambda_{irr}} = 0 \; and \; \lambda_{irr} \neq \lambda_{isos}$*)* (Maafi and Brown, 2007).

The closed-form integration of the differential equation of this type of photoreaction could be achieved in the following manner (Maafi and Brown, 2007):

Since only A absorbs, the total medium absorbance eq.4 can be simplified and expressed by a single term:

$$A_{Tot}^{\lambda irr}(t) = \varepsilon_A^{\lambda irr} C_A(t)\, l_{\lambda irr} \qquad \text{eq.13}$$

Therefore, substitution of eq.13 into eq.5 yields the following equation:

$$\frac{dC_A}{dt} = -\Phi_{AB}^{\lambda irr} P_{\lambda_{irr}} (1 - 10^{-A_{tot}^{\lambda_{irr}}(t)}) \qquad \text{eq.14}$$

Since $C_A(t) = \frac{A_{Tot}^{\lambda irr}(t)}{\varepsilon_A^{\lambda irr}\, l_{\lambda irr}}$, eq.14 can be re-arranged as:

$$\frac{dA_{tot}^{\lambda_{irr}}(t)}{1-10^{-A_{tot}^{\lambda_{irr}}(t)}} = (-\Phi_{AB}^{\lambda irr} P_{\lambda_{irr}} \varepsilon_A^{\lambda irr}\, l_{\lambda irr})\, dt \qquad \text{eq.15}$$

The differential equation of eq.15 can be solved by variable separation as:

$$\int \frac{dA_{tot}^{\lambda_{irr}}(t)}{1-10^{-A_{tot}^{\lambda_{irr}}(t)}} = \int (-\Phi_{AB}^{\lambda irr} P_{\lambda_{irr}} \varepsilon_A^{\lambda irr}\, l_{\lambda irr})\, dt \qquad \text{eq.16}$$

This would yield:

$$A_{tot}^{\lambda_{irr}}(t) = log[1 + \left(10^{A_A^{\lambda_{irr}}(0)} - 1\right) e^{-(\Phi_{AB}^{\lambda irr} P_{\lambda_{irr}} \varepsilon_A^{\lambda irr} l_{\lambda irr} ln(10)).t}] \quad \text{eq.17}$$

The integrated rate-law equation expressing the temporal variation of the absorbance of species A, when the medium is irradiated at λ_{irr} and the absorbance recorded at a different observation wavelength (λ_{obs} which may or may not be equal to λ_{irr}), is derived from eq.17 as:

$$A_A^{\lambda_{irr}/\lambda_{obs}}(t) = \frac{l_{\lambda_{obs}}}{l_{\lambda_{irr}}} \times Log\left[1 + \left(10^{-\left(A_{tot}^{\lambda_{irr}/\lambda_{irr}}(0) \times \frac{l_{\lambda_{irr}}}{l_{\lambda_{obs}}}\right)} - 1\right) \times e^{-k_{AB}^{\lambda_{irr}} \times t}\right] \quad \text{eq.18}$$

with $A_A^{\lambda_{irr}/\lambda_{irr}}(0)\ and\ A_A^{\lambda_{irr}/\lambda_{obs}}(t)$ being the absorbances of A at the initial and at a given time t, respectively. The former, $A_A^{\lambda_{irr}/\lambda_{irr}}(0)$, is recorded at the same wavelength of irradiation. $l_{\lambda_{irr}}$ and $l_{\lambda_{obs}}$ are the optical path-lengths of the irradiation and monitoring light beams in the sample, respectively. The latter parameters may or may not be equal (depending on the experimental set up as shown in scheme 2).

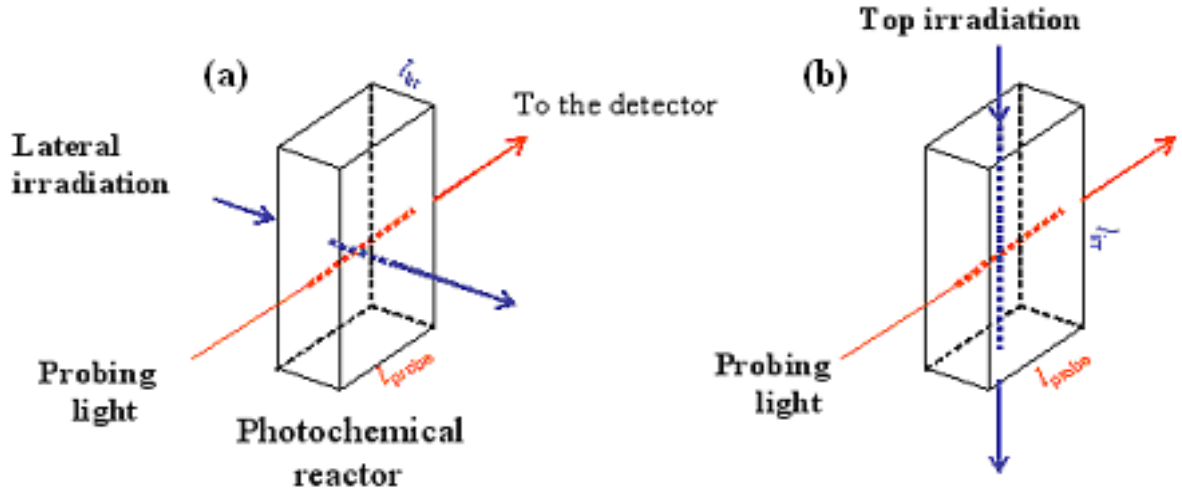

Scheme 2: The sample cuvettes and the possible paths of irradiation and probing lights. (Maafi and Brown, 2005a)

$k_{AB}^{\lambda_{irr}}$ is the overall photoreaction rate-constant, which is expressed as:

$$k_{AB}^{\lambda_{irr}} = \Phi_{AB}^{\lambda_{irr}} \times \varepsilon_{A}^{\lambda_{irr}} \times l_{\lambda_{irr}} \times P_{\lambda_{irr}} \times Ln(10) \qquad \text{(eq.19)}$$

With $\Phi_{AB}^{\lambda_{irr}}$ being the quantum yield of the photoreaction at the irradiation wavelength, $\varepsilon_{A}^{\lambda_{irr}}$ the absorption coefficient of species A at λ_{irr}, and $P_{\lambda_{irr}}$ the radiant power of the light beam at λ_{irr}.

However, in most cases, A is not the only absorbing species in the medium. Therefore, the expression of the total absorbance must encompass not only the absorbance of A but also those of the other concurrent species (B,C,...etc)

(iii) Non-isosbestic irradiations where both species absorb ($\boldsymbol{\lambda_{irr} \neq \lambda_{isos}}$, $\boldsymbol{\varepsilon_{A}^{\lambda_{irr}} \neq 0}$ ***and*** $\boldsymbol{\varepsilon_{B}^{\lambda_{irr}} \neq 0}$)

In most AB(1Φ) photoreactions, both species A and B absorb at the irradiation wavelength. This means that the total absorbance, used in the formula of the photokinetic factor, depends on both the absorbances of A and B, i.e.

$$A_{tot}^{\lambda_{irr}/\lambda_{obs}} = A_{A}^{\lambda_{irr}/\lambda_{obs}} + A_{B}^{\lambda_{irr}/\lambda_{obs}} \quad \text{(eq.20)}$$

The total absorbance of the medium's species over time is not constant as varying amounts of reactant and products, which have different absorbtivities, are present at different time points of the photoreaction. Since the total absorbance of the medium changes over time, the photokinetic factor is not constant through the reaction progress. As a consequence, the corresponding differential equation (eq.5) cannot be integrated in a closed-form. Furthermore, the equations corresponding to the previous, less common, irradiation scenarios (eqs.6 and 18) do not fit the data corresponding to this case. So far, no mathematical model equation (i.e. the integrated rate-law) has ever been proposed to describe the kinetics of these photoreactions. (Glass et al., 2004; Mauser and Gauglitz, 1998)

Therefore, in order to circumvent this situation, the new methodology for semi-empirical photokinetic model elaboration was adopted. Analysis of the kinetics of the non-isosbestic irradiation of an AB(1Φ) system where only A absorbs suggests that photoreactions of this kind but where both A and B absorb the irradiation wavelength might follow a similar general LOG-EXP mathematical model (eq.18) but where the absorbance of B is also taken into consideration. Based on this assumption and RK-4-generated synthetic data, a semi-

empirical model for AB(1Φ) photoreactions irradiated at non-isosbestic wavelengths where both species A and B absorb could be defined and optimised as:

$$A_{tot}^{\lambda_{irr}/\lambda_{obs}}(t) = A_{tot}^{\lambda_{irr}/\lambda_{obs}}(\infty) + \frac{A_A^{\lambda_{irr}/\lambda_{obs}}(0) - A_{tot}^{\lambda_{irr}/\lambda_{obs}}(\infty)}{A_A^{\lambda_{irr}/\lambda_{irr}}(0) - A_{tot}^{\lambda_{irr}/\lambda_{irr}}(\infty)} \times \frac{l_{\lambda_{obs}}}{l_{\lambda_{irr}}} Log\left[1 + \left(10^{\left[\left(A_A^{\lambda_{irr}/\lambda_{irr}}(0) - A_{tot}^{\lambda_{irr}/\lambda_{irr}}(\infty)\right) \times \frac{l_{\lambda_{irr}}}{l_{\lambda_{obs}}}\right]} - 1\right) \times e^{-k_{AB}^{\lambda_{irr}} \times t}\right] \quad (eq.21)$$

The coefficients $A_{tot}^{\lambda_{irr}/\lambda_{obs}}(t)$, $A_{tot}^{\lambda_{irr}/\lambda_{obs}}(0)$, $A_{tot}^{\lambda_{irr}/\lambda_{obs}}(\infty)$, $A_{tot}^{\lambda_{irr}/\lambda_{irr}}(0)$ and $A_{tot}^{\lambda_{irr}/\lambda_{irr}}(\infty)$ in Eq.21 are the measured (along $l_{\lambda_{obs}}$) total absorbances of the medium respectively recorded at reaction time t, at the initial time (t = 0) and either at the end of the reaction, where t = ∞. The reaction medium is monitored while irradiated at a given irradiation wavelength and simultaneously monitored at either a different observation wavelength ($\lambda_{irr}/\lambda_{obs}$) or at the same wavelength ($\lambda_{irr}/\lambda_{irr}$). It is assumed that the reaction is quantitative and proceeds without by–products.

The corresponding concentration profiles equations are;

$$C_A\,(t) = C_A\,(\infty) + \frac{Log\left[1 + \left(10^{\left[\left(\varepsilon_A^{\lambda_{irr}} - \varepsilon_B^{\lambda_{irr}}\right) \times \left(C_A\,(0) - C_A\,(\infty)\right) \times l_{\lambda_{irr}}\right]} - 1\right) \times e^{-k_{AB}^{\lambda_{irr}} \times t}\right]}{\left(\varepsilon_A^{\lambda_{irr}} - \varepsilon_B^{\lambda_{irr}}\right) \times l_{\lambda_{irr}}} \quad (eq.21a)$$

$$C_B\ (t) = C_B\ (\infty) \times \left(1 - \frac{Log\left[1 + \left(10^{\left[\left(\varepsilon_A^{\lambda_{irr}} - \varepsilon_B^{\lambda_{irr}}\right) \times \left(C_A\ (0) - C_A\ (\infty)\right) \times l_{\lambda_{irr}}\right]} - 1\right) \times e^{-k_{AB}^{\lambda_{irr}} \times t}\right]}{\left(\varepsilon_A^{\lambda_{irr}} - \varepsilon_B^{\lambda_{irr}}\right) \times \left(C_A\ (0) - C_A\ (\infty)\right) \times l_{\lambda_{irr}}} \right) \qquad (eq.21b)$$

The model was tested and developed by fitting AB(1Φ) synthetic kinetic traces generated by feeding RK-4 NIM calculations with various sets of photoreactions parameters. Equation 21 was found to fit over 100 generated RK-4 synthetic kinetic traces. Nevertheless, at this stage, it was only possible to determine the value of $k_{\cdot}^{\lambda_{irr}}$ as a fitting parameter of model eq.21 to the generated traces without having defined its analytical expression and its limits of applicability.

Thus, the next stage of the development procedure was to determine an analytical expression for $k_{AB}^{\lambda_{irr}}$ and define the limits of applicability of this expression and hence the model. The rate-law (eq.5) formed the basis for deriving the rate-constant expression, which was evaluated against previous and additional RK-4 synthetic traces to be defined as;

$$k_{AB}^{\lambda_{irr}} = \Phi_{AB}^{\lambda_{irr}} \times \varepsilon_A^{\lambda_{irr}} \times l_{\lambda_{irr}} \times P_{\lambda_{irr}} \times F_{\lambda_{irr}}^{B} = \beta_{\lambda_{irr}} \times P_{\lambda_{irr}} \qquad \text{(eq. 22)}$$

where $F_{\lambda_{irr}}^{B}$ is the photokinetic factor calculated using the absorbance of the photoproduct, $A_B^{\lambda_{irr}/\lambda_{irr}}(\infty)$, measured at the irradiation wavelength and at the end of the reaction ($i.e. A_{tot}^{\lambda_{irr}} = A_B^{\lambda_{irr}/\lambda_{irr}}(\infty)$ in eq.3).

By comparing the rate-constant values obtained from model fitting ($k_{AB,Mod.}^{\lambda_{irr}}$) and those determined using the rate-constant equation (eq.22) ($k_{AB,Cal.}^{\lambda_{irr}}$) for each kinetic trace, the limits of applicability of eq.21 could be defined. Different sets of kinetic traces with the same photoreactions parameters except for one variable in each set were also generated with the variable being given different values spanning a wide range of eventualities. The condition imposed on the system for applicability of eqs. 21 and 22 was that $k_{AB,Mod.}^{\lambda_{irr}}$ and $k_{AB,Cal.}^{\lambda_{irr}}$ values should differ by no more than 10%.

It was found that the rate-constant is defined by eq.22 whenever the value of $F_{\lambda_{irr}}^{B}$ was equal to or exceeded 1.2. This corresponds to a photoproduct absorbance value equal to or below 0.64 at λ_{irr} across $l_{\lambda_{irr}}$ at the end of the photoreaction. These simulation experiments also revealed that when $F_{\lambda_{irr}}^{B}$<1.2, model eq.21 still fits the corresponding traces, yet the k value determined by fitting will only represent a fitting parameter and cannot be considered as the true rate-constant of the reaction since in these cases, eq.22 no longer defines k. Nonetheless, in such cases, this parameter can still be used to compare the effect of a variable on photodegradation rate for experiments within the same settings but cannot be used for different experiments or for the determination of photoreactions attributes. Furthermore, since the absorbance of species B is given by

$$A_B^{\lambda_{irr}/\lambda_{irr}}(\infty) = \varepsilon_B^{\lambda_{irr}} \times l_{\lambda_{irr}} \times C_0 \qquad \text{eq.23}$$

then, this limitation can be circumvented by either reducing the irradiation optical path-length ($l_{\lambda_{irr}}$) or the initial concentration (C_0) in such proportions to bring $A_B^{\lambda_{irr}/\lambda_{irr}}(\infty) \leq 0.64$.

3.2. Stage 2: AB(1Φ) model validation

In this study, the most extensive testing of eq.21 with synthetic RK-4 data has been performed. Validation was performed using over 150 new synthetic kinetic traces different from the ones used for the development stage, yet still within the limits of the model's applicability. This was achieved in two steps.

First, the kinetic traces were fitted with model eq.21 in order to establish the validity of the model to fit more AB(1Φ) kinetic traces. In this respect, the equation showed a good fitting in all RK-4 cases. This indicates that the overall mathematical formulation of the model (Log-Exp) is suitable to describe AB(1Φ) kinetic traces. Some examples of the input parameters used to feed RK-4 calculations to generate synthetic kinetic traces for AB(1Φ) photoreactions for model development purposes are presented in table 1. The corresponding synthetic kinetic traces together with the model fitted traces are shown in figure 1**.**

Table 1: Sets of data used to generate some AB(1Φ) kinetic traces using fourth order Runge-Kutta method and to calculate kinetic traces using equations 21 and 22; together with the rate constants and the % variance between $k_{AB,Mod.}^{\lambda_{irr}}$ and $k_{AB,RK.}^{\lambda_{irr}}$.

	series 1	series 2	series 3	series 4	series 5	series 6	series 7
ΦAB	0.04	0.14	0.14	0.54	0.54	0.74	0.94
$\varepsilon_A^{\lambda_{irr}}$	25046	5046	15046	9046	25046	3046	5046
$\varepsilon_B^{\lambda_{irr}}$	13666	13666	3666	33666	10666	5666	3666
Co (M)	1.50E-05	1.50E-05	1.50E-05	5.00E-06	2.00E-05	1.50E-05	1.50E-05
P (Einstein. $S^{-1}.cm^{-3}$)	3.00E-06	3.00E-06	3.00E-06	3.00E-06	3.00E-06	3.00E-06	3.00E-06
***lirr* (cm)**	2.5	2.5	2.5	2.5	2.5	2.5	2.5
***lobs* (cm)**	1	1	1	1	1	1	1
$F_{\lambda_{irr}}^B$	1.35E+00	1.35E+00	1.97E+00	1.47E+00	1.33E+00	1.82E+00	1.97E+00
$k_{AB,RK.}^{\lambda_{irr}}$	0.0109	6.80E-03	0.0315	0.054	0.1465	0.0308	0.07
$k_{AB,Mod.}^{\lambda_{irr}}$	1.02E-02	7.16E-03	3.12E-02	5.40E-02	1.34E-01	3.08E-02	7.02E-02
% error	7.319268	5.052573	1.020682	0.041575	8.924844	0.052267	0.305368

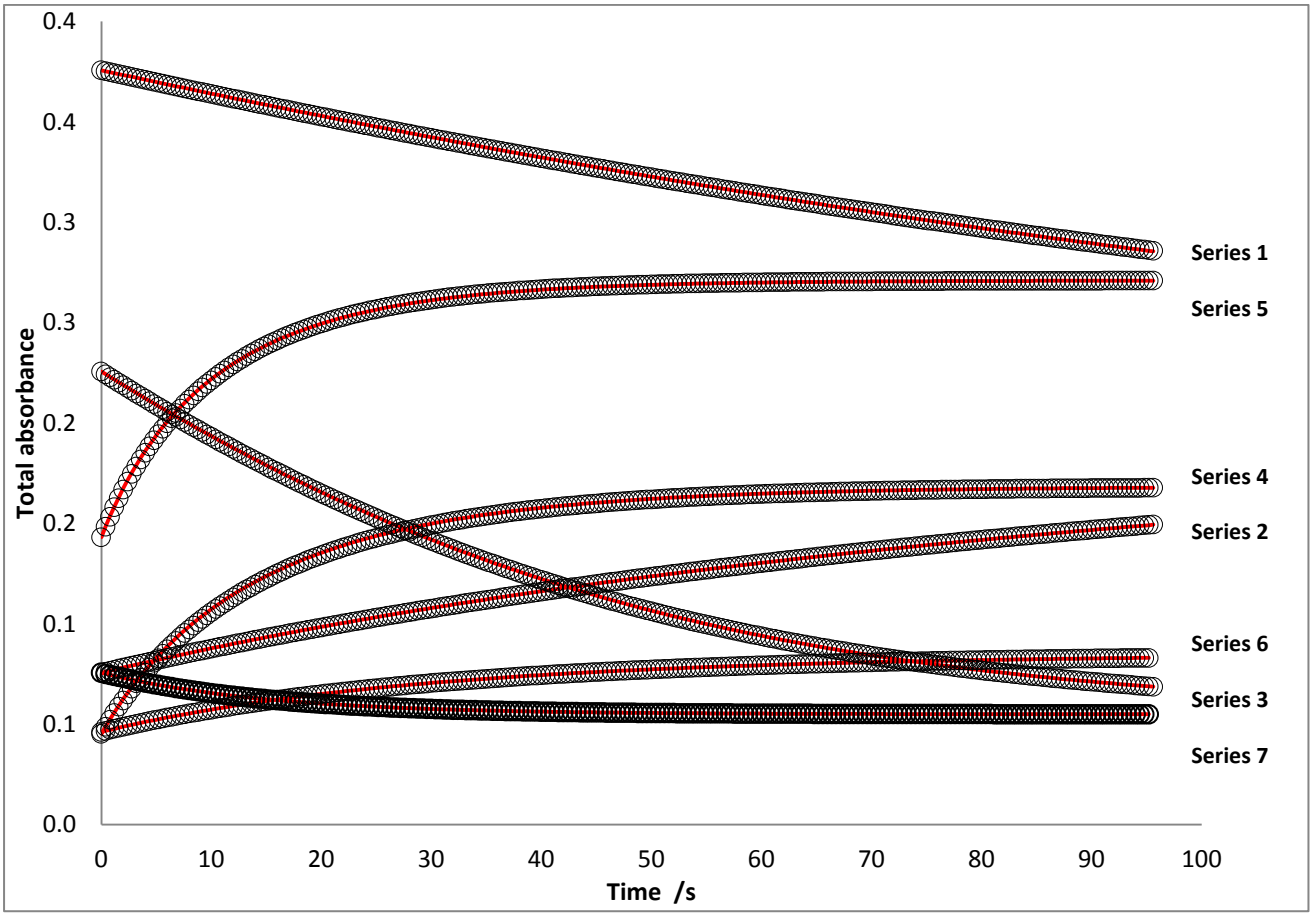

Figure 1: Sample Runge-Kutta generated traces and the corresponding model traces

The following validation step consisted in a quantitative comparison of the rate-constant values obtained from model fitting ($k_{AB,Mod.}^{\lambda_{irr}}$) and those determined using the rate-constant equation (eq.22) ($k_{AB,Cal.}^{\lambda_{irr}}$) for each simulation scenario. The model was deemed accurate if there was a good correlation between the aforementioned rate constants with a percentage error less than 10%.

Figures 2a and 2b are illustrations for the correlation of rate constants, plotted in two different graphs so the values of all $k_{AB,Mod.}^{\lambda_{irr}}$ and $k_{AB,Cal.}^{\lambda_{irr}}$could be well represented on the graphical scales due to the wide range of values. Furthermore, the condition that $F_{\lambda_{irr}}^{B} \geq 1.2$ was respected for each simulation case

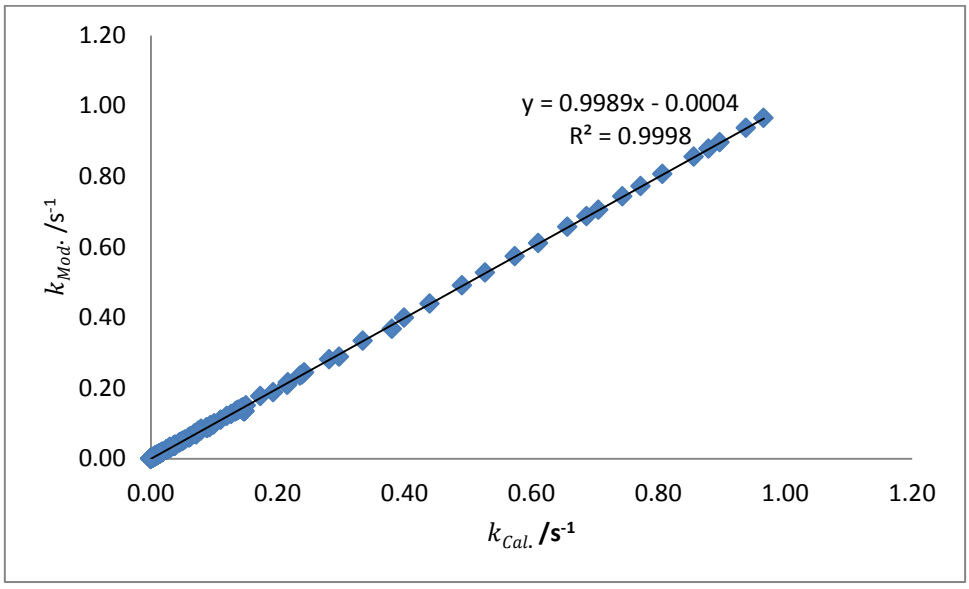

Figure 2a: Linear correlation between $k_{AB,Mod.}^{\lambda_{irr}}$ and $k_{AB,Cal.}^{\lambda_{irr}}$ for low rate constants ranging from 1.93 x 10^{-6} to 9.66 x 10^{-1} s^{-1}.

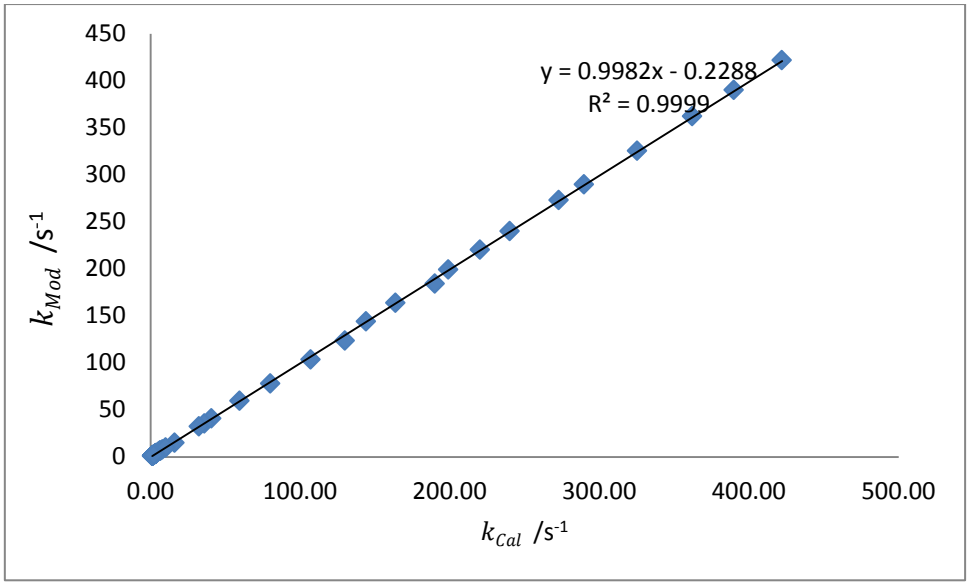

Figure 2b: Linear correlation between $k_{AB,Mod.}^{\lambda_{irr}}$ and $k_{AB,Cal.}^{\lambda_{irr}}$ for relatively high rate constants ranging from 1.05 to 4.22 x 10^2 s^{-1}.

As shown in figures 2a and b, the squared correlation coefficient (r^2) values are very close to unity indicating that there is a very good agreement between $k_{AB,Mod.}^{\lambda_{irr}}$ and $k_{AB,Cal.}^{\lambda_{irr}}$ for all the selected traces in this study with less than 10% error between the two sets of values. These results together with the good fitting of the traces are all indicative of the reliability and accuracy of the model to describe the photoreaction kinetics of AB(1Φ) systems at any monochromatic irradiation and observation wavelengths.

3.3. A new method for the study of AB(1Φ) photoreactions kinetics

In order to use the semi-empirical model to describe experimental or synthetic AB(1Φ) photoreaction kinetic data following monochromatic irradiation, a simple systematic approach should be followed. First, the kinetic traces at the observed wavelength following irradiation are fitted with eq. 6 for isosbestic irradiations or eq. 21 for non-isosbestic

irradiations. This is achieved by varying the rate-constant value of the model ($k_{AB,Mod.}^{\lambda_{irr}}$) equation until an accurate fitting is achieved and the rate-constant value is thus determined.

$\varepsilon_A^{\lambda_{irr}}$ should then be determined from the initial absorbance spectrum at $t_{(0)}$ using the Beer Lambert law as;

$$\varepsilon_A^{\lambda_{irr}} = \frac{A_A^{\lambda_{irr}/\lambda_{irr}}(0)}{l_{\lambda_{obs}} \times C_0} \ (eq.24)$$

The value of $F_{\lambda_{irr}}^B$ can be calculated using the total absorbance of the photoproduct at the irradiation wavelength at $t = \infty$, using eq.23. The photoreaction quantum yield can then be determined by rearranging the rate-constant equation (eq.22) as;

$$\Phi_{AB}^{\lambda_{irr}} = \frac{k_A^{\lambda_{irr}}}{\varepsilon_A^{\lambda_{irr}} \times l_{\lambda_{irr}} \times P_{\lambda_{irr}} \times F_{\lambda_{irr}}^B} \ (eq.25)$$

4. Discussion

The good fittings and correlations obtained for over 250 AB(1Φ) synthetic kinetic traces are indicative of not only the suitability of the model to describe unimolecular photoreactions kinetics but also of the reliability of the novel methodology for the development of semi-empirical integrated rate-laws and rate-constants analytical expressions.

The expressions of these models clearly reflect the dependence of unimolecular photoreactions on reaction quantum yield, the radiant power of the light source, the sample volume and irradiation path-length as well as the PP absorbance for cases where both A and B absorb at the wavelength of irradiation. The dependence of k on all of these parameters makes it unsuitable for the comparison of different photoreactions rates between different studies and laboratories, predominantly due to the difficulty in replicating the same radiant power conditions. On the other hand, the quantum yield is indicative of the intrinsic photoreactivity of a particular molecule in a given medium, and can be compared between different studies, although it is not informative of the rate of photoreactions.

Furthermore, besides allowing the determination of a photoreaction's rate-constant, the semi-empirical integrated rate-law model also allows the determination of quantum yields from the rate-constant equation without the need for prior separation of the medium's species or additional experiments.

Comparison of the expressions of thermal zero, first and even second order kinetic models with model eq.21 clearly suggests that photoreactions are ill-described by the former models and obey a different kinetic order that is more accurately and specifically described by the latter equations. This type of photoreactions can, thus, be attributed a new kinetic order termed the **Φ-order** kinetics.

IV.II. Application of the AB(1Φ) model for the study of nifedipine and nisoldipine photodegradation kinetics

1. Introduction

A large number of photochemical systems undergo unimolecular photo-transformations. Amongst these, many drugs have been shown to photo-decompose with light in one photochemical step yielding a single product via the AB(1Φ), unimolecular, photoreaction mechanism. Some members of the 1,4-dihydtopyridine calcium channel blockers antihypertensives have been found to be particularly sensitive to light and to undergo relatively rapid unimolecular photoreactions following absorption of UV/Vis irradiation. The most photolabile drug entities of the dihyropyridines, namely, nifedipine (Nif) and nisoldipine (Nis), have been selected as experimental drug candidates for the description and quantitative evaluation of their kinetics using the Φ-order kinetic model for AB(1Φ) photoreactions.

Both Nif and Nis are used in the treatment of hypertension. Chemicaly, they are characterised by the presence of a nitro group at the *ortho* position of the phenyl ring that renders them particularly prone to photolability. Their photodegradation mechanism (Scheme 1) involves an oxidation of the dihyropyridine moiety to a pyridine ring and the reduction of the aromatic nitro part to a nitroso group (Marinkovic et al., 2000). This change in chemical structure results in a significant loss of therapeutic efficacy (Onoue et al., 2008; Pizarro-Urzua and Nunez-Vergara, 2005; De Vries and Van Henegouwen, 1998, Alvarez-Lueje et al., 1998).

As a consequence, a number of studies have been devoted to the study of the photodegradation of Nif and Nis under various conditions (Piechocki and Thoma, 2010; Tonnesen, 2004; Albini and Fasani, 1998; Pietta et al, 1981; Fasani et al., 2006; Gorner, Mielkarek et al., 2005; Huang et al., 1996; Marinkovic et al., 2000).

Kinetic studies employing separation techniques were largely preferred because they allow monitoring of the photoreactant concentration throughout the photoreaction. Conversely, spectroscopic methods, such as spectrophotometry, were less frequently used to study photoreactions kinetics due to the overlap between the spectra of the initial species and its photoproduct.

Furthermore, treatment of the kinetic data was generally achieved using thermal kinetics equations of the zero- and/or first-order (Piechocki and Thoma, 2010; Tonnesen, 2004;

Albini and Fasani, 1998; Kawabe et al, 2008; Onoue et al., 2008; Pizarro-Urzua and Nunez-Vergara, 2005; De Vries and Van Henegouwen, 1998; Pietta et al, 1981; Fasani et al., 2006 1-9, Shamsipur et al., 2003). A fewer number of studies proposed approaches to rationalise the photodegradation kinetics with other models (Matsuda et al, 1989; Mielcarek et al., 2005). However, the lack of coherence and uniformity in the kinetic treatment of photoreactions has resulted in many controversies and inconsistencies in the interpretation, quantification and attribution of kinetic orders to the photodecomposition rates of these drugs.

The photoconversion of Nis in methanolic solutions, for instance, monitored using UV spectrophotometry and reversed-phase high performance chromatography RP–HPLC, was attributed a first–order kinetics (Mielkarek et al., 2005), whereas another similar spectrophotometric study in ethanol described Nis kinetics by an apparent first–order up to a concentration of $3x10^{-5}$ M and the zero–order for concentrations higher than $2x10^{-4}$ M (Huang et al., 1996). In the solid state, Nis photodegradation, as monitored by HPLC, was ascribed a zero–order kinetics under daylight but the reaction order could not be clearly identified under UV illumination. In the latter case, Nis degradation showed a more complicated kinetic behaviour whereby the decrease of its concentration was linear with time up to *ca.* 60% of the initial concentration then it followed a much slower pattern (Marinkovic et al., 2003).

Building on previous studies relative to the modelling of unimolecular photochemical reactions kinetics (Maafi and Brown, 2005; Maafi and Brown, 2007; Maafi, 2010), a full quantitative study based on the Φ-order kinetics for the elucidation of Nif and Nis kinetics in solution as model candidates of unimolecular photoreactive drugs, will be presented. The rationalisation and quantification of some photo-stabilising strategies will also be explored, based on the Φ-order rate-constant expression. A quantitative study of the effect of initial drug concentration on photodegradation rates will first be presented followed by a quantitative evaluation and rationalisation of the photoprotective effects of photoactive yet non-reactive additives.

2. Nif and Nis photoreactions

The photoconversion of Nif and Nis leads to the formation of a nitroso derivative of the drugs as the major photoproduct (PP) (Scheme 1) (Piechoki and Thoma, 2010; Tonnesen, 2004; Albini and Fasani, 1998; Pietta et al, 1981; Fasani et al , 2006; Gorner, 2010; Mielkarek et al., 2005)

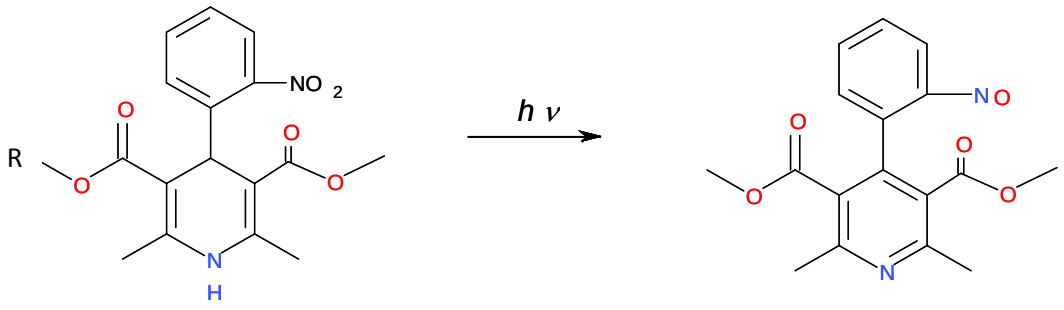

NIF PP

Scheme 1: Photo-transformation of Nif and Nis.

The absorbance spectra of Nif and Nis in ethanol are characterised by two main absorption regions at 200–250 and 300–420 nm, spanning the UVB, UVA and part of the visible spectral ranges (figure 2). The main peak maxima are located at around 238 and 340 nm with the former having **Nif:** R = CH_3 **Nis:** R = $CH_2CH(CH_3)_2$ an the latter broader peak. The drugs spectral characteristics are predominantly due to the contribution of the absorptions of the nitrobenzene and the dihydropyridine chromophores in both molecules. The long wavelength band (300–420 nm) belongs exclusively to the dihydropyridine ring which undergoes aromatisation upon exposure to irradiation. Disappearance of this band during the photoreaction is accompanied by the appearance of new peaks in the 200-300 nm region. The UVB transition, on the other hand, is attributed to the contribution of both chromophores (Krufurst and Kufan, 1983).

The photodegradation of these antihypertensives is easily evidenced by a change in the UV spectra of the drug solutions (figure 2), which show relatively similar spectral charactersitics. Exposure of ethanolic solutions of Nis to monochromatic irradiation results in the gradual increase in the absorbance regions of 200–230 nm and 260–320 nm with a peak appearing in the latter region at 280 nm and a shoulder at approximately 314 nm. A decrease in absorbance is also observed between 230 and 260 nm and 320–420 nm, with the appearance of three isosbestic points at 232, 259 and 320 nm. The region between 390–420 nm represents an exclusive absorption region for the mother compounds (Nif and Nis) as the spectrum of *PP* tails off at approximately 370 nm.

The smooth evolution of the spectra with the simultaneous formation of clearly identifiable isosbestic points suggest that both photoreactions occur quantitatively without formation of by–products. Further irradiation of the resulting *PP* at various wavelengths did not lead to further spectral changes, indicating that the *PP* is photostable.

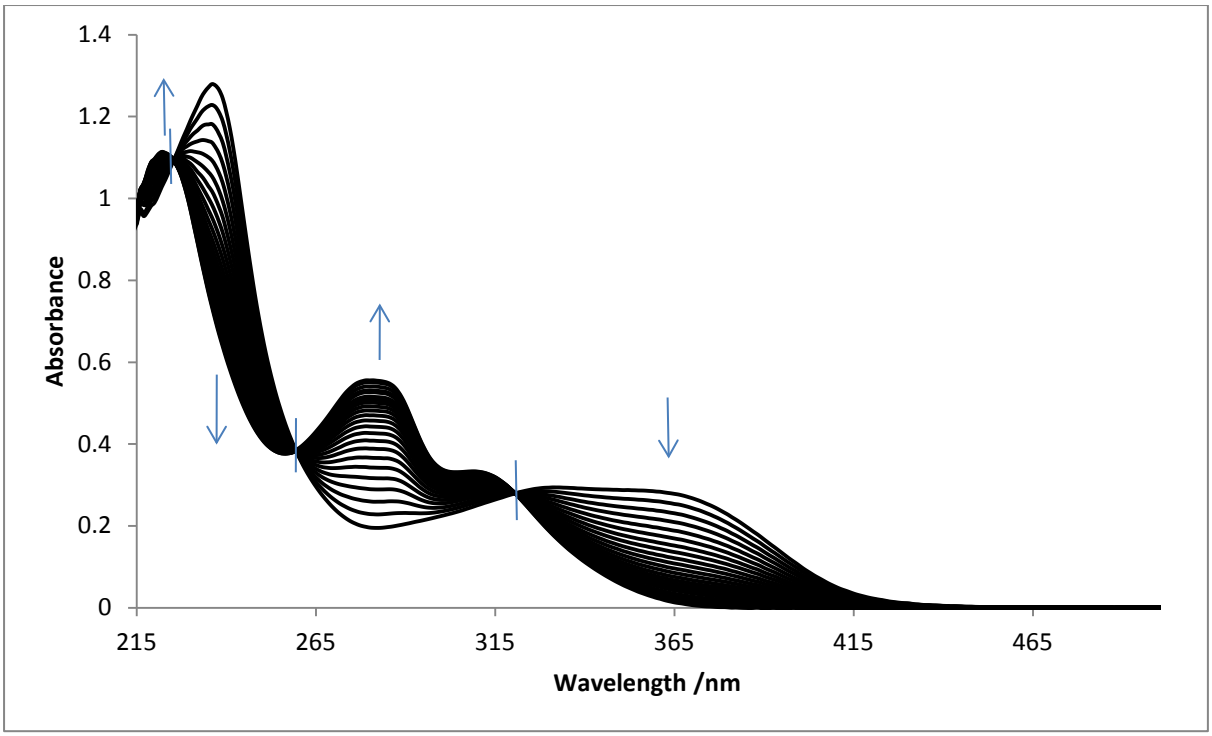

Figure 1: Evolution of the electronic absorption spectra of 5.88 x 10^{-5} M Nis in ethanol subjected to a continuous irradiation with a 390 nm monochromatic beam (total irradiation time 2000 s at a radiant power of P_{390} = 7.76 x 10^{-7} einstein.s^{-1}.dm^{-3}. The arrows indicate the direction of the peaks' evolution during the photoreaction and the vertical lines cross the spectra at the isosbestic points (232, 259 and 320 nm).

The hipsochromic shift observed in the absorption range 320–420 nm has been assigned to the π→π* electronic transition in the dihydropyridine ring, while the hyperchromic effect in

the 259-320 nm range is ascribed to the π→π* electronic transitions in the aromatic ring (Mielcarek et al., 2005a). The latter may also involve an underlying π→π* transition of the dihydropyridine in agreement with the spectral contribution of each chromophore to the overall Nif/Nis electronic spectrum (Kurfurst and Kufan, 1983).

The mechanism underlying the photodegradation reactions of Nif/Nis with radiation involves an intramolecular electron transfer from the dihydropyridine to the nitrophenyl group leading to a radical ion pair (Martens et al., 1983; Fasani et al., 2006). The favourable pathway for the decay of the latter intermediate involves a proton transfer followed by the elimination of a water molecule to produce the primary photoproduct (*PP*, scheme 1) (Zhu et al., 2003; Fasani et al., 2006). The spatial proximity of the oxygen atom of the *ortho*-nitro group on the phenyl ring to the hydrogen atom of the non–coplanar dihydropyridine favours the proton transfer which represents a key step in the phototransformation of both drugs (Zhu et al., 2003; Cotta-Ramusino and Vari, 1999; Fasani et al., 2006).

3. Modelling Nif/Nis photodegradation kinetics

Nif and Nis photodegradation kinetics were studied by exposing freshly prepared ethanolic solutions to different irradiation wavelengths (λ_{irr} = 223, 235, 250, 282, 321, 345, 370, 390 nm for Nif and λ_{irr} = 259, 281, 320, 345, 370, 380 and 390 nm for Nis) spanning different regions of their respective absorption spectrum including isosbestic points.

The variation of absorbance over time for each irradiation wavelength was recorded at the same observation wavelength (λ_{obs} = 390 nm). These traces were labelled by their irradiation/observation wavelengths ($\lambda_{irr}/\lambda_{obs}$). The fitting of the experimental traces was then performed using the suitable model equation (i.e. eqs. 6 or 21 for non–isobestic and isosbetic irradiations, respectively).

Application of Φ-order model equations 6 or 21, as appropriate, to the experimental kinetic traces of Nif and Nis resulted in a full and accurate fitting of all the kinetic traces recorded for the various irradiation and observation wavelengths (figure 2). This confirms that Nif and Nis photo-decomposition with light irradiation follows the Φ-order kinetics. In addition, besides an accurate fitting of all the synthetic NIM traces, fitting Nif and Nis experimental kinetic traces with the Φ-order model further confirms the validity and reliability of this model to describe AB(1Φ) photorecations kinetics, thereby offering a novel, precise and simple kinetic treatment strategy to describe unimolecular photoreactions kinetics.

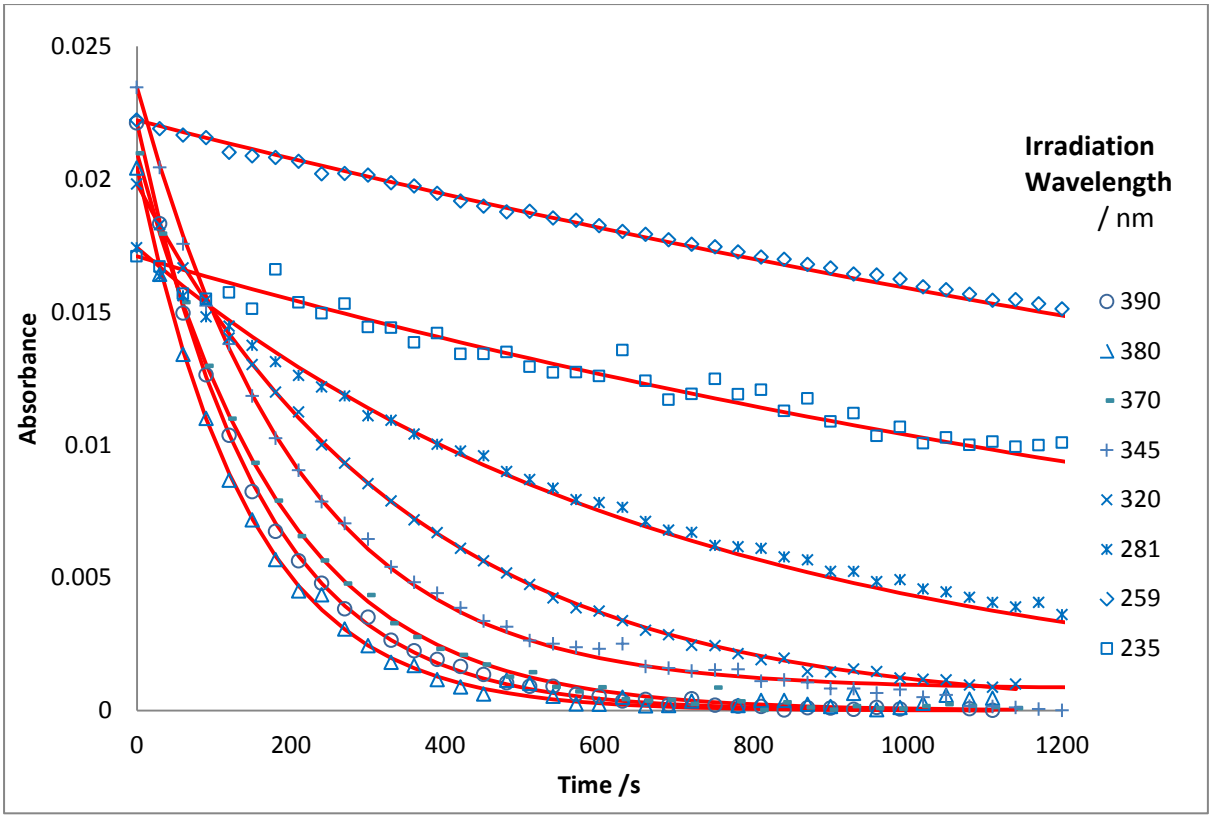

Figure 2: The photokinetic traces of *NIS* in ethanol (7.84 x 10^{-6} M) at λ_{irr}= 235, 259, 281, 320, 345, 370, 380 and 390 nm and observed at λ_{obs}= 390nm. The symbols represent the experimental data while the lines represent the model fitted traces using the appropriate model equation.

A further advantage procured by the model is the ability to determine useful kinetic parameters such as the overall rate-constant and photo-conversion quantum yields.

4. The correlation between quantum yield and wavelength

Fitting the models to the kinetic traces allows the determination of the respective values of $k_{NIS}^{\lambda_{irr}}$ and $k_{NIF}^{\lambda_{irr}}$ for each irradiation experiment which together with its analytical formula (eqs. 9 or 22) allow the determination of quantum yield values of the drugs photodegradation at any monochromatic irradiation (table 1).

A significant difference between irradiation of the first and second absorption regions (200 – 280, and 300 – 400 nm, respectively) can be observed from table 1. A faster degradation was observed upon exposure to irradiation wavelengths in the 340–390 nm region compared to irradiations in the 235–320 nm region of the spectrum. As indicated by the rate-constant values, both Nif and Nis reactivity to irradiation in the UVC-UVB regions is much slower than that observed under UVA irradiation. This could indicate that Nif and Nis photodegradation causative spectral range spans the UVA/visible regions. However, since various experimental, spectroscopic and reactants' parameters are involved in the rate-constant equation (eq.22), the former conclusion must be considered with caution and other parameters such as the quantum yields of photoreaction must also be considered in conjunction with the rate-constant values.

The quantum yields of photodegradation were calculated for each irradiation experiment from the re-arranged rate-constant equation of the photoreaction (eq.25). The results shown in table 1, indicate that overall the photochemical quantum yields of both Nif and Nis increase with increasing irradiation wavelength. For Nif degradation, the value obtained with λ_{irr} = 321 and 370 nm (table 1) respectively agree with the literature quantum yields determined in 2-propanol and methanol ($\Phi_{NIF\rightarrow PP}^{313}$ = 0.30 and 0.33, respectively) at 313 nm using a method based on aberchrome (Gorner, 2010), and in acetonitrile and methanol ($\Phi_{NIF\rightarrow PP}^{366}$ = 0.27 – 0.35 and $\Phi_{NIF\rightarrow PP}^{254}$= 0.23 – 0.24, respectively) when exposed to irradiation beams of a 35 cm bandwidth emitting maximally at 366 and 254 nm while using HPLC data corresponding to 25 % depletion of Nif (Fasani et al., 2008). Nis quantum yield values agree

with those reported in the literature in methanol recorded as 0.35 at λ_{irr} = 366 nm (Fasani et al., 2006) and λ_{irr} = 365 nm (Mielcarek et al., 2005a). However, at 259 nm, $\Phi_{NIS\rightarrow PP}^{259}$ is more than 10–fold lower than the reported value of $\Phi_{NIS\rightarrow PP}^{\lambda_{irr}}$ = 0.25 for λ_{irr} = 254 nm (Fasani et al., 2006). This discrepancy might be due to the large bandwidth of the filtered irradiation beam resulting in polychromatic light, used for the latter study which can only lead to average quantum yield values due to the contribution of other nearby wavelengths. The discrepancy effect of polychromatic irradiation on quantum yield values that is more important at 254 nm than at 366 nm, might be explained by a more pronounced variation of the quantum yield values in the 250–300 nm than in the 350–390 nm region (table 2 and figure 3).

When moving from the 280 to the 390 nm irradiation wavelength, the quantum yield values were found to almost and more than triple for NIS and NIF respectively; suggesting that the photodegradation of the drugs is mainly due to UVA and visible radiations.

Table 2: Quantum yield and overall reaction rate-constant values of Nif and Nis for a different monochromatic irradiations.

λ_{irr} /nm	$A_{NIF/NIS}^{\lambda_{irr}/390}(0)$	$P_{\lambda_{irr}}$ /einstein.s^{-1}.dm^{-}	$k_{NIF/NIS}^{\lambda_{irr}} \times 10^3$ /s^{-1}	$\Phi_{NIF/NIS\rightarrow PP}^{\lambda_{irr}}$
NIF photodegradation kinetic parameters				
390	0.0151	9.11 x 10^{-7}	7.50	0.509
370	0.0263	7.67 x 10^{-7}	7.20	0.322
345	0.0248	4.37 x 10^{-7}	4.05	0.305
321	0.0261	3.18 x 10^{-7}	2.36	0.267
282	0.0162	1.88 x 10^{-7}	0.440	0.109

250	0.0142	1.50×10^{-7}	0.265	0.025
235	0.0182	2.36×10^{-7}	0.135	0.004
223	0.0144	2.98×10^{-7}	0.180	0.0057
NIS photodegradation kinetic parameters				
235	0.0171	8.64×10^{-7}	0.500	0.0041±0.0001
259	0.0222	2.64×10^{-7}	0.335	0.028±0.0111
281	0.0174	4.98×10^{-7}	1.240	0.122±0.0085
320	0.0198	3.53×10^{-7}	2.800	0.304±0.0157
345	0.0235	5.99×10^{-7}	5.100	0.326±0.0088
370	0.0210	6.32×10^{-7}	5.700	0.334±0.0200
380	0.0204	8.04×10^{-7}	7.300	0.345±0.0179
390	0.0221	1.02×10^{-6}	6.500	0.351±0.0069

A plot of quantum yield values against irradiation wavelength (figure 3) shows that quantum yield of photodegradation increases by more than 85 and 125 times with increasing wavelength from 235 to 390 nm for both Nis and Nif, respectively. These values become more significant (> 0.1) for wavelengths higher than 280 nm. However, the electronic transition situated in the 320–390 nm region is responsible for the highest phototransformation of both drugs ($\Phi^{\lambda_{irr}}_{NIS/NIF \rightarrow PP} > 0.25$). The higher quantum yield values at the longer wavelengths of the absorption spectrum, corresponding to lower radiation energy, may suggest that the lowest singlet–state of the molecule, that is more readily and efficiently reached following higher wavelengths absorption, is much more efficient in the photoconversion of Nis and Nif than are the other higher excited states or other higher

vibrational levels of the lower excited state, which underlines the important contribution of the π→π* electronic transition of the dihydropyridine ring in their photochemistry.

Furthermore, photodegradation quantum yields are well correlated with irradiation wavelength (figure 3) via sigmoidal functions for both drugs (eqs. 26 and 27). A good agreement is found between experimental and calculated (eq. 28) values of the quantum yields (as indicated by the inset linear relationship in figure 3. Therefore, the sigmoid equation may be found useful to estimate the quantum yield absolute values at any irradiation wavelength between 235 and 390 nm.

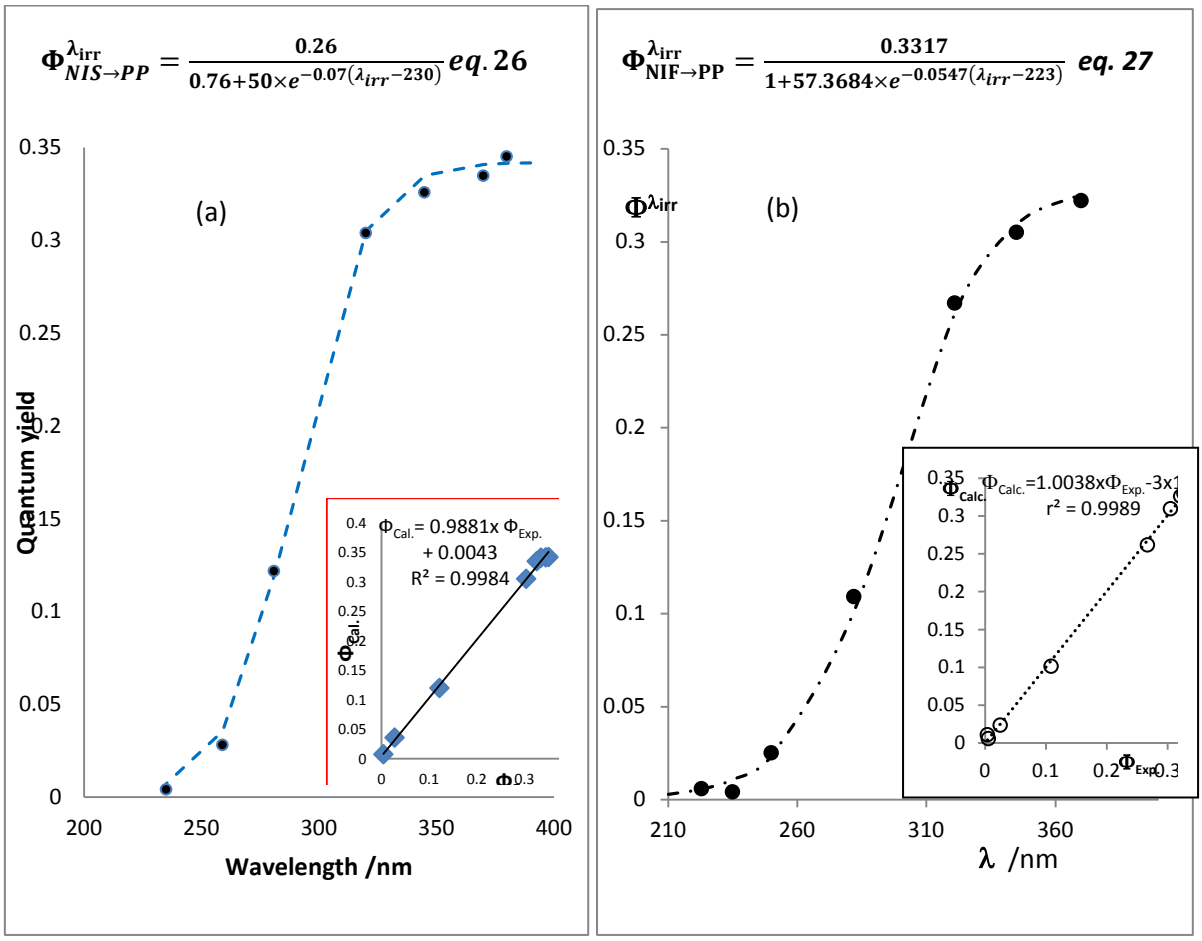

Figure 3: Sigmoid-like pattern of *(a) NIS* and (b) NIF photodegradaion quantum yield values with irradiation wavelength. Inset: experimental ($\Phi_{\text{Exp.}}^{\lambda_{\text{irr}}}$) versus calculated ($\Phi_{\text{Cal.}}^{\lambda_{\text{irr}}}$) quantum yield values.

The similarity in the sigmoidal evolution of quantum yields with irradiation wavelength for both dihydropyridine analogues indicates that the structural difference between the two molecules consisting in an extended alkyl chain (*R*) on the ester (–COO–R) group for Nis compared to a methyl in Nif does not significantly affect the photochemical efficiency of the main structural dihydropyridine–phenyl photochromic backbone. Additionally, the presence of the nitro group at the ortho position of the aromatic ring of both drugs renders such molecules more prone to photolability as suggested by the relatively high quantum yields recorded for both molecules compared to other dihydropyridine members (Garcia et al., 2014).

Moreover, the above monochromatic irradiation experiments treated using the Φ-order kinetic elucidation method provided a new tool for the accurate determination drugs quantum yield values at different wavelengths. This has, in turn, allowed a more precise understanding of the contribution of different wavelengths to the photoreactivity of the molecules. These findings strongly underline the necessity of using monochromatic light for the determination of quantum yields that proved to be wavelength-dependent. Furthermore, this approach not only allows the fitting of photokinetic traces and subsequent rate-constant determination but it also offers the advantage of facilitating quantum yield determination from the rate-constant analytical expression and this using the whole spectrophotometric data trace and not just segments of the kinetic trace to which

different rate-constants would be attributed (Piechocki and Thoma, 2010; Tonnesen, 2004; Albini and Fasani, 1998). Furthermore, this is achieved without requiring a prior separartion of the different components involved in the photoreaction since model fitting can more simply be achieved on the spectrophotometric kinetic traces of the reaction medium.

5. Photostabilisation by increasing drug concentration

Various concentrations of Nif and Nis in ethanol were selected within their linearity range (2.5 x 10^{-6} -1.5 x 10^{-4} M and 3.92 x 10^{-6} M - 1.58 x 10^{-4} M, respectively) to investigate the effect of concentration on photodegradation rate. This was done by conducting irradiaition experiments of the same wavelength on drug solutions using different initial concentrations. This procedure was repeated for different irradiation wavelengths ($\lambda_{NIF}^{irr} =$ 390, 354, 321 and 281 nm; λ_{NIS}^{irr} = 320, 350 or 390 nm) while maintaining all other variables constant for all the experiments. Evolution of the kinetic traces was monitored at an observation wavelength of λ_{obs} = 390 nm.

These traces were, then, fitted to the adequate model equation (eqs. 6 or 21) and a good fitting was achieved for all the traces (figure 4), further confirming the reliability of the models to describe the evolution of AB(1Φ) photoreactions. The rate-constants of photoreactions were thus determined and used to evaluate the effect of initial concentration on photoreaction rate (table 3).

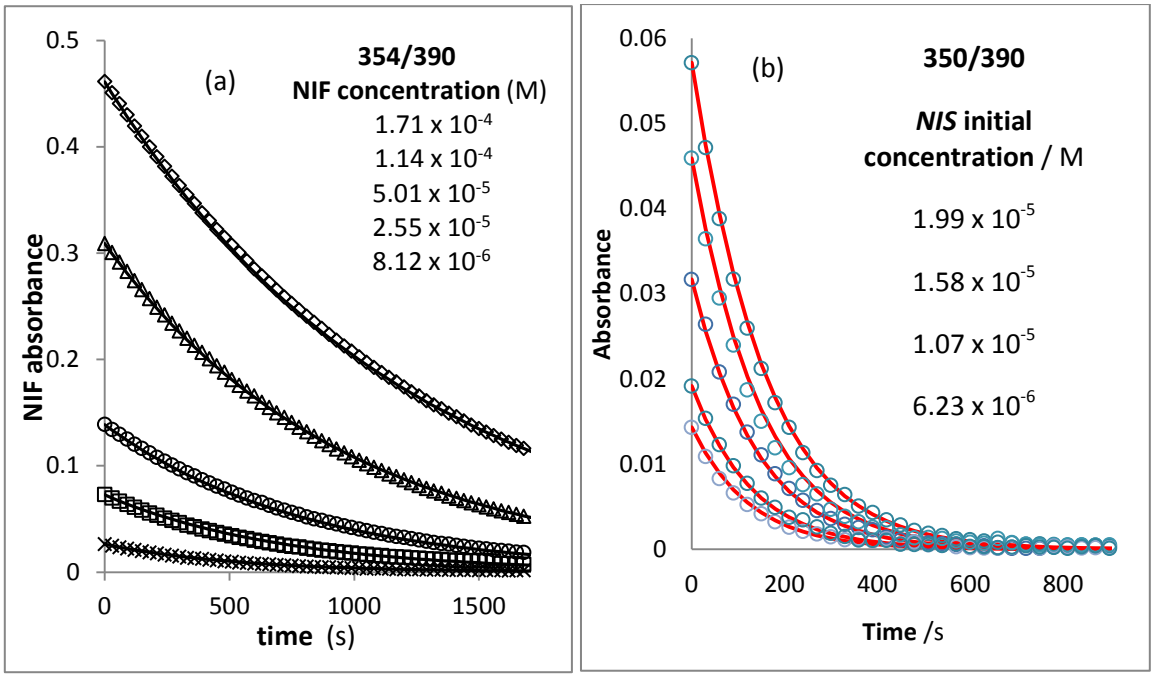

Figure 4: Photokinetic traces for the photodegradation of (a) NIF and (b) NIS ethanolic solutions of various concentrations following irradiation at (a) 354 nm (b) 350nm and observation at 390 nm.

Increasing initial drug concentration had the effect of noticeably decreasing photodegradation rate-constants for both Nif and Nis for irradiation experiments conducted at wavelengths where both the reactant and PP absorb (281, 321, 354 for NIF; and 320 and 350 for NIS). For UVA irradiations (320, 321, 350, 354 nm), a 4- to 6- fold increase in initial concentration resulted in 2 – 42 % reduction in reaction rate-constant. At this wavelength range, a higher reduction in photodegradation rate was observed for Nif than Nis as the concentrations increments were higher for the former (table 3). Increasing Nif concentration while irradiating in the UVB region (281 nm) resulted in a more significant photodegradation retardation than other irradiation regions with a four-fold concentration increase achieving an over 4-fold reduction in rate-constant (table 4). This finding could be due to the synergistic contribution of different concomitant effects at this wavelength

namely (i) a concentration inhibitory effect in addition to (ii) a reduction in the radiant power available for Nif due to the competitive absorption of incident radiation by the forming PP since the PP absorbance is higher than the mother compound at this wavelength; and (iii) a low quantum yield inherent to Nif and Nis at this wavelength. This strongly implies that protection of these molecules from light exposure is particularly important at wavelengths ranges above 300 nm.

Table 3: Initial concentrations and overall rate-constants of Nif and Nis photodegradation measured at various irradiation wavelengths.

λ_{irr}	$A^{\lambda_{irr}/390}(0)$	$k^{\lambda_{irr}}$ /s	$C\ (0) \times 10^5\ /M$	% reduction in photodegradation rate
NIF Photodegradation				
281	0.277	0.00009	10.2	77
	0.146	0.00022	5.28	43
	0.068	0.00039	2.37	-
321	0.461	0.00082	17.1	42
	0.309	0.00105	11.4	26
	0.073	0.00141	2.56	-
354	0.144	0.00389	5.21	10

	0.069	0.00414	2.41	4
	0.027	0.00430	0.84	-
390	0.129	0.00454	4.65	6
	0.070	0.00483	2.44	1
	0.028	0.00489	0.87	-
NIS Photodegradation				
320	0.013	0.0043	0.396	-
	0.025	0.0041	0.826	5
	0.03	0.0039	1.01	9
	0.045	0.00375	1.53	13
	0.059	0.0035	2.06	19
350	0.014	0.0082	0.449	-
	0.019	0.0080	0.623	2
	0.032	0.0077	1.07	6
	0.046	0.0075	1.58	9
	0.057	0.0072	1.99	12
390	0.011	0.007	0.35	-
	0.022	0.007	0.73	0
	0.033	0.0069	1.12	1
	0.054	0.0069	1.86	1
	0.080	0.0066	2.81	6

On the other hand, when irradiation was performed at wavelengths where only the reactant absorb the incident irradiation wavelength (i.e. 390 nm), increasing initial concentration had very little or no effect on photodegradation rate (table 3). This is predominantly due to the fact that PP does not competitively absorb irradiation at this wavelength and therefore, the radiant power available to Nif/Nis remains constant despite the reaction progress and PP formation.

The reduction in photoreaction rate-constant with increasing Nif/Nis initial concentration when irradiated at wavelengths where PP also absorbs is also implicitly conveyed by the photokinetic factor in the rate-constant expression (eq. 22). Increasing initial concentration causes a reduction of the value of the photokinetic factor ($F_{PP}^{\lambda_{irr}}$), which in turn, reduces the rate-constant value. Therefore, it can be inferred that initial concentration is inversely related to photodegradation rate at wavelengths ranges where PP absorbs. A linear relationship between $F_{PP}^{\lambda_{irr}}$ and $k_{NIF/NIS}^{\lambda_{irr}}$ can be established as depicted in figure 5.

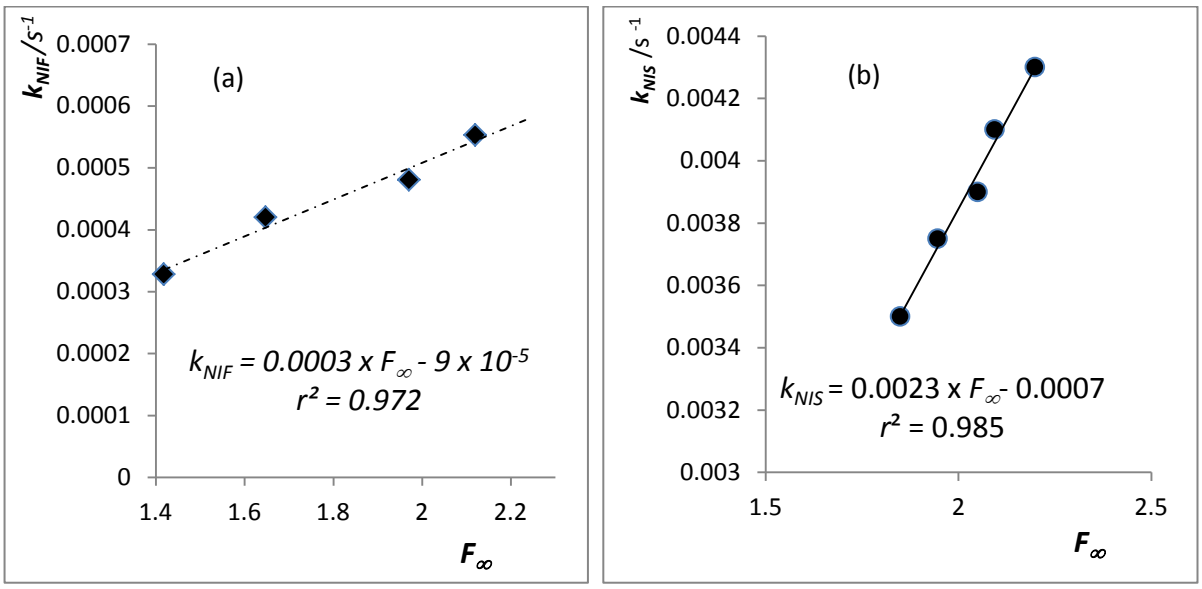

Figure 5: A Linear relationship between the overall rate–constant of (a)Nif and (b)Nis photodegradation with the photokinetic factor of the photoproduct when irradiating various concentrations of the drug solutions at 321/320nm and observing at 390 nm.

On the other hand, the rate-constant expression for irradiations at wavelengths where only the reactant absorbs, (eq.19), does not depend on concentration since the photokinetic factor remains constant ($F_{\infty}^{\lambda_{irr}} = F_{PP}^{\lambda_{irr}} \approx 2.3$). As such, at 390 nm where only Nif/Nis absorb, increasing the initial concentration did not cause any significant reduction in photodegradation rates (table 4).

Furthermore, a concentration self-inhibitory effect is also expected for more complex photoreaction mechanisms where more photoproducts are formed and absorb at the wavelength of irradiation since an inverse relationship exists between species concentration, and thus absorbance, and the corresponding photokinetic factor and thus rate-constant. Likewise, it can also be expected that when irradiation is performed at wavelengths where the photoproducts do not absorb the incident irradiation, then the photoreaction rate will not be dependent on initial concentration.

These findings account for a number of qualitative results reported in the literature, where less photodegradation was observed with higher initial reactant concentrations (Piechocki and Thoma, 2010; Tonnesen, 2004). Moreover, the attribution of the first kinetic order to the photodegradation of Nis at concentrations up to 3 x 10^{-5} M yet the zero-order for photoreactions using concentrations above 2 x 10^{-4} M, in a previous study (Huang et al., 1996); can be explained by a photoreaction slow-down due to increasing initial concentrations.

This concentration self-photo-inhibitory effect holds the potential to be used as a photo-protective means, especially at an industrial production level where initially bulk concentrations are used, and therefore, less photo-degradation would be expected before diluting and/or formulating a photoactive drug, where other photo-protective means might become necessary. Furthermore, preparation of concentrated stock solutions with the aim of minimising photo-

degradation and thus increasing a drug's shelf-life by diluting the drug at the dispensing or administration stage, represent another photo-protective strategy that can be deduced from the above results.

6. Photo-stabilisation by photo-absorbing additives

A commonly employed photo-protective method used with photo-active compounds is through the use of photo-protective excipients in the formulation (Piechocki and Thoma, 2010; Tonnesen, 2004; Albini and Fasani, 1998; Thoma and Klimek, 1991). The effect of excipient-dyes and food colouring agents on improving drug photostability have generally been studied using estimations based on thermal zero- and first-order reaction models, often only using the early stages of the photo-reaction kinetic trace (Piechocki and Thoma, 2010; Tonnesen, 2004).

In this study, the photo-stabilising effect of increasing concentrations of some widely used food colourants on Nif and Nis photo-degradation together with the ability of the Φ-order equations to quantify and rationalise this effect were investigated.

The electronic absorption spectra (figure 6) of the selected excipients used (tartrazine, TRZ, Sunset Yellow, SSY, and Quinoline Yellow, QY) (Scheme 3) are characterised by two broad absorption regions (200 - 320 nm and 320-550 nm) that overlap the absorption bands of Nif

and Nis spectra. When irradiated within the same experimental conditions used for Nif/Nis photo-degradation, these dyes were found to be photo-stable. Concentrations within the linearity ranges of the dyes in ethanol were used for photo-protection experiments. Monitoring the spectra of the photo-reacting drug and the evolving species without recording the spectra of the dye present in solution could be achieved by considering the dye solution as blank on the spectrophotometer before adding the drug.

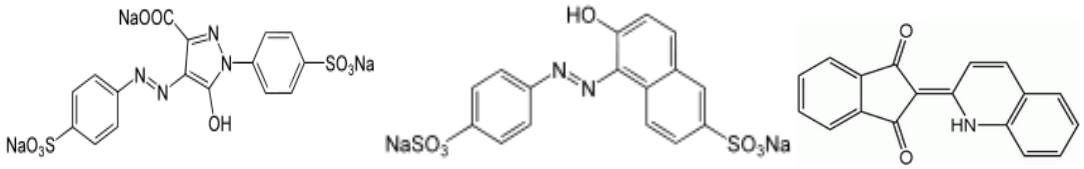

Tartrazine (TRZ) Sunset yellow (SSY) Quinoline Yellow (QY)

Scheme 3: chemical structures of TRZ, SSY and QY

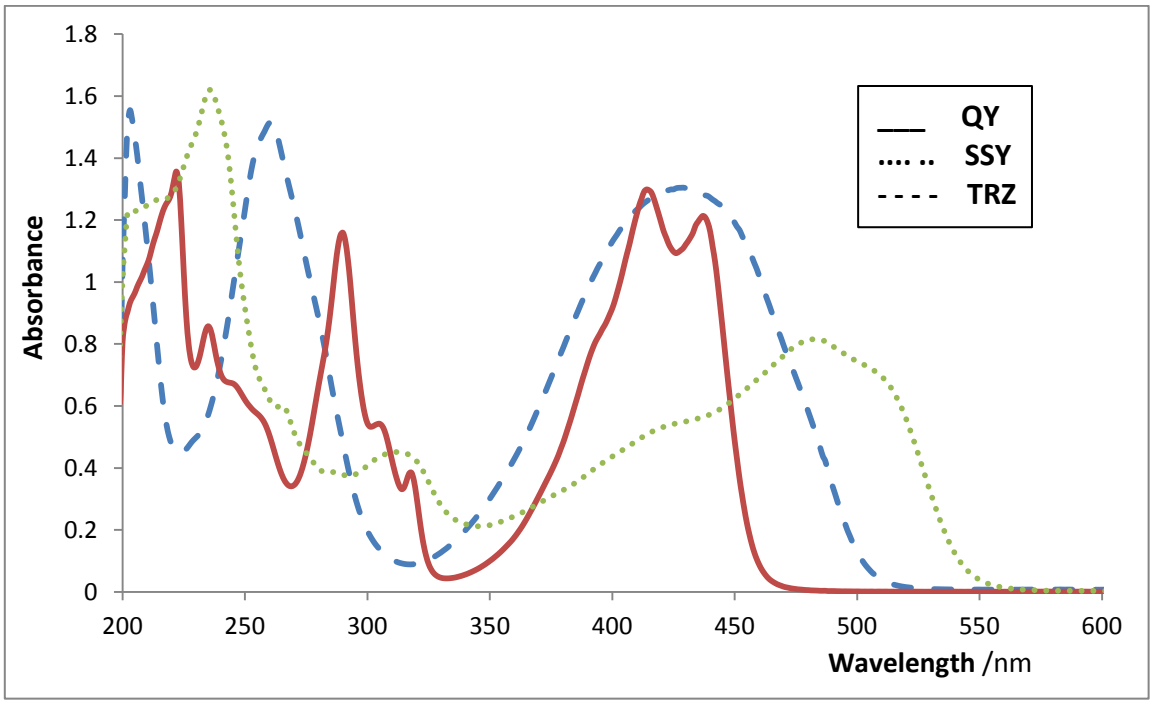

Figure 6: Absorption spectra of tartrazine (TRZ, 8.13 x 10^{-6} M), quinoline yellow (QY, 4.84 x 10^{-5} M) and sun set yellow (SSY, 2.73 x 10^{-5} M), in ethanol.

Since only Nif/Nis photo-degradation kinetic traces were observed without interference of the dye's trace, the semi-empirical model equation 18 was used to fit the drugs kinetic traces. An accurate fitting was obtained for all the photo-degradation kinetic data following irradiation at $\lambda_{irr} = 390$ nm in the presence of each additive (TRZ, QY, SSY for NIF; and TRZ, QY for NIS) as observed at $\lambda_{obs} = 390$ nm (figure 7). Over 70% photo-stabilisation was achieved for the highest dye-concentrations used (Table 4). The rate-constants of photoreaction, determined through the fitting, were found to be inversely proportional to the photo-absorbing dye concentration (Table 4), thereby indicating a concentration-dependent photo-protective effect of the additives used on the dihyropyridines photo-degradation.

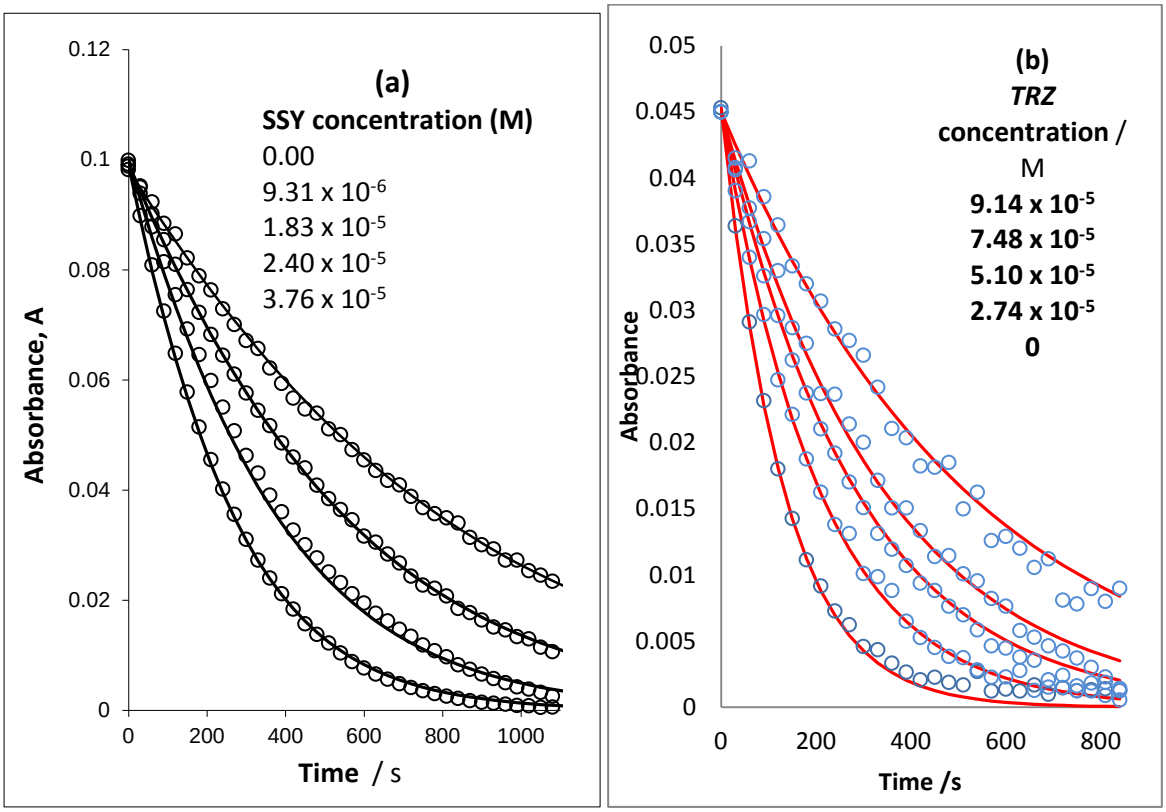

Figure 7: The effect of increasing dyes concentration on the photodergradation traces of (a) Nif (3.52 x 10^{-5} M) and (b) Nis (1.56 x 10^{-5} M*)* solutions in ethanol when irradiated and observed at 390 nm.

Table 4: Dyes absorbance, overall reaction rate–constants, photokinetic factors, and percentage reduction in reaction rates of NIF and NIS photo-degradation in the presence of various concentrations of dyes when irradiated and observed at 390 nm.

	$A_{dye}^{\lambda_{irr}}$ [a]	$k_{NIF/NIS}^{\lambda_{irr}}$ /s^{-1}	$\frac{k_{NIF/NIS}^{\lambda_{irr}}\left(A_{dye}^{\lambda_{irr}}=0\right)}{k_{NIF/NIS}^{\lambda_{irr}}\left(A_{dye}^{\lambda_{irr}}\neq 0\right)}$	% reduction [b]
NIF [c,d]	0	0.0067	1	0
Tartrazine (TRZ)	0.252	0.00430	1.558	33.48
	0.518	0.00315	2.127	53.98
	0.978	0.00210	3.191	69.22
	1.364	0.00164	4.085	74.86
	1.948	0.00130	5.154	79.25
Quinoline Yellow (QY)	0.319	0.0043	1.558	26.86
	0.741	0.0032	2.094	38.80
	1.025	0.0026	2.577	47.76
	1.940	0.0018	3.722	64.18
Sun set Yellow (SSY)	0.160	0.0033	2.030	22.98
	0.324	0.0026	2.566	33.58
	0.490	0.0022	2.979	38.80
	0.742	0.0015	4.351	49.22
NIS [c,d]	0	0.0080		0
Tartrazine (*TRZ*)	0.379	0.0052	1.54	35
	0.762	0.0039	2.05	51.25
	1.147	0.0032	2.50	60.00
	1.415	0.0022	3.64	72.5
Quinoline Yellow (*QY*)	0.261	0.0067	1.19	16.25
	0.472	0.0055	1.45	31.25
	0.792	0.0040	2.00	50

	1.137	0.0032	2.50	60

[a]: absorbance of the dye measured at the irradiation wavelength of 390 nm.

[b]: The concentrations of NIF were 4.6537 x 10-5 M for the TRZ experiment , 5.73104 x 10-5 M for the QY experiments and 3.49 x 10-5 M for SSY experiments. The constant concentration of *NIS* was 1.56 x 10^{-5} M All the experiemnts were conducted at 390/390.

[c]: the radiant power value for the experiments performed at an irradiation of λ_{irr} = 390 nm was P_{390} = 9.5 x 10^{-7} einstein.dm^{-3}.s^{-1} and for NIF and P_{390} =1.74 x 10^{-6} – 1.78 x 10^{-6} einstein.dm^{-3}.s^{-1} for NIS.

This study confirms similar results obtained using different additives such as curcumin, fast yellow, chrysoine, apocarotinal and cochineal in solution (Thoma and Klimek, 1991), and tartrazine (Teraoka et al., 1988) and curcumin (Tonnesen, 2001) in film coating materials for Nif; and of β–carotene for Nis (Mielcarek et al., 2005b). However, the quantification of these effects on the photoreaction rate, using physicochemical/mathematical methods, has, thus far, not been rationalised. Thus, Φ-order kinetic studies represent a new and accurate tool for the quantification and prediction of the effects of inert photo-absorbing additives on photodegradation kinetics. This is achieved by considering the dye's absorbance of incident irradiation in addition to that of PP in the photokinetic factor expression, $F_{\infty}^{\lambda_{irr}}$ (i.e. $A_{tot}^{\lambda_{irr}/\lambda_{irr}}(\infty) = A_{PP}^{\lambda_{irr}/\lambda_{irr}}(\infty) + A_{Excip.}^{\lambda_{irr}}$), when calculating $k_{NIF/NIS}^{\lambda_{irr}}$ as;

$$k_{NIF}^{\lambda_{irr}} = \Phi_{NIF\rightarrow PP}^{\lambda_{irr}} \times \varepsilon_{NIF}^{\lambda_{irr}} \times l_{\lambda_{irr}} \times P_{\lambda_{irr}} \times F_{\lambda_{irr}}^{dye} \qquad (eq.29)$$

As shown in figure 7, a linear relationship is found between $F_{\lambda_{irr}}^{dye}$ and $k_{NIF/NIS}^{\lambda_{irr}}$, with intercepts close to zero and correlation coefficients exceeding 0.98. These linear equations can be used to estimate the rate-constant values of photo-degradation in the presence of infinite concentrations of the dye. Nevertheless, despite being theoretically possible,

practically the concentrations of the dyes used are often limited by the maximum allowed daily intake. Furthermore, it also likely that a dye will exert its maximal photo-stabilising effect at concentrations near the upper linearity range concentration. This is because increasing the dye's concentration above the latter will no longer lead to a significant increase in absorbance. Therefore, it is also possible to minimise the amount of photo-protective additive to be used based on its linearity range as higher concentrations are unlikely to deliver higher photo-protection.

The photo-stabilising effect of the dyes on the drugs is due to a reduction in the value of $F_{\infty}^{\lambda_{irr}}$ with increasing amounts of excipinet-photoabsorbers as well as a reduced amount of radiation available to the reactant, which, in turn, leads to a decrease in $k_{NIF/NIS}^{\lambda_{irr}}$. As a consequence, the dyes are not chemically reactive but act as competitive absorbers of the incident radiation with the drug in solution, thereby reducing the amount of radiation available to the drug compared to photodegradation in the absence of competitive photo-absorbers. This effect should not, however, have any incidence on the photodegradation mechanism (AB(1Φ)) and inherent quantum yield of the drug at any given wavelength, as might have, previously, been suggested (Mielcarek et al., 2005a), unless the drug or its intermediate react with the additive.

The applicability of the model to describe AB(1Φ) kinetics in the presence of stable photo-additives was further evaluated using RK synthetic traces for increasing dye absorbance values. Again, the traces were well fitted with the model and linear correlations were found

between $F_{dye}^{\lambda_{irr}}$ and $k_{A\rightarrow B}^{\lambda_{irr}}$ for dye absorbance values up to *ca.* 2.5 (corresponding to $F_{dye}^{\lambda_{irr}}$> 0.4), with the latter value being the limit of applicability of the Φ-kinetics equations (figure 8).

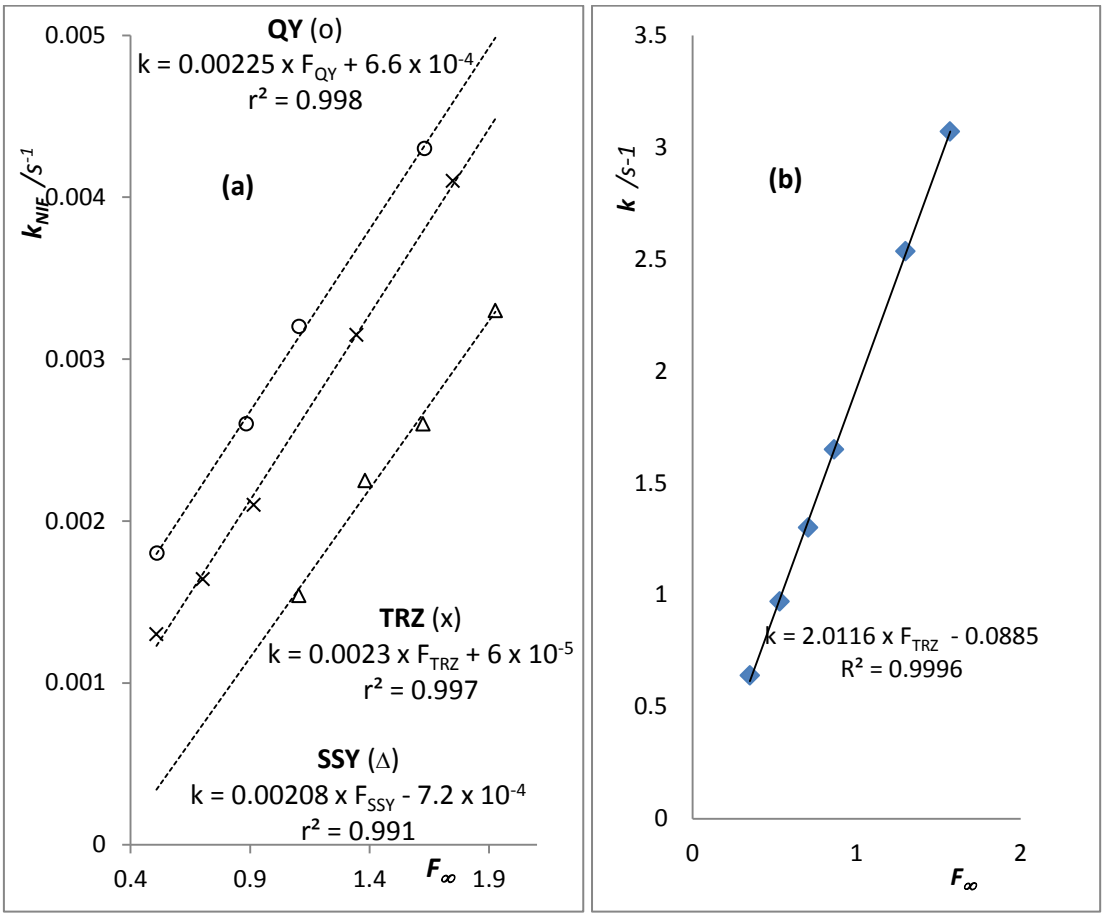

Figure 8: Linear relationships between the overall kinetic rate-constant of (a) NIF and (b) NIS photodegradation in the presence of various dye concentrations (table 3) and the corresponding photokinetic factors (inversely related to increasind dye concentration).

The good fitting of the Φ-model to the kinetic traces together with a linear correlation established between $F_{\lambda_{irr}}^{dye}$ and $k_{NIF/NIS}^{\lambda_{irr}}$ under the experimental conditions used whereby the dye solution is considered as the blank for subsequent spectrokinetic recordings, indicate that the Φ kinetics are suitable for the qualitative as well as the quantitative study

and prediction of the effects of photo- and thermally- stable excipients on drugs photodegradation.

7. Conclusions

The Φ-kinetics method proved to be useful and accurate in the description and elucidation of Nif and Nis photodegradation kinetics in solution. The kinetic parameters of these reactions were determined and the dependence of quantum yield on irradiation wavelength was further confirmed and quantitatively rationalised. Furthermore, an inhibitory effect of initial drug concentration was also demonstrated and quantitatively described. Photo-absorbing chemically inert additives were also shown to halt the drugs photo-degradation process. This Φ-order kinetic description and elucidation method that was theoretically and, hereby, experimentally validated may also be extended and applied to any photo-active molecule reacting via the unimolecular AB(1Φ) photoreaction mechanism.

References

Albini A. and Fasani E. Drugs Photochemistry and Photostability. The Royal Society of Chemistry: Cambridge; 1998.

Alvarez-Lueje A., Naranjo L., Nunez-Vergara L.J., Squella J.A., 1998. Electrochemical study of nisoldipine: analytical application in pharmaceutical forms and photodegradation. J. of Pharm. and Biomed. Anal. 16, 853–862.

Cotta-Ramusino, M., and Vari, M.R., 1999. Force field and semi-empirical MO conformational analysis of dihydropyridine calcium-channel antagonists. J. Mol. Struct. (Theochem.). 492, 257-268.

De Vries H, Van Henegouwen GMJB. Photoactivity of nifedipine in vitro and in vivo. J. Photochem. Photobiol. B: Biol. 1998; 43: 217-221.

Fasani E, Dondi D, Ricci A, Albini A. Photochemistry of 4-(2-nitrophenyl)-1,4-dihydropyridines. Evidence for electron transfer and formation of an intermediate. Photochem. Photobiol. 2006; 82:225-230.

Gorner H. Nitro group photoreduction of 4-(2-nitrophenyl)- and 4-(3-nitrophenyl)-1,4-dihydropyridines. Chem. Phys. 2010; 373: 153-158.

Huang C., Liu H. Ren J., Du X., 1996. Studies of photodegradation stability of nisoldipine. Chinese J. Pharm. **27, 1; 26-27**

Kawabe K, Nakamura H, Hino E, Suzuki S. Photochemical stabilities of some difydropyridine calcium-channel blockers in powdered pharmaceutical tablets.J. Pharm. Biomed. Anal. 2008; 47: 618-624.

Krufurst A., Kuhan J., 1983. Quantum chemical interpretation of electronic absorption spectra of the hantzsch dihydropyridines. Coll. Czech. Chem. Commun. 43, 1422-1428.

M. Maafi, The potential of AB(1 □) systems successful actimometers for the visible range. Phys. Chem. Chem. Phys. 2010; 12: 13248–13254.

Maafi M, Brown RG. The kinetic model for AB(1 □) systems. A closed form integration of the differential equation with a variable photokinetic factor. J. Photochem. Photobiol. A: Chem. 2007; 187: 319-324.

Maafi M, Brown RG. General analytical solutions for the kinetics of AB(k,□] and ABC(k,□] systems. Int. J. Chem. Kinet. 2005; 37(3): 162-174.

;

Marinkovic V.D., Agbaba D., Karljikovic-Rajic K., Vladimirov S., Nedeljkovic J.M., 2003. Photochemical degradation of solid-state nisoldipine monitored by HPLC. J. of Pharm. and Biomed. Anal. 32, 929-935

Martens, F.M., Verhoeven, J.W., Varma, C.A.G.O., Bergwerf, P., 1983. photooxidation of 1,4-dihydropyridines by various electron acceptors: a laser flash photolysis study. J. Photochem., 22, 99-113.

Matsuda Y, Teraoka R, Sugimoto I. Comparative evaluation of photostability of solid-state nifedipine under ordinary and intensive light irradiation conditions. Int. J. Pharm. 1989; 54: 211-221.

Mielcarek J., Augustyniak W., Grobelny P., Nowacka G., 2005a. Photoprotection of 1,4-dihydropyridine derivatives by dyes. Int. J. of Pharm. 304, 145–151.

Mielcarek J., Grobelny P., Szamburska P. 2005b. The effect of beta-carotene on the photostability of nisoldipine. Methods Find. Exp. Clin. Pharmacol. 27(3), 167.

Onoue S, Igarashi N, Yamauchi Y, Murase N, Zhou Y, Kojima T, Yamada S, Tsuda Y. in vitro phototoxicity of dihydropyridine derivatives : a photochemical and photobiological study. Eur. J. Pharm. Sci. 2008; 33: 262-270.

Piechocki JT and Thoma K. Pharmaceutical Photostability and Photostabilisation Technology. Informa Healthcare: London; 2010.

Pietta P, Rava A, Biondi P. High-performence liquid chromatography of nifedipine, its metabolites and photochemical degradation products. J. Chrom. 1981; 210: 516-521.

Pizarro-Urzua NA, Nunez-Vergara LJ. Nifedipine and nitrodipine reactivity towards singlet oxygen. J. Photochem. Photobiol. A: Chem. 2005; 175:129-137.

Shamsipur M., B. Hemmateenejad, M. Akhond, K. Javidnia, R. Miri, A study of the photodegradation kinetics of nifedipine by multivariate curve resolution analysis, Journal Pharmaceutical and Biomedical Analysis, 31 (2003) 1013-1019.

Tonnesen H.H. Photostability of Drugs and Drug Formulations (second Edition). CRC Press: London; 2004.

Piechocki JT and Thoma K. Pharmaceutical Photostability and Photostabilisation Technology. Informa Healthcare: London; 2010.

Zhu, X.Q., Li, H.R., Li, Q., Ai, T., Lu, J.Y., Yang, Y., Cheng, J.P., 2003. Detrmination of the C4-11 bond dissociation energies of NADH models and their radical cations in acetonitrile. Chem. Eur. J. 9, 871-880.

Chapter V: Modelling and elucidation of photoreversible, AB(2Φ), photoreactions kinetics - Application to montelukast and fluvoxamine photodegradation.

V.I. AB(2Φ) model development and validation

1. AB(2Φ) photoreactions

Photo-reversible reactions, whereby an initial species A photoreacts into PP, B, which itself photo-reverts back to A, represent another common photoreaction mechanism. Such systems undergo two reversible photochemical reactions between the mother compound and its isomer (scheme 1), and are thus labelled AB(2Φ) photoreactions.

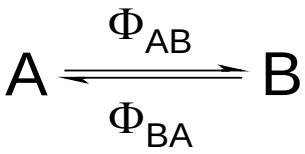

Scheme 1: Generic photoreaction system for the AB(2Φ) mechanism.

However, despite their simple mechanistic nature and widespread applications, no integrated rate-law has, thus far, been found for this type of reactions due to the presence of a time-dependent photokinetic factor in their rate-law equation. Therefore, as was achieved for AB(1Φ) photoreactions, the methodology for the development and validation of semi-empirical integrated rate-laws was employed to determine the model equation that governs AB(2Φ) photoreactions.

2. Elaboration of a kinetic model for AB(2Φ) reactions

2.1. Stage 1: AB(2Φ) model development

2.1.1. Isosbestic irradiations

In the case where irradiation of a sample solution is realised at an isosbestic wavelength, $\lambda_{irr} = \lambda_{isos}$, the general integrated rate–law of AB(2Φ) reaction systems has been obtained through a closed–form integration (Maafi and Brown, 2005a), as

$$A_{tot}^{\lambda_{isos}/\lambda_{obs}}(t) = A_{tot}^{\lambda_{isos}/\lambda_{obs}}(\infty) + \left(A_{tot}^{\lambda_{isos}/\lambda_{obs}}(0) - A_{tot}^{\lambda_{isos}/\lambda_{obs}}(\infty)\right) \times e^{-k_{A\leftrightharpoons B}^{\lambda_{isos}} \times t} \quad \text{(eq.1)}$$

or;

$$C_A(t) = C_A(\infty) + \left(C_A(0) - C_A(\infty)\right) \times e^{-k_{A\leftrightharpoons B}^{\lambda_{isos}} \times t} \quad \text{(eq. 2)}$$

$$C_B(t) = C_B(\infty) - C_B(\infty) \times e^{-k_{A\leftrightharpoons B}^{\lambda_{isos}} \times t} \quad \text{(eq. 3)}$$

with $C_A(\infty)$ and $C_B(\infty)$ representing the concentrations of the species at either the end of the reaction or *pss* (t = ∞) and $k_{A\leftrightharpoons B}^{\lambda_{isos}}$ being the overall rate–constant of the reaction performed at an isosbetic irradiation.

The monoexponential form of the equation indicates that isosbestic irradiations induce first–order kinetics for AB(2Φ) reactions. This is primarily due to the fact that when $\lambda_{irr} = \lambda_{isos}$, the photokinetic factor does not vary with reaction time (as the medium absorbance at the irradiation wavelength, λ_{isos}, is time–independent).

$k_{A\leftrightharpoons B}^{\lambda_{isos}}$ has the analytical expression;

$$k_{A\leftrightharpoons B}^{\lambda_{isos}} = \left(\Phi_{A\to B}^{\lambda_{isos}} + \Phi_{B\to A}^{\lambda_{isos}}\right) \times \varepsilon_A^{\lambda_{isos}} \times l_{\lambda_{isos}} \times P_{\lambda_{isos}} \times F_{pss}^{\lambda_{isos}} \qquad (eq.4)$$

With,

$$F_{pss}^{\lambda_{isos}} = \frac{1 - 10^{-\left(A_{tot}^{\lambda_{isos}/\lambda_{isos}}(pss) \times \frac{l_{\lambda_{isos}}}{l_{\lambda_{obs}}}\right)}}{A_{tot}^{\lambda_{isos}/\lambda_{isos}}(pss) \times \frac{l_{\lambda_{isos}}}{l_{\lambda_{obs}}}} \qquad (eq.5)$$

The reaction initial velocity ($v_0^{\lambda_{isos}}$) can then be determined from the derivative of eq.1 at t_0 as eq.6;

$$v_{0.Mod}^{\lambda_{isos}} = -k_{A\leftrightharpoons B}^{\lambda_{isos}} \times \left(A(0) - A(\infty)\right) \qquad (eq.6)$$

The value of the initial velocity can also be obtained graphically as the tangent of the initial stages of the kinetic trace, and compared to its theoretical expression (eq.7).

$$v_{0.Cal}^{\lambda_{isos}/\lambda_{obs}} = -(\varepsilon_A^{\lambda_{obs}} - \varepsilon_B^{\lambda_{obs}}) \times l_{\lambda_{obs}} \times \Phi_{A\to B}^{\lambda_{isos}} \times C_A(0) \times \varepsilon_A^{\lambda_{isos}} \times l_{\lambda_{isos}} \times P_{\lambda_{isos}} \times F_{\lambda_{isos}} \quad (eq.7)$$

However, since only a few isosbestic points are usually present on the electronic spectra of AB(2Φ) reactions, it is worth considering the most predominant non-isosbestic irradiation case.

2.1.2. Non-isosbestic irradiations

In an AB(2Φ) photoreaction system; the differential equation (DE) expressing the time variation of the concentrations of species A and B (C_A(t) and C_B(t), respectively), considering that the solution is subjected to a monochromatic and continuous irradiation, is homogeneously and continuously stirred, the concentration of the excited-state is assumed to be negligible, the medium temperature is constant, and at the (non-isosbestic) irradiation wavelength (λ_{irr}) species A and B absorb different amounts of light (P), i.e., the absorption coefficients (ε) of the species are different and have non-zero values ($\varepsilon_A^{\lambda_{irr}} \neq \varepsilon_B^{\lambda_{irr}} \neq 0$); is

$$\frac{dC_A\ (t)}{dt} = -\frac{dC_B\ (t)}{dt} = \left(\Phi_{B\to A}^{\lambda_{irr}} \times \varepsilon_B^{\lambda_{irr}} \times C_B\ (t) - \Phi_{A\to B}^{\lambda_{irr}} \times \varepsilon_A^{\lambda_{irr}} \times C_A\ (t)\right) \times l_{\lambda_{irr}} \times P_{\lambda_{irr}} \times F^{\lambda_{irr}} \quad (eq.8)$$

where $\Phi_{A\to B}^{\lambda_{irr}}$ and $\Phi_{B\to A}^{\lambda_{irr}}$ are the forward and reverse quantum yields of the photochemical steps realised at the irradiation wavelength (λ_{irr}), $P_{\lambda_{irr}}$ is the radiant power, $l_{\lambda_{irr}}$ is the optical path length of the irradiation beam inside the sample, and $F^{\lambda_{irr}}$ the photokinetic factor expressed as:

$$F_{\lambda_{irr}} = \frac{1-10^{-\left(A_{tot}^{\lambda_{irr}/\lambda_{irr}}(t)\times\frac{l_{\lambda_{irr}}}{l_{\lambda_{obs}}}\right)}}{A_{tot}^{\lambda_{irr}/\lambda_{irr}}(t)\times\frac{l_{\lambda_{irr}}}{l_{\lambda_{obs}}}} \qquad \text{(eq.9)}$$

Since $F_{\lambda_{irr}}$is a time-dependent function, eq.8 cannot be integrated in a closed form. To circumvent this problem, the methodology based on RK numerical integration was adopted to develop and validate a semi-empirical integrated rate-law that describes the kinetics of

AB(2Φ) photoreaction systems when subjected to continuous monochromatic irradiation. The programme was fed with plausible photo-reversible reaction parameters to produce the corresponding kinetic traces representing the variation of the species' concentration/absorbance over time. Such traces were used to test, optimise and then validate a template formula of the integrated rate-law. The template formula was set as the one derived for unimolecular AB(1Φ) photoreaction systems (eq. 21). This formula was optimised to take into account the absorbance of both A and B, present at the photostationary state (*pss*).

The proposed formula was then fitted with around 50 traces to test the ability of the model to fit AB(2Φ) kinetic traces, determine the overall rate-constant expression, and its limits of applicability. The optimised equation for AB(2Φ) systems is given in Eq.3:

$$A_{tot}^{\lambda_{irr}/\lambda_{obs}}(t) = A_{tot}^{\lambda_{irr}/\lambda_{obs}}(pss) + \frac{A_{tot}^{\lambda_{irr}/\lambda_{obs}}(0) - A_{tot}^{\lambda_{irr}/\lambda_{obs}}(pss)}{A_{tot}^{\lambda_{irr}/\lambda_{irr}}(0) - A_{tot}^{\lambda_{irr}/\lambda_{irr}}(pss)} \times \frac{l_{\lambda_{obs}}}{l_{\lambda_{irr}}}$$

$$\times Log\left[1 + \left(10^{\left[\left(A_{tot}^{\lambda_{irr}/\lambda_{irr}}(0) - A_{tot}^{\lambda_{irr}/\lambda_{irr}}(pss)\right) \times \frac{l_{\lambda_{irr}}}{l_{\lambda_{obs}}}\right]} - 1\right) \times e^{-k_{A \leftrightharpoons B}^{\lambda_{irr}} \times t}\right] (eq.10)$$

The coefficients, $A_{tot}^{\lambda_{irr}/\lambda_{obs}}(t)$, $A_{tot}^{\lambda_{irr}/\lambda_{obs}}(0)$, $A_{tot}^{\lambda_{irr}/\lambda_{obs}}(pss)$, $A_{tot}^{\lambda_{irr}/\lambda_{irr}}(0)$ and $A_{tot}^{\lambda_{irr}/\lambda_{irr}}(pss)$ in eq.10 are the measured total absorbances of the medium recorded at reaction time t, at the initial time t_0 and at the photo-stationary state, (*pss,* where t = ∞), respectively, when the reaction medium is irradiated at a given irradiation wavelength and simultaneously monitored at either a different observation wavelength ($\lambda_{irr}/\lambda_{obs}$) or at the

same wavelength ($\lambda_{irr}/\lambda_{irr}$). It is assumed that the reaction is quantitative and proceeds without by-products.

In this mathematical description, it is assumed that experimental measurements (A_{tot}) of spectroscopic and kinetic data are achieved under the observation ($l_{\lambda_{obs}}$) and not the excitation ($l_{\lambda_{irr}}$) conditions (with $l_{\lambda_{obs}}$ being the optical path length of the monitoring light inside the sample). It is important to notice that these optical path lengths ($l_{\lambda_{irr}}$ and $l_{\lambda_{obs}}$) may not be equal, and the absorbance of the medium in the excitation conditions (i.e measured along $l_{\lambda_{irr}}$) may not be directly accessible.

The analytical expression of the exponential factor, $k_{A\leftrightharpoons B}^{\lambda_{irr}}$ in eq.10, which represents the overall reaction rate-constant, was worked out from the rate-law equation at *pss* where $\frac{dC}{dt} = 0$, and is given by;

$$k_{A\leftrightharpoons B}^{\lambda_{irr}} = \left(\Phi_{A\to B}^{\lambda_{irr}} \times \varepsilon_A^{\lambda_{irr}} + \Phi_{B\to A}^{\lambda_{irr}} \times \varepsilon_B^{\lambda_{irr}}\right) \times l_{\lambda_{irr}} \times P_{\lambda_{irr}} \times F_{pss}^{\lambda_{irr}} \qquad (eq.11)$$

Where,

$$F_{pss}^{\lambda_{irr}} = \frac{1 - 10^{-\left(A_{tot}^{\lambda_{irr}/\lambda_{irr}}(pss) \times \frac{l_{\lambda_{irr}}}{l_{\lambda_{obs}}}\right)}}{A_{tot}^{\lambda_{irr}/\lambda_{irr}}(pss) \times \frac{l_{\lambda_{irr}}}{l_{\lambda_{obs}}}} \qquad (eq.12)$$

The concentration profiles, $C_A\ (t)$ and $C_B\ (t)$, are dependent on the species absorption coefficients, and given by

$$C_A\ (t) = C_A\ (\infty) + \frac{Log\left[1 + \left(10^{\left[\left(\varepsilon_A^{\lambda_{irr}} - \varepsilon_B^{\lambda_{irr}}\right) \times \left(C_A\ (0) - C_A\ (\infty)\right) \times l_{\lambda_{irr}}\right]} - 1\right) \times e^{-k_{A \leftrightharpoons B}^{\lambda_{irr}} \times t}\right]}{\left(\varepsilon_A^{\lambda_{irr}} - \varepsilon_B^{\lambda_{irr}}\right) \times l_{\lambda_{irr}}} \qquad (eq.13)$$

$$C_B\ (t) = C_B\ (\infty) \times \left(1 - \frac{Log\left[1 + \left(10^{\left[\left(\varepsilon_A^{\lambda_{irr}} - \varepsilon_B^{\lambda_{irr}}\right) \times \left(C_A\ (0) - C_A\ (\infty)\right) \times l_{\lambda_{irr}}\right]} - 1\right) \times e^{-k_{A \leftrightharpoons B}^{\lambda_{irr}} \times t}\right]}{\left(\varepsilon_A^{\lambda_{irr}} - \varepsilon_B^{\lambda_{irr}}\right) \times \left(C_A\ (0) - C_A\ (\infty)\right) \times l_{\lambda_{irr}}}\right) \qquad (eq.14)$$

However, when monitoring a photoreaction by spectrophotometry, it is necessary to use the logarithmic integrated rate–law equation describing the variation of the total observed absorption ($A_{tot}^{\lambda_{irr}/\lambda_{obs}}(t)$) with time:

The derivative of this equation at t_0 yields the initial velocity expression ($\upsilon_{0\ (mod.)}^{\lambda_{irr}/\lambda_{obs}}$) as:

$$v_{0\,(mod.)}^{\lambda_{irr}/\lambda_{obs}} = \left(\frac{dA_{tot}^{\lambda_{irr}/\lambda_{obs}}}{dt}\right)_0$$

$$= \frac{A_{tot}^{\lambda_{irr}/\lambda_{obs}}(0) - A_{tot}^{\lambda_{irr}/\lambda_{obs}}(pss)}{A_{tot}^{\lambda_{irr}/\lambda_{irr}}(0) - A_{tot}^{\lambda_{irr}/\lambda_{irr}}(pss)} \times \frac{k_{A\leftrightharpoons B\,(mod.)}^{\lambda_{irr}}}{\frac{l_{\lambda_{irr}}}{l_{\lambda_{obs}}} \times Ln(10)}$$

$$\times \left(10^{\left(A_{tot}^{\lambda_{irr}/\lambda_{irr}}(pss) - A_{tot}^{\lambda_{irr}/\lambda_{irr}}(0)\right) \times \frac{l_{\lambda_{irr}}}{l_{\lambda_{obs}}}} - 1\right) \quad (eq.15)$$

The initial velocity can also be determined theoretically, ($v_{0\,(cld.)}^{\lambda_{irr}/\lambda_{obs}}$), from the differential rate-law (eq.8) at t_0, rewritten as a function of total medium absorbance as;

$$v_{0\,(cld.)}^{\lambda_{irr}/\lambda_{obs}} = \left(\varepsilon_B^{\lambda_{obs}} - \varepsilon_A^{\lambda_{obs}}\right) \times l_{\lambda_{obs}} \times \Phi_{A\to B}^{\lambda_{irr}} \times \varepsilon_A^{\lambda_{irr}} \times l_{\lambda_{irr}} \times P_{\lambda_{irr}} \times F_0^{\lambda_{irr}} \times C_0 \quad (eq.16)$$

where $F_0^{\lambda_{irr}}$ is calculated using the initial absorbance $A_{tot}^{\lambda_{irr}/\lambda_{irr}}(0)$ instead of $A_{tot}^{\lambda_{irr}/\lambda_{irr}}(pss)$ in eq.12.

2.2. Stage 2: AB(2Φ) model validation

The theoretical validation of model eq.10 was performed in three stages. The first step consisted in checking that the model traces fitted more numerical simulation traces. This was achieved using approximately 100 RK-4 theoretical kinetic traces that were different from the ones used in the model development process. An example of the photoreaction parameters used to generate these data together with their kinetic and model fitted traces is given in table 1 and figure 1.

Table 1: Examples of reaction parameters used to feed RK–4 calculation of traces.

Attributes Sample #	C_0 [a] / M	$l_{\lambda_{irr}}$ [b] / cm	$\varepsilon_A^{\lambda_{irr}}$ / M^{-1} cm^{-1}	$\varepsilon_B^{\lambda_{irr}}$ / M^{-1} cm^{-1}	$\Phi_{A\to B}^{\lambda_{irr}}$	$\Phi_{B\to A}^{\lambda_{irr}}$	$P_{\lambda_{irr}}$ / einstein s^{-1} dm^{-3}
1	2.0×10^{-5}	2	6748	32159	0.50	0.20	1.0×10^{-6}
2	2.0×10^{-5}	1	8587	30269	0.85	0.17	9.3×10^{-7}
3	2.0×10^{-5}	1	8587	30269	0.17	0.17	3.4×10^{-6}
4	7.5×10^{-6}	1	55984	10837	0.60	0.20	1.5×10^{-6}
5	1.0×10^{-5}	1.7	35984	10837	0.70	0.40	2.0×10^{-6}
6	6.0×10^{-5}	1	5231	30273	0.10	0.50	7.0×10^{-6}
7	1.0×10^{-5}	2	22231	71273	0.10	0.30	3.0×10^{-7}

[a]: $C_0 = C_A(0)$ and $C_B(0) = 0$. [b]: $l_{\lambda_{irr}}$ = 1cm.

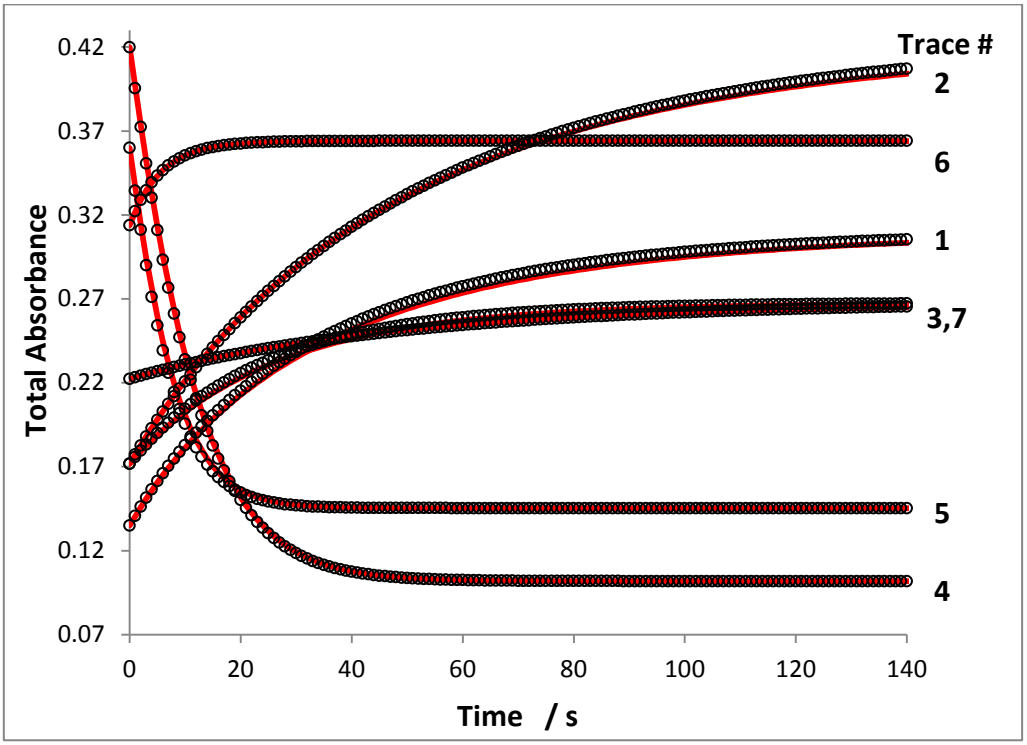

Figure 1: Examples of semi-empirical eq. 10 model fitting, (lines), of simulated RK–4 kinetic traces (circles), $A_{tot}^{\lambda_{irr}/\lambda_{irr}}$ *vs*. time, for AB(2Φ) photochemical reactions. The RK–4 calculations are based on table 1 data.

The semi-empirical integrated rate-law readily fitted all the simulation kinetic traces with high accuracy, thereby providing an initial proof of the validity of the model. The next validation step consisted in comparing the overall rate-constant values obtained by trace fitting ($k^{\lambda_{irr}}_{A\leftrightharpoons B\ (mod.)}$) to the theoretically calculated ones ($k^{\lambda_{irr}}_{A\leftrightharpoons B\ (cld.)}$) using eq.11. As can be seen in figure 2, the overall reaction rate-constants ($k^{\lambda_{irr}}_{A\leftrightharpoons B}$) values ranged from $2\text{x}10^{-3}$ to 1.8 s^{-1}, spanning more than three orders of magnitude. For each reaction case, a good agreement was found between the two sets of values with a percentage error never exceeding 10%.

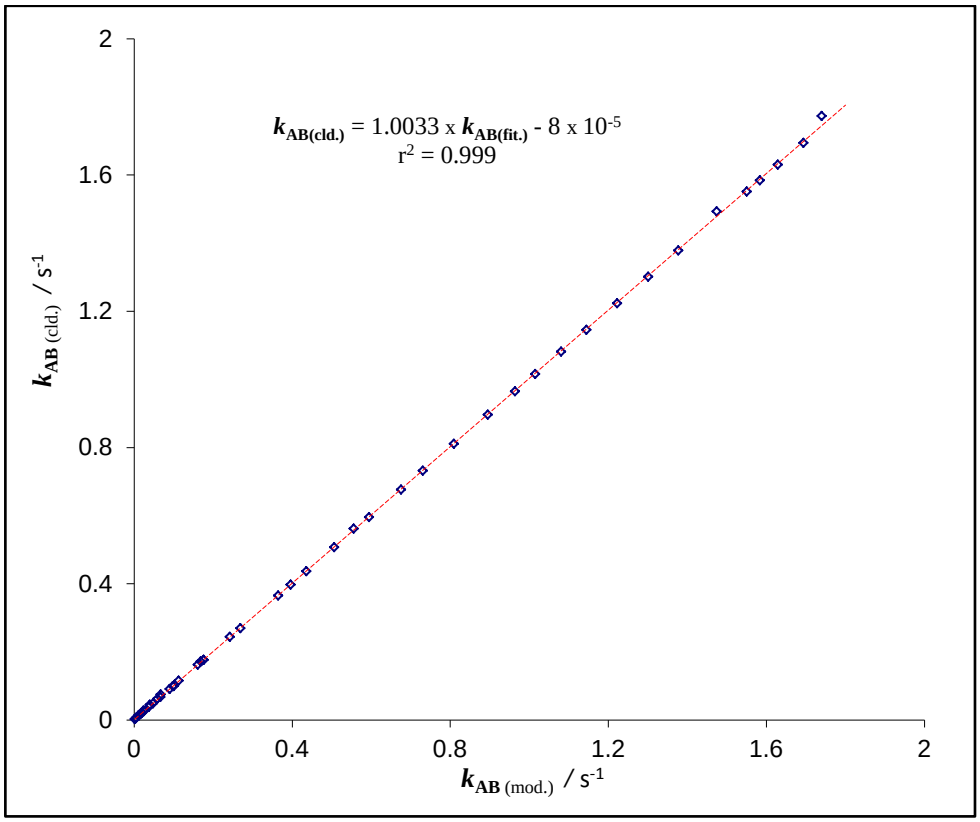

Figure 2: Correlation between the calculated values of overall rate-constants of the reaction ($k^{\lambda_{irr}}_{A \leftrightharpoons B\ (cld.)}$) against those generated from the fitting of RK–4 data using eq.10 ($k^{\lambda_{irr}}_{A \leftrightharpoons B\ (mod.)}$).

The final validation step of the theoretical part consisted in comparing the initial velocity values determined using the model derivative at t_0, (eq. 15, $\upsilon_{0\ (mod.)}^{\lambda_{irr}/\lambda_{obs}}$) to those calculated using the rate-law expression at t_0 (eq.16, $\upsilon_{0\ (cld.)}^{\lambda_{irr}/\lambda_{obs}}$) for all photoreaction cases.

A good agreement was found between the two sets of values that spanned the range of 2.2×10^{-5} to 3.8×10^{-1} s^{-1} with a straight correlation, a coefficient close to unity and a percentage error not exceeding 5% (figure 3).

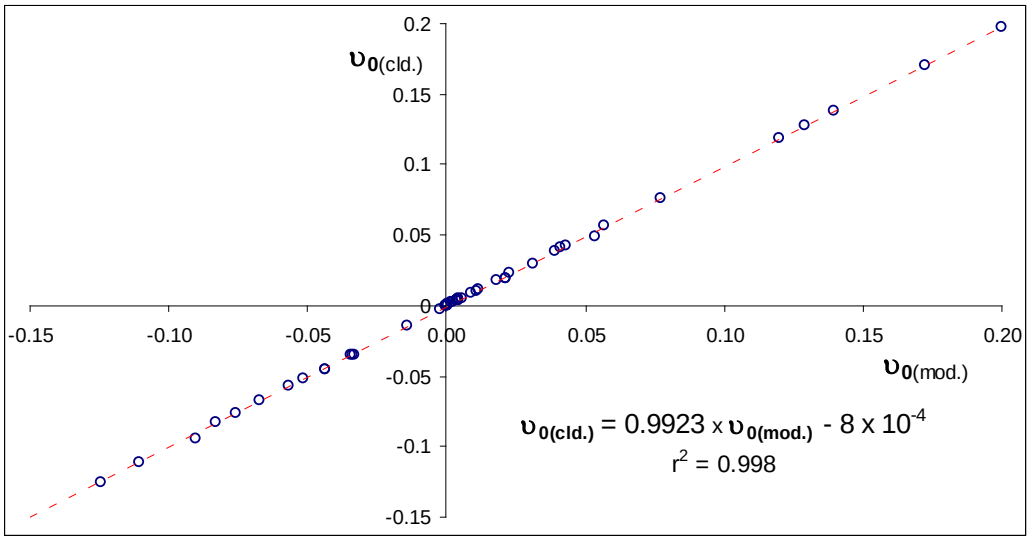

Figure 3: A plot of calculated and model initial velocity values; $\upsilon_{0\,(cld.)}^{\lambda_{irr}/\lambda_{obs}}$ and $\upsilon_{0\,(mod.)}^{\lambda_{irr}/\lambda_{obs}}$. υ_0 is expressed in s^{-1}.

These findings are strongly indicative of the validity of model equation (eq.10) to describe the kinetic evolution of AB(2Φ) photoreactions. However, the applicability of the model and rate-constant expressions relied on the condition that the value of $F_{pss}^{\lambda_{irr}}$must exceed or equal 1.2. Nevertheless, this condition can easily be met by reducing either the initial concentration C(0) or the irradiation path-length ($l_{\lambda_{irr}}$). Furthermore, this model provides means of determining reaction parameters such as overall photoreaction rate-constant and initial velocity from model fitting and eq.15, respectively, without resorting to the prior determination of reaction attributes such as ε and Φ.

The accurate fitting and correlations obtained between theoretical and model-derived kinetic parameters clearly indicate that photo-reversible drug degradation reactions obey a different kinetic order than thermal kinetics, namely, the Φ–order kinetics. Moreover, it is also worth noting that the terms of the integrated rate-law model together with the rate-constant expression indicate the inherent and exclusive dependence of photoreactions on parameters such as $k_{AB}^{\lambda_{irr}}, t, \varepsilon_{A\ or\ B}^{\lambda_{irr}}, \Phi_{A\to B\ or\ B\to A}^{\lambda_{irr}}, C_{A\ or\ B}(pss),\ l_{\lambda_{irr}},\ l_{\lambda_{obs}}$and $P_{\lambda_{irr}}$ most of which are not involved in thermal reactions.

A summary of the stepwise approach adopted in the above method used for deriving semi-integrated rate-laws describing the kinetics of photoreaction systems is provided in the following diagram (Diagram 1).

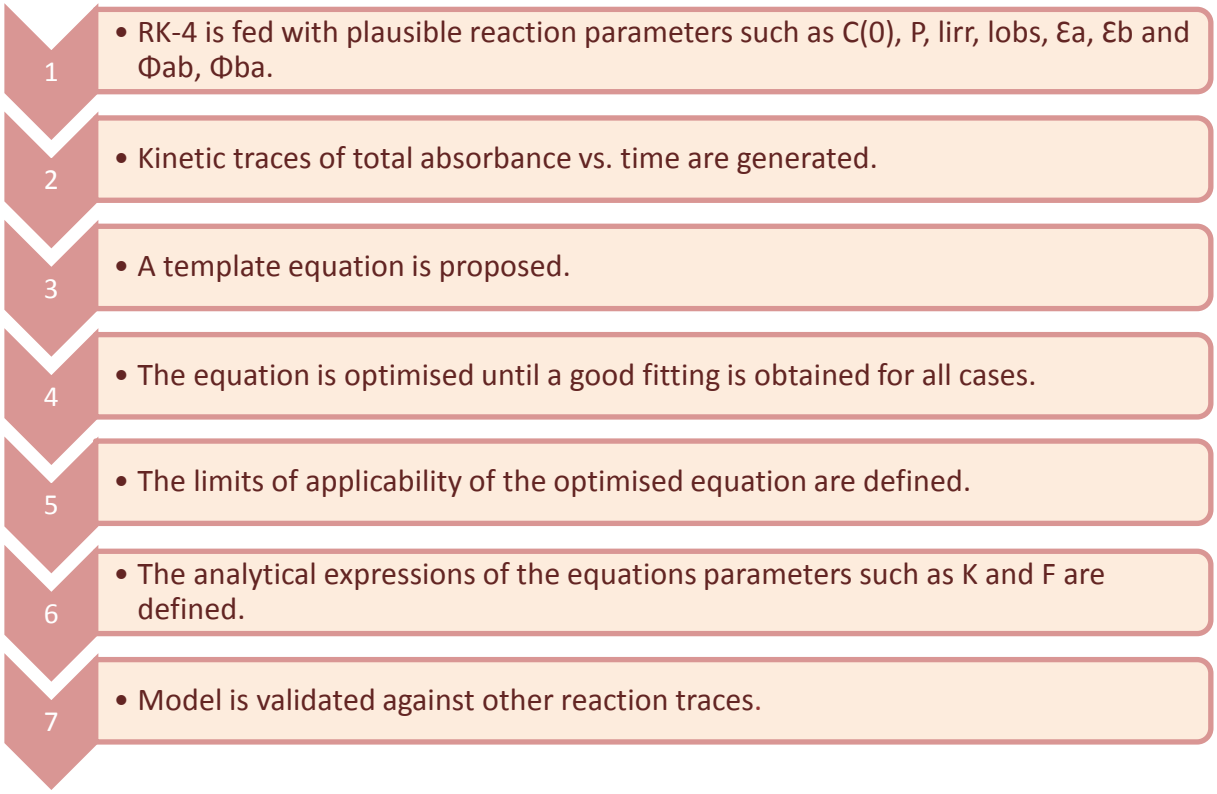

Diagram 1: Stepwise method used to derive the integrated rate-law for AB(2Φ) systems.

Based on the above results, a three-step kinetic implementation procedure can be proposed for the elucidation of AB(2Φ) photoreactions kinetics.

3. A stepwise approach for the kinetic study of AB(2Φ) reactions

Unlike AB(1Φ) photoreactions, elucidation of AB(2Φ) photokinetics necessitates additional data due to the overlapping electronic spectra of A and its photoproduct (B) at *pss.* As a result, $\varepsilon_B^{\lambda_{irr}}$ can not be determined from the UV-Vis traces. Therefore, the values of $\Phi_{A\to B}^{\lambda_{irr}}$ and $\Phi_{B\to A}^{\lambda_{irr}}$ can not be calculated using eqs. 11 and 16, since the extracted fitting parameters ($k_{A\leftrightharpoons B}^{\lambda_{isos}}$ and $v_0^{\lambda_{isos}/\lambda_{obs}}$ or $k_{A\leftrightharpoons B}^{\lambda_{irr}}$ and $v_0^{\lambda_{irr}/\lambda_{obs}}$) are not sufficient to work out the three unknowns of the reaction (i.e. $\Phi_{A\to B}^{\lambda_{irr}}$, $\Phi_{B\to A}^{\lambda_{irr}}$ and $\varepsilon_B^{\lambda_{irr}}$) if their values are not known prior to the experiment. Thus, solving a photoreaction kinetics through the use of fitting parameters for the unknown values until a good fitting is reached leads to a degenerate kinetic solution with inextricable identifiability and/or distinguishability issues (Maafi and Brown, 2005b). Accordingly, it is necessary to use further data, obtained by an alternative analytical method, that allows the determination of the PP electronic absorption spectrum in addition to the data obtained by spectrophotometric monitoring. Therefore, a simple elucidation method for photoreversible reactions that can be implemented in three steps was devised and is hereby presented.

3.1. Determination of the equilibrium constant under isosbestic irradiation

This step is required for the determination of the PP absorption spectrum. This is achieved by monitoring the variation of the species concentrations throughout the photoreaction time when exposed to monochromatic isosbestic irradiation, and this using an analytical separation method such as HPLC. When the solution is irradiated at an isosbestic wavelength, the absorption coefficient of the photoproduct is known since $\varepsilon_A^{\lambda_{isos}} = \varepsilon_B^{\lambda_{isos}}$ and therefore, the number of unknowns reduces to only $\Phi_{A\to B}^{\lambda_{isos}}$ and $\Phi_{B\to A}^{\lambda_{isos}}$. The species *pss*

concentrations, as determined by HPLC, allow the determination of the equilibrium constant (eq.17) as follows,

$$\frac{dC_A}{dt} = \frac{-dC_B}{dt} = 0 \ (eq.17)$$

Eq.17 can be rewritten as;

$$\Phi_{A\to B}^{\lambda_{isos}} \times \varepsilon_A^{\lambda_{isos}} \times C_A \times l_{\lambda_{isos}} \times P_{\lambda_{isos}} \times F_{pss}^{\lambda_{isos}} = \Phi_{B\to A}^{\lambda_{isos}} \times \varepsilon_B^{\lambda_{isos}} \times C_B \times l_{\lambda_{isos}} \times P_{\lambda_{isos}} \times F_{pss}^{\lambda_{isos}} \ (eq.18)$$

that can be rearranged into;

$$\Phi_{A\to B}^{\lambda_{isos}} \times \varepsilon_A^{\lambda_{isos}} \times C_A = \Phi_{B\to A}^{\lambda_{isos}} \times \varepsilon_B^{\lambda_{isos}} \times C_B \quad (eq.19)$$

Since $\varepsilon_A^{\lambda_{isos}}$=$\varepsilon_B^{\lambda_{isos}}$

$$\mathrm{K}_{\leftrightharpoons}^{\lambda_{isos}} = \frac{k_{B\to A}^{\lambda_{isos}}}{k_{A\to B}^{\lambda_{isos}}} = \frac{C_B(pss)}{C_A(pss)} = \frac{\Phi_{A\to B}^{\lambda_{isos}}}{\Phi_{B\to A}^{\lambda_{isos}}} \qquad (eq.20)$$

It is worth noticing that $\mathrm{K}_{\leftrightharpoons}^{\lambda_{isos}}$ is concentration–independent. This feature finds its importance in the fact that the HPLC experiment that serves in its determination is usually performed at initial concentrations of species A that are usually too high for spectrophotometric analysis, normally realised at lower concentrations where $F_{\lambda_{irr}}(\infty)$ > 1.2.

3.2. Determination of the photoisomer absorption spectrum

The reconstruction of the full spectrum of the photoisomer (B), can then be performed at lower concentrations in the second step of the elucidation method. This is achieved from the value of $\mathrm{K}_{\leftrightharpoons}^{\lambda_{isos}}$, which remains unchanged for the same irradiation wavelength, and the spectrum of the reactive medium recorded at *pss* under the same isosbestic irradiation used for the HPLC experiment ($A_{tot}^{\lambda_{isos}/\lambda_{obs}}(pss)$).

Since,

$$\mathrm{K}_{\leftrightharpoons}^{\lambda_{isos}} = \frac{k_{B\to A}^{\lambda_{isos}}}{k_{A\to B}^{\lambda_{isos}}} = \frac{C_B(pss)}{C_A(pss)} (eq.20)$$

And

$$C(0) = C_A(pss) + C_B(pss) \qquad \text{(eq.21)}$$

$C_B(pss)$ can be expressed as a function of $C_A(pss)$ as,

$$C_B(pss) = \mathrm{K}_{\leftrightharpoons}^{\lambda_{isos}} \times C_A(pss) \qquad (eq.22)$$

By substituting of (eq.22) into (eq.21), $C_A(pss)$ can be expressed as,

$$C_A(pss) = \frac{C(0)}{1 + \mathrm{K}_{\leftrightharpoons}^{\lambda_{isos}}} \qquad (eq.23)$$

From (eq.22), $C_A(pss)$ can be expressed as,

$$C_A(pss) = \frac{C_B(pss)}{\mathrm{K}_{\leftrightharpoons}^{\lambda_{isos}}} \qquad (eq.24)$$

Substitution of (eq.24) into (eq.23) leads to the expression of $C_B(pss)$as a function of $C(0)$as,

$$C_B(pss) = \frac{\mathrm{K}_{\leftrightharpoons}^{\lambda_{isos}} \times C(0)}{1 + \mathrm{K}_{\leftrightharpoons}^{\lambda_{isos}}} \qquad (eq.25)$$

After rearrangement, the mathematical expression of $\varepsilon_B^{\lambda_{obs}}$can be obtained following the substitution of eqs. 24 and 25 into $A_{tot}^{pss} = A_A^{pss} + A_B^{pss}$ as;

$$\varepsilon_B^{\lambda_{obs}} = \frac{(\mathrm{K}_{\leftrightharpoons}^{\lambda_{isos}} + 1) \times A_{tot}^{\lambda_{isos}/\lambda_{obs}}(pss) - \varepsilon_A^{\lambda_{obs}} \times l_{obs} \times C_A(0)}{l_{obs} \times \mathrm{K}_{\leftrightharpoons}^{\lambda_{isos}} \times C_A(0)} \qquad (\mathrm{eq.}\,26)$$

This expression allows the reconstruction of the electronic absorption spectrum of B using the total absorbance spectrum of the medium at *pss* following isosbestic irradiation. Therefore, following this step, irrespective of the wavelength selected to perform irradiation, the number of unknowns will constantly be two in total, as the spectrum of the photoproduct (ε_B^{λ}) becomes accessible.

3.3. Quantum yields determination at any wavelength

3.3.1. Quantum yields determination at isosbestic wavelengths

In the case of isosbestic irradiations, fitting the experimental data with eq.1, allows the determination of $k_{A\leftrightharpoons B}^{\lambda_{isos}}$. Then, from eqs.6 and 7, the forward quantum yield can be determined as;

$$\Phi_{A\to B}^{\lambda_{isos}} = \frac{v_{0\ (mod.)}^{\lambda_{isos}/\lambda_{obs}}}{\left(\varepsilon_B^{\lambda_{obs}} - \varepsilon_A^{\lambda_{obs}}\right) \times l_{\lambda_{obs}} \times \varepsilon_A^{\lambda_{isos}} \times l_{\lambda_{isos}} \times P_{\lambda_{isos}} \times F_0^{\lambda_{isos}} \times C_0} \ (eq.27)$$

While the reverse quantum yield is determined from the rate-constant expression (eq.4) as;

$$\Phi_{B\to A}^{\lambda_{isos}} = \frac{k_{A\leftrightharpoons B}^{\lambda_{isos}}}{\varepsilon_A^{\lambda_{isos}} \times l_{\lambda_{isos}} \times P_{\lambda_{isos}} \times F_{\lambda_{isos}}} - \Phi_{A\to B}^{\lambda_{isos}} \qquad (eq.28)$$

3.3.2. Quantum yields determination for non-isosbestic wavelengths

In the last step of the method, the quantum yields ($\Phi_{A\to B}^{\lambda_{irr}}$ and $\Phi_{B\to A}^{\lambda_{irr}}$) for any irradiation wavelength can readily be worked out from eqs. 15 and 16, for $\Phi_{A\to B}^{\lambda_{irr}}$determination, eq.29, and by rearranging eq.11 for $\Phi_{B\to A}^{\lambda_{irr}}$, yielding eq. 30.

$$\Phi_{A\to B}^{\lambda_{irr}} = \frac{v_{0\,(mod.)}^{\lambda_{irr}/\lambda_{obs}}}{\left(\varepsilon_B^{\lambda_{obs}} - \varepsilon_A^{\lambda_{obs}}\right) \times l_{\lambda_{obs}} \times \varepsilon_A^{\lambda_{irr}} \times l_{\lambda_{irr}} \times P_{\lambda_{irr}} \times F_0^{\lambda_{irr}} \times C_0} \qquad (eq.29)$$

$$\Phi_{B\to A}^{\lambda_{irr}} = \frac{k_{A\leftrightharpoons B}^{\lambda_{irr}}}{\varepsilon_A^{\lambda_{irr}} \times l_{\lambda_{irr}} \times P_{\lambda_{irr}} \times F_{\lambda_{irr}}} - \Phi_{A\to B}^{\lambda_{irr}} \qquad (eq.30)$$

4. Discussion

Unlike thermal kinetics treatment methods, the Φ-order models offer the possibility to fit the entire kinetic traces for AB(2Φ) photoreactions. Nevertheless, based on spectrophotometric data, application of eq.10 would not be sufficient to determine the values of the unknown parameters ($\Phi_{A\to B}^{\lambda_{irr}}$, $\Phi_{B\to A}^{\lambda_{irr}}$ and $\varepsilon_B^{\lambda_{irr}}$) and/or ascertain whether the reaction follows an AB(1Φ) or AB(2Φ) mechanism, also known as a distinguishability problem. Therefore, the elucidation of the specific mechanism underlying a photoreaction can only be achieved using additional information obtained by an alternative analytical separation method such as HPLC. However, the accuracy of the model in fitting entire photoreactions kinetic traces, as opposed to partial thermal fitting, in addition to providing an accurate means for kinetic parameters determination far outweigh the additional

requirement for an analytical separation step to determine the species equilibrium concentrations under isosbestic irradiation. In addition, the good fitting of the experimental data with eqs. 1 or 10 certainly provides further evidence that the reaction is of the Φ–order kinetics.

In addition, the expression of $k_{A \leftrightharpoons B}^{\lambda_{irr}}$ (eq.11) indicates that the photodegradation overall rate-constant of AB(2Φ) photodrugs inherently depends on the irradiation wavelength, the absorption coefficients of the reactant and its photoproduct ($\varepsilon^{\lambda_{irr}}$), the forward and reverse quantum yields ($\Phi^{\lambda_{irr}}$), the optical path-length travelled by the irradiation light inside the sample ($l_{\lambda_{irr}}$), the radiant power ($P_{\lambda_{irr}}$) and initial drug concentration through the photokinetic factor ($F_{\infty}^{\lambda_{irr}}$). This rationalises, for the first time, the set of parameters affecting the overall rate-constant of these systems. It may contribute to a better interpretation of the literature data and reiterates the importance of using monochromatic irradiation for these photokinetic studies. It is also worth noting that in $k_{A \leftrightharpoons B}^{\lambda_{irr}}$ analytical expression, the terms $\varepsilon^{\lambda_{irr}} \times \Phi^{\lambda_{irr}}$ relative to A and B add up in a similar way to that observed for both photoreactions performed with isosbestic irradiation, and thermal reactions, where individual photoreactions rates add up to make the overall rate-constant.

Furthermore, $F_{\infty}^{\lambda_{irr}}$ expression suggests that $k_{A \leftrightharpoons B}^{\lambda_{irr}}$ depends on initial concentration as implicitely conveyed by the non-linear factor $\left(1 - 10^{-A_{tot}^{\lambda_{irr}/\lambda_{irr}(0)}}\right)$. Therefore, provided that all other experimental parameters and conditions are kept identical, an increase of the

initial concentration is expected to exert a self-photostabilising effect on the photoreaction rate. On the other hand, the initial velocity of the reaction is also expected to increase with initial concentration as explicitly conveyed by the rate-law equation.

IV.II. Application of the AB(2Φ) kinetic model for the study of montelukast and fluvoxamine photodegradation kinetics

1. Introduction

Photochromic molecules have found wide applications in numerous research areas ranging from photodynamic materials science to photo-nanomedicine (Fomina et al, 2012; Feliciano et al, 2010). Research in targeted drug delivery has recently turned its attention towards triggered drug delivery through the use of stimuli-responsive delivery devices (Fomina et al, 2012; Wohl and Engebersen, 2012; Tomatsu et al, 2011; Feliciano et al, 2010). Within this field, light represents a particularly attractive stimulus that is currently being actively explored since it can be remotely applied and controlled in space and time thereby affording more precise control over drug release site and dosage (Fomina et al, 2012; Tomatsu et al, 2011). A number of advantages are thus procured such as reduction of undesirable side-effects, higher drug levels reaching target sites, enhanced *in vivo* action, reduced drug degradation and precise control over dosage regimen (Fomina et al, 2012; Tomatsu et al, 2011).

In particular, photoreversible, AB(2Φ), systems seem to have acquired considerable interest in the field of photo-responsive systems and have been employed along with light-triggered nanocarriers, photoresponsive hydrogels, polymeric capsules as well as effector

photochromic molecules tethered to specific target receptors (Fomina et al, 2012; Wohl and Engebersen, 2012; Tomatsu et al, 2011; Feliciano et al, 2010). Such systems undergo two reversible photochemical reactions between the mother compound and its isomer (Scheme 1). The interest in these molecules has arisen as a result of their reversible photoreaction properties as they can photo-isomerise between the *cis*- and *trans*- isomeric configurations upon appropriate spectral irradiation. The ensuing conformational change brings about the required result such as drug release from the carrier or receptor switching or silencing. On the other hand, the system can usually revert back to its original form upon a different spectral irradiation rendering this process reversible and repeatable. Examples of photo-isomerisable molecules include azobenzenes, stilbenes and spiropyrans (Tomatsu et al, 2011).

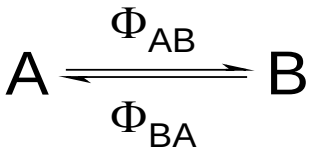

Scheme 1 : Generic photoreaction system of the AB(2Φ) mechanism.

In addition to photo-isomerisable technologies, a number of drugs such as some antipsychotics, tricyclic antidepressants, cephalosporin antibiotics and corticosteroids have been shown to undergo photo-isomerisation in response to light irradiation (Ming, 2012). As a result, most often, the photo-isomerised drug looses its therapeutic efficacy as it switches to its inactive or even toxic conformation.

The wide applications of photo-isomerisable technologies and widespread use of these drugs renders the precise understanding of their photokinetic behaviour and parameters of particular importance. For the purpose of this kinetic modelling and elucidation study, the widely prescribed and photo-isomerisable drugs, montelukast (Monte) and fluvoxamine (Fluvo) have been selected.

Montelukast sodium (Monte), sodium 1-(1(R)-(3-(2-(7-chloro-2-quinolinyl)-(E)-ethenyl)phenyl) 3-(1-hydroxy-1-methylethyl)phenyl)propyl)thio)methyl) cyclopropranе) acetate, is an oral drug used in the treatment of asthma and seasonal allergies (Schoors et al, 1995). It is classed as a leukotriene receptor antagonist since it acts by binding to the cystenyl leukotriene receptor $CysLT_1$ in the lungs and bronchial tubes (Schoors et al, 1995). It thus blocks the action of leukotriene D4 on these receptors and reduces bronchoconstriction and inflammation (Schoors et al, 1995). Fluvo, 2–{[(E)–{5–Methoxy–1–[4–(trifluoromethyl)phenyl]pentylidene} amino]oxy}ethanamine (*E–Fluvo*)., on the other hand, is a selective serotonin (5–hydroxytryptamine, 5–HT) neuronal re–uptake inhibitor (SSRI) used in the treatment of depression and anxiety (Fukui et al., 2014; Figgitt et al., 2000; Benfield et al., 1986).

Both drugs were shown to be photolabile, especially in solution (Smith et al., 2004; Panahia et al., 2014) even at low levels of UV radiation exposure. Their photodegradation follows the *trans-cis* photo-isomerisation mechanism, AB(2Φ), whereby the (*E*)-isomer rotates to the (*Z*)-geometry (Smith et al., 2004; Miolo et al., 2002; Kwon et al., 2005) (Schemes 2&3).

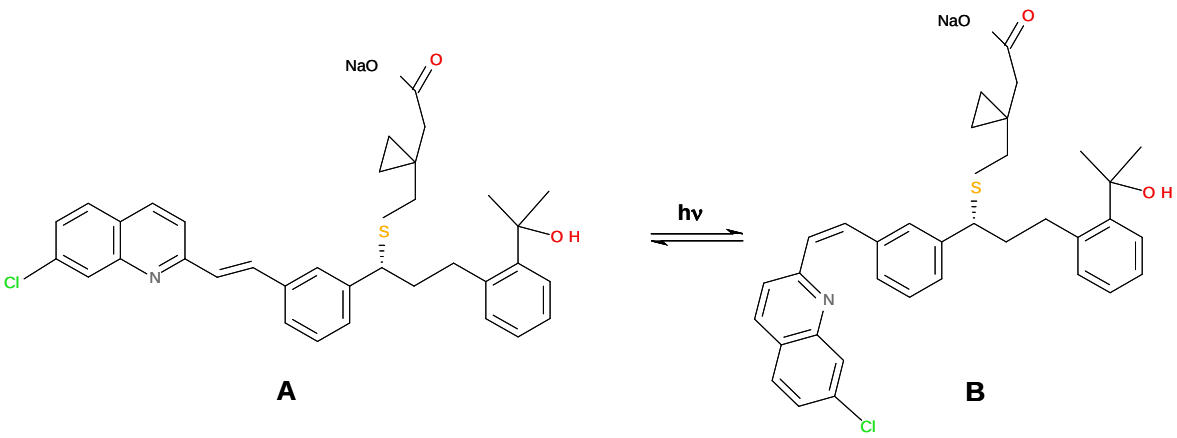

Scheme 2. *Trans* to *cis* Photoisomerism of Monte upon exposure to UV-irradiation.

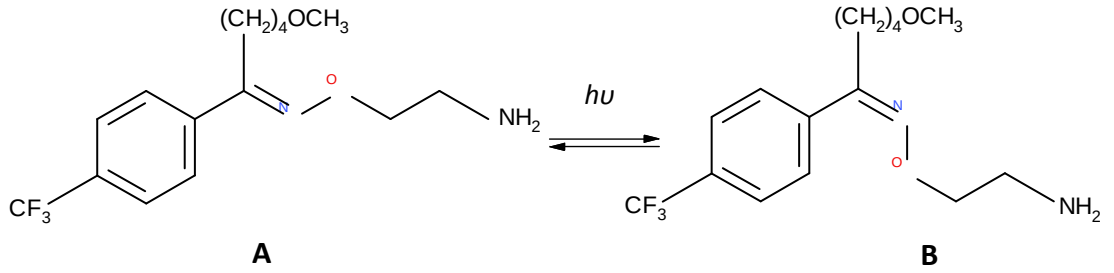

Scheme 3: *E/Z* (Anti/Syn) reversible photoisomerism of *Fluvo* upon exposure to UV–irradiation.

While no phototoxicity has been linked to *Z*–Fluvo photoproduct, it was nonetheless found to be a 150–times less potent than its *E*–counterpart when tested on cortical synaptosomes (Panahia et al., 2014; Iijima et al., 1997). UVB irradiation was found to be responsible for this process and thus *in vivo* photodegradation was also deemed possible as UVB is able to reach blood vessels in the dermis (Miolo et al., 2002). The pharmacological effects of Z-Monte isomer, on the other hand, are currently unknown.

As a result, special handling precautions are warranted for both drugs to avoid exposure to light and subsequent photodegradation. Various strategies have been employed for this purpose such as by using amber glass vials (Zhao et al., 1997), wrapping with black paper (Radhakrishna et al., 2003) or aluminium foil paper (Thibert et al., 1996) and storage in the dark, or analysis under amber/red light conditions (Arison et al., 1999).

Thus far, the kinetics of these systems have been studied using the classical zero or first order thermal kinetics despite a lack of consistency and reproducibility (Roman et al., 2011; Alsarra, 2004; Al Omari et al., 1999) and scarce attempts have been made to determine the photodegradation quantum yields of these as well as other photo-isomerising drugs (Ming, 2012).

Therefore, the aim of this kinetic study is to describe the photokinetic behaviour of Monte and Fluvo in solution by applying the Φ-order semi-empirical integrated rate-law to their experimental kinetic traces. This will, then, allow a full elucidation of the photokinetic parameters of these drugs to be undertaken. Finally, the effects of some photo-absorbing additives on the photodegradation rates of Monte and Fluvo will also be evaluated and quantified using the Φ-order model equations.

2. Results and discussion

2.1. Monte and Fluvo photoreactions

The electronic absorption spectrum of Monte in ethanol is characterised by an intense peak at *ca.* 210 nm and a broad and vibrational transition spanning the 250 – 400 nm UV region due to a $\pi \rightarrow \pi^*$ transition of the conjugated double bond system around which isomerisation takes place. The spectral evolution of the solution when exposed to a continuous monochromatic irradiation (figure 4) shows an increase and a decrease of the absorbances in the 200-258 nm and 258-400 nm regions, respectively with a single isosbestic point at λ_{isos} = 258 nm. This indicates that *trans* and *cis* Monte isomers spectra totally overlap and share the same overall shape of the absorption spectra with no new spectral features appearing. These findings also suggest that the reaction is quantitative and proceeds without by-products.

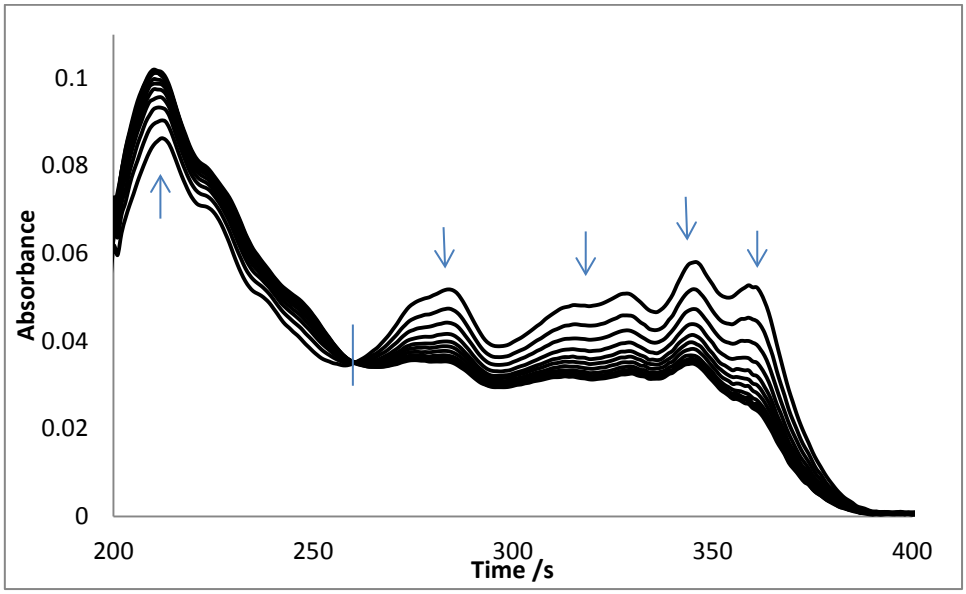

Figure 4: Evolution of the electronic absorption spectra of 1.85×10^{-6} M Monte in ethanol subjected to a continuous irradiation with a 360 nm monochromatic beam (total irradiation time 700 s at a radiant power of P_{360} = 9.86 x 10^{-7} einstein.s^{-1}.dm^{-3}). The arrows indicate the direction of the peaks' evolution during the photoreaction and the vertical line crosses the spectra at the isosbestic point.

The native electronic absorption spectrum of *E–Fluvo* isomer is characterised by two main absorption bands of 200–226 nm and 226–320 nm spanning the UVC and UVB regions. This molecule absorbs mainly in the UVB region of the spectrum as is the case for non–conjugated oximes, with the long wavelength absorption transition having a $\pi \rightarrow \pi^*$ character (Gilbert and Bagott, 1991). When exposed to a monochromatic irradiation within that region, the absorbance of the solution decreases in the regions of 200–215 nm and 226–285 nm and increases in the absorbance bands of 215- 226 nm and 285-320 nm. The clearly defined isosbestic points at 215, 226 and 285 nm and the smooth evolution of the spectra indicate that the photoreaction is quantitative and proceeds without by–products. The spectra of the two isomers overlap and share a similar overall shape with a 40 % maximum variation in absorbance observed at *ca.* 245 nm (figure 5).

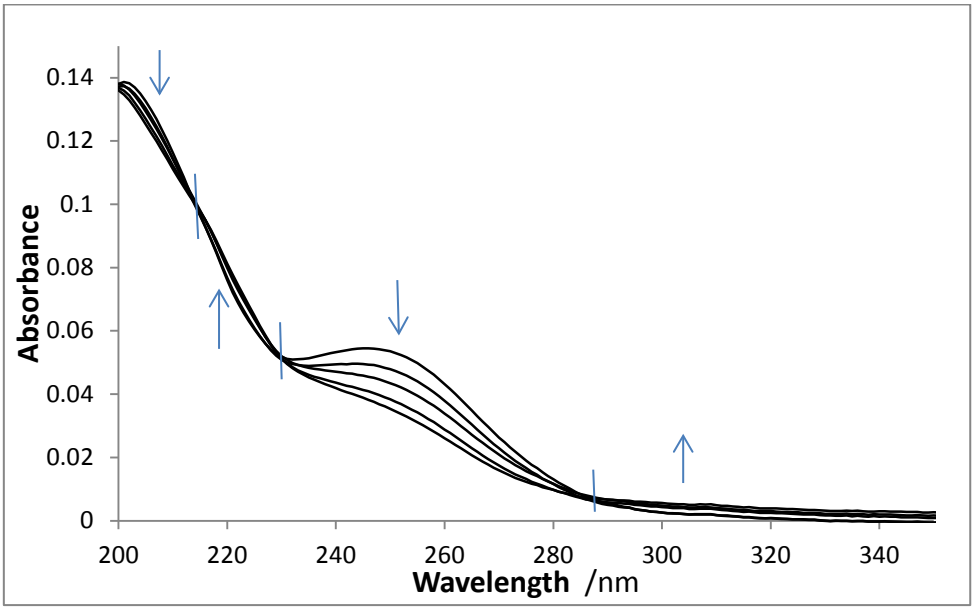

Figure 5: Evolution of the electronic absorption spectra of 4.01 x 10^{-6} M *Fluvo* in water subjected to steady state irradiation with a 270–nm monochromatic beam (total irradiation time 26 min at a radiant power of 7.37 x 10^{-7} einstein.s^{-1}.dm^{-3}). The arrows indicate the direction of the absorbance evolution during the photoreaction and the vertical lines cross the spectra at the isosbestic points (215, 226, 285 nm).

2.2. Elucidation of Monte/Fluvo photodegradation kinetics

Thus far, the photo-degradation of Monte has generally been studied in organic media by monitoring the variation of its concentration by HPLC (Roman et al., 2011; Al Omari et al., 2007; Alsarra, 2004). The kinetic data have been treated with thermal kinetic equations with little or no justification as to why a particular order was ascribed. Monte photodegradation was described by the first order kinetics in early studies (Al Omari et al., 2007; Alsarra, 2004) and the zero-order kinetics in a more recent study (Roman et al., 2011). The latter was based on the generation of three plots by attempting a 0, 1^{st}- and 2^{nd}-orders kinetics fitting and an evaluation of the highest correlation coefficients of the graphs fitting. The highest correlation coefficient was recorded for the zero-order fitting of the kinetic data (r^2 = 0.996). Nevertheless, a first-order kinetics could also have been proposed since the corresponding correlation coefficient was almost as high (r^2 values of 0.9937).

The photodegradation kinetics of *Fluvo* were attributed the pseudo–first order kinetics under fluorescent lamp irradiation with a beam's bandwidth of 110 nm, ranging between 290–400 nm with maximum emission at 312 nm and differing half–life times were recorded depending on the spectral output of the irradiation sources (Miolo et al., 2002, Kwon et al., 2005).

The lack of photokinetic studies and the conflicting photoreactions orders ascribed to the same molecule in the literature are widely encountered in the area of drugs

photodegradation kinetics. The cases of benzydamine hydrochloride and ketrolac thromethamine (Piechocki and Thoma, 2010) represent another example where each of the data sets were well fitted with both zero- and first-order kinetics.

In the following study, solutions of Monte in ethanol and Fluvo in water were exposed to various monochromatic irradiation wavelengths spanning their absorption spectra (i.e. 220, 258, 284, 328, 345 and 360 nm for Monte and λ_{irr} = 290, 285, 280, 270, 260, 245, and 226 nm for Fluvo). In each case, the kinetic trace of the degradation was recorded at observation wavelengths of λ_{obs} = 345 nm and λ_{obs} = 245 nm, for Monte and Fluvo, respectively, that correspond to the most extensive variation of the absorbance (figures 4 and 5). The kinetic traces followed a smooth decrease at these observation wavelengths, eventually reaching a plateau region. This behaviour corresponds to the AB(2Φ) mechanism proposed for both drugs.

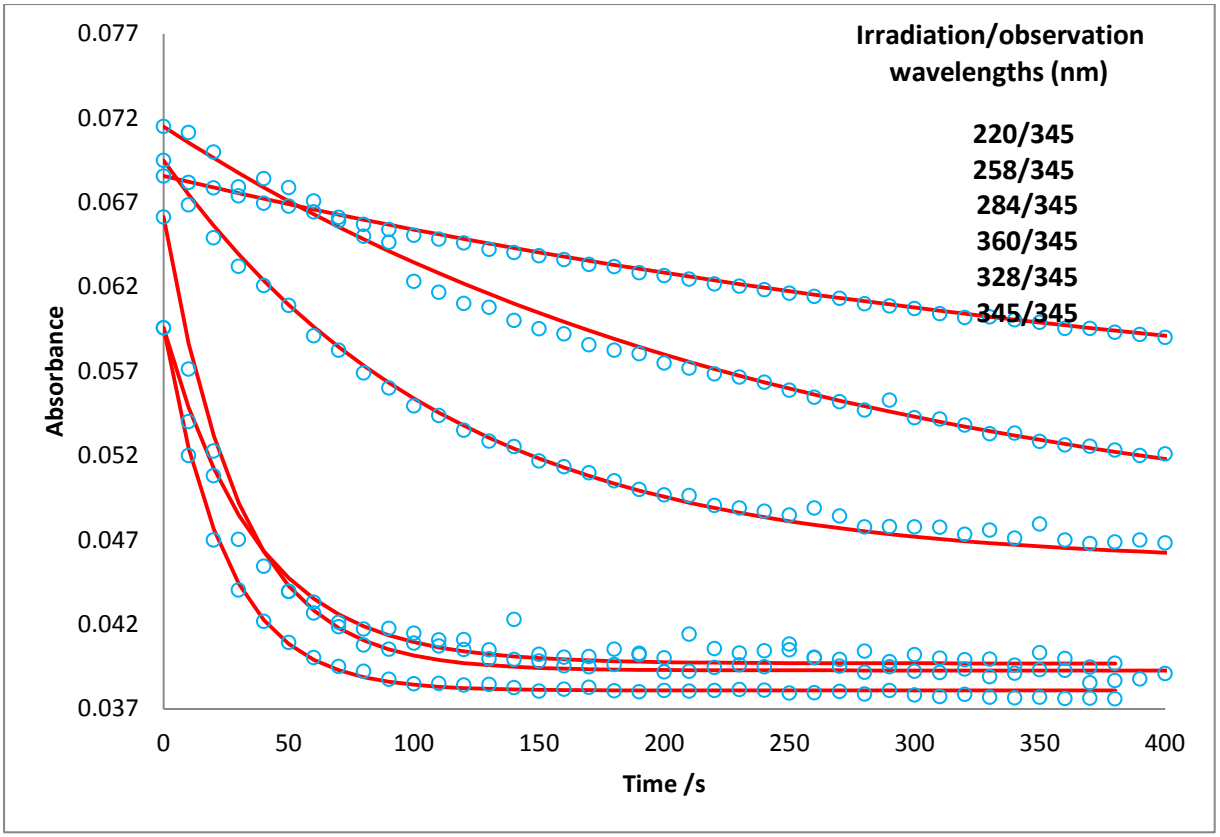

Figure 6: The photokinetic traces of Monte in ethanol (1.85 x 10^{-6} M) at λ_{irr}= 220, 258, 284, 360, 328 and 345 nm and observed at λ_{obs} = 345nm. The circles represent the experimental data while the lines represent the fitting traces using eq.10.

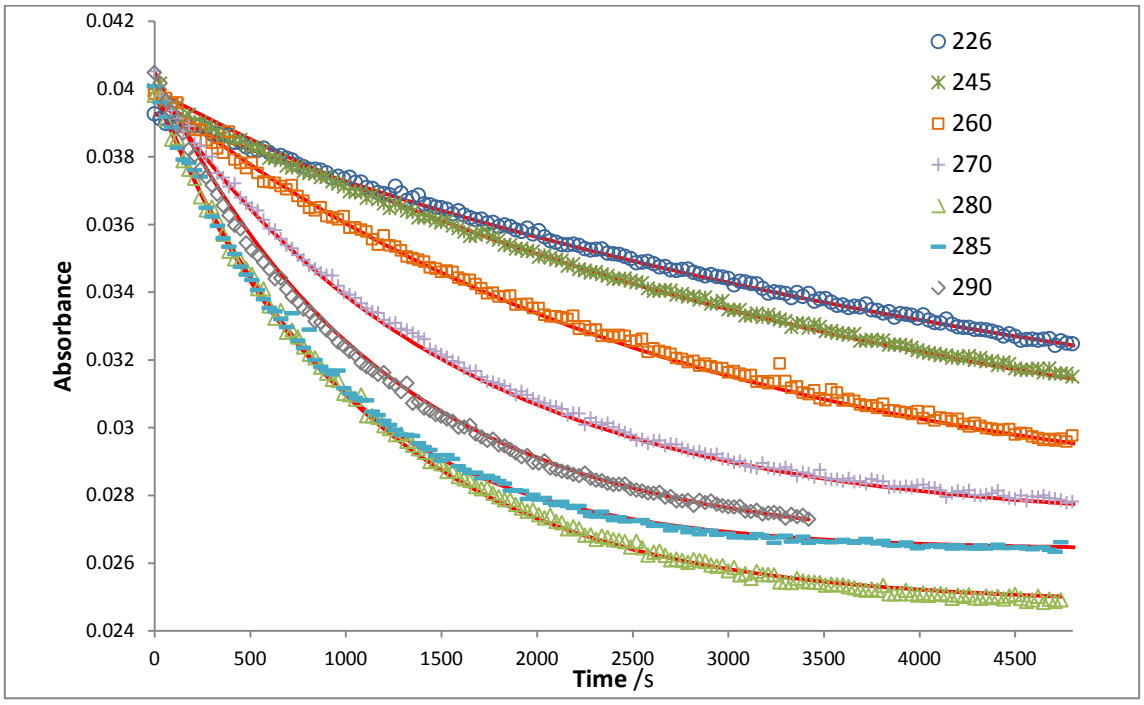

Figure 7: The photokinetic traces of *Fluvo* photodegradation in water (2.95 x 10^{-6} M) at λ_{irr} = 226, 245, 260, 270, 280, 285 and 290nm and observed at λ_{obs}= 245nm. The geometric shapes represent the experimental data while the continuous lines represent the model fitted traces using the appropriate model equation.

The experimental traces were all accurately fitted by eq.10 (figures 6 and 7), indicating that Monte and Fluvo photodegradation follow the Φ-order kinetics.

Table 2: Overall photoreaction rate-constants and kinetic parameter values of Monte for a set of monochromatic irradiations performed in ethanol at 22°C.

$\boldsymbol{\lambda_{irr}}$ **/nm**	$\boldsymbol{A_{tot}^{\lambda_{irr}/345}(0)}$	$\boldsymbol{P_{\lambda_{irr}}}$ **/einstein.** $\mathbf{s^{-1}.dm^{-3}}$	$\boldsymbol{A_{pss}^{\lambda irr}(\infty)}$	$\boldsymbol{k_{NIF}^{\lambda_{irr}}}$ **/s^{-1}**
220	0.068	8.009 x 10^{-7}	0.088	0.0021
258	0.071	6.362 x 10^{-7}	0.044	0.0039
284	0.069	6.932 x 10^{-7}	0.043	0.0092
328	0.060	1.187 x 10^{-6}	0.033	0.028
345	0.060	1.428 x 10^{-6}	0.038	0.042

360	0.066	1.332 x 10^{-6}	0.026	0.035

The overall rate-constants obtained from the fitting of the traces (table 2), suggested that photoreaction rate increase with wavelength. Nonetheless, the rate-constant values must be considered with caution because they cannot be directly compared for the present experiments, since they depend on both spectral, reactivity and experimental conditions used, as expressed in eq.11. This limits the utility of the experimentally determined AB(2Φ) reactions' rate-constants especially when polychromatic light and/or first-order kinetics are employed. Hence, it is becomes necessary to determine more informative photoreactions parameters such as the individual photochemical quantum yield values at different wavelengths.

The elucidation of Monte and Fluvo kinetics amounts to the determination of the three system unknowns, namely the forward ($\Phi^{\lambda}_{A\rightarrow B}$) and reverse ($\Phi^{\lambda}_{B\rightarrow A}$) quantum yields, and the spectrum of the photoproduct ($\varepsilon^{\lambda}_{B}$). These parameters cannot be determined from the kinetic traces alone because the useful equations (mainly eqs. 10, 11 and 16) cannot be solved for the three aforementioned parameters due to the fact that these equations, even though linearly-independent, are non-linear. Accordingly, it is necessary to use further data, obtained through an alternative analytical technique, in addition to the electronic absorption spectra. The three-step elucidation method proposed above for AB(2Φ) reactions was hereby adopted.

2.3. Elucidation of Monte and Fluvo photokinetics

2.3.1. Determinaltion of the equilibrium constant at an isosbestic irradiation ($K_{\leftrightharpoons}^{\lambda_{isos}}$)

When irradiating the sample solution at an isosbestic wavelength, ($\lambda_{irr} = \lambda_{isos}$), the reaction photokinetic traces follow the first-order kinetics according to the corresponding integrated rate-law eq. 1. Determination of the isomers concentrations at equilibrium by HPLC allows us the determination of the equilibrium constant ($K_{\leftrightharpoons}^{\lambda_{isos}}$) of the photoreaction undertaken at the isosbestic wavelength. This value can then serve in the determination of the photoproduct absorption coefficients at all wavelengths (i.e. the isomer's spectrum).

To this end, E-Monte ethanolic and E-Fluvo aqueous solutions were subjected to a 258 and 226 monochromatic isosbestic irradiations, respectively. The photoreactions were monitored by HPLC and the corresponding E- and Z- isomers concentrations traces were fitted with the integrated rate-law equation 1. This allowed the determination of the rate–constant $k_{A\leftrightharpoons B}^{\lambda_{isos}}$, as well as the *pss* concentrations of the reactive species and hence the respective equilibrium constants $K_{A\leftrightharpoons B}^{\lambda_{isos}}$ for Monte and Fluvo photodegradation at these wavelengths (figures 8 & 9, table 3).

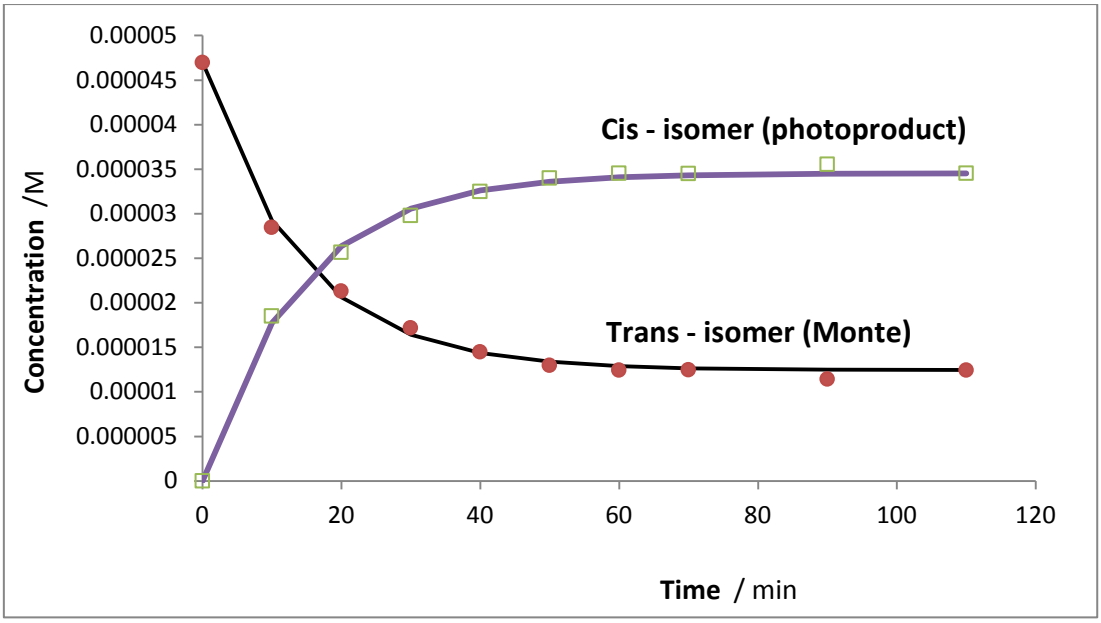

Figure 6: Evolution of Monte concentration over photodegradation time and formation of the *cis*-isomer photoproduct monitored by HPLC upon exposure to isosbestic monochromatic irradiation of 258 nm (P_{258}= 6.43 x 10^{-7} einstein.s^{-1}.dm^{-3}).

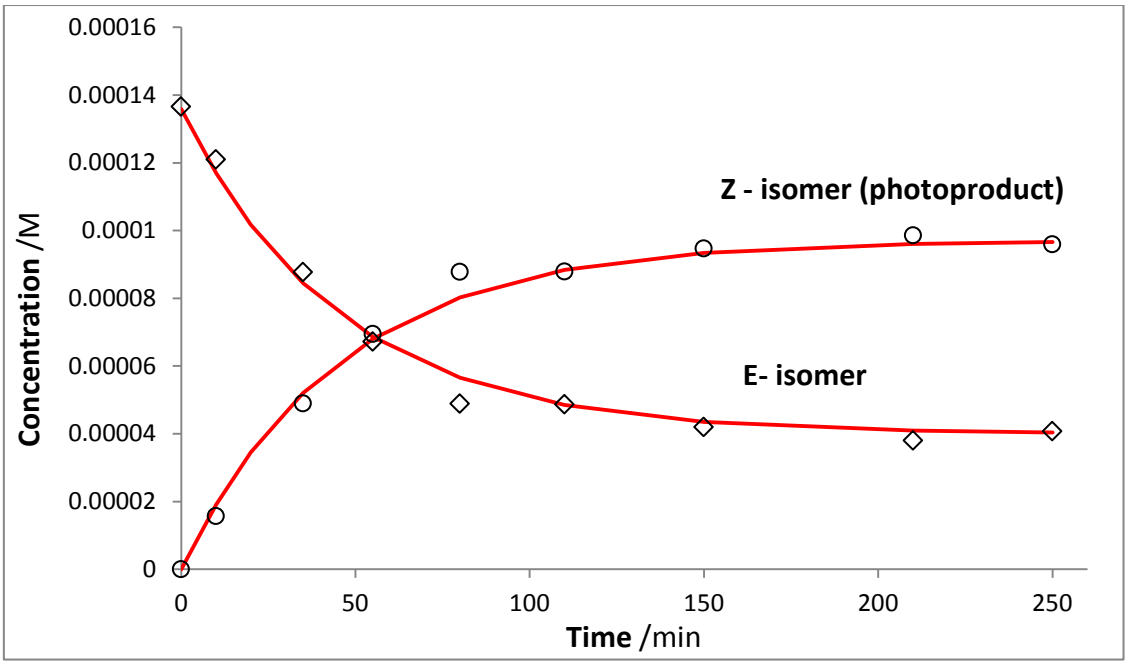

Figure 7: Change in aqueous *E*–*Fluvo* solution (1.37 x 10^{-4} M) and its *Z*–isomer photoproduct concentrations over 4 hours upon exposure to an isosbestic monochromatic irradiation of 226 nm (P_{226}= 1.88 x 10^{-6} einstein.s^{-1}.dm^{-3}) as monitored by HPLC.

All kinetic traces were accurately fitted with eq. 1 (figures 6 & 7). This allowed the determination of the overall reaction rate-constant ($k_{A\leftrightarrows B}^{\lambda_{isos}}$) as well as the initial velocity using the elucidation method described above.

The absolute value of the forward quantum yield ($\Phi_{A\rightarrow B}^{\lambda_{isos}}$) can readily be determined from eq.7. This value ($\Phi_{A\rightarrow B}^{\lambda_{isos}}$) in combination with eq.4, leads to the determination of the value of the reverse quantum yield at the isosbestic point ($\Phi_{B\rightarrow A}^{\lambda_{isos}}$). As a result, the ratio of the species concentrations at *pss* for the isosbestic irradiation ($\mathrm{K}_{\leftrightarrows}^{\lambda_{isos}}$) is given by

$$\mathrm{K}_{\leftrightarrows}^{\lambda_{isos}} = \frac{C_B(pss)}{C_A(pss)} = \frac{\Phi_{A\rightarrow B}^{\lambda_{isos}}}{\Phi_{B\rightarrow A}^{\lambda_{isos}}} = \frac{k_1}{k_2} \qquad (eq.31)$$

The results shown in table 3 indicate that the *E*–Monte and -Fluvo isomers are more than twice as photoefficient as their respective *Z*–isomer counterparts, as indicated by the value of $\mathrm{K}_{\leftrightarrows}^{\lambda_{isos}}$, which resulted, in a higher proportion of the *Z*–isomers at *pss*. While in thermal chemistry, the E-isomers are normally formed in higher yields than the Z-isomers due to the more stable lowest energy configuration of the former, in photochemistry, E *to Z* isomerisation is much more efficient. This is due to the formation of a different excited-state intermediate with a different dipole moment and electronic configuration than the ground state, hence the different excited-state chemistry (Beijersberge Van Henegouwen, 1997). Furthermore, the reverse photoreaction steps occur via a different excited-state

intermediate whereby, in the solvents used, the *E* intermediate is more stabilised than its *Z* counterpart (Beijersberge Van Henegouwen, 1997). Furthermore, *E* isomers are usually associated with higher absorption coefficients than their counterpart. Consequently, the E-Z photo-isomerisation process is more efficient than the reverse process and occurs at longer wavelengths (Neckers et al., 1995; Singh, 2005).

Table 3: Overall rate–constant and equilibrium constant for the photodegradation of an aqueous *Fluvo* solution (1.37 x 10^{-4} M) exposed to isosbestic monochromatic irradiation at 226 nm, as monitored by *HPLC.*

λ_{isos} /nm	$A_0^{\lambda_{isos}}$	$C_0^{\lambda_{isos}}$ / M	$l_{\lambda_{isos}}$ / cm	$l_{\lambda_{obs}}$ / cm	$C_A(pss)$ / M	$C_B(pss)$ / M	$P_{\lambda_{isos}}$ /einstein.s^{-1}.dm^{-3}	$k_{A\leftrightharpoons B}^{\lambda_{isos}}$ / s^{-1}	$K_{A\leftrightharpoons B}^{\lambda_{isos}}$
226	2.41	1.37x10^{-4}	1	1	4.07x10^{-5}	9.59x10^{-5}	1.88x10^{-6}	3.83x10^{-4}	2.35
258	0.92	4.7x10^{-5}	2	1	1.24 x10^{-5}	3.45x10^{-5}	6.43x10^{-7}	1.17x10^{-3}	2.75

2.3.2. Recovery of the isomer's absorption spectrum

The reconstruction of the whole spectrum of the *cis*-isomer is the second step of the elucidation method. This can be achieved by conducting the above isosbestic monochromatic irradiation of the drugs using lower initial concentrations in order to allow UV/Vis spectrophotometric

monitoring of the photoreaction. The previously determined, concentration-independent, equilibrium constant, $K_{\rightleftharpoons}^{\lambda_{isos}}$, at these wavelengths together with the total absorbance spectrum of the medium at pss $A_{tot}^{\lambda_{isos}/\lambda_{obs}}(pss)$ enable the determination of the absorption coefficients of the photoproduct isomer using eq. 26 (figures 8 and 9);

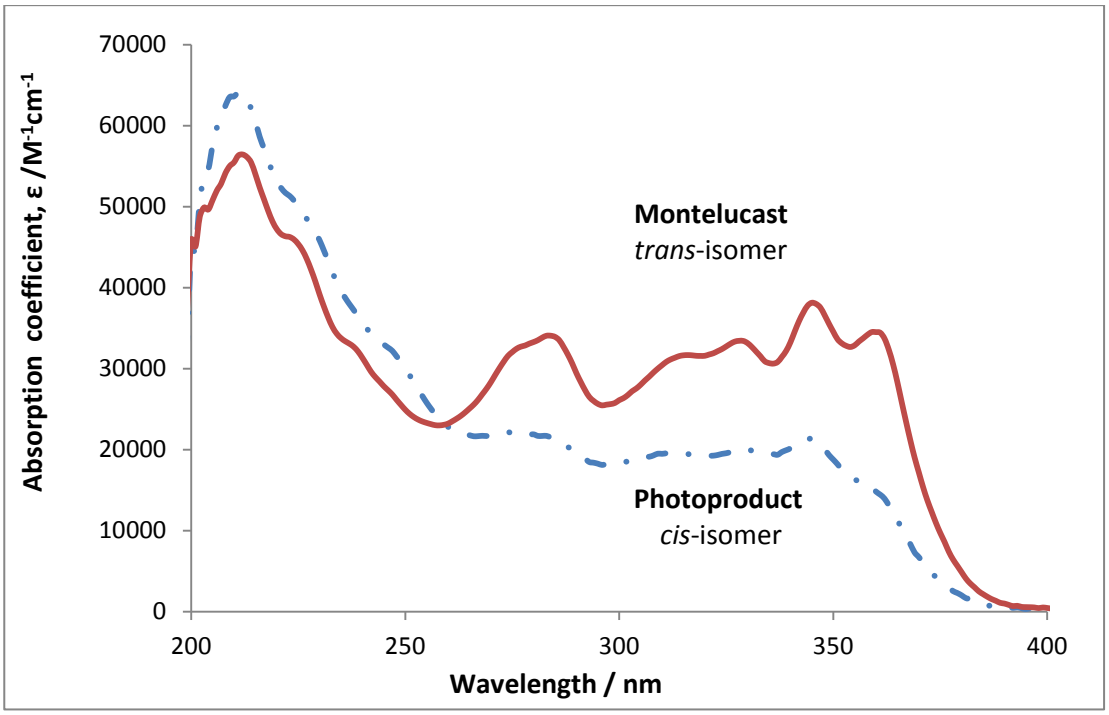

Figure 8: Electronic absorption spectra (expressed as absorption coefficient units) of Monte and its *cis*-isomer photoproduct.

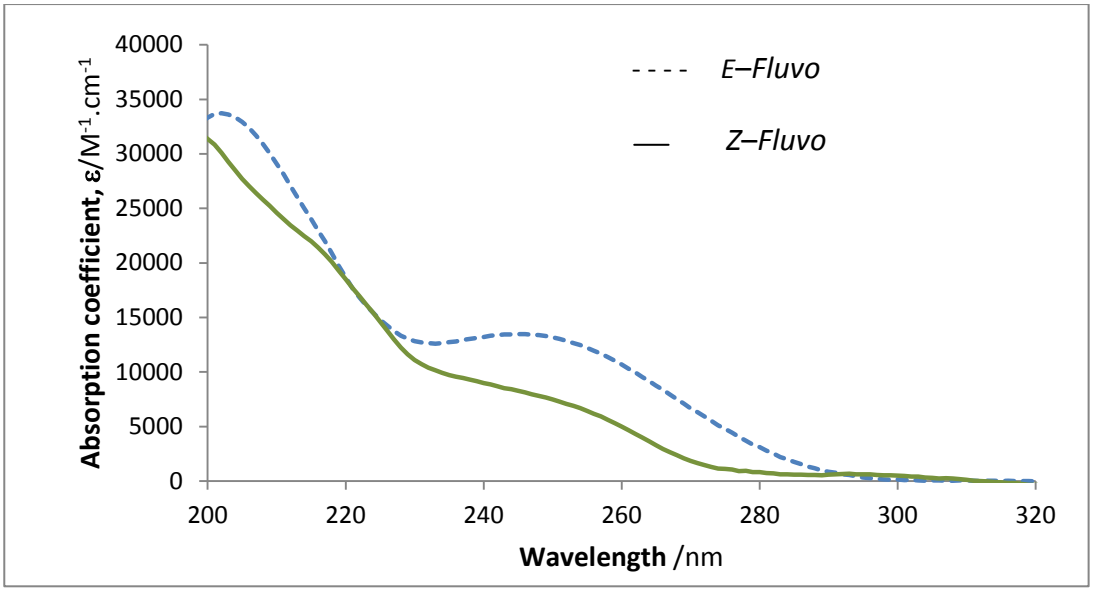

Figure 9: Electronic absorption spectra (expressed as absorption coefficient units) of *E*– (native) and *Z–Fluvo (photoproduct)*.

2.3.3. Isomers' quantum yields at any irradiation wavelength

Determination of the absorption coefficients of the Cis-isomer at any wavelength allows the determination of the forward and reverse photochemical quantum yields of the photoisomerisation process in the final step of the kinetic elucidation from equations 15, 16 and 11, (tables 5 and 6).

Table 5: Quantum yields, overall rate-constant, absorption coefficient and initial velocity values for Monte photodegradation reactions under various monochromatic irradiations.

λ_{irr} /nm	$A_{Monte}^{\lambda_{irr}/345}(0)$	$P_{\lambda_{irr}}$ /einstein. $s^{-1}.dm^{-3}$	$A^{\lambda irr}(pss)$	$k_{Monte}^{\lambda_{irr}}$ /s^{-1}	$v_{0\,(mod.)}^{\lambda_{irr}/\lambda_{obs}}$ / s^{-1}	$\varepsilon_{Trans}^{\lambda_{irr}}$ / $M^{-1}cm^{-1}$	$\varepsilon_{Cis}^{\lambda_{irr}}$ / $M^{-1}cm^{-1}$	$F^{\lambda_{irr}}(0)$	$\Phi_{A\to B}^{\lambda_{irr}}$	$\Phi_{B\to A}^{\lambda_{irr}}$
220	0.068	8.009×10^{-7}	0.088	0.0021	-3.51×10^{-5}	47235	53121	1.910	0.012 ± 0.0011	0.0033 ± 0.0004

258	0.071	6.362 x 10^{-7}	0.044	0.0039	-7.2x10^{-5}	23003	23762	1.999	0.065 ± 0.0007	0.024 ± 0.0057
284	0.069	6.932 x 10^{-7}	0.044	0.0092	-0.00021	34076	21517	1.999	0.072 ± 0.0046	0.039 ± 0.0063
328	0.060	1.187 x 10^{-6}	0.033	0.028	-0.00054	33446	19988	2.055	0.145 ± 0.0121	0.061 ± 0.0282
345	0.060	1.428 x 10^{-6}	0.038	0.042	-0.00086	38149	21345	2.014	0.16 0± 0.0125	0.060 ± 0.0034
360	0.066	1.332 x 10^{-6}	0.026	0.035	-0.0009	34519	14823	2.003	0.180 ± 0.0129	0.021 ± 0.0068

Table 6: Quantum yields, overall rate–constant, absorption coefficient and initial velocity values for *Fluvo* photodegradation reactions under various monochromatic irradiations, as determined by the Φ–order kinetics.

λ_{irr} /nm	$A_{Fluvo}^{\lambda_{irr}/245}(0)$	$P_{\lambda_{irr}}$ /einstein. $s^{-1}.dm^{-3}$	$A^{\lambda irr}(pss)$	$k_{A\leftrightharpoons B}^{\lambda_{irr}}$ /s^{-1}	$v_{0\,(mod.)}^{\lambda_{irr}/\lambda_{obs}}$ / s^{-1}	$\varepsilon_A^{\lambda_{irr}}$ / $M^{-1}cm^{-1}$	$\varepsilon_B^{\lambda_{irr}}$ / M^{-1} cm^{-1}	$F^{\lambda_{irr}}(0)$	$\Phi_{A\to B}^{\lambda_{irr}}$	$\Phi_{B\to A}^{\lambda_{irr}}$
226	0.0393	6.09 x 10^{-7}	0.0420	0.000197	-2.20x10^{-6}	14254	13802	2.086	0.00383 ± 0.00003	0.00157 ± 0.00027
245	0.0399	5.86 x 10^{-7}	0.0281	0.000268	-3.09x10^{-6}	13478	8273	2.095	0.00612 ±0.00042	0.0038 ± 0.001331
260	0.0398	4.60 x 10^{-7}	0.0191	0.000380	-4.56 x10^{-6}	10687	4997	2.14	0.0128 ± 0.00064	0.0085 ± 0.00096
270	0.0405	5.21 x 10^{-7}	0.0109	0.000670	-8.31 x10^{-6}	6679	1859	2.19	0.0361 ± 0.00195	0.025 ± 0.0035
280	0.0398	5.51 x 10^{-7}	0.0031	0.000875	-1.28 x10^{-5}	3109	829	2.25	0.0931± 0.00275	0.0535±0.0127
285	0.0400	4.70 x 10^{-7}	0.0031	0.00048	-1.32 x10^{-5}	1774	586	2.27	0.2167 ± 0.0059	0.0844 ± 0.0075
290	0.0402	2.56 x 10^{-7}	0.0028	0.00152	-6.69 x10^{-6}	859	596	2.28	0.4349 ± 0.0205	0.0573 ± 0.0184

The results in tables 5 and 6 show that $\Phi_{A\rightarrow B}^{\lambda_{irr}}$ for the E-Z isomerisation increases with increasing irradiation wavelength and is higher than the reverse quantum yield at all irradiation wavelengths. For Fluvo, the most pronounced variation of the quantum yield ratios ($1.4 > \Phi_{A\rightarrow B}^{\lambda_{irr}}/\Phi_{B\rightarrow A}^{\lambda_{irr}} > 7.6$) is situated in the longest wavelength, 280 to 290 nm, region (ranging between 1.7 and 7.5), whereas, a much more modest change in $\Phi_{A\rightarrow B}^{\lambda_{irr}}/\Phi_{B\rightarrow A}^{\lambda_{irr}}$ is observed in the region 245-280 nm ($1.4 > \Phi_{A\rightarrow B}^{\lambda_{irr}}/\Phi_{B\rightarrow A}^{\lambda_{irr}} > 1.7$).

The quantum yield values recorded for Fluvo are relatively higher than those reported in the literature for Fluvo in different aqueous media (1.87×10^{-3} to 8.55×10^{-3}) when irradiated using a fluorescent lamp with a beam's bandwith of 110 nm ranging between 290 and 400 nm. This, however could be due to the use of non-monochromatic light and the contribution of shorter wavelengths which would result in lower average quantum yield values (Kwon et al., 2005).

A plot of $\Phi_{A\rightarrow B}^{\lambda_{irr}}$ values against λ_{irr} shows linear (eq. 32) and sigmoidal relationships (eq. 33) between these parameters for Monte and Fluvo, respectively (figure 10).

$$\Phi_{A\rightarrow B,Monte}^{\lambda_{irr}} = 0.0012\times \boldsymbol{\lambda_{irr}} - 0.2555 \quad \text{(eq. 32)}$$

$$\Phi_{A\rightarrow B,Fluvo}^{\lambda_{irr}} = \frac{1}{0.07 + 400 \times \mathrm{e}^{-(0.13\times(\boldsymbol{\lambda_{irr}}-250))}} \quad \text{(eq. 33)}$$

These correlations allow the determination of quantum yield values of Monte and Fluvo at any wavelength in their respective solvents.

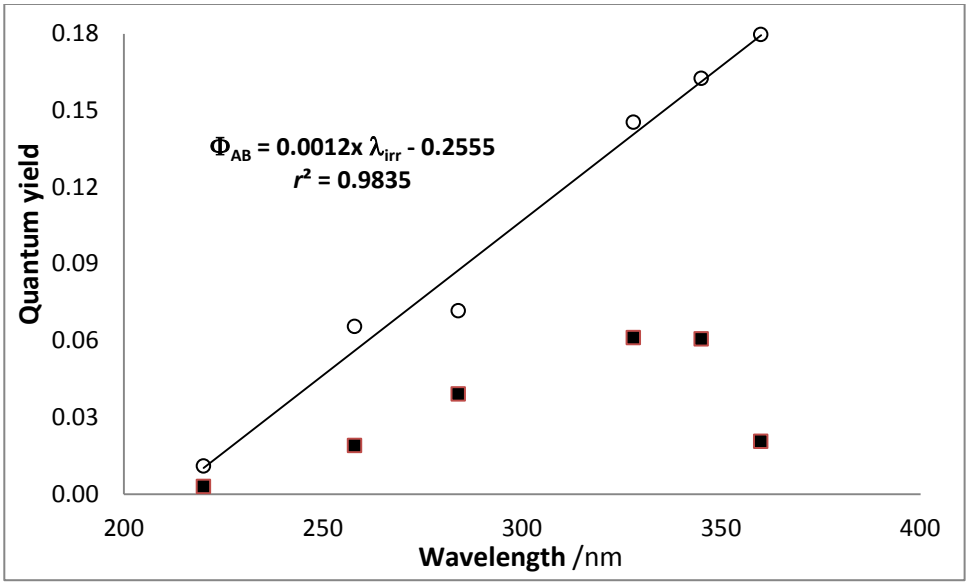

Figure 10: Average forward ($\Phi_{A\rightarrow B}^{\lambda_{irr}}$) (circles) and reverse ($\Phi_{B\rightarrow A}^{\lambda_{irr}}$) (plain squares) quantum yields for Monte photodegradation, calculated for irradiation wavelengths 220, 258, 285, 328, 345 and 360 nm.

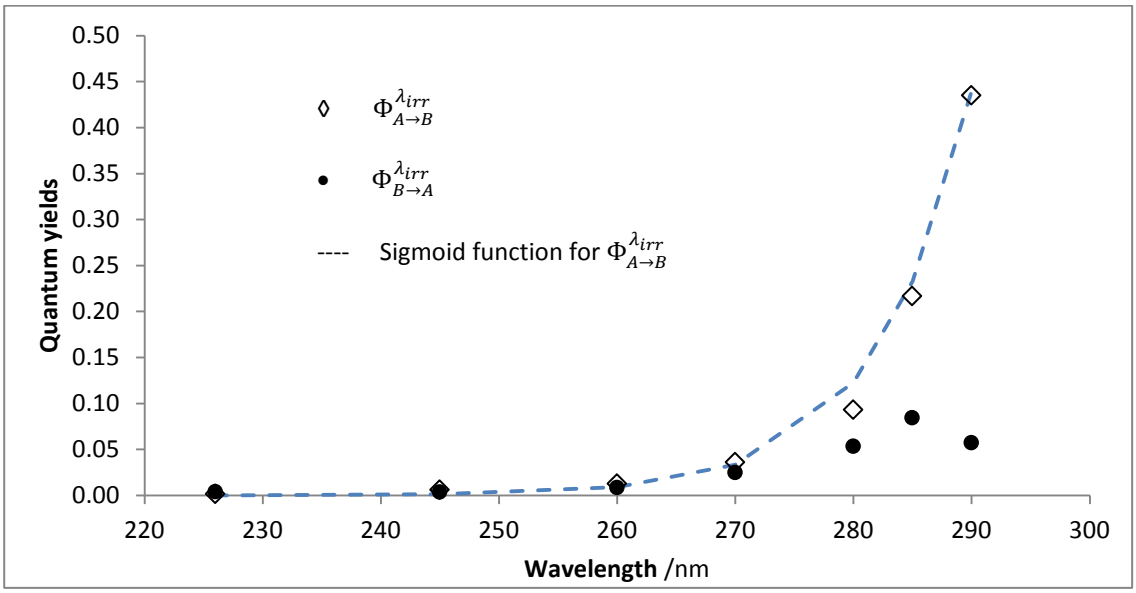

Figure 11: Average forward ($\Phi_{A\rightarrow B}^{\lambda_{irr}}$) (diamonds) and reverse ($\Phi_{B\rightarrow A}^{\lambda_{irr}}$) (plain circles) *Fluvo* quantum yields for irradiation wavelengths 226, 245, 260, 270, 280, 285 and 290 nm.

The reverse quantum yields, on the other hand, follow a concave pattern with irradiation wavelength (Figs.10 and 11), and a 3 and 54–fold maximum span of variation was recorded for Monte and Fluvo $\Phi_{B\rightarrow A}^{\lambda_{irr}}$ values, respectively; whereas a 15 and 114 variation span was recorded for their respective forward quantum yield values. The differing magnitude of photo–efficiencies between *E*– and its *Z*–*Fluvo* isomer suggests a difference in the excited–states associated with each species. The more pronounced difference between the isomers' quantum yields that was recorded in the longest wavelength region indicates that the excited–sate of lowest energy is much more efficient for *E*– than for *Z*–*isomers.* This is likely to be due to the more stable excited-state configuration associated with the E-isomer configuration which favours this transition process. Furthermore, the oxime group within *E*–*Fluvo* was twice as photochemically efficient as the ethene bond in the stilbene–like Montelukast ($\Phi_{A\rightarrow B}^{\lambda_{irr}}$ = 0.012–0.18). This implies a trend of higher forward quantum yield values for lower–energy excited–states and could also indicate that the lowest energy $n\rightarrow\pi^*$ transition has a higher contribution in the photoisomerisation process than the $\pi\rightarrow\pi^*$ for Fluvo. Overall, *these* results indicate that not only the chemical nature, the geometry of the molecule but also the irradiation conditions impact the drugs photochemical behaviour.

The above results also indicate that (i) the UVA and UVB regions of the spectrum, respectively are the most efficient causative spectral range for Monte and Fluvo photodegradation; (ii) the E-Z photo-isomerisation process is more efficient than the reverse photoreaction; and (iii) that photoreactions quantum yields are, *a priori*, wavelength-dependent.

Pharmaceutically, the photoreversibility of these reactions has the advantage of limiting the depletion of the initial active ingredient to the amounts recorded at the *pss*, however, the more pronounced E-Z isomerisation as a favoured photoprocess especially at longer wavelengths of the drug's absorption spectrum would result in a significant decrease in active ingredient concentration, which may lead to a diminution or loss of therapeutic efficacy and/or even phototoxicity.

This kinetic elucidation method is the first kinetic-based method for the determination of the absolute values for AB(2Φ) forward and reverse quantum yield values at any monochromatic irradiation wavelength. The quantum yield of a given reaction has, traditionally, been calculated by dividing the number of reacted drug molecules (most often obtained by chromatography), by the number of absorbed photons, or radiant power, determined for the light-source (Ricci et al, 2003; Ricci et al 2001). However, this approach presents some important limitations since not only the initial drug-molecule but also its photoproducts and the products thermally- or photochemically-generated from the photoproducts themselves, can all contribute to the absorption of the incident photons of the light-source. Therefore, the actual number of photons absorbed by the initial drug-molecule is, in actual facts, less than the radiant power received by the sample. Furthermore, the classical approach yields a unique (average) quantum yield value for the whole reaction and does not distinguish between the individual (additional) photoreaction steps that may be involved in the overall photodegradation process. It also assumes a monochromatic excitation irradiation and/or a wavelength-independent quatum yield while in actual facts, the quantum yield is often wavelength-dependent as was previously shown

and the excitation beam encompasses the contribution of several wavelengths despite the use of filters in an attempt to narrow down the incident wavelength range. ,

Therefore, kinetic methods as the one presented here, represent a more reliable and accurate alternative for the determination of the quantum yields of photoreaction systems, since the integrated rate-laws and the overall rate-constant equations implicitly take into account not only the various individual photochemical reaction-steps but also and more importantly the absorption contribution of the various species involved thereby circumventing the limitations associated with the classical approach.

These results stress out the usefulness and necessity of a full kinetics elucidation of drug photodegradation. They also confirm that reliable conclusions about the photoreactivity of a compound can only be reached, as suggested earlier, when using monochromatic irradiation coupled to a treatment using the Φ–order kinetics.

These findings strongly suggest that the current ICHQ1b guidelines would benefit from introducing recommendations on the photostability assessment of drugs at low concentrations in solution as well as the implementation of a standardisable, specific and accurate photokinetic analytical approach, like the one proposed above. Such data would not only shed light on the photokinetic behaviour and photodegradation parameters of the drug under ambient lighting conditions but may also lay down a platform for an understanding of the drugs behaviour *in vivo* since drugs systemic distribution in patients'

skin and eyes occurs mostly at low concentration within biological fluids and tissues (Ferguson and Dover, 2006). This is further emphasised in the ICH S10 document on the photosafety testing of pharmaceuticals where a maximum substrate concentration of 100 μg/ml is recommended, in addition to using several dilutions during the testing procedure (ICH S10, 2013). Furthermore, low concentration studies become even more important given the fact that the rate of photodegradation of drugs increases with lower concentration (as encountered *in vivo*), as demonstrated theoretically (by the Φ–order kinetics) and experimentally. These findings can also explain the reasons underlying topical and systemic drug-induced phototoxicity reactions reported in numerous studies on all age-groups (Kutlubay et al., 2014; Arnold et al., 2014; Feldmeyer et al., 2013; Drucker and Rosen, 2011).

Furthermore, moderate and even low intensity irradiation levels were shown to cause significant photodegradation, as shown in these studies. Such irradiation levels closely corroborate the irradiation levels likely to be encountered by the drugs systemically. The ICH S10 also recommends an irradiance dose of approximately 5J/cm^2 UVA doses for the *in vitro* 3T3 Neutral Red Uptake phototoxicity test (3T3 NRU PT) to corroborate natural irradiation conditions comparable to those obtained during prolonged outdoor activities on summer days around noon time, in temperate zones and at sea levels (ICH S10, 2013).

Therefore, the conditions of the present study are likely to mimic the conditions to which drugs are exposed in the body since small concentrations (ca**.** 1.28 μg/ml) and low radiation power (1-1.8 J/h/cm^2) are employed. The use of photokinetic studies using low drug concentration studies in solutions and low/moderate irradiation levels in conjunction with

an accurate, specific and quantitative photokinetic data treatment method, like the Φ–order kinetic approach, would represent a strong initial assessment platform, that provides reliable data about the inherent photoreactivity of a molecule in solution, that would feed in the evaluation of drugs' photosafety and photodegradation *in vivo*.

3. Photostabilisation with non-reactive photoabsorbing additives

3.1. Photostabilisation of Fluvo photodegradation using excipient–dyes

Although retardation of drugs photodegradation by photo-absorbing additives has been attempted for many drugs, there are currently no standardised and reproducible methods to evaluate and quantify these effects. In this respect, the Q1b document (ICH,1996) does not provide any guidelines. As such, in this section, the utility of the Φ–order kinetics in evaluating, quantifying and predicting the photostabilising effects of photoabsorbing additives on the photodegradation of photoreversibly reacting drug molecules, such as Fluvo, will be studied.

The UV–absorbing food additive/excipient–dye *TRZ* was selected as its spectrum overlaps that of *Fluvo*, and could therefore act as an absorption competitor. For this purpose, photodegradation experiments of a known concentration of Fluvo solution in the presence of TRZ were conducted using various concentrations of the photoabsorbing additive. In order to monitor the evolution of Fluvo photodegradation spectra by spectrophotometry without interference of the additive's spectrum, the additive's solution of the desired

concentration was first added to the quartz cell and considered as the blank before adding the required volume of Fluvo stock solution and irradiating it at λ_{irr}=280 nm. The resultant kinetic traces observed at λ_{obs} = 245 nm were fitted with the Φ–order equation (Fig.6) and their respective reactions rate–constants were determined from the fitting (Table 3).

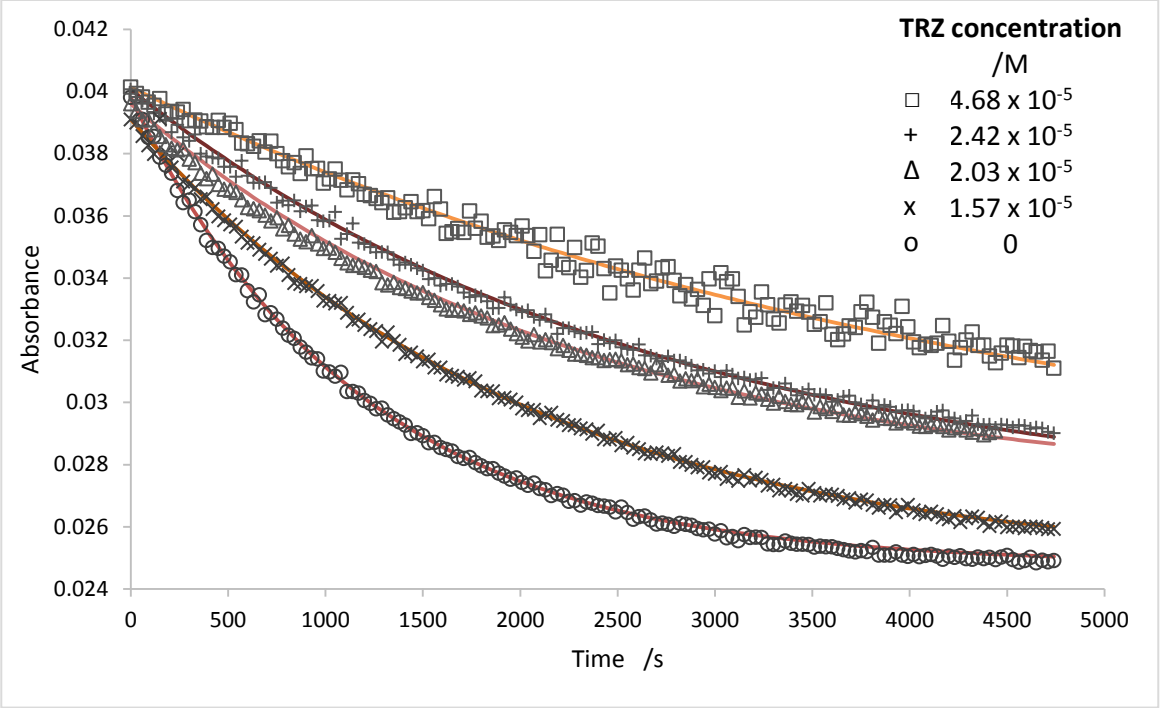

Figure 6: Effect of increasing *TRZ* concentrations on the photodegradation traces of 2.95 x 10^{-6} M aqueous *Fluvo* solutions when irradiated at 280 nm and observed at 245 nm.

The Φ–order kinetics applied well to all the kinetic traces irrespective of the dye's concentration, which had to be within its linearity range. The rate-constant values (table 3) indicate that increasing TRZ concentrations resulted in a decrease of photodegradation rate and thus increased photostabilisation. This indicates that the photodegradation pattern of the drug is not altered by the presence of the photoabsorbing additive as the Φ–order kinetics still apply. The corresponding rate-constant equation reveals that the reduction in

photoreaction rate is due to a reduction in the photokinetic factor value ($F_{\lambda_{irr}}^{dye}$) due to an increased medium absorbance of the incident radiation in the presence of the dye (i.e. $A_{tot}^{\lambda_{irr}/\lambda_{obs}}(\infty)$ is calculated by also comprising the additive's absorbance as $A_{tot}^{\lambda_{irr}/\lambda_{obs}}(\infty) = A_{E\ and\ Z-Fluvo}^{\lambda_{irr}/\lambda_{obs}}(\infty) + A_{dye}^{\lambda_{irr}/\lambda_{obs}}$)

Table 3: Dye absorbances, overall reaction rate–constants, photokinetic factors, and percentage reduction in reaction rates of *Fluvo* photodegradation in the presence of various concentrations of *TRZ* when irradiated at 280 nm and observed at 245 nm.

	$A_{dye}^{\lambda_{irr}}$ [a]	$F_{\infty}^{\lambda_{irr}}$	$k_{Fluvo}^{\lambda_{irr}}$ /s^{-1}	$\frac{k_{Fluvo}^{\lambda_{irr}}\left(A_{dye}^{\lambda_{irr}}=0\right)}{k_{Fluvo}^{\lambda_{irr}}\left(A_{dye}^{\lambda_{irr}}\neq 0\right)}$	% reduction [b]
Fluvo [c,d]	0	2.28	0.00087	1	0
Tartrazine (*TRZ*)	0.314	1.18	0.00051	1.71	41.4
	0.406	1.01	0.00044	1.98	49.4
	0.483	0.89	0.00037	2.32	56.9
	0.933	0.51	0.00022	3.87	74.1

[a]: Absorbance of the dye measured at the irradiation wavelength of 280 nm for concentrations given in Fig.6.
[b]: The constant concentration of *Fluvo* was 2.95 x 10^{-6} M.
[c]: The radiant power value for the experiments was P_{390} = 5.06 x 10^{-6} – 5.18 x 10^{-6} einstein.dm^{-3}.s^{-1}.

[d]: the optical path lengths: $l_{\lambda_{irr}}$= 2 cm; $l_{\lambda_{obs}}$= 1 cm

Furthermore, as predicted by the rate-constant equation, a good linear relationship was found between $k_{A\leftrightharpoons B}^{\lambda_{irr}}$ and $F_{\lambda_{irr}}^{dye}$ with an intercept close to zero and a correlation coefficient close to unity (Fig. 7).

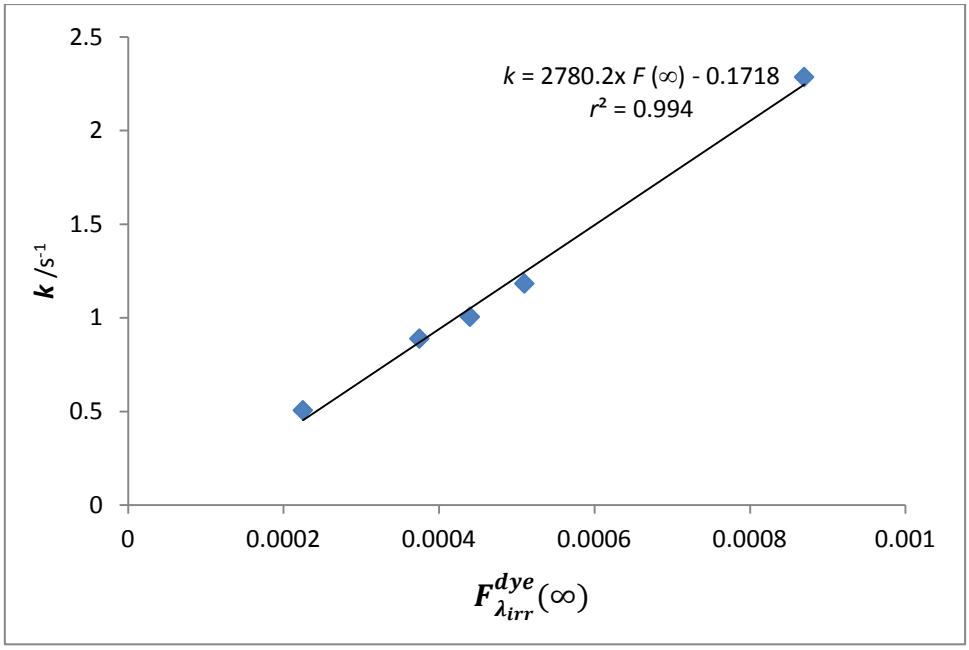

Figure 7: Linear relationship between *Fluvo* overall rate–constant of photodegradation in the presence of increasing concentrations of *TRZ* with the corresponding photokinetic factors ($F_{\lambda_{irr}}^{dye}(\infty)$).

Therefore, in addition to accurately fitting photoreactions kinetic traces and allowing the determination of rate-constants and quantum yields, the Φ–order kinetics also offer an easy and useful tool to evaluate and quantify photostabilisation of drugs in solution.

4. Conclusions

The photodegradation kinetic traces of the AB(2Φ) photoreactive drugs Monte and Fluvo are well described by the newly proposed Φ–order kinetics, which also allow a full elucidation of the kinetic parameters characterising photoreversible reaction systems in addition to the accurate quantification of the photostabilisation effect by absorption competitors or increasing concentration. These results strongly suggest that

photodegradation reactions of drugs are better described by the Φ-order kinetics rather than the commonly employed but controversial thermal orders.

The stepwise approach proposed here to elucidate AB(2Φ) drugs photoreactions resolves the identifiability issues inherent to non-linear equation systems since it allows the determination of the unique kinetic parameters that characterise the photoreaction system being studied. This method also offers the possibility of determining the spectrum of the photoproduct without requiring its physical separation from the medium.

The above drug-photodegradation study method and results based on monochromatic irradiation experiments has clearly shown that photoreactions quantum yield values depend on the irradiation wavelength. Therefore, polychromatic or even filtered-light irradiation experiments are unlikely to provide the true photodegradation quantum yields. For Monte, for instance, more than 15-fold variation was recorded for the forward and reverse quantum yield values within the wavelength range of 220-360 nm.

This study also shows the new framework and perspectives offered by the Φ–order kinetic model for the accurate and full elucidation of drugs photodegradation kinetics. It also constitutes a precise and photoreactions-specific tool for both the systematic evaluation and quantification of photolability and/or photostabilisation of drugs. This method is not only easy to implement in different laboratories but also yields reproducible results that can be used to inform both photostability and photosafety studies. Thus, this photoreactions' study

method and data treatment procedure could represent a reliable and universally-applicable quantitative assessment tool to evaluate drugs photoreactivity prior to conducting in vivo safety studies.

The above findings also confirm the robustness of the photokinetic model development methodology that was employed to devise the Φ–order kinetics and the wide array of applications that can be derived from its mathematical equations. Therefore, this methodology could be used for the development of model equations for more extended photdegradation mechanisms still awaiting integrated rate-laws.

References

Al Omari M.M., Zoubi R.M., Hasan E.I., Khader T.Z., Badwan A.A., 2007. Effect of light and heat on the stability of montelukast in solution and in its solid state. J. Pharm. Biomed. Ana. 45(3), 465-471.

Alsarra I.A., 2004. Develeopment of a stability-indicating HPLC method for the determination of montelukast in tablets and human plasma and its applications to pharmacokinetic and stability studes. Saudi Pharm. J. 12(4), 136-142.

Arison B.H., Baillie T.A., Balani S.K., Dufresne C., 1999. US Patent Number 5,952,347, Application number US19980037949.

Arnold C., C. Pedroza, E. Tyson, Seminars in Perinatology. 2014, 38, 452–464.

Benfield, P. and A. Ward, Fluvoxamine: a review of its pharmacodynamics and pharmacokinetic properties, and therapeutic efficacy in depression illness. Drugs. 32, 313–334, 1986.

Beijersberge Van Henegouwen G.M.J., 1997. Medicinal Photochemistry: Phototoxic and Phototherapeutics Aspects of Drugs. In Tests B and Meyer U.A. Advances in Drug Research. 29, 81-169.

Drucker A.M., C.F. Rosen, Drug Saf. 2011, 34, 821–837.

Feldmeyer L., G. Shojaati, K.S. Spanaus, A. Navarini, B. Theler, D. Donghi, M. Urosevic-Maiwald, M. Glatz, L. Imhof, M.J. Barysch, R. Dummer, M. Roos, L.E. French, C. Surber, G.F.L. Hofbauer, J. Am. Acad. Dermatol. 2013, 69, 530–536.

Feliciano M., Vytla D., Medeiros K.A., Chambers J.J., 2010. The $GABA_A$ receptor as a target for photochromic molecules. Bioorg. & Med. Chem. 18, 7731-7738.

Ferguson J. In Photodermatology (Eds: J. Ferguson, J.S. Dover),.Photodermatology. Manon Publishing Ltd. London, 2006, pp. 66 –71.

Figgitt, D.P. and K.J. McClellan, Fluvoxamine: An updated review of its use in the management of adults with anxiety disorders. Drugs. 60, 925-954, 2000.

Fukui, N., Y. Suzuki, T. Sugai, J. Watanabe, S. Ono, N. Tsuneyama and T. Someya, Promoter variation in the catechol-*O*-methyltransferase gene is associated with remission of symptoms during fluvoxamine treatment for major depression. Psych. Res., 218, 353–355, 2014.

Fomina N., Sankaranarayanan J., Almutairi A., 2012. Photochemical mechasnisms of light-triggered release from nanocarriers. Advanced Drug Delivery Reviews. 64, 1005-1020.

Gilbert A., J. Bagott, Essentials of molecular photochemistry. Blackwell Science. Oxford, 1991

ICH, Guidance for industry Q1B photostability testing of new drug substances and products, Fed. Regist. 1996, 62, 27115-27112.

ICH (S10), 2013. ICH Harminised Tripartite Guideline Photosafety Evaluation of Pharmaceuticals S10. Online: http://www.ich.org/fileadmin/Public_Web_Site/ICH_Products/Guidelines/Safety/S10/S10_Step_4.pdf . Accessed on 22/11/2014.

Kutlubay Z., A. Sevim, B. Engin, Y. Tuzun, Clin. in Dermato. 2014, 32, 73-79.

Kwon, J.W. and K.L. Armbrust, Photo-isomerization of fluvoxamine in aqueous solutions. J. Pharm. Biomed. Anal., 37, 643–648, 2005.

Iijima, K., M. Suzuki, T. Sakaizumi and O. Ohashi, Molecular structure of gaseous acetoxime determined by electron diffraction. J. Mol. Struct., 413-414, 327-331, 1997.

Ming L., 2012. Organic Chemistry of drug degradation. RSC Drug Discovery Series No.29. The Royal Society of Chemistry, Cambridge.

Miolo, G., S. Caffieri, L. Levorato, M. Imbesi , P. Giusti, T. Uz, R. Manev and H. Manev, Photoisomerization of fluvoxamine generates an isomer that has reduced activity on the 5-hydroxytryptamine transporter and does not affect cell proliferation. Eur. J. Pharmacol., 450, 223– 229, 2002.

D.C. Neckers, D.H. Volman, G. Von Bunau, Advances in photochemistry, vol. 19. John Wiley & Sons, New York, 1995.

Panahia, H.A., Y.T.E. Monirib and E. Keshmirizadeh, Synthesis and characterization of poly[N-isopropylacrylamide-co-1-(N,N-bis-carboxymethyl)amino-3-allylglycerol] grafted to magnetic nano-particles for the extraction and determination of fluvoxamine in biological and pharmaceutical samples. J. Chromatogr. A., 1345, 37–42, 2014.

Piechocki J.T., Thoma K., 2010. Pharmaceutical Photostability and Photostabilisation Technology. Informa Healthcare, London

Radhakrishna T., Narasaraju A., Ramakrishna M., Satyanarayana A., 2003. Simultaneous determination of montelukast and loratadine by HPLC and derivative spectrophotometric methods. J. Pharm. Biomed. Anal. 31, 359-368.

Ricci A, Fasani E., Mella M., Albini A., 2003. General patterns in the photochemistry of pregna-1,4-dien-3,20-diones. J. Org. Chem. 68, 4361-4366.

Ricci A, Fasani E., Mella M., Albini A., 2001. Noncommunicating photoreaction paths in some pregna-1,4-dien-3,20-diones. J. Org. Chem. 66, 8086-8093.

Roman J., Breier A.R., Steppe M., 2011. Stability indicating LC method to determination of sodium montelukast in pharmaceutical dosage form and its photodegradation kinetics. J. Chromato. Sci. 49, 540-546.

Schoors DF, De Smet M, Reiss T, Margolskee D, Cheng H, Larson P, Amin R, Somers G., 1995. Single dose pharmacokinetics, safety and tolerability of MK-0476, a new leukotriene D4-receptor antagonist, in healthy volunteers. Br. J. Clin. Pharmacol. 40(3):277-80.

J. Singh, Photochemistry And Pericyclic Reactions. New Age International, New Delhi, 2005

Thibert R., Mach H., Clas S. D., Meisner D.R., Vadas E.B., 1996. Characterization of the self-association properties of a leukotriene D_4 receptor antagonist, MK-0476. Int. J. Pharm. 134, 59-70.

Tomatsu I., Peng K., Kros A., 2011. Photoresponsive hydrogels for biomedical applications. Advanced Drug Delivery Reviews. 63, 1257-1266.

Tonnesen H.H, 2004. Photostability of Drugs and Drug Formulations (second Edition). CRC Press: London; 2004.

Wohl B.M., Engebersen J.F.J., 2012. Responsive layer-by-layer materials for drug delivery. Journal of Controlled Release. 158, 2-14.

Zhao J.J., Rogers J.D., Holland S.D., Larson P., Amin R.D., Haesen R., Freeman A., Seiberling M., Merz M., Cheng H., 1997. Pharmacokinetics and bioavailability of montelukast sodium (MK-0476) in healthy young and elderly volunteers. Biopharm. Drug Dispos. 18, 769-777.

Chapter VI: Modelling and elucidation of the kinetics of multiple consecutive photoreactions $AB_4(4\Phi)$ - Application to the photoreaction of riboflavin.

VI. I. $AB_4(4\Phi)$ model development and validation

1. Introduction

Consecutive photoreactions, involving two or more irreversible steps, are ubiquitous in nature and are involved in the photodegradation of many molecules (Gorner, 2010; Piechocki, 2010; Wu 2010; Fasani et al., 2008, Jiao et al., 2008; Baranda et al., 2006; Massad et al., 2006; Albini and Fasani 1998; Bosca and Miranda, 1998). These reactions involve the formation of intermediate photoproduct(s) before a final photoproduct is formed. The more complex nature of this type of reactions has halted further any possible advances in the elucidation of the integrated rate-law equations that underlie their kinetic evolution.

Thus, the first aim of this study was to develop and validate a kinetic model that accurately describes the kinetics of irreversible consecutive photoreactions involving up to four photoproducts, the $AB_4(4\Phi)$ photoreactions (scheme 1). Another objective consisted in the application of this model to describe and elucidate the kinetics of Riboflavin (Ribo) photoreaction in ethanol, as an example of a photoactive molecule photodegrading via the consecutive photoreaction $AB_2(2\Phi)$ mechanism. As part of this objective, a stepwise elucidation method was also developed to allow a complete kinetic description of any reaction of the $AB_2(2\Phi)$ type. Finally, the utility of Ribo as an actinometer for the visible 400-480 nm range was also investigated and the significance of some new photokinetic parameters such as the pseudo-rate-constant, β, was unravelled.

$$A \xrightarrow{\Phi_{A\rightarrow B}} B_1 \xrightarrow{\Phi_{B1\rightarrow B2}} B_2 \xrightarrow{\Phi_{B2\rightarrow B3}} B_3 \xrightarrow{\Phi_{B3\rightarrow B4}} B_4$$

Scheme 1: The reaction mechanism for $AB_4(4\Phi)$ consecutive photoreactions.

2. Results and discussion

2.1. Kinetic model elaboration for consecutive photoreactions

The differential equations defining the variation of the concentrations $C_A\ (t), C_{B_{1-4}}(t)$ of reactant A and photoproducts B_{1-4}, (Scheme 1), with photoreaction time, are given by eqs 1a-e. This system of equations was derived considering that the solution is subjected to a monochromatic λ_{irr} continuous irradiation, is homogeneously and continuously stirred, the medium temperature is constant, the concentration of the excited state species is assumed to be negligible, and at the (non-isosbestic) irradiation wavelength (λ_{irr}), species A and B_{1-4} are characterised by different absorption coefficients ε i.e. they absorb different amounts of light ($P_{\lambda_{irr}}$)

$$\frac{dC_A\ (t)}{dt} = -\Phi_{A\to B_1}^{\lambda_{irr}} \times \varepsilon_A^{\lambda_{irr}} \times l_{\lambda_{irr}} \times P_{\lambda_{irr}} \times F_{\lambda_{irr}}(t) \times C_A\ (t) \qquad (eq.1a)$$

$$\frac{dC_{B_1}(t)}{dt} = \left(\Phi_{A\to B_1}^{\lambda_{irr}} \times \varepsilon_A^{\lambda_{irr}} \times C_A\ (t) - \Phi_{B_1\to B_2}^{\lambda_{irr}} \times \varepsilon_{B_1}^{\lambda_{irr}} \times C_{B_1}(t)\right) \times l_{\lambda_{irr}} \times P_{\lambda_{irr}} \times F_{\lambda_{irr}}(t) \qquad (eq.1b)$$

$$\frac{dC_{B_2}(t)}{dt} = \left(\Phi_{B_1\to B_2}^{\lambda_{irr}} \times \varepsilon_{B_1}^{\lambda_{irr}} \times C_{B_1}(t) - \Phi_{B_2\to B_3}^{\lambda_{irr}} \times \varepsilon_{B_2}^{\lambda_{irr}} \times C_{B_2}(t)\right) \times l_{\lambda_{irr}} \times P_{\lambda_{irr}} \times F_{\lambda_{irr}}(t) \qquad (eq.1c)$$

$$\frac{dC_{B_3}(t)}{dt} = \left(\Phi_{B_2\to B_3}^{\lambda_{irr}} \times \varepsilon_{B_2}^{\lambda_{irr}} \times C_{B_2}(t) - \Phi_{B_3\to B_4}^{\lambda_{irr}} \times \varepsilon_{B_3}^{\lambda_{irr}} \times C_{B_3}(t)\right) \times l_{\lambda_{irr}} \times P_{\lambda_{irr}} \times F_{\lambda_{irr}}(t) \qquad (eq.1d)$$

$$\frac{dC_{B_4}(t)}{dt} = \Phi_{B_3\to B_4}^{\lambda_{irr}} \times \varepsilon_{B_4}^{\lambda_{irr}} \times C_{B_4}(t) \times l_{\lambda_{irr}} \times P_{\lambda_{irr}} \times F_{\lambda_{irr}}(t) \qquad (eq.1e)$$

where $\Phi_{A\to B_1}^{\lambda_{irr}}$, $\Phi_{B_1\to B_2}^{\lambda_{irr}}$, $\Phi_{B_2\to B_3}^{\lambda_{irr}}$ and $\Phi_{B_3\to B_4}^{\lambda_{irr}}$ are the quantum yields of the consecutive photoreaction steps, realised at λ_{irr} (nm). The excitation beam traverses the sample with an optical path-length, $l_{\lambda_{irr}}$(cm). $\varepsilon_A^{\lambda_{irr}}, \varepsilon_{B_{1-4}}^{\lambda_{irr}}$($M^{-1}cm^{-1}$), are the molar absorption coefficients of

the species and $P_{\lambda_{irr}}$ (einstein.s^{-1}dm^{-3}) is the radiant power of the monochromatic beam. $F_{\lambda_{irr}}(t)$, the photokinetic factor, is expressed as;

$$F_{\lambda_{irr}}(t) = \frac{1 - 10^{-\left(A_{tot}^{\lambda_{irr}/\lambda_{irr}}(t) \times \frac{l_{\lambda_{irr}}}{l_{\lambda_{obs}}}\right)}}{A_{tot}^{\lambda_{irr}/\lambda_{irr}}(t) \times \frac{l_{\lambda_{irr}}}{l_{\lambda_{obs}}}} \qquad (eq.2)$$

with $l_{\lambda_{obs}}$(cm) being the path-length of the monitoring light of the spectrophotometer through the sample and $A_{\mathrm{tot}}^{\lambda_{irr}/\lambda_{irr}}(t)$, the total absorbance of the medium irradiated and observed at λ_{irr}.

Mathematical integration of the photoreaction rate-laws (eqs. 1) cannot be achieved through closed-form due to the presence of the time-dependent photokinetic factor $F_{\lambda_{irr}}(t)$. Therefore, a new methodology based on Runge-Kutta 5 numerical integration methods (RK-4 NIM) was employed to determine semi-empirically integrated rate-laws describing the evolution of different species concentrations with time for consecutive photoreactions.

2.1.1. Stage1: Model equations development

The kinetics of unimolecular and reversible photoreactions have been shown to follow a log-exponential evolution with reaction time. Based on this observation together with the consecutive mechanistic nature of $AB_4(4\Phi)$ reactions, log-exponential models for the evolution of each individual species of the photoreaction was devised and tested using RK-5

generated kinetic traces for a variety of simulated consecutive photoreaction traces of the $AB_4(4\Phi)$ type. The devised semi-empirical models are;

$$C_A(t) = \frac{Log\left(1 + \left(10^{\left|\varepsilon_A^{\lambda_{irr}} - \varepsilon_{B_1}^{\lambda_{irr}}\right| \times l_{\lambda_{irr}} \times C_A(0)} - 1\right) \times e^{-k_{A \to B_1}^{\lambda_{irr}} \times t}\right)}{\left|\varepsilon_A^{\lambda_{irr}} - \varepsilon_{B_1}^{\lambda_{irr}}\right| \times l_{\lambda_{irr}}} (Eq.3a)$$

$$C_{B_1}(t) = \frac{k_{A \to B_1}^{\lambda_{irr}}}{\left|\varepsilon_A^{\lambda_{irr}} - \varepsilon_{B_1}^{\lambda_{irr}}\right| \times (k_{B_1 \to B_2}^{\lambda_{irr}} - k_{A \to B_1}^{\lambda_{irr}}) \times l_{\lambda_{irr}}}$$
$$\times \left[Log\left(1 + \left(10^{\left|\varepsilon_A^{\lambda_{irr}} - \varepsilon_{B_1}^{\lambda_{irr}}\right| \times l_{\lambda_{irr}} \times C_A(0)} - 1\right) \times e^{-k_{A \to B_1}^{\lambda_{irr}} \times t}\right)\right.$$
$$\left. - Log\left(1 + \left(10^{\left|\varepsilon_A^{\lambda_{irr}} - \varepsilon_{B_1}^{\lambda_{irr}}\right| \times l_{\lambda_{irr}} \times C_A(0)} - 1\right) \times e^{-k_{B_1 \to B_2}^{\lambda_{irr}} \times t}\right)\right] (Eq.3b)$$

$$C_{B_2}(t) = \frac{k_{A \to B_1}^{\lambda_{irr}} \times k_{B_1 \to B_2}^{\lambda_{irr}}}{\left|\varepsilon_A^{\lambda_{irr}} - \varepsilon_{B_1}^{\lambda_{irr}}\right| \times l_{\lambda_{irr}}}$$
$$\times \left[\frac{Log\left(1 + \left(10^{\left|\varepsilon_A^{\lambda_{irr}} - \varepsilon_{B_1}^{\lambda_{irr}}\right| \times l_{\lambda_{irr}} \times C_A(0)} - 1\right) \times e^{-k_{A \to B_1}^{\lambda_{irr}} \times t}\right)}{\left(k_{B_1 \to B_2}^{\lambda_{irr}} - k_{A \to B_1}^{\lambda_{irr}}\right) \times \left(k_{B_2 \to B_3}^{\lambda_{irr}} - k_{A \to B_1}^{\lambda_{irr}}\right)}\right.$$
$$- \frac{Log\left(1 + \left(10^{\left|\varepsilon_A^{\lambda_{irr}} - \varepsilon_{B_1}^{\lambda_{irr}}\right| \times l_{\lambda_{irr}} \times C_A(0)} - 1\right) \times e^{-k_{B_1 \to B_2}^{\lambda_{irr}} \times t}\right)}{\left(k_{B_1 \to B_2}^{\lambda_{irr}} - k_{A \to B_1}^{\lambda_{irr}}\right) \times \left(k_{B_2 \to B_3}^{\lambda_{irr}} - k_{B_1 \to B_2}^{\lambda_{irr}}\right)}$$
$$\left. + \frac{Log\left(1 + \left(10^{\left|\varepsilon_A^{\lambda_{irr}} - \varepsilon_{B_1}^{\lambda_{irr}}\right| \times l_{\lambda_{irr}} \times C_A(0)} - 1\right) \times e^{-k_{B_2 \to B_3}^{\lambda_{irr}} \times t}\right)}{\left(k_{B_2 \to B_3}^{\lambda_{irr}} - k_{B_1 \to B_2}^{\lambda_{irr}}\right) \times \left(k_{B_2 \to B_3}^{\lambda_{irr}} - k_{A \to B_1}^{\lambda_{irr}}\right)}\right] (Eq.3c)$$

$$C_{B3}(t) = \frac{k_{A \to B1}^{\lambda_{irr}} \times k_{B1 \to B2}^{\lambda_{irr}} \times k_{B2 \to B3}^{\lambda_{irr}}}{\left|\varepsilon_A^{\lambda_{irr}} - \varepsilon_{B1}^{\lambda_{irr}}\right| \times l_{\lambda_{irr}}} \times$$

$$\left[\frac{Log\left(1+\left(10^{\left|\varepsilon_A^{\lambda_{irr}}-\varepsilon_{B1}^{\lambda_{irr}}\right|\times l_{\lambda_{irr}}\times C_A(0)}-1\right)\times e^{-k_{\mathrm{A\to B1}}^{\lambda_{irr}}\times t}\right)}{(k_{\mathrm{B3\to B4}}^{\lambda_{irr}}-k_{\mathrm{A\to B1}}^{\lambda_{irr}})\times(k_{\mathrm{B1\to B2}}^{\lambda_{irr}}-k_{\mathrm{A\to B1}}^{\lambda_{irr}})\times(k_{\mathrm{B2\to B3}}^{\lambda_{irr}}-k_{\mathrm{A\to B1}}^{\lambda_{irr}})}\right.$$

$$-\frac{Log\left(1+\left(10^{\left|\varepsilon_A^{\lambda_{irr}}-\varepsilon_{B1}^{\lambda_{irr}}\right|\times l_{\lambda_{irr}}\times C_A(0)}-1\right)\times e^{-k_{\mathrm{B1\to B2}}^{\lambda_{irr}}\times t}\right)}{(k_{\mathrm{B1\to B2}}^{\lambda_{irr}}-k_{\mathrm{A\to B1}}^{\lambda_{irr}})\times(k_{\mathrm{B2\to B3}}^{\lambda_{irr}}-k_{\mathrm{B1\to B2}}^{\lambda_{irr}})\times(k_{\mathrm{B3\to B4}}^{\lambda_{irr}}-k_{\mathrm{B1\to B2}}^{\lambda_{irr}})}$$

$$+\frac{Log\left(1+\left(10^{\left|\varepsilon_A^{\lambda_{irr}}-\varepsilon_{B1}^{\lambda_{irr}}\right|\times l_{\lambda_{irr}}\times C_A(0)}-1\right)\times e^{-k_{\mathrm{B2\to B3}}^{\lambda_{irr}}\times t}\right)}{(k_{\mathrm{B2\to B3}}^{\lambda_{irr}}-k_{\mathrm{A\to B1}}^{\lambda_{irr}})\times(k_{\mathrm{B2\to B3}}^{\lambda_{irr}}-k_{\mathrm{B1\to B2}}^{\lambda_{irr}})\times(k_{\mathrm{B3\to B4}}^{\lambda_{irr}}-k_{\mathrm{B2\to B3}}^{\lambda_{irr}})}$$

$$+\frac{Log\left(1+\left(10^{\left|\varepsilon_A^{\lambda_{irr}}-\varepsilon_{B1}^{\lambda_{irr}}\right|\times l_{\lambda_{irr}}\times C_A(0)}-1\right)\times e^{-k_{\mathrm{B3\to B4}}^{\lambda_{irr}}\times t}\right)}{(k_{\mathrm{B1\to B2}}^{\lambda_{irr}}-k_{\mathrm{A\to B1}}^{\lambda_{irr}})\times(k_{\mathrm{B2\to B3}}^{\lambda_{irr}}-k_{\mathrm{B1\to B2}}^{\lambda_{irr}})\times(k_{\mathrm{B3\to B4}}^{\lambda_{irr}}-k_{\mathrm{B1\to B2}}^{\lambda_{irr}})}$$

$$-\frac{Log\left(1+\left(10^{\left|\varepsilon_A^{\lambda_{irr}}-\varepsilon_{B1}^{\lambda_{irr}}\right|\times l_{\lambda_{irr}}\times C_A(0)}-1\right)\times e^{-k_{\mathrm{B3\to B4}}^{\lambda_{irr}}\times t}\right)}{(k_{\mathrm{B3\to B4}}^{\lambda_{irr}}-k_{\mathrm{A\to B1}}^{\lambda_{irr}})\times(k_{\mathrm{B1\to B2}}^{\lambda_{irr}}-k_{\mathrm{A\to B1}}^{\lambda_{irr}})\times(k_{\mathrm{B2\to B3}}^{\lambda_{irr}}-k_{\mathrm{A\to B1}}^{\lambda_{irr}})}$$

$$\left.-\frac{Log\left(1+\left(10^{\left|\varepsilon_A^{\lambda_{irr}}-\varepsilon_{B1}^{\lambda_{irr}}\right|\times l_{\lambda_{irr}}\times C_A(0)}-1\right)\times e^{-k_{\mathrm{B3\to B4}}^{\lambda_{irr}}\times t}\right)}{(k_{\mathrm{B2\to B3}}^{\lambda_{irr}}-k_{\mathrm{A\to B1}}^{\lambda_{irr}})\times(k_{\mathrm{B2\to B3}}^{\lambda_{irr}}-k_{\mathrm{B1\to B2}}^{\lambda_{irr}})\times(k_{\mathrm{B3\to B4}}^{\lambda_{irr}}-k_{\mathrm{B2\to B3}}^{\lambda_{irr}})}\right](eq.3d)$$

$$C_{B4}(t)$$

$$=\frac{Log\left(1+\left(10^{\left|\varepsilon_A^{\lambda_{irr}}-\varepsilon_{B1}^{\lambda_{irr}}\right|\times l_{\lambda_{irr}}\times C_A(0)}-1\right)\times e^{-k_{\mathrm{B3\to B4}}^{\lambda_{irr}}\times t}\right)-log\left(10^{\left|\varepsilon_A^{\lambda_{irr}}-\varepsilon_{B1}^{\lambda_{irr}}\right|\times l_{\lambda_{irr}}\times C_A(0)}\right)}{\left|\varepsilon_A^{\lambda_{irr}}-\varepsilon_{B1}^{\lambda_{irr}}\right|\times l_{\lambda_{irr}}}$$

$$\times\left[\frac{k_{\mathrm{A\to B1}}^{\lambda_{irr}}\times k_{\mathrm{B1\to B2}}^{\lambda_{irr}}\times k_{\mathrm{B2\to B3}}^{\lambda_{irr}}}{(k_{\mathrm{B3\to B4}}^{\lambda_{irr}}-k_{\mathrm{A\to B1}}^{\lambda_{irr}})\times(k_{\mathrm{B1\to B2}}^{\lambda_{irr}}-k_{\mathrm{A\to B1}}^{\lambda_{irr}})\times(k_{\mathrm{B2\to B3}}^{\lambda_{irr}}-k_{\mathrm{A\to B1}}^{\lambda_{irr}})}\right.$$

$$-\frac{k_{\mathrm{A\to B1}}^{\lambda_{irr}}\times k_{\mathrm{B1\to B2}}^{\lambda_{irr}}\times k_{\mathrm{B2\to B3}}^{\lambda_{irr}}}{(k_{\mathrm{B1\to B2}}^{\lambda_{irr}}-k_{\mathrm{A\to B1}}^{\lambda_{irr}})\times(k_{\mathrm{B2\to B3}}^{\lambda_{irr}}-k_{\mathrm{B1\to B2}}^{\lambda_{irr}})\times(k_{\mathrm{B3\to B4}}^{\lambda_{irr}}-k_{\mathrm{B1\to B2}}^{\lambda_{irr}})}$$

$$\left.+\frac{k_{\mathrm{A\to B1}}^{\lambda_{irr}}\times k_{\mathrm{B1\to B2}}^{\lambda_{irr}}\times k_{\mathrm{B2\to B3}}^{\lambda_{irr}}}{(k_{\mathrm{B2\to B3}}^{\lambda_{irr}}-k_{\mathrm{A\to B1}}^{\lambda_{irr}})\times(k_{\mathrm{B2\to B3}}^{\lambda_{irr}}-k_{\mathrm{B1\to B2}}^{\lambda_{irr}})\times(k_{\mathrm{B3\to B4}}^{\lambda_{irr}}-k_{\mathrm{B2\to B3}}^{\lambda_{irr}})}\right]$$

$$+\frac{k_{\mathrm{B1\to B2}}^{\lambda_{irr}}\times k_{\mathrm{B2\to B3}}^{\lambda_{irr}}\times k_{\mathrm{B3\to B4}}^{\lambda_{irr}}\times Log\left(1+\left(10^{\left|\varepsilon_A^{\lambda_{irr}}-\varepsilon_{B1}^{\lambda_{irr}}\right|\times l_{\lambda_{irr}}\times C_A(0)}-1\right)\times e^{-k_{\mathrm{A\to B1}}^{\lambda_{irr}}\times t}\right)-log\left(10^{\left|\varepsilon_A^{\lambda_{irr}}-\varepsilon_{B1}^{\lambda_{irr}}\right|\times l_{\lambda_{irr}}\times C_A(0)}\right)}{\left|\varepsilon_A^{\lambda_{irr}}-\varepsilon_{B1}^{\lambda_{irr}}\right|\times l_{\lambda_{irr}}\times(k_{\mathrm{B3\to B4}}^{\lambda_{irr}}-k_{\mathrm{A\to B1}}^{\lambda_{irr}})\times(k_{\mathrm{B1\to B2}}^{\lambda_{irr}}-k_{\mathrm{A\to B1}}^{\lambda_{irr}})\times(k_{\mathrm{B2\to B3}}^{\lambda_{irr}}-k_{\mathrm{A\to B1}}^{\lambda_{irr}})}$$

$$+\frac{k_{\mathrm{A\to B1}}^{\lambda_{irr}}\times k_{\mathrm{B2\to B3}}^{\lambda_{irr}}\times k_{\mathrm{B3\to B4}}^{\lambda_{irr}}\times Log\left(1+\left(10^{\left|\varepsilon_A^{\lambda_{irr}}-\varepsilon_{B1}^{\lambda_{irr}}\right|\times l_{\lambda_{irr}}\times C_A(0)}-1\right)\times e^{-k_{\mathrm{B1\to B2}}^{\lambda_{irr}}\times t}\right)-log\left(10^{\left|\varepsilon_A^{\lambda_{irr}}-\varepsilon_{B1}^{\lambda_{irr}}\right|\times l_{\lambda_{irr}}\times C_A(0)}\right)}{\left|\varepsilon_A^{\lambda_{irr}}-\varepsilon_{B1}^{\lambda_{irr}}\right|\times l_{\lambda_{irr}}\times(k_{\mathrm{B1\to B2}}^{\lambda_{irr}}-k_{\mathrm{A\to B1}}^{\lambda_{irr}})\times(k_{\mathrm{B2\to B3}}^{\lambda_{irr}}-k_{\mathrm{B1\to B2}}^{\lambda_{irr}})\times(k_{\mathrm{B3\to B4}}^{\lambda_{irr}}-k_{\mathrm{B1\to B2}}^{\lambda_{irr}})}$$

$$-\frac{k_{\mathrm{A\to B1}}^{\lambda_{irr}}\times k_{\mathrm{B1\to B2}}^{\lambda_{irr}}\times k_{\mathrm{B3\to B4}}^{\lambda_{irr}}\times Log\left(1+\left(10^{\left|\varepsilon_A^{\lambda_{irr}}-\varepsilon_{B1}^{\lambda_{irr}}\right|\times l_{\lambda_{irr}}\times C_A(0)}-1\right)\times e^{-k_{\mathrm{B2\to B3}}^{\lambda_{irr}}\times t}\right)-log\left(10^{\left|\varepsilon_A^{\lambda_{irr}}-\varepsilon_{B1}^{\lambda_{irr}}\right|\times l_{\lambda_{irr}}\times C_A(0)}\right)}{\left|\varepsilon_A^{\lambda_{irr}}-\varepsilon_{B1}^{\lambda_{irr}}\right|\times l_{\lambda_{irr}}\times(k_{\mathrm{B2\to B3}}^{\lambda_{irr}}-k_{\mathrm{A\to B1}}^{\lambda_{irr}})\times(k_{\mathrm{B2\to B3}}^{\lambda_{irr}}-k_{\mathrm{B1\to B2}}^{\lambda_{irr}})\times(k_{\mathrm{B3\to B4}}^{\lambda_{irr}}-k_{\mathrm{B2\to B3}}^{\lambda_{irr}})}$$

$$(eq.3e)$$

It is worth noting that in the case where only one photoreaction step is involved (i.e. $k_{B_1\rightarrow B_2}^{\lambda_{irr}} = k_{B_2\rightarrow B_3}^{\lambda_{irr}} = k_{B_3\rightarrow B_4}^{\lambda_{irr}} = 0$) , these sets of equations reduce down to the AB(1Φ) equations.

The general form of the rate-constants $k_{\mathrm{i}\rightarrow\mathrm{j}}^{\lambda_{irr}}$($s^{-1}$) is given in eq.4 where *i* corresponds to the reacting species (either the initial reactant or photoproduct) and *j* represents its subsequent photoproduct in a given reaction step.

$$k_{\mathrm{i}\rightarrow\mathrm{j}}^{\lambda_{irr}} = \Phi_{\mathrm{i}\rightarrow\mathrm{j}}^{\lambda_{irr}} \times \varepsilon_{\mathrm{i}}^{\lambda_{irr}} \times l_{\lambda_{irr}} \times \frac{1-10^{-\varepsilon_{\mathrm{i}}^{\lambda_{irr}}\times l_{\lambda_{irr}}\times C(0)}}{\varepsilon_{\mathrm{i}}^{\lambda_{irr}}\times l_{\lambda_{irr}}\times C(0)} \times P_{\lambda_{irr}} = \beta_{\mathrm{i}\rightarrow\mathrm{j}}^{\lambda_{irr}} \times P_{\lambda_{irr}} (eq.4)$$

Spectroscopic monitoring of the photoreaction does not offer the evolution traces of the individual species concentrations involved in the photoreaction but instead, presents the sum of the species absorbances at various photoreaction times. The equation describing the variation of the total absorbance with reaction time, is defined on the basis of the individual species time-concentration equations (eqs. 3) as;

$$A_{\mathrm{Tot}}^{\lambda_{irr}/\lambda_{obs}}(t) = \sum (C_i(t) \times \varepsilon_i^{\lambda_{obs}} \times l_{\lambda_{obs}}) \ (eq.5)$$

This model equation offers the possibility to monitor the evolution of a given consecutive photoreaction using simple UV/Vis spectrophotometry without requiring chromatographic separation of the medium's species at various time points of the reaction.

The proposed general semi-empirical model equation (eq.5) was found to adequately fit the RK-5 synthetic kinetic traces for cases where the photokinetic factor, $F_{\lambda_{irr}}(\infty)$, value was equal to or exceeding 1.8 (i.e. $A^{\lambda_{irr}/\lambda_{obs}}(\infty) < 0.22$); a limitation that can usually be circumvented by reducing the initial species concentration or the irradiation path-length.

The observed initial velocity, $v_{o\ Cal.}^{\lambda_{irr}/\lambda_{obs}}$ of the photoreaction can be determined from eq.1 as;

$$v_{o,\ Cal.}^{\lambda_{irr}/\lambda_{obs}} = (\varepsilon_B^{\lambda_{obs}} - \varepsilon_A^{\lambda_{obs}}) \times l_{\lambda_{obs}} \times \Phi_{A\to B_1}^{\lambda_{irr}} \times \varepsilon_A^{\lambda_{irr}} \times l_{\lambda_{irr}} \times P_{\lambda_{irr}} \times F_{\lambda_{irr}}(0) \times C_A\ (0)$$

$$= \delta_{\lambda_{irr}} \times P_{\lambda_{irr}}\ (eq.6a)$$

with $C_A\ (0)$ being the initial reactant concentration of species A and $F_{\lambda_{irr}}(0)$, the photokinetic factor at t_0 (i.e. in eq.2, $A_{tot}^{\lambda_{irr}/\lambda_{irr}}(t) = A_A^{\lambda_{irr}/\lambda_{irr}}(0)$).

Furthermore, the observed initial velocity of the reaction, $v_{o\ Mod.}^{\lambda_{irr}/\lambda_{obs}}$, can also be determined from the differentiation of eqs. 3a and 5 at t_0 as;

$$v_{o,\ Mod.}^{\lambda_{irr}/\lambda_{obs}} = \frac{l_{\lambda_{obs}} \times k_{\mathrm{A}\to B_1}^{\lambda_{irr}}}{l_{\lambda_{irr}} \times \ln(10)} \times \left(1 - 10^{-\left(\left|\varepsilon_A^{\lambda_{irr}} - \varepsilon_{B_1}^{\lambda_{irr}}\right| \times l_{\lambda_{irr}} \times C_A\ (0)\right)}\right)\ (Eq.6b)$$

2.1.2. Stage 2: Validation of the model equations

The accuracy of the above equations to describe the kinetic evolution of species involved in consecutive photoreactions types was tested against 125 new RK-5-generated kinetic traces with varying input parameters within the limits of applicability of the model. This was achieved by feeding the RK-5 programme with varied but plausible input values for the initial concentration (C(0)), radiant power ($P_{\lambda_{irr}}$), irradiation path-length ($l_{\lambda_{irr}}$), reactant and photoproducts' absorption coefficients ($\varepsilon^{\lambda_{irr}}$) and quantum yields ($\Phi^{\lambda_{irr}}$). The different simulation scenarios were carefully selected to provide a wide array of reaction eventualities (table 1).

Table 1: Sets of data used to generate some $AB_4(4\Phi)$ kinetic traces shown in figure1 using fifth order Runge-Kutta method and to calculate the fitted kinetic traces using the $AB_4(4\Phi)$-order model; together with the rate constants obtained for each photoreaction step.

	Trace 1	Trace 2	Trace 3	Trace 4	Trace 5	Trace 6	Trace 7
$C_o \times 10^6$ (M)	10	8.0	4.0	8.0	9.0	7.0	4.0
$Px10^6$ (einstein. $s^{-1}.cm^{-3}$)	5.0	3.0	5.0	6.0	8.0	6.0	7.0
$\boldsymbol{l}_{\lambda_{irr}}$(cm)	1	2.5	5	1.4	1	2	2
$\boldsymbol{\varepsilon}_{A}^{\lambda_{irr}}$ ($M^{-1}cm^{-1}$)	3500	5500	16000	2500	8550	2200	3750
$\boldsymbol{\varepsilon}_{B_1}^{\lambda_{irr}}$($M^{-1}cm^{-1}$)	5800	3200	14000	12400	6500	6500	4800
$\boldsymbol{\varepsilon}_{B_2}^{\lambda_{irr}}$($M^{-1}cm^{-1}$)	5900	1500	12000	1100	4200	8700	6700
$\boldsymbol{\varepsilon}_{B_3}^{\lambda_{irr}}$($M^{-1}cm^{-1}$)	6300	3666	10000	5000	3100	5000	3200
$\boldsymbol{\varepsilon}_{B_4}^{\lambda_{irr}}$($M^{-1}cm^{-1}$)	7000	5700	8000	4000	2249	1050	2100
$\boldsymbol{\Phi}_{A\rightarrow B_1}^{\lambda_{irr}}$	0.1	0.02	0.03	0.1	0.01	0.05	0.02
$\boldsymbol{\Phi}_{B_1\rightarrow B_2}^{\lambda_{irr}}$	0.2	0.1	0.001	0.1	0.2	0.03	0.08
$\boldsymbol{\Phi}_{B_2\rightarrow B_3}^{\lambda_{irr}}$	0.3	0.1	0.02	0.1	0.2	0.01	0.1
$\boldsymbol{\Phi}_{B_3\rightarrow B_4}^{\lambda_{irr}}$	0.1	0.05	0.06	0.1	0.1	0.02	0.05
$\boldsymbol{k}_{A\rightarrow B_1}^{\lambda_{irr}}$ (s^{-1})	0.00387	0.00175	0.01955	0.00490	0.00155	0.00290	0.00234
$\boldsymbol{k}_{B_1\rightarrow B_2}^{\lambda_{irr}}$ (s^{-1})	0.01250	0.00495	0.00059	0.02300	0.02270	0.00520	0.01185
$\boldsymbol{k}_{B_2\rightarrow B_3}^{\lambda_{irr}}$ (s^{-1})	0.01905	0.00230	0.01061	0.00230	0.01510	0.00240	0.02032
$\boldsymbol{k}_{B_3\rightarrow B_4}^{\lambda_{irr}}$ (s^{-1})	0.00675	0.00320	0.02768	0.00900	0.00480	0.00255	0.00501

The rate-constant equation proposed above (eq. 4) was used to calculate the theoretical rate-constant value for each photoreaction step ($k_{Cal.}^{\lambda_{irr}}$). Besides, the proposed concentration model equations (eqs. 3) were fitted to the RK-5 generated kinetic traces corresponding to the time evolution of each species concentration throughout the photoreaction. Equation 5 was used to fit the absorbance kinetic trace of the sum of all the species absorbances with time. Fitting was achieved and equation rate-constant value ($k_{mod.}^{\lambda_{irr}}$) for each species kinetic trace were determined.

A good fitting of the model to all synthetic kinetic traces was obtained for $AB_4(4\Phi)$ and its sub-mechanisms (figure 1).

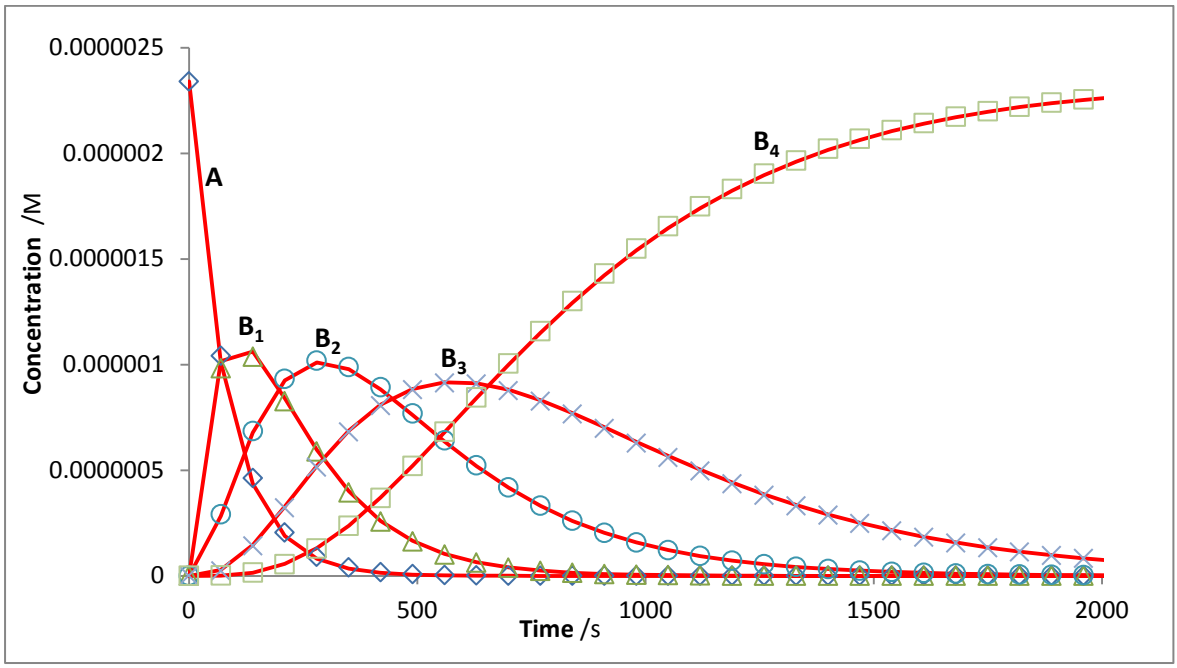

Figure 1: Individual concentration evolution profiles of reactant (A) and photoproducts (B_1, B_2, B_3, B_4) corresponding to trace 6 data in Table 1. The shapes represent the species RK-5

obtained concentrations profiles while the continuous lines correspond to Φ-order semi-empirical equations (eqs. 3).

A sample representation of the evolution of the absorbance profiles for the photoreactions simulated cases of table 1 together with the model-fitted traces are depicted in figure 2.

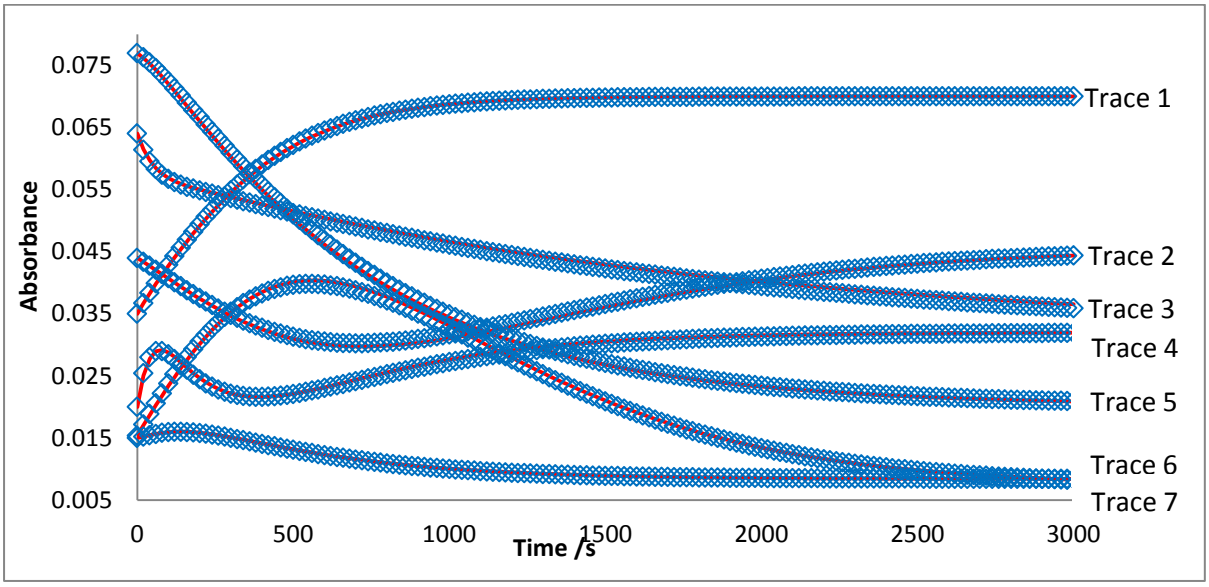

Figure 2: Sample Runge-Kutta generated $AB_4(4\Phi)$ kinetic traces (circles) and the corresponding $AB_4(4\Phi)$-model fitted traces (lines).

Additionally, for each kinetic trace, the calculated ($k_{Cal.}^{\lambda_{irr}}$) and model fitting-determined ($k_{Mod.}^{\lambda_{irr}}$) rate-constant values differed by no more than 10%. The close correlation obtained between the two sets of values (figure 3) provides validation for the accuracy of the semi-empirical integrated rate-law equations (eqs. 3a-e) to describe the kinetic evolution of consecutive photoreactions.

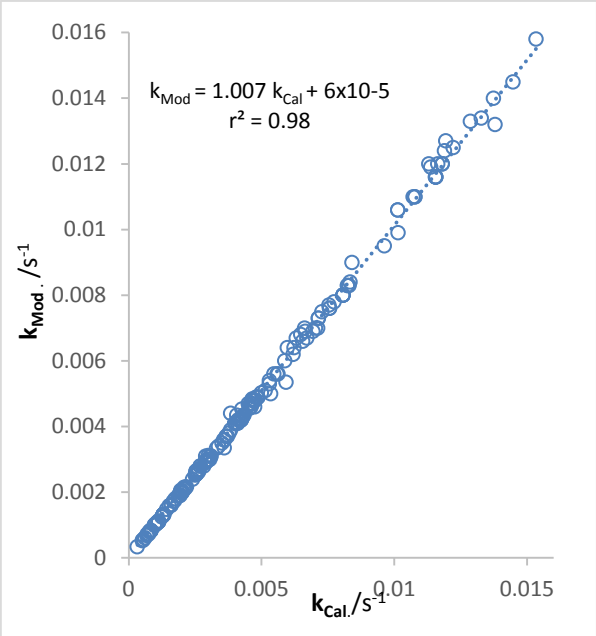

Figure 3: Correlation between the rate-constant values calculated theoretically using the $AB_4(4\Phi)$ rate-constant equations ($k_{Cal.}^{\lambda_{irr}}$) and those determined from the fitting of RK–4 data with the $AB_4(4\Phi)$ model equations ($k_{Mod.}^{\lambda_{irr}}$), for over 100 simulation photokinetic traces.

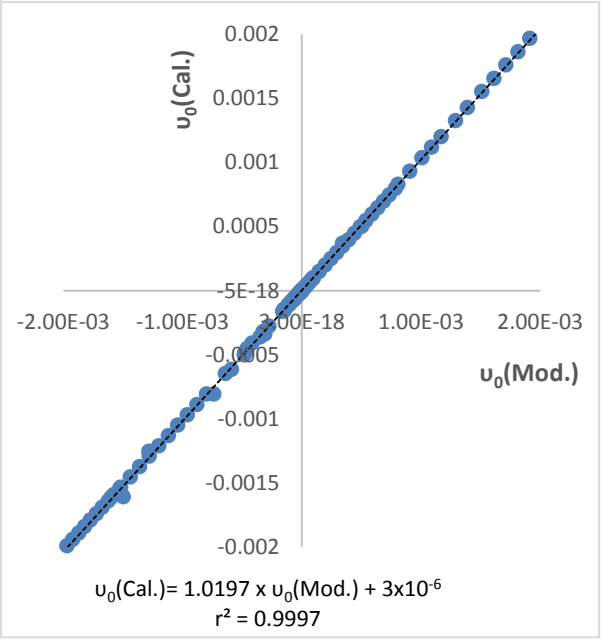

Figure 4: Correlation between the initial velocity values of over 150 RK-4 generated kinetic traces, obtained theoretically ($\upsilon_{o\ Cal.}^{\lambda_{irr}/\lambda_{obs}}$) using the rate-law equation and those obtained from the model differential equation ($\upsilon_{o\ Mod.}^{\lambda_{irr}/\lambda_{obs}}$), at t_0.

A third validation step consisted in the determination of the initial velocity of all the simulated RK-5 reaction cases using (i) the rate-law equation for the change in absorbance at t_0, (eq.6a) and (ii) the derivative of the semi-empirical integrated rate-law at t_0 (eq.6b). The model would prove to be valid if for each photoreaction case, the values of $\upsilon_{o\ Theo.}^{\lambda_{irr}/\lambda_{obs}}$ and

$\upsilon_{o\ Mod.}^{\lambda_{irr}/\lambda_{obs}}$ differed by no more than 10%. As shown in figure 4, a very good correlation was found between the initial velocity value determined by the two methods, thereby providing further evidence on the validity and accuracy of the semi-empirical model.

As a result of the above findings, the proposed semi-empirical model (eq. 5) was tested against experimental photokinetic data using the photolabile drug Riboflavin which was shown to photoreact via the $AB_2(2\Phi)$ consecutive photoreaction mechanism.

IV.II. Application of the $AB_4(4\Phi)$ kinetic model for the study of riboflavin photodegradation kinetics

1. Introduction

Riboflavin (Ribo), also known as vitamin B_2 is a water soluble vitamin that is widely consumed. It is present in various food products such as liver, kidney, eggs, meat, fresh vegetables, dairy products as well as yeast (Dewick, 1998). It is also extensively used as a component of vitamin preparations and parenteral nutrition solutions (Ahmed et al., 2004). Dietary deficiency, although uncommon, manifests itself by disturbances of the skin and eyes (Dewick, 1998). Being also an essential component of many bodily enzymes and coenzymes, vitamin B_2 proved to be vital to the normal functioning of a number of systemic oxidation-reduction reactions as well as several metabolic pathways (Dewick, 1998). Furthermore, recent findings have also revealed that Ribo can inactivate high levels of a broad range of viruses and bacteria present in red blood cells, fresh frozen plasma and platelet concentrates (Corbin, 2002).

Ribo is a member of the 7,8-dimethyl substituted isoalloxazines or the flavins family as the molecule consists of an isoalloxazine ring linked to D-ribitol. Although thermally stable, Ribo has long been known to photodegrade with light (Sheraz et al. 2014; Koziol, 1966b)**.** An extensive number of studies and research papers have been devoted to the photochemistry of Ribo in both aqueous and organic solvents (Sheraz et al. 2014). Its photodegradation was shown to occur sequentially in a two-step consecutive reaction in alcohols and aqueous buffered acidic solutions. It phototransforms into an intermediate formylmethylflavin (FMF) which, in turn, irreversibly photoreacts to produce lumichrome (LC) (Ahmed et al., 2011; Ahmed et al., 2010a; Ahmad et al., 2006a; Moore and Ireton, 1977). In basic solutions, Ribo

hydrolysis renders the photoreaction mechanism more complex (Ahmed et al., 2011; Ahmed et al., 2010a; Koziol; 1966a).

While studies on Ribo photoproducts, photoreactions mechanisms and to some extent photostabilising means are abundant, the kinetics of photodegradation reactions have been less appreciably explored. The published kinetic studies on Ribo photodegradation were conducted using classical treatments of thermal reactions and were ascribed the apparent first-order kinetics (Ahmed et al., 2011; Ahmed et al., 2010a; Ahmed et al., 2004).

Despite being widely used, this kinetic treatment strategy, originally developed to describe thermal reactions kinetics, has been shown to present several drawbacks and inadequacies when applied to the study of photoreactions kinetics. The results thus obtained cannot be generalised or even compared between different studies.

Compounded to the kinetic treatment issue, is the wide use of polychromatic or filtered light irradiation composed of several wavelength beams to conduct photokinetic studies. The use of such irradiation settings results in different wavelength beams having different effects on the reaction kinetics. Consequently, not only is it difficult to replicate similar irradiation conditions and intensities using this type of irradiation settings but it is also impossible to clearly define and delineate the actual effect of each irradiation wavelength impacting on the photoreaction and its kinetics.

In order to palliate these problems, the use of monochromatic light beams combined with an accurate actinometric method, on the one hand, was deemed to be the most effective experimental approach to generate reproducible results and study photoreaction kinetics (Maafi and Maafi, 2015; Maafi and Maafi, 2014a, Maafi and Maafi, 2014b; Maafi and Maafi, 2013; Moore, 2004). The quantitative analysis of these results, on the other hand, must also rely on a reproducible and specific analytical treatment method. The recently developed, Φ-order kinetics have offered the possibility to conduct reliable quantitative analysis of photoreactions kinetics that can be universally used, reproduced and compared (Maafi and Maafi, 2015; Maafi and Maafi, 2014a, Maafi and Maafi, 2014b; Maafi and Maafi, 2013).

The objectives of this chapter were to unravel the kinetics of Ribo photodegradation using the above Φ-order model. Furthermore, the method used to determine the kinetic parameters that are specific to this reaction will also be described. Finally, the significance of two newly determined and kinetically important photokinetic parameters, namely the pseudo-initial rate-constant and velocitiy, will also be discussed in more details.

2. Results and discussion

2.1. Riboflavin photodegradation

The photodegradation of Ribo in ethanol was reported to occur via the $AB_2(2\Phi)$ consecutive photoreaction mechanism (Scheme 2). An intermediate aldehyde photoproduct, FMF, is

formed by intramolecular photoreduction of the isoalloxazine ring system followed by oxidation of the ribityl side-chain. This first photoreaction step was shown to occur predominantly from the triplet state of the photo-excited Ribo molecule (Koziol, 1966a; Grodowski, 1977; Heelis 1982). It was suggested that the ribityl chain rich in hydroxyl oxygen atoms promotes the transition from the excited singlet to the excited triplet state and stabilises the latter by steric protection (Koziol, 1966a). The triplet state quantum yields were reported to be around 0.6 in methanol (Chacon et al., 1998) and 0.7 in ethanol (Moore et al.1977). Triplet state lifetimes of 3.7 and 19 µs were also reported for Ribo in aqueous and methanolic solutions, respectively (Grodowski et al. 1977; Sikorska et al. 2005). The second photolysis step in Ribo degradation was also reported to occur from the lowest triplet state of the photo-activated FMF which undergoes a bimolecular redox reaction to generate LC (Ahmed et al. 2006a).

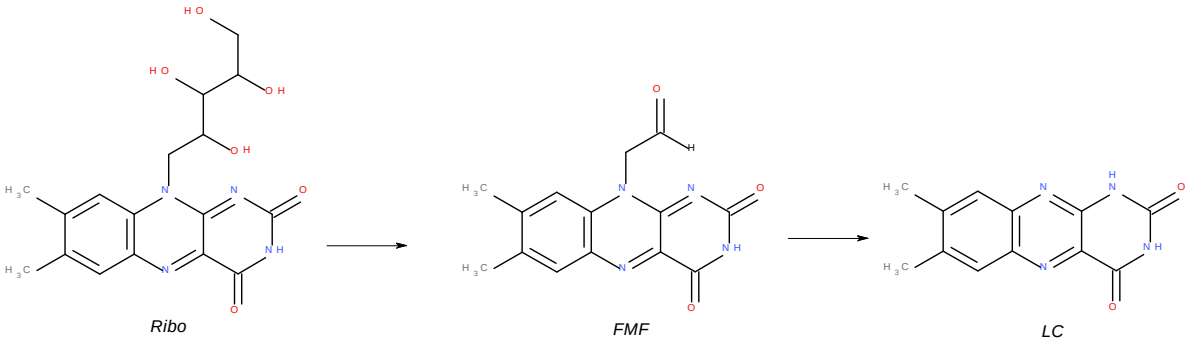

Scheme 2: Consecutive $AB_2(2\Phi)$ photoreaction mechanism of *Ribo* upon exposure to UV–irradiation.

The electronic absorption spectrum of *Ribo* in ethanol is characterised by four absorption bands spanning the UV and visible regions of the spectrum (figure 5). Two intense peaks characterise the UVC region with two broad absorption bands situated at longer

wavelengths with maxima at 360 and 445 nm. The absorbance bands in the near UV and visible parts of the spectrum have mainly been attributed to π-π^* transitions (Sikorska et al., 2005; Koziol, 1966a; Grodowski, 1977; Ahmad et al. 2006a). Monochromatic irradiation of Ribo ethanolic solution results in the photo-bleaching of the solution through the disappearance of the visible absorption peak with a concomitant decrease in absorbance in the UV region and the appearance of a shoulder at around 390 nm. The appearance of isosbestic points (405, 383, 320, 303, 260, and 233 nm) characterise the smooth evolution of the photoreaction (figure 5).

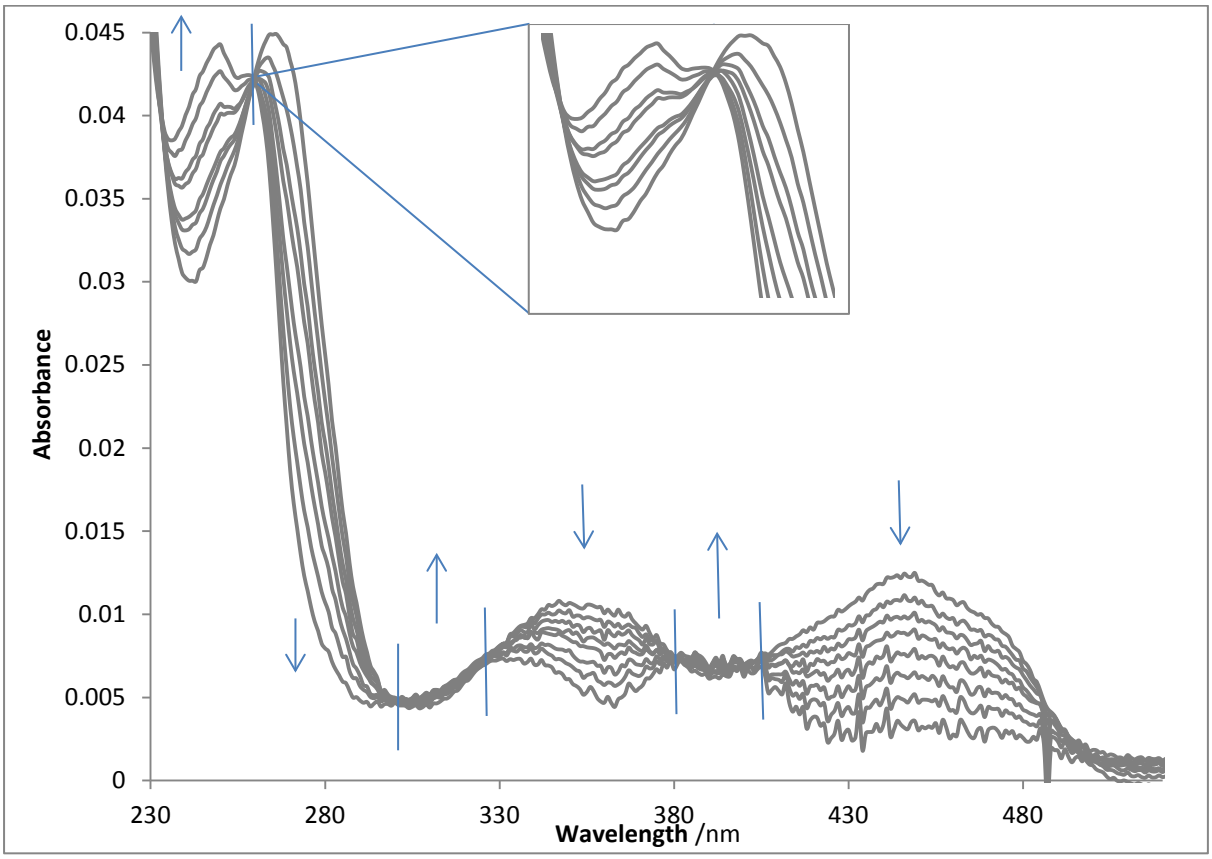

Figure 5: Evolution of the electronic absorption spectra of 1.11 x 10^{-6} M *Riboflavin* in ethanol subjected to continuous irradiation with a 460 nm monochromatic beam (at a

radiant power of P_{270} = 1.36 x 10^{-6} einstein.s^{-1}.dm^{-3}) for 4 hours. The arrows indicate the direction of the absorbance evolution during the photoreaction and the vertical lines cross the spectra at the isosbestic points (405, 383, 320, 303, 260, and 233 nm).

2.2. Φ-order photokinetics of Riboflavin

It has been reported that wavelengths in the range of 350-500 nm cause *Ribo* photodegradation with the wavelength range of 415 – 455 nm being the most damaging (Sheraz et al., 2014). Furthermore, photo-irradiation experiments of Ribo in ethanol revealed a considerably slower photoreaction under UVB irradiation compared to irradiations undertaken in the visible region of the spectrum. Consequently, the present kinetic study was predominantly concerned with the elucidation of Ribo photoreaction kinetics in the most photoactive visible absorbance region of 400 – 480 nm.

Monochromatic irradiation experiments were performed at different wavelengths ($\lambda_{irr} = 400, 420, 445, 460 \text{ and } 480$ nm) in order to cover the whole wavelength range of interest. The changes in absorbance of the medium were monitored at different observation wavelengths (λ_{obs}) including the wavelength of irradiation ($\lambda_{obs} = \lambda_{irr}$ so that $\varepsilon_{B_1}^{\lambda_{irr}} = \varepsilon_{B_1}^{\lambda_{obs}}$), for each irradiation experiment.

Continuous irradiation of Ribo under different wavelengths results in the gradual reduction of absorbance as observed at 445 nm (figure 6). Fitting of these traces was performed using eq. 5 where $C_{B_3}(t), C_{B_4}(t)$ in eq.5, and $k^{\lambda_{irr}}_{B_2 \rightarrow B_3}$ in eq.4 were given the zero value.

An accurate fitting of the semi-empirical model (eq. 5) to the experimental kinetic traces was obtained for all experimental kinetic traces of Ribo photodegradation. This finding further confirms the consecutive $AB_2(2\Phi)$ nature of Ribo photoreaction in ethanol.

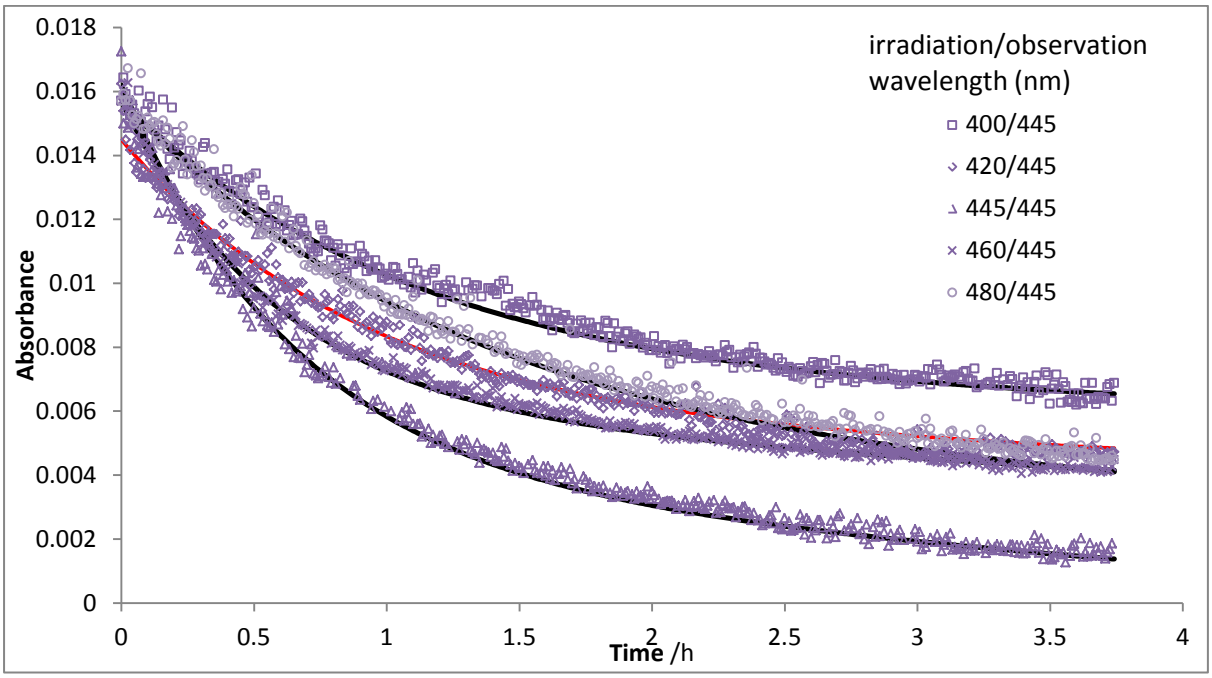

Figure 6: The photokinetic traces for the photodegradation of *Riboflavin* in ethanol (≈1.2 x 10^{-6} M) under continuous irradiations at λ_{irr}= 400, 420, 445, 460 and 480nm and observation at λ_{obs}= 445nm. The geometric shapes represent the experimental data wehereas the continuous lines represent the model fitted traces using model equation (eq.5).

Fitting of the model allowed the determination of the individual rate-constants of the consecutive photoreaction steps rate-constants, $k_{\mathrm{A}\rightarrow B_1}^{\lambda_{irr}}$ and $k_{B_1\rightarrow B_2}^{\lambda_{irr}}$, respectively. $k_{\mathrm{A}\rightarrow B_1}^{\lambda_{irr}}$ was found to be 10 to 40 - fold higher than $k_{B_1\rightarrow B_2}^{\lambda_{irr}}$ for the 400-480 nm irradiation range. On the other hand, both rate-constant values were found to increase with irradiation wavelength between 400 and 460 nm, reaching their maximum at 460 nm and decreasing again at 480 nm. Photoreactions rate-constants provide some indication about photoreactions rates, mainly when only one variable is changed within the same experimental settings. However, they do not reflect the photochemical efficiencies of molecules at given wavelengths nor can they be used to compare photoreaction rates from different studies or experimental conditions. Therefore, a photokinetic elucidation method should be adopted in order to allow the determination of individual photoreaction quantum yields for each step of the $AB_2(2\Phi)$ reactions.

2.3. Elucidation of $AB_2(2\Phi)$ photoreaction kinetics

A comprehensive kinetic elucidation of a bimolecular consecutive, $AB_2(2\Phi)$, photoreaction system entails the determination of the values of six parameters, namely; $\varepsilon_{B_1}^{\lambda_{irr}}$, $\varepsilon_{B_2}^{\lambda_{irr}}$, $k_{\mathrm{A}\rightarrow B_1}^{\lambda_{irr}}$, $k_{B_1\rightarrow B_2}^{\lambda_{irr}}$, $\Phi_{A\rightarrow B_1}^{\lambda_{irr}}$ and $\Phi_{B_1\rightarrow B_2}^{\lambda_{irr}}$. This can be achieved using the $AB_2(2\Phi)$ Φ-order kinetic model (eq.5). The study on Ribo photodegradation kinetics in ethanol illustrates this methodology.

The absorption coefficients, $\varepsilon_A^{\lambda_{irr}}$ and $\varepsilon_{B_2}^{\lambda_{irr}}$, corresponding to Ribo and its final photoproduct, *LC,* respectively, were determined from the initial (t = 0) and final (t = ∞) absorption spectra of the photodegradation reaction. $\varepsilon_{B_2}^{\lambda_{irr}}$ was determined using eq.7a;

$$\varepsilon_{B2}^{\lambda_{irr}} = \frac{A_{tot}^{\lambda_{irr}/\lambda_{obs}}(\infty)}{l_{\lambda_{obs}} \times C_A\ (0)}\ (eq.7a)$$

However, due to the overlapping spectra of the intermediate photoproduct, FMF, with those of Ribo and LC concomitantly present in the medium, the absorption spectrum of FMF cannot be determined directly from the observed spectra of the medium.

The quantum yield of the first photoreaction step, ($\Phi_{A\rightarrow B_1}^{\lambda_{irr}}$) is determined from the rate-constant eq.4 as;

$$\Phi_{A\rightarrow B_1}^{\lambda_{irr}} = \frac{k_{\mathrm{A}\rightarrow B_1}^{\lambda_{irr}} \times A_{tot.}^{\lambda_{irr}/\lambda_{irr}}(0)}{\varepsilon_A^{\lambda_{irr}} \times l_{\lambda_{irr}} \times P_{\lambda_{irr}} \times \left(1 - 10^{-A_{tot.}^{\lambda_{irr}/\lambda_{irr}}(0)}\right)} (eq.7b)$$

The reconstruction of the concentration profiles of species A, B_1, and B_2 versus irradiation time for each time point of absorbance measurement was realised by first attributing plausible arbitrary values to the three unknowns, $\varepsilon_{B_2}^{\lambda_{irr}}$, $k_{\mathrm{A}\rightarrow B_1}^{\lambda_{irr}}$, $k_{B_1\rightarrow B_2}^{\lambda_{irr}}$, and substituting them in the concentration equations (eqs. 3a, 3b and 3c) for $C_A(t)$, $C_{B1}(t)$ and $C_{B2}(t)$, respectively, for all the time point intervals. From then, the total absorbance spectrum could be determined for the chosen values using model equation (eq.5). Fitting of the latter trace to the experimental absorbance trace was evaluated and the values altered until a

perfect fitting of the model trace to the experimental trace is obtained. The value of $\varepsilon_{B_1}^{\lambda_{irr}}$ for that irradiation wavelength can also be determined from $v_{o\ Cal.}^{\lambda_{irr}/\lambda_{obs}}$, eq.6b as;

$$\varepsilon_{B_1}^{\lambda_{obs}} = \frac{v_o^{\lambda_{irr}/\lambda_{obs}}}{l_{\lambda_{obs}} \times \Phi_{A\to B_1}^{\lambda_{irr}} \times \varepsilon_A^{\lambda_{irr}} \times l_{\lambda_{irr}} \times P_{\lambda_{irr}} \times F^{\lambda_{irr}/\lambda_{irr}}(0) \times C_A\ (0)} + \varepsilon_A^{\lambda_{obs}}\ (eq.7c)$$

The accuracy of the thus determined rate-constant values can be verified/ corrected and/or further refined by fitting the model using these values to the kinetic traces of the same irradiation experiment observed at different wavelengths. This step necessitates, the determination and refinement of an intelligently selected value for $\varepsilon_{\mathrm{B1}}^{\lambda_{\mathrm{obs.}}}$ and further refinement, if necessary, of the rate-constant value, that is constant for all observation kinetic traces corresponding to the same irradiation experiment, until a good fit is realised for all the kinetic traces. The method of refining the fitting of the model to a number (3-4) of observation kinetic traces ensures a close precision in the estimation of the kinetic parameters of this photoreaction type. Furthermore, the higher the number of observed kinetic traces, the higher the precision of the determined kinetic parameters, which should also be compared against other irradiation and observation cases to ensure precision and accuracy. Furthermore, this task could be further simplified if the spectra of the intermediate photoproduct(s) were already determined from the literature.

This method allows the reconstruction of the individual concentration profiles of the species present in the medium at various times as well as their absorption coefficients profiles over the studied irradiation wavelengths (figure 7).

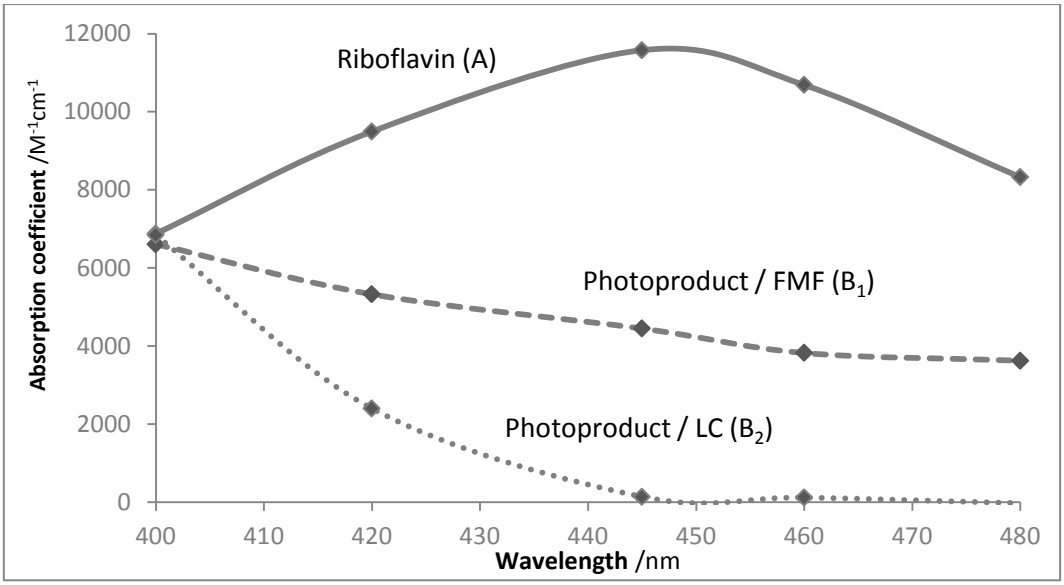

Figure 7: Electronic absorption spectra (expressed as absorption coefficient units) of Riboflavin and its photoproducts B_1 and B_2.

Finally, the quantum yield of the second photoreaction step can be determined from the equation of the rate-constant for the phototransformation of B_1 into B_2 ($k_{B_1\rightarrow B_2}^{\lambda_{irr}}$) as given by eq.7d;

$$\Phi_{B_1\rightarrow B_2}^{\lambda_{irr}} = \frac{k_{B_1\rightarrow B_2}^{\lambda_{irr}} \times \varepsilon_{B_1}^{\lambda_{irr}} \times l_{\lambda_{irr}} \times C_A(0)}{\varepsilon_{B_1}^{\lambda_{irr}} \times l_{\lambda_{irr}} \times P_{\lambda_{irr}} \times \left(1 - 10^{-\varepsilon_{B_1}^{\lambda_{irr}} \times l_{\lambda_{irr}} \times C_A(0)}\right)} (eq.7d)$$

It, then, becomes possible to determine the individual concentration profiles (Figure 8) of A, B_1 and B_2 by substitution of the values of $\varepsilon_A^{\lambda_{irr}}$, $\varepsilon_{B_1}^{\lambda_{irr}}$, $k_{\mathrm{A}\rightarrow B_1}^{\lambda_{irr}}$ *and* $k_{B_1\rightarrow B_2}^{\lambda_{irr}}$ into the Φ-model concentration equations (eqs. 3a-3c) This can be achieved for each monochromatic irradiation experiment.

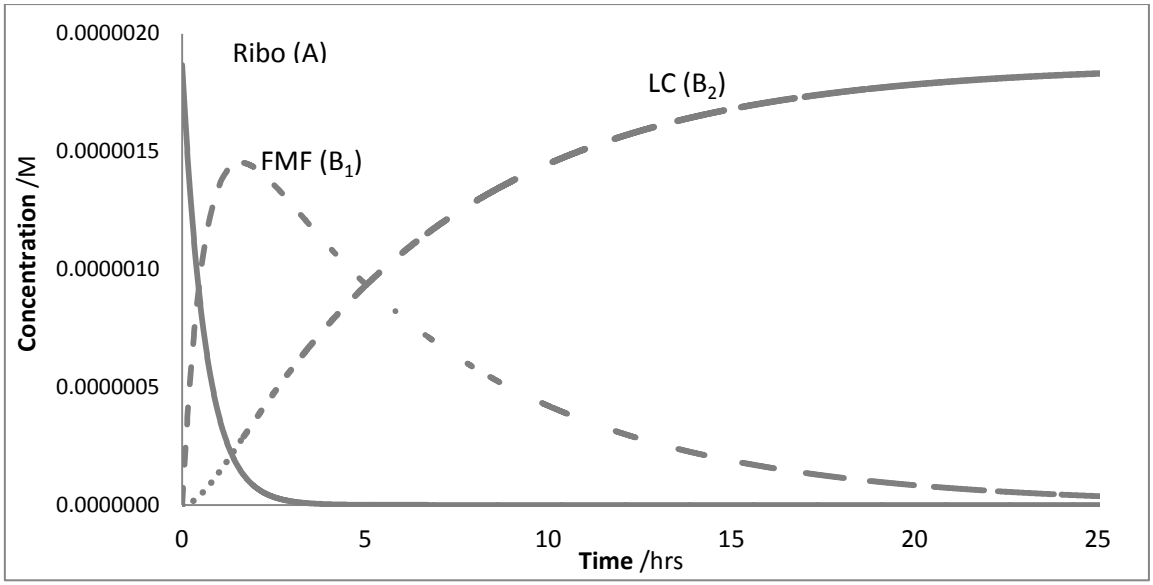

Figure 8: Evolution of the concentration profiles of Ribo (1.8 x 10^{-6} M) and its photoproducts (B_1 and B_2) upon irradiation at 445 nm (P_{445} = 1.26 x 10^{-6} einstein. s^{-1}.dm^{-3}), as determined using the $AB_2(2\Phi)$-model concentration equations (eqs. 3a-3c).

The kinetic attributes of Ribo photodegradation in ethanol are presented in Table 2. The elucidation method presents (i) the quantum yield values of each photoreaction step; (ii) the absorbance spectra of the photoproducts and (iii) the kinetic concentration profiles of the reactant and photoproducts. Furthermore, this can be achieved without the need for a physical separation of the species using the method described above.

Table 2: Quantum yields, overall rate–constant and absorption coefficient values for *Riboflavin* photodegradation reactions and its two photoproducts measured at various monochromatic and continuous irradiations.

λ_{irr}/nm	$C(0)$ x 10^6 / M	$P_{\lambda_{irr}}$ x 10^6 /einstein.s^{-1}.dm^{-3}	$\varepsilon_A^{\lambda_{irr}}$/$M^{-1}cm^{-1}$	$\varepsilon_{B_1}^{\lambda_{irr}}$/$M^{-1}cm^{-1}$	$\varepsilon_{B_2}^{\lambda_{irr}}$/ M^{-1} cm^{-1}	$k_{A\rightarrow B_1}^{\lambda_{irr}}$ x 10^4 /M^{-1}.s^{-1}.dm^{-3}.einstein	$k_{B_1\rightarrow B_2}^{\lambda_{irr}}$ x 10^4 /M^{-1}.s^{-1}.dm^{-3}.einstein	$\Phi_{A\rightarrow B_1}^{\lambda_{irr}}$ x 10^2	$\Phi_{B_1\rightarrow B_2}^{\lambda_{irr}}$ x 10^2
400	1.46	1.29	6880	6607	6840	2.4	0.06	0.354±0.0003	0.008±0.001
420	1.03	1.30	9494	5325	2400	3.2	0.22	0.625± 0.021	0.009±0.002
445	1.87	1.26	11578	4447	141	4.7	0.36	0.687±0.027	0.096±0.018
460	1.55	1.39	10685	2822	120	5.1	0.40	0.764±0.012	0.126±0.043
480	1.11	1.39	8325	3625	0	3.5	0.34	0.756±0.118	0.127±0.035

2.4. Wavelength-quantum yield correlation

The individual quantum yield values (table 2) increased with irradiation wavelength in the visible region of the spectrum (figure 9). This variation however, was more pronounced for the second photoreaction step (LC) with a 5-fold increment between the lowest and highest recorded quantum yields compared to only a 1.5-fold variation for the quantum yields corresponding to the initial photoreaction step (FMF). The quantum yield values $\Phi_{A\rightarrow B_1}^{\lambda_{irr}}$ were 6 – 20 times higher than the subsequent $\Phi_{B_1\rightarrow B_2}^{\lambda_{irr}}$. Remarkably, a linear correlation could be established between the first and second photoreactions quantum yields values for increasing irradiation wavelengths, thereby suggesting a concordance in the incremental increase of the two sets of quantum yield values with wavelength (figure 10). Overall, the quantum yield values for Ribo photodegradation were one to three orders of magnitude smaller than those recorded in earlier chapters for nifedipine, nisoldipine, montelukast and fluvoxamine.

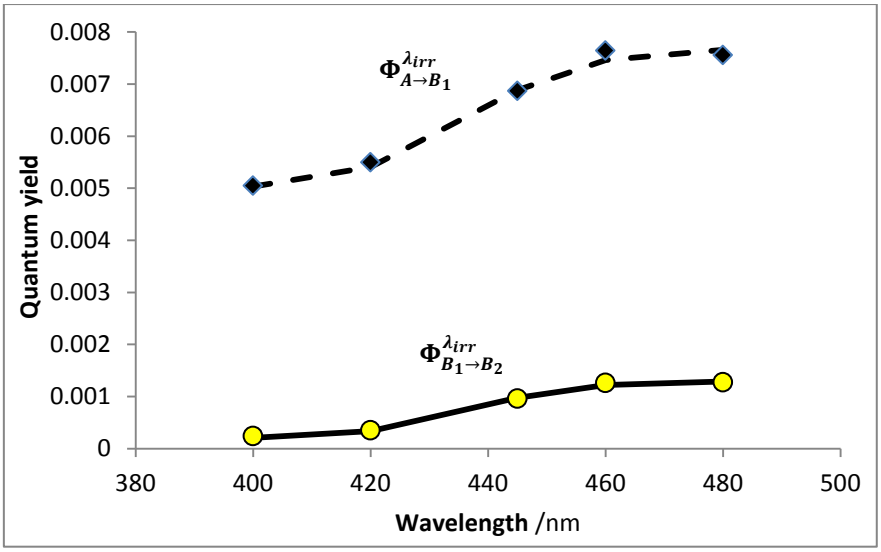

Figure 9: Quantum yield values for the two consecutive photoreaction steps of Ribo (1.8 x 10^{-6} M) photodegradation in ethanol for different irradiation wavelengths (shapes); together with the sigmoid-fitted functions for quantum yield variation with wavelength (lines).

The variation of both sets of quantum yield values were described by sigmoid functions (eqs.8),

$$\Phi_{A\rightarrow B_1}^{\lambda_{irr}} = \frac{0.0006}{0.22 + 0.155 \times e^{-0.1(\lambda_{irr}-439.9)}} + 0.004965 \qquad (eq.8a)$$

$$\Phi_{B_1\rightarrow B_2}^{\lambda_{irr}} = \frac{0.0002}{0.18 + 0.13 \times e^{-0.11(\lambda_{irr}-439.9)}} + 0.00019 \qquad (eq.8b)$$

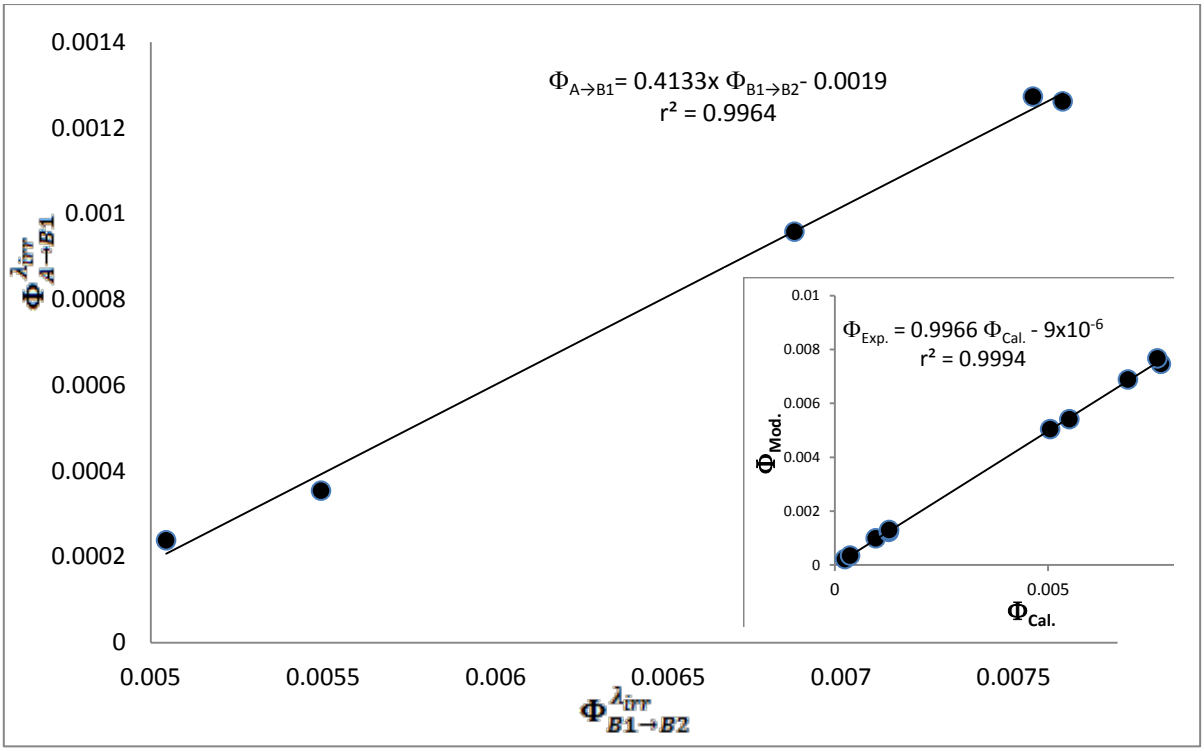

Figure 10: Correlation between the quantum yields corresponding to the first and second photoreaction steps of Riboflavin photodegradation in ethanol. Inset: Correlation between quantum yield values for Riboflavin photodegradation in ethanol determined experimentally by model fitting ($\Phi_{Mod.}$) and those calculated ($\Phi_{Cal.}$) from the sigmoid function equations (eqs. 8a or 8b).

The above functions were determined by conducting a few irradiation experiments at selected monochromatic wavelengths. Besides, they offer the possibility to determine the quantum yields of photoreactions at any wavelength. The sigmoid nature of photoreaction quantum yield evolution with irradiation wavelength has also been found for a number of drugs Nis, Nif, Fluvo and Monte.

The accuracy of these functions to describe the quantum yields evolution with wavelength was evaluated by comparing the experimental quantum yield values ($\Phi_{Mod.}$) obtained

through the elucidation method described above to those calculated from the sigmoid functions ($\Phi_{cal.}$), for each irradiation wavelength. The inset in Figure 10 shows a very good correspondence between the two sets of values thereby providing a new tool for the determination of the quantum yield values of Ribo photodegradation in ethanol for any monochromatic wavelength in the 400-480 nm range from eqs. 8a and 8b without the need to conduct any experiment.

2.5. Pseudo-rate-constant

In order to establish the utility of Ribo as a potential actinometer for the visible monochromatic irradiation range 400-480 nm, ethanolic solutions of Ribo of the same concentration were irradiated at various known radiant power intensities for different irradiation wavelengths. The resulting kinetic traces were fitted with the Φ-order model eq.5 (figure 11), and the rate-constants (eq.4) were determined.

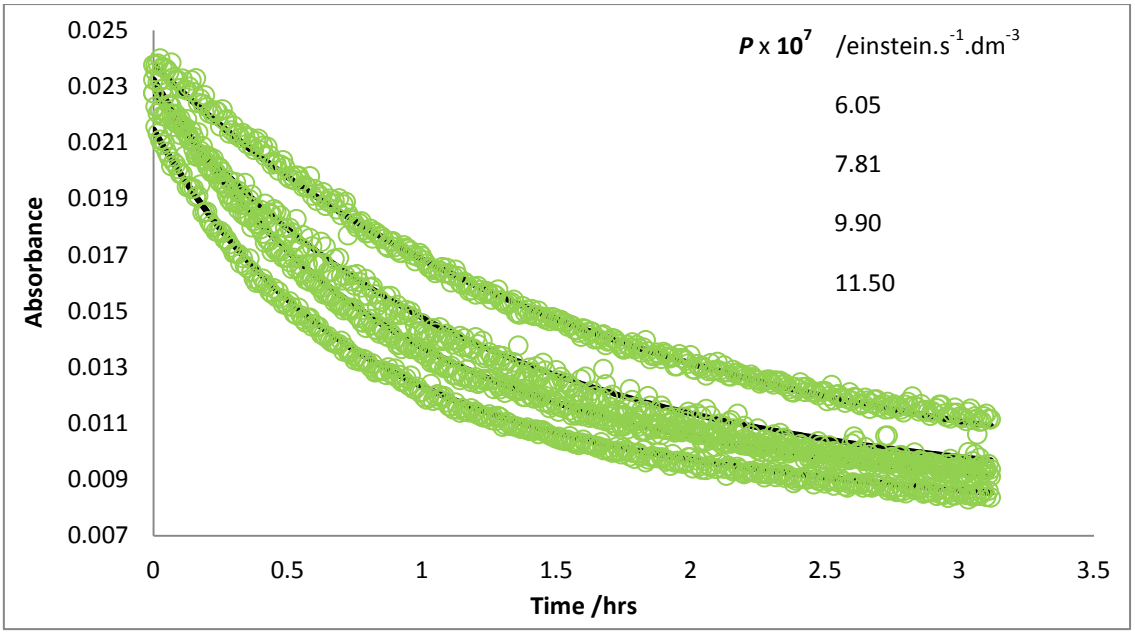

Figure 11. Effect of increasing the irradiation radiant power ($P_{\lambda_{irr}}$) on the kinetic traces of Ribo (1.50 x 10^{-6} M) when irradiated and observed at 445 nm. The circles represent the experimental data while the lines represent the model fitted traces.

As can be predicted from eq. 4, the correlation between the rate-constants, determined by model fitting, with their respective radiant power value for each wavelength set of actinometry experiments, yielded straight lines (r^2>0.96) with intercepts close to zero (Table 3). A similar linear correlation could be established between the initial velocity values, determined from eq.6b and their corresponding radiant power with $\delta_{\lambda_{irr}}$as the gradient of the line and near-zero intercepts (table 3).

Table 3: Correlation between $k_{A\rightarrow B_1}^{\lambda_{irr}}$, $k_{B_1\rightarrow B_2}^{\lambda_{irr}}$, and υ_o with radiant power ($P_{\lambda_{irr}}$), for Ribo (1.8 x 10^{-6} M) photodegradation in ethanol ($l_{\lambda_{irr}}$= 2 cm; $l_{\lambda_{obs}}$= 1 cm) together with the

corresponding $\beta_{\lambda_{irr}}$ or $\delta_{\lambda_{irr}}$ and the span of radiant power employed for various monochromatic irradiations.

Irradiation wavelength $\boldsymbol{\lambda_{irr}}$ / nm	**Equation of the line** [a]	**Correlation coefficient,** $\boldsymbol{r^2}$	$\boldsymbol{P_{\lambda_{irr}}}$ **range** $\times \mathbf{10^7}$ /einst.s^{-1}.dm^{-3}
	$\boldsymbol{k^{\lambda_{irr}}_{A\rightarrow B_1} = \beta^{\lambda_{irr}}_{A\rightarrow B_1} \times P_{\lambda_{irr}}}$		
420	$302.22\times P_{420} - 3\times 10^{-5}$	0.99	6.27 – 1.30
445	$421.9\times P_{445} - 5\times 10^{-5}$	0.98	6.05 – 12.5
460	$305.1\times P_{460} + 8\times 10^{-5}$	0.99	7.46 – 1.39
480	$225.8\times P_{480} + 4\times 10^{-5}$	0.97	8.17 – 19.2
	$\boldsymbol{k^{\lambda_{irr}}_{B_1\rightarrow B_2} = \beta^{\lambda_{irr}}_{B_1\rightarrow B_2} \times P_{\lambda_{irr}}}$		
420	$3.52\times P_{420} - 5\times 10^{-7}$	0.97	6.27 – 1.30
445	$43.7\times P_{445} - 3\times 10^{-5}$	0.98	6.05 – 12.5
460	$41.9\times P_{460} - 2\times 10^{-5}$	0.96	7.46 – 1.39
480	$39.7\times P_{480} - 2\times 10^{-5}$	0.96	8.17 – 19.2
	$\boldsymbol{v_o = \delta_{\lambda_{irr}} \times P_{\lambda_{irr}} + intercept}$		
420	$-2.88 \times P_{420} + 6\times 10^{-7}$	0.95	6.27 – 1.30
445	$-4.15 \times P_{445} - 3\times 10^{-7}$	0.95	6.05 – 12.5
460	$-2.49 \times P_{460} - 1\times 10^{-6}$	0.94	7.46 – 1.39
480	$-7.21 \times P_{480} + 5\times 10^{-6}$	0.97	8.17 – 19.2

[a] $k^{\lambda_{irr}}$ and intercepts expressed in s^{-1}.dm^{-3}. M^{-1}.einstein; $\beta_{\lambda_{irr}}$ in M^{-1}.

These experimental results are in agreement with eqs.4 and 6a, since a proportional relationship between radiant power and each of the rate-constant and initial velocity was observed and recorded. The gradient $\beta_{\lambda_{irr}}$ is wavelength-dependent and holds the same value for experiments conducted using the same molecule, initial concentration and solvent, although the radiant power may be different. $\beta_{\lambda_{irr}}$ reflects the rate-constant of a photoreaction for each mole of photons absorbed. In other words, it is independent of the intensity of radiation and can thus be described as the pseudo-rate constant of photoreactions. This parameter offers tremendous advantages in the area of photoreactions kinetics since, unlike the rate constant, it allows effective comparisons of photoreactions rates to be made between the same set of studies or between different studies and even for different molecules. This is because the radiant power is hardly replicable between different irradiation experiments and laboratories, and as a result the rate-constant could, thus far, not be used to compare different photoreactions rates of different photokinetic studies (Maafi and Maafi, 2015a; Maafi and Maafi, 2015a, Moore, 2004). This represents a critical issue that has hampered further advances in the field of photoreactions kinetics and has prevented effective comparisons to be made between different photokinetic studies of the same or different photochromic molecules. This problem has further prevented any kinetic models developments for photoreactions.

Therefore, the use of *monochromatic* light regardless of the light type source together with the *pseudo-rate-constant,* $\beta_{\lambda_{irr}}$, allows (i) the universal standardisation of photokinetic

studies irrespective of the light source used, provided that the study is conducted using monochromatic beams; (ii) a standard and quantitative kinetic data treatment method of photodegradation results and (iii) the provision of full and effective quantitative analytical methods for the evaluation and prediction of photoreactions behaviours for different study reports or for the study of a given variable within the same set of experiments.

Using this approach, photoreactions rates can be quantitatively compared and predicted for any irradiation intensities used. Furthermore, even for experiments where the concentrations and/or irradiation path-lengths (e.g. Exp.$_1$ and Exp.$_2$) are different, their corresponding $\beta_{Exp_1}^{\lambda_{irr}}$ and $\beta_{Exp_2}^{\lambda_{irr}}$ can be adjusted to account for the variation in concentration and/or irradiation path-length in order to compare the photoreactions rates of the molecule(s). The adjustment is achieved by dividing $\beta_{Exp._2}^{\lambda_{irr}}$ by the ratio $(F_{Exp._2}^{\lambda_{irr}} \times l_{Exp._2}^{\lambda_{irr}})/(F_{Exp._1}^{\lambda_{irr}} \times l_{Exp._1}^{\lambda_{irr}})$ and comparing it to $\beta_{Exp._1}^{\lambda_{irr}}$ or dividing $\beta_{Exp._1}^{\lambda_{irr}}$ by the ratio $(F_{Exp._1}^{\lambda_{irr}} \times l_{Exp._1}^{\lambda_{irr}})/(F_{Exp._2}^{\lambda_{irr}} \times l_{Exp._2}^{\lambda_{irr}})$ and comparing it to $\beta_{Exp._2}^{\lambda_{irr}}$.

The utility of the pseudo-rate constant can be illustrated using Ribo results where a correlation of $\beta_{A\rightarrow B_1}^{\lambda_{irr}}$ and $\beta_{B_1\rightarrow B_2}^{\lambda_{irr}}$ with wavelength (figure 12) shows a higher rate of photodegradation at 445 nm for both photoreaction steps. This indicates that irrespective of the radiant power, the rate of Ribo photodegradation in ethanol is highest at 445 nm. Also, for all wavelengths, $\beta_{A\rightarrow B_1}^{\lambda_{irr}}$ was shown to be about 10-fold higher than $\beta_{B_1\rightarrow B_2}^{\lambda_{irr}}$, indicating a much faster initial photoreaction rate for the degradation of A into B_1 than the

phototransformation of B_1 into B_2. The equations correlating $\beta_{\lambda_{irr}}$ with wavelength (figure 12), allow the determination of the value of $\beta_{\lambda_{irr}}$ for any wavelength in the 400-480 nm range for Ribo solution in ethanol at a concentration of 1.8 x 10^{-6} M and irradiation path-length of 2 cm. Furthermore, two other strategies exist for the determination of this factor that can be achieved experimentally through a correlation between $k_{\lambda_{irr}}$ and $P_{\lambda_{irr}}$, if the latter parameter is known or can be determined, or simply using its analytical formula eq.9a.

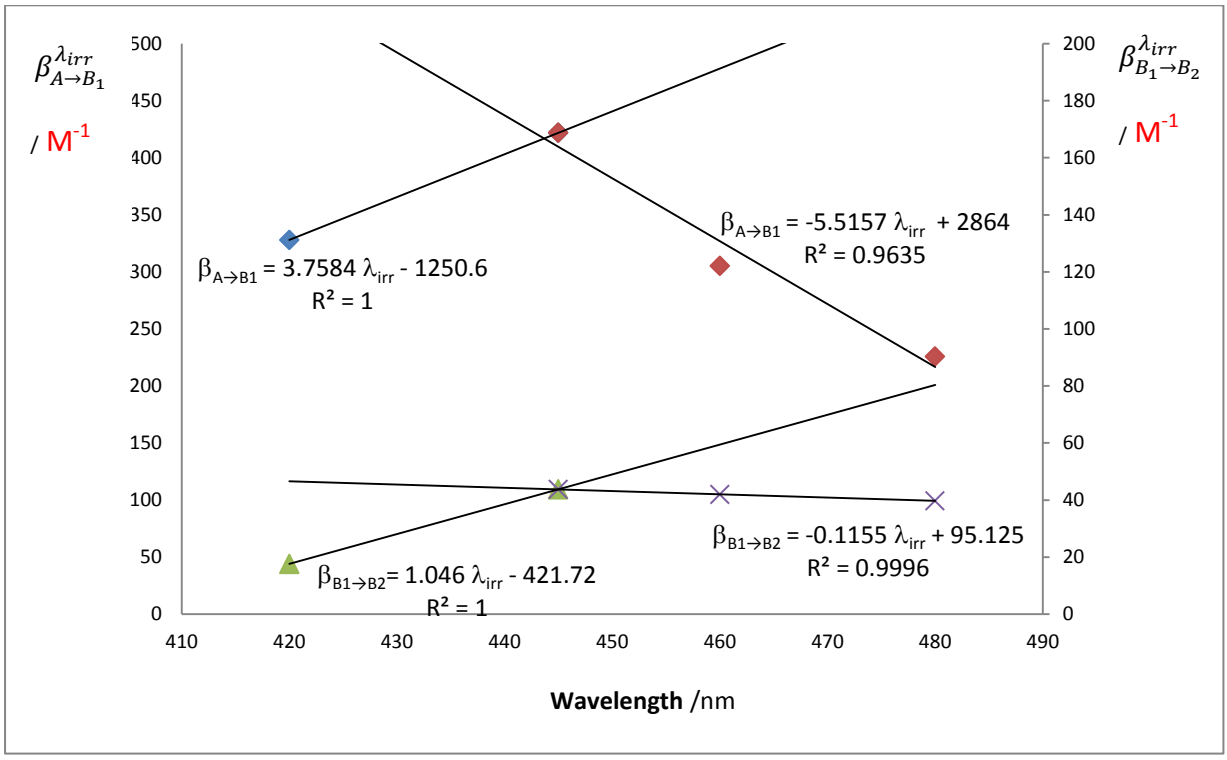

Figure 12: Variation of the pseudo-rate-constant with irradiation wavelength for each photoreaction step of Ribo (1.8 x 10^{-6} M) photodegradation in ethanol ($l_{\lambda_{irr}}$ = 2 cm; $l_{\lambda_{obs}}$ = 1 cm).

2.6. Ribo actinometry

A further benefit procured by the pseudo-rate-constant is the provision of new actinometric systems in the form of photoreactive molecules such as riboflavin, nifedipine, montelukast, nisoldipine and fluvoxamine (Maafi and Maafi, 2015a; Maafi and Maafi, 2015b; Maafi and Maafi, 2014a, Maafi and Maafi, 2014b; Maafi and Maafi, 2013). In the case of Ribo, the linear correlation between its rate-constants of photodegradation with radiant power (Table 3) highlights its utility as an actinometric tool in the 400-480 nm spectral range. The determination of the radiant power intensity of a monochromatic beam of unknown intensity can be achieved by preparing an ethanolic solution of $1.8 \text{ x } 10^{-6}$ M and irradiating it with the irradiation source of interest. The rate-constant(s) of the solution photodegradation can then be determined by $AB_2(2\Phi)$ kinetic model (eq.5) fitting. The determined $k_{A\rightarrow B_1}^{\lambda_{irr}}$ or $k_{B_1\rightarrow B_2}^{\lambda_{irr}}$ together with the corresponding $\beta_{A\rightarrow B_1}^{\lambda_{irr}}$ or $\beta_{B_1\rightarrow B_2}^{\lambda_{irr}}$, respectively can then be substituted into eq. 9a derived from eq. 4, to determine the unknown, $P_{\lambda_{irr}}$.

$$P_{\lambda_{irr}} = \frac{k_{A\rightarrow B_1}^{\lambda_{irr}}}{\beta_{A\rightarrow B_1}^{\lambda_{irr}}} = \frac{k_{B_1\rightarrow B_2}^{\lambda_{irr}}}{\beta_{B_1\rightarrow B_2}^{\lambda_{irr}}} \ (eq.9a)$$

A similar procedure can also be adopted using the gradient $\delta_{\lambda_{irr}}$ to determine the radiant power using eq.9b derived from eq.6a as

$$P_{\lambda_{irr}} = \frac{\boldsymbol{v_o}^{\lambda_{irr}/\lambda_{obs}}}{\delta_{\lambda_{irr}}} \text{ (eq.9b)}$$

The initial velocity of a photoreaction can be determined using different strategies; (i) from the derivative of the model at t_0, (eq.6b), (ii) from its analytical formula (eq.6a), or (iii) from

the gradient of the line formed by the very first experimental points of the kinetic trace. On the other hand, the parameter $\delta_{\lambda_{irr}}$can be determined from table 3 or from its analytical expression (in eq.6a). This factor takes the function of a pseudo-initial velocity as it reflects the initial velocity per quantum of light absorbed by the sample. As was argued for the pseudo-rate constant, $\delta_{\lambda_{irr}}$provides a new quantitative tool for the evaluation, comparison and prediction of initial photoreaction velocity between studies using different monochromatic beam intensities.

3. Conclusion

The RK-5 NIM methodology was used to elaborate a photokinetic model for consecutive photoreactions involving up to four photoproducts ($AB_4(4\Phi)$). This model proved to be reliable when tested against RK-5 NIM traces. On the other hand, the use of this integrated rate-law elaboration methodology to develop semi-empirical Φ-order kinetic models that faithfully describe photoreactions kinetics has overcome the integration problem of photoreactions differential equations that was at the origin of the erroneous use of 0^{th}, 1^{st} and 2^{nd}-order models despite an often encountered ambiguousness and inadequacy to describe photoreactions kinetics.

The photodegradation reaction of Ribo in ethanol was well described by the $AB_2(2\Phi)$ kinetic model. The latter allowed not only the fitting of the kinetic traces of photodegradation but also a complete elucidation of the kinetics of Ribo photodegradation in ethanol within the 400-480 nm range, that encompassed rate-constant and quantum yields determination for

each consecutive photoreaction step. The quantum yields of Ribo photodegradation were found to increase with increasing wavelength in the visible region of the spectrum, a correlation that could be quantified by sigmoid functions. Such correlations offer the possibility of calculating Ribo quantum yields corresponding to any visible irradiation wavelength. Furthermore, the model also allowed the establishment of Ribo as an actinometer for the irradiation range 400 - 480 nm. This type of kinetic studies opened for the first time new horizons for the harmonisation of photoreactions kinetics through the use of monochromatic light irradiation and the pseudo-rate constant, β a new photokinetic tool that reflects the rate-constant of photoreactions independent of irradiation intensity and which can be used to compare the kinetics of the same or different molecules under different radiant-power intensities. Furthermore, the $AB_2(2\Phi)$ kinetic elucidation method, as applied to determine Ribo kinetics, offers the possibility to elucidate the kinetics of any photoactive molecule reacting through the $AB_2(2\Phi)$ mechanism. Additionally, the NIM-based methodology has allowed the modelling of the kinetic traces of many photoreaction types and thus the photodegradation kinetics of several drugs. It thus allows a complete kinetic study to be effectuated on photoreactions.

References

Ahmad I., Sheraz M.A., Ahmed S., Kazi S.H., Mirza T., Aminuddin M., 2011. Stabilizing effect of citrate buffer on the photolysis of riboflavin in aqueous solution. Results in Pharma Sciences, 1, 11–15.

Ahmad I., Ahmed S., Sheraz M.A., Vaid F.H.M., Ansari I.A., 2010a. Effect of divalent anions on photodegradation kinetics and pathways of riboflavin in aqueous solution. International Journal of Pharmaceutics, 390, 174–182.

Ahmad I., Fasihullah Q., Vaid Faiyaz H.M., 2006a. Photolysis of formylmethylflavin in aqueous and organic solvents. Photochemical and Photobiological Sciences, 5(7), 680-685.

Ahmad I., Fasihullah Q., Vaid Faiyaz H.M., 2006b. Effect of light intensity and wavelengths on photodegradation reactions of riboflavin in aqueous solution. Journal of Photochemistry and Photobiology B: Biology, 82, 21–27.

Ahmed I., Fassihullah Q., Noor A., Ansari I.A., Ali Q.N.M., 2004. Photolysis of riboflavin in aqueous solution: a kinetic study, International Journal of Pharmaceutics. 280, 199-208.

Albini A. and Fasani E., 1998. Drugs Photochemistry and Photostability. The Royal Society of Chemistry, Cambridge.

Baranda A.B., Alonsoa R.M., Jime´neza R.M., Weinmann W., 2006. Instability of calcium channel antagonists during sample preparation for LC–MS–MS analysis of serum samples. Forensic Science International, 156, 23–34.

Bosca F., Miranda M.A., 1997. Photosensitizing drugs containing the benzophenone chromophore. Journal of Photochemistry and Photobiology B: Biology, 43, 1-26.

Chacon J.N., McLearie J., Sinclair R.S., 1988. Singlet oxygen yields and radical contributions in the dye-sensitised photo-oxidation in methanol of esters of polyunsaturated fatty acids (oleic, linoleic, linolenic and arachidonic). Photochemistry and Photobiology. 47, 647-656.

Corbin F., 2002. Pathogen inactivation of blood components: Current status and introduction of an approach using riboflavin as a photosensitizer. International Journal of hematology, 76, 253-257.

Dewick P.M., 1998. Medicinal natural products, John Wiley & Sons, Chichester.

Fasani E, Albini A, Mella M., 2008. Photochemistry of Hantzsch 1,4-dihydropyridines and pyridines. Tetrahedron, 64, 3190-3196.

Gorner H., 2010. Photocyclization of 2,6-dichlorodiphenylamines in solution. Journal of Photochemistry and Photobiology A: Chemistry, 211, 1–6.

Heelis P.F., 1982. The photophysical and photochemical properties of flavins (isoalloxazines). Chemistry Society Reviews. 11, 15-39.

Jiao S., Zheng S., Yin D., Wang L., Chen L., 2008. Aqueous photolysis of tetracycline and toxicity of photolytic products to luminescent bacteria. Chemosphere 73, 377–382.

Koziol J., 1966a. Studies on flavins in organic solvents-I. Spectral characteristics of riboflavin, riboflavin tetrabutyrate and lumichrome. Photochemistry and Photobiology, 5, 41-54.

Koziol J., 1966 b. Studies on flavins in organic solvents-II. Photodecomposition of riboflavin in the presence of oxygen. Photochemistry and Photobiology, 5, 55-62.

Maafi M. and Maafi W., 2015a. Quantitative assessment of photostability and photostabilisation of Fluvoxamine and its design for actinometry. Photochemical Photobiological Sciences.14(5),982-94

Maafi M. and Maafi W., 2015b. Quantification of Unimolecular Photoreaction Kinetics: Determination of Quantum Yields and Development of Actinometers—The Photodegradation Case of Cardiovascular Drug Nisoldipine. International Journal of Photoenergy, 2015.

Maafi M., Maafi W., 2014a. Φ-order kinetics of photoreversible drug reactions. Int. J. of Pharm. 471, 536-543.

Maafi M., Maafi W., 2014b. Montelukast photodegradation: Elucidation of Φ-order kinetics, determination of quantum yields and application to actinometry. Int. J. Pharm. 471, 544-552.

Maafi W., Maafi M., 2013. Modelling Nifedipine Photodegradation, Photostability and Actinometric Properties. Int. J. Pharm. 456(1), 153-164.

Maafi M., 2010. The potential of AB(1Φ) systems for direct actinometry. Diarylethenes as successful actimometers for the visible range. Phys. Chem. Chem. Phys. 12, 13248–13254.

Maafi M, Brown R.G., 2007. The kinetic model for AB(1Φ) systems. A Closed-form integration of the differential equation with a variable photokinetic factor. J. Photochem. Photobiol. A: Chem. 187, 319-324.

Massad W. A., Marioli J. M., Garcı´a N. A., 2006. Photoproducts and proposed degradation pathway in the riboflavin-sensitised photooxidation of isoproterenol. Pharmazie, 61,1019–1021.

Moore D.E., 2004. Photophysical and photochemical aspects of drug stability. In Tonnesen H.H, 2004. Photostability of Drugs and Drug Formulations (second Edition). CRC Press: London; 2004.

Moore W.M. and Ireton R.C., 1977. The photochemistry of riboflavin-V. The photodegradation of isoalloxazines in alcoholic solvents. Photochemistry and Photobiology, 25, 347–356.

Moore W.M., McDaniels J.C and Hen J.A., 1977. The photochemistry of riboflavin-VI. The photophysical properties of isoalloxazines. Photochemistry and Photobiology 25 (6), 505-512

Piechocki J.T., Thoma K., 2010. Pharmaceutical Photostability and Photostabilisation Technology. Informa Healthcare: London.

Sheraz M.A., Kazi S.H., Ahmed S., Anwar Z., Ahmed I., 2014. Photo, thermal and chemical degradation of riboflavin. Beilstein Journal of Organic Chemistry, 10, 1999-2012.

Sikorska E., Khmelinskii E., Komasa A., Koput J., Ferreira L.F.V., Herance J.R., Bourdelande J.L., Williams S.L., Worrall D.R., Insin´ska-Rak M., Sikorski M., 2005. Spectroscopy and photophysics of flavin related compounds: Riboflavin and iso-(6,7)-riboflavin. Chemical Physics. 314, 239–247.

Tonnesen H.H., 2004 Photostability of drugs and drug formulations (second Ed.). CRC Press, London.

Wu Y., Kookana R., 2011. Aqueous Photodegradation of Selected Antibiotics under Different Conditions. *2010 International Conference on Biology, Environment and Chemistry, IPCBEE vol.1, IACSIT Press, Singapore, 191-194.*

Chapter VII: The utility of Φ-order kinetics in the development of actinometers

1. Introduction

The energy quanta of the photons flux absorbed by a sample is responsible for the electronic excitations of photoactive molecules. The rate at which the photons impact on the sample affects the rate of a given photoreaction, as conveyed by the rate-constant equation. A variation in the number of photons incident on a sample per unit time induced by altering irradiation intensity will, thus, have a direct effect on photoreaction rate. It is, therefore, important to quantify the number of photons reaching a sample per unit time and area during the study of photoreactions kinetics. This process is known as actinometry and has traditionally been performed using either chemical or physical devices.

Chemical actinometry is performed by irradiating a chemical system, of known quantum yield (Φ) values, under the same conditions as the studied sample and subsequently determining the number of molecules that have photoreacted per unit volume per unit time (Rate). This is usually determined by monitoring the concentration of a secondary species that forms after irradiation has stopped by reaction between the photoproduct of the actinometer and a specific chemical substance added to the reaction medium.The actinomter photoreaction rate together with the known quantum yield value of the chemical actinometer can then be used to determine the photon flux per unit volume per unit time (*N*) using the following equation (Khun et al., 2004):

$$N = \frac{Rate}{\Phi} \ (\text{eq. } 1)$$

Physical actinometry, on the other hand, relies on physical devices that convert the energy or the number of the incident photons falling on photodiodes into a quantifiable electrical signal translated into a direct readout. They tend to be preferred to chemical actinometers due to their simple, fast and precise performance (Khun et al., 2004). Nevertheless, they represent a more expensive option and their sensitivity may decrease with use, or may be altered by aging and occasional recalibration is recommended. Furthermore, sometimes visually unnoticeable damage may occur to the photodiodes during exposure to high irradiation levels leading to irreversible reduction in sensitivity and severe inhomogeneities on the surface (Khun et al., 2004).

For the photostability testing of new active substances and medicinal products, the ICH recommends the use of quinine chemical actinometry for the recommended 320-400 nm spectral irradiation range (ICH, 1996). However, this actinometer has rarely been used for this purpose as it was shown to be sensitive to oxygen content of the medium and undergo thermal reaction (Baertschi et al., 2010; Baertschi, 1997; De Azevedo Filho et al., 2011). The most widely used ferrioxalate actinometer has also been attributed major drawbacks due to its cumbersome experimental usage and a rapid reaction completion compared to most photoreactions (Moore, 2004) which have rendered accurate quantum yield determination a challenging task.

In view of the important limitations associated with physical and chemical actinometers, including the ICH recommended one, the added utility of the Φ-order kinetics in allowing

the development of more accurate and easy-to-use drug-based actinometers will be detailed in this chapter. For this purpose, the theoretical background underlying this actinometry study will first be explained. Subsequently, the utility of the previously studied drugs to act as actinometers will be explored and a stepwise actinometry method provided.

2. Results and discussion

2.1. Theoretical background

The Φ-order kinetic equations provide a useful tool for the development of actinometers. The linear relationship bewteen the rate-constant and the radiant power, conveyed by equation (eq. 1) and that between initial photoreaction velocity and radiant power (eq. 2) can advantageously be explored for the proposal of a new methodology to conduct actinometry.

$$k_{A \leftrightharpoons B}^{\lambda_{irr}} = \left(\Phi_{A \to B}^{\lambda_{irr}} \times \varepsilon_A^{\lambda_{irr}} + \Phi_{B \to A}^{\lambda_{irr}} \times \varepsilon_B^{\lambda_{irr}}\right) \times l_{\lambda_{irr}} \times F_{\lambda_{irr}}(\infty) \times P_{\lambda_{irr}}$$

$$= \beta_{\lambda_{irr}} \times P_{\lambda_{irr}} \qquad (eq.1)$$

$$\upsilon_{0\ (cld.)}^{\lambda_{irr}/\lambda_{obs}} = \left(\varepsilon_B^{\lambda_{obs}} - \varepsilon_A^{\lambda_{obs}}\right) \times l_{\lambda_{obs}} \times \Phi_{A \to B}^{\lambda_{irr}} \times \varepsilon_A^{\lambda_{irr}} \times l_{\lambda_{irr}} \times F_{\lambda_{irr}}(0) \times C_0 \times P_{\lambda_{irr}}$$

$$= \quad \delta_{\lambda_{irr}} \times P_{\lambda_{irr}} \quad (eq.2)$$

The validation of a new actinometer can be achieved by conducting irradiation experiments of various intensities and fitting the data with the Φ-order kinetics in order to

experimentally confirm the applicability of eq. 1 and/or 2 to the proposed molecule and confirm its suitability for actinometry within the studied spectral irradiation range, as described in the following section.

2.2. Actinometry using NIF, NIS, Monte and Fluvo

Rearranging equations 1 and 2, into eq. 3, illustrates the utility of the Φ-order-derived equations in actinometry studies.

$$P_{\lambda_{irr}}^{unk.} = \frac{k_{A \leftrightharpoons B}^{\lambda_{irr}}}{\beta_{\lambda_{irr}}} = \frac{\nu_0^{\lambda_{irr}/\lambda_{obs}}}{\delta_{\lambda_{irr}}} (eq. 3)$$

The use of these equations for the development and validation of new actinometers will be demonstrated using the previously studied AB(1Φ) and AB(2Φ) photoreaction systems, as described in subsequent sections of this chapter.

2.3. Actinometer validation through peudo-rate constant determination

The utility of Nif, Nis, Monte and Fluvo as actinometers can be confirmed by verifying the linear correlation between the rate-constant and radiant power. This is conducted by preparing various solutions of approximately the same concentration for each compound and performing a series of irradiation experiments of different intensities. These experiments were performed for different irradiation wavelengths, as illustrated in table 1. The kinetic traces obtained at a selected observation wavelength were then fitted with the

Φ-order semi-empirical integrated rate-law (figure 1), which then allowed the determination of each photoreaction rate-constant (table 1).

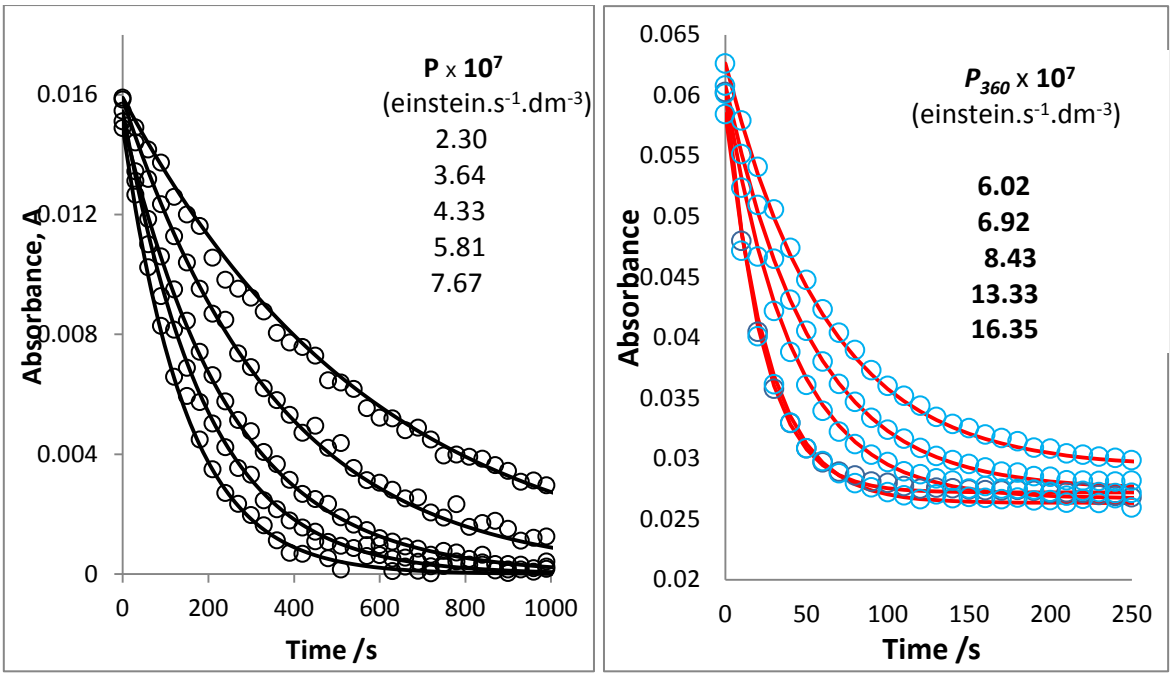

Figure 1: Effect of increasing the irradiation radiant power on the kinetic traces of photodegradation of NIF (5.14 x 10^{-6} M) and Monte (1.85 x 10^{-6} M) λ_{irr} / λ_{obs}= 370/390 nm and 360/360 nm, respectively. The circles represent the experimental data while the lines represent the model fitted traces.

As shown in figure 1, increasing the radiant power of the irradiation source had the effect of accelerating the photoreaction rate. A plot of the variation of the rate-constant-values for each wavelength irradiation experiment with radiant power shows a linear correlation between these parameters with a gradient $\beta_{\lambda_{irr}}$ and an intercept close to zero, as predicted by eq. 1 (table 1).

Table 1: Correlation equations for the variation of photodegradation overall rate-constants ($k_{AB}^{\lambda_{irr}}$) for NIF, Monte, NIS and Fluvo with radiant power ($P_{\lambda_{irr}}$), the corresponding $\beta_{\lambda_{irr}}$ factors, and the span of radiant power employed for various monochromatic irradiations.

Irradiation wavelength λ_{irr} / nm	Equation of the line [a] $k_{A\leftrightharpoons B}^{\lambda_{irr}} = \beta_{\lambda_{irr}} \times P_{\lambda_{irr}} + intercept$	Correlation coefficient, r^2	$P_{\lambda_{irr}} \times 10^7$ einst.s^{-1}.dm^{-3}
NIF			
390	$8489.2 \times P_{390} - 3 \times 10^{-4}$	0.993	2.87 – 9.11
370	$9775.9 \times P_{370} + 2 \times 10^{-4}$	0.988	2.30 – 7.37
345	$8116.9 \times P_{345} + 4 \times 10^{-4}$	0.987	2.39 – 5.19
321	$9131.8 \times P_{321} - 3 \times 10^{-4}$	0.997	1.20 – 3.46
Monte			
360	$28069 \times P_{360} + 8 \times 10^{-4}$	0.996	6.02 – 16.3
345	$24932 \times P_{345} + 4 \times 10^{-3}$	0.980	4.99 – 14.1
328	$17064 \times P_{328} + 7.9 \times 10^{-3}$	0.999	5.67 – 13.1
258	$2250.7 \times P_{258} + 1.1 \times 10^{-3}$	0.984	4.53 – 10.0
NIS			
390	$7902.7 \text{ x } P_{390} - 5\text{x}10^{-6}$	0.996	3.81 – 10.9
370	$8850.8 \text{ x } P_{370} + 5\text{x}10^{-7}$	0.999	5.55 – 11.9
345	$8391.1 \text{ x } P_{345} - 7\text{x}10^{-6}$	0.998	2.42 – 7.20
320	$7558.4 \text{ x } P_{320} + 2\text{x}10^{-5}$	0.996	1.34 – 4.35
Fluvo			
260	$818.4 \times P_{260} + 3 \times 10^{-7}$	0.99	2.93 – 4.60
270	$1249 \times P_{270} + 3 \times 10^{-5}$	0.96	2.50 – 5.21
280	$1584 \times P_{280} - 1 \times 10^{-6}$	0.99	2.70 – 5.51
285	$1998 \times P_{285} + 2 \times 10^{-5}$	0.98	2.63 – 4.81
290	$2077 \times P_{290} + 5 \times 10^{-5}$	0.99	2.56 – 4.42

[a] $k_{A\leftrightharpoons B}^{\lambda_{irr}}$ expressed in s^{-1} and $\beta_{\lambda_{irr}}$ in einst^{-1}.dm^3

It is interesting to note that for all studied drugs, a correlation can be found between the factor $\beta_{\lambda_{irr}}$ and irradiation wavelength (figure 2). This allows the determination of the $\beta_{\lambda_{irr}}$

factors at any wavelength within the selected range of each drug, and helps the development of an actinometric method.

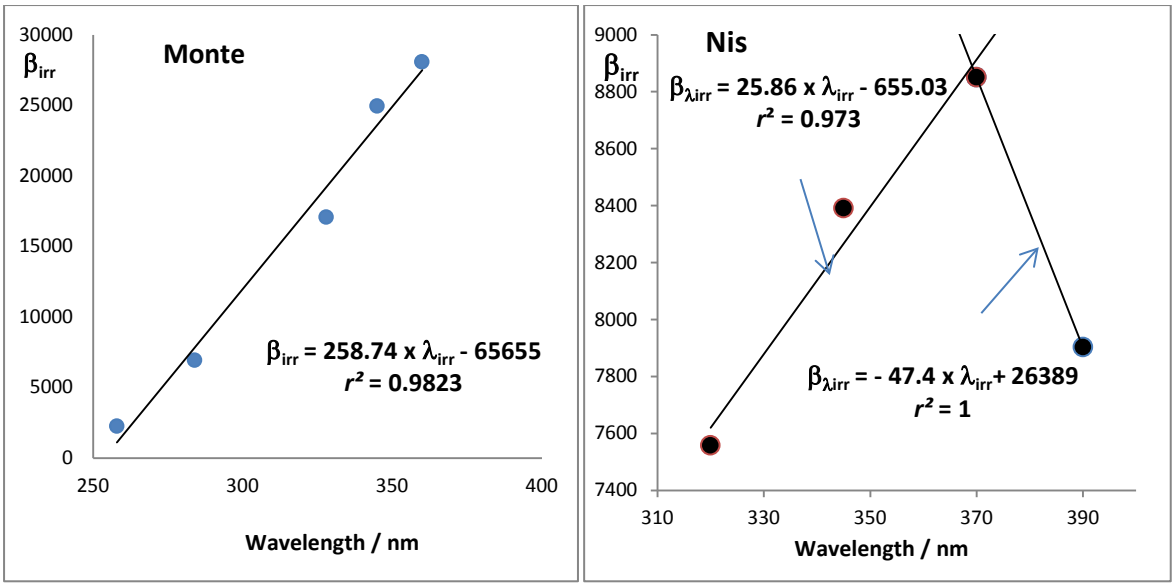

Figure 2: Linear correlation of the $\beta_{\lambda_{irr}}$ factor with irradiation wavelength for Monte and Nis. $\beta_{\lambda_{irr}}$ is expressed in einst^{-1}.dm^{3}.

Therefore, the value of $\beta_{\lambda_{irr}}$ can also be determined from these correlation equations in figure 2. A good correlation exists between the beta values determined experimentally, or using the corresponding correlation equation ($\beta_{Exp.}$) and those calculated using the mathematical equation for $\beta_{\lambda_{irr}}$ derived from eq.1 (eq.4, $\beta_{Cal.}$) (figure 3).

$$\beta_{Cal.}^{\lambda_{irr}} = \left(\Phi_{A\to B}^{\lambda_{irr}} \times \varepsilon_A^{\lambda_{irr}} + \Phi_{B\to A}^{\lambda_{irr}} \times \varepsilon_B^{\lambda_{irr}}\right) \times l_{\lambda_{irr}} \times F_{\lambda_{irr}}(\infty) \quad (eq.4)$$

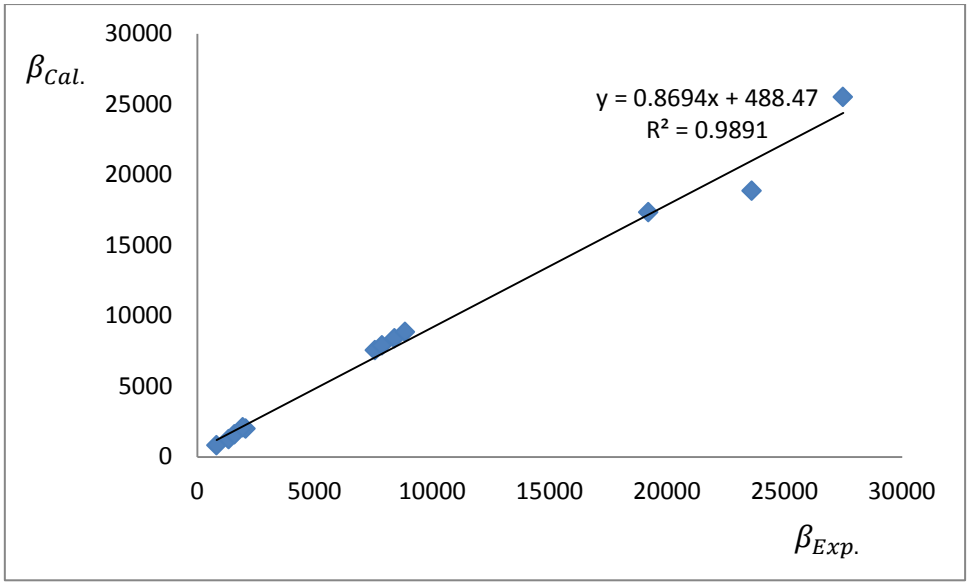

Figure 3: Correlation between the values of β determined experimentally ($\beta_{Exp.}$) and those determined using eq.4 ($\beta_{Cal.}$).

This implies that the factor $\beta_{\lambda_{irr}}$ can also be calculated directly from its correlation equation with wavelength (figure2) without the need to perform any experiments. This allows the determination of the value of $\beta_{\lambda_{irr}}$ at any wavelength within the spectral range of interest. The thus determined $\beta_{\lambda_{irr}}$ value can then be fed into eq.3a to determine the unknown radiant power value of the irradiation beam as;

$$P_{\lambda_{irr}} = \frac{k_{AB}^{\lambda_{irr}}}{\beta_{\lambda}} (eq.3a)$$

It is also worth noting that the factor $\beta_{\lambda_{irr}}$ represents a photokinetic parameter that is independent of the radiant power and can therefore be used to compare photoreaction rates of different studies for a given molecule since it is not dependent on irradiation intensity, which is hardly replicable between different settings. This factor can even be used

to compare the photoreaction rates of different photoreactive molecules for experiments using the same initial concentration and irradiation path lengths within the same or different laboratory settings. Furthermore, if these experiments are conducted using a different irradiation path-length and/or initial concentration from the parameters of our or another experiment (($l_{\lambda_{irr,actual}}, C_{actual}(0)$), then an amendment must first be made on $\beta_{\lambda_{irr,actual}}$before its value can be compared to the one corresponding to the different experimental settings (hereby being, $l_{\lambda_{irr,Exp.}} = 2\ cm, C_{Exp.}(0)$ corresponding to $F_{\infty,\ Exp.}^{\lambda_{irr}}$).. This is achieved by multiplying $\beta_{\lambda_{irr,actual}}$by the product ($F_{\infty,actual}^{\lambda_{irr}} \times l_{\lambda_{irr,actual}}$) and dividing it by the product ($2 \times F_{\infty,\ Exp.}^{\lambda_{irr}}$). This would then allow a direct comparison of the photoreaction rates between different studies, using the same or different molecules, to be made, even when the radiant power is different. As such, the $\beta_{\lambda_{irr}}$factor, or the pseudo-rate-constant, reflects the rate of photoreactions regardless of the radiant power used and provides a new and accurate tool for comparing photoreactions rates, as is commonly performed in thermal kinetics.

2.4. Actinometer validation through initial velocity determination

For this purpose, the kinetic traces generated for Nis and Fluvo actinometry experiments above were selected as examples of AB(1Φ) and AB(2Φ) photoreactions (figure 4).

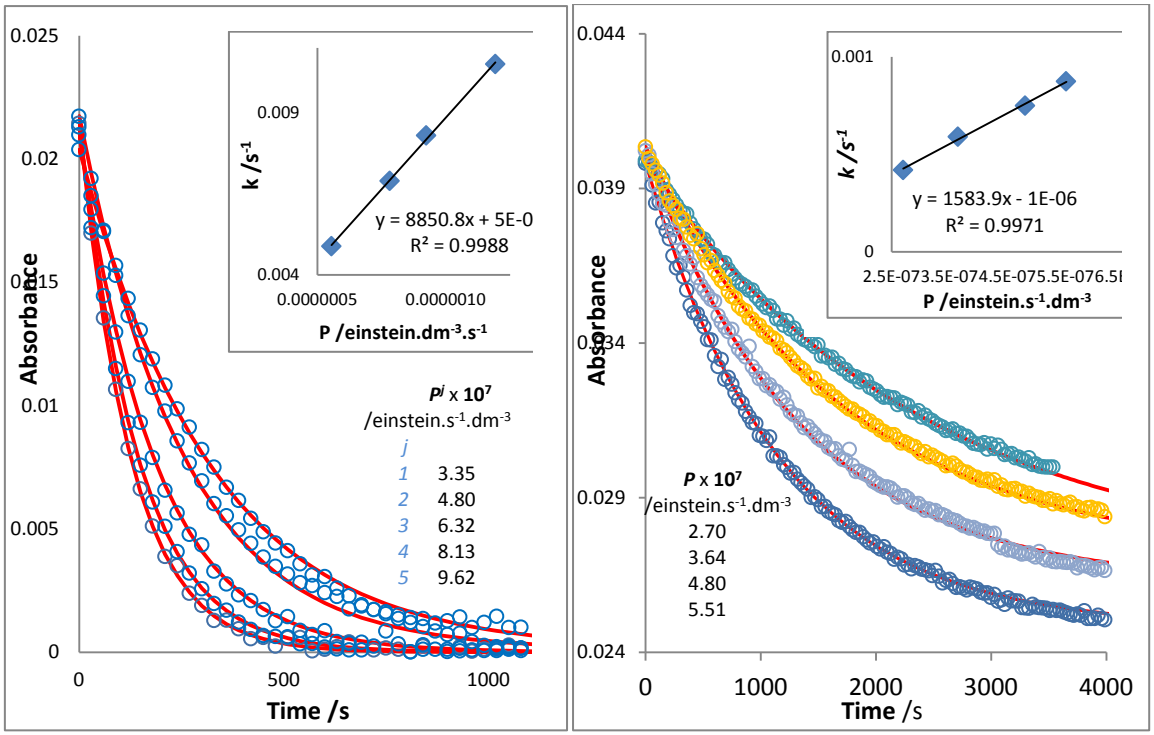

Figure 4: Effect of increasing the irradiation radiant power ($P_{\lambda_{irr}}$) on the kinetic traces of photodegradation of *NIS* (6.56 x 10^{-6} M) and *Fluvo* (2.97 x 10^{-6} M) λ_{irr} / λ_{obs}= 370/390 nm and 280/245 respectively. The circles represent the experimental data while the lines represent the model fitted traces.

The actinometry study can also be performed through the determination of the initial velocity ($v_0^{\lambda_{irr}/\lambda_{obs}}$) of each photoreaction using the derivative of the model equation at t_0 ; $v_{0\,(mod.)}^{\lambda_{irr}/\lambda_{obs}}$ (eq. 5)

$$v_{0\ (mod.)}^{\lambda_{irr}/\lambda_{obs}} = \left(\frac{dA_{tot}^{\lambda_{irr}/\lambda_{obs}}}{dt}\right)_0$$

$$= \frac{A_{tot}^{\lambda_{irr}/\lambda_{obs}}(0) - A_{tot}^{\lambda_{irr}/\lambda_{obs}}(pss)}{A_{tot}^{\lambda_{irr}/\lambda_{irr}}(0) - A_{tot}^{\lambda_{irr}/\lambda_{irr}}(pss)} \times \frac{k_{A\leftrightharpoons B\ (mod.)}^{\lambda_{irr}}}{\frac{l_{\lambda_{irr}}}{l_{\lambda_{obs}}} \times Ln(10)}$$

$$\times \left(10^{\left(A_{tot}^{\lambda_{irr}/\lambda_{irr}}(pss) - A_{tot}^{\lambda_{irr}/\lambda_{irr}}(0)\right) \times \frac{l_{\lambda_{irr}}}{l_{\lambda_{obs}}}} - 1 \right) \quad (eq.5)$$

The values of the initial velocities were then plotted against the corresponding radiant power value for each wavelength (**Table 2**).

Table 2: Correlation equations for the variation of the initial reaction velocities ($v_0^{\lambda_{irr}/\lambda_{obs}}$) with radiant power ($P_{\lambda_{irr}}$), for *NIS* (6.56 x 10^{-6} M) and *Fluvo* (2.95 x 10^{-6}M) photodegradation ($l_{\lambda_{irr}}$= 2 cm; $l_{\lambda_{obs}}$= 1 cm) together with the radiant power span used for various monochromatic irradiations.

Irradiation wavelength λ_{irr} / nm	**Equation of the line [a] $v_0^{\lambda_{irr}/\lambda_{obs}} = \delta_{\lambda_{irr}} \times P_{\lambda_{irr}} + intercept$**	**Correlation coefficient, r^2**	**$P_{\lambda_{irr}} \times 10^7$ /einst.s^{-1}.dm^{-3}**
Nis			
390	- 197.98 x P_{390} - 5x10^{-6}	0.94	3.81 – 10.9
370	- 226.05 x P_{370} + 7x10^{-5}	0.96	5.55 – 11.9
345	- 124 x P_{345} - 1x10^{-5}	0.98	2.42 – 7.20
320	- 130.26 x P_{320} - 4x10^{-6}	0.99	1.34 – 4.35
Fluvo			
260	- 10.58 x P_{260} + 4.8x10^{-7}	0.93	2.93 – 4.60
270	- 14.57 x P_{270} – 8.9x10^{-7}	0.98	2.50 – 5.21
280	- 25.16 x P_{280} + 1.3x10^{-6}	0.99	2.70 – 5.51
285	- 28.11 x P_{285} + 1.8x10^{-7}	0.99	2.63 – 4.81
290	- 31.08 x P_{290} + 1x10^{-6}	0.99	2.56 – 4.42

As shown in **Table 2**, a linear relationship was found between $\nu_0^{\lambda_{irr}/\lambda_{obs}}$ and $P_{\lambda_{irr}}$ with a gradient $\delta_{\lambda_{irr}}$, an intercept close to zero and a correlation coefficient close to unity, further confirming the suitability of Nis and Fluvo to act as actinometers.

The value of $\nu_0^{\lambda_{irr}/\lambda_{obs}}$ can also be determined from the gradient of the first experimental points of a kinetic trace ($\upsilon_{0\ (Exp.)}^{\lambda_{irr}/\lambda_{obs}}$). These values correlate well with those determined from eq. 5 ($\upsilon_{0\ (Mod.)}^{\lambda_{irr}/\lambda_{obs}}$), as shown in figure 5.

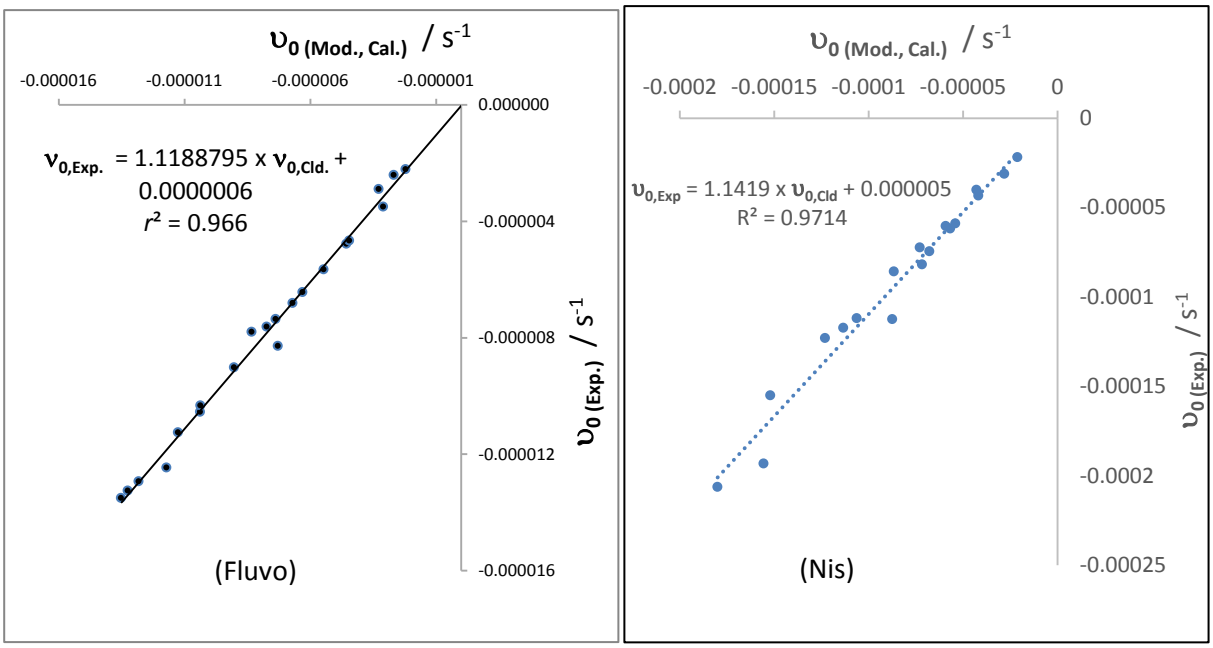

Figure 5: Correlation between the initial velocity values $\nu_{0(Mod,Cal.)}^{\lambda_{irr}/\lambda_{obs}}$ and $\nu_{0(Exp.)}^{\lambda_{irr}/\lambda_{obs}}$ for all the sets of *Fluvo and Nis* actinometry experiments in Table 2.

A linear correlation between the gradients of eq.2, ($\delta_{\lambda_{irr}}$) (Table 2) and irradiation wavelength can also be established as shown in figure 5. Similar to $\beta_{\lambda_{irr}}$, these correlation equations allow the determination of the value of $\delta_{\lambda_{irr}}$ for any wavelength without the need to conduct any experiment.

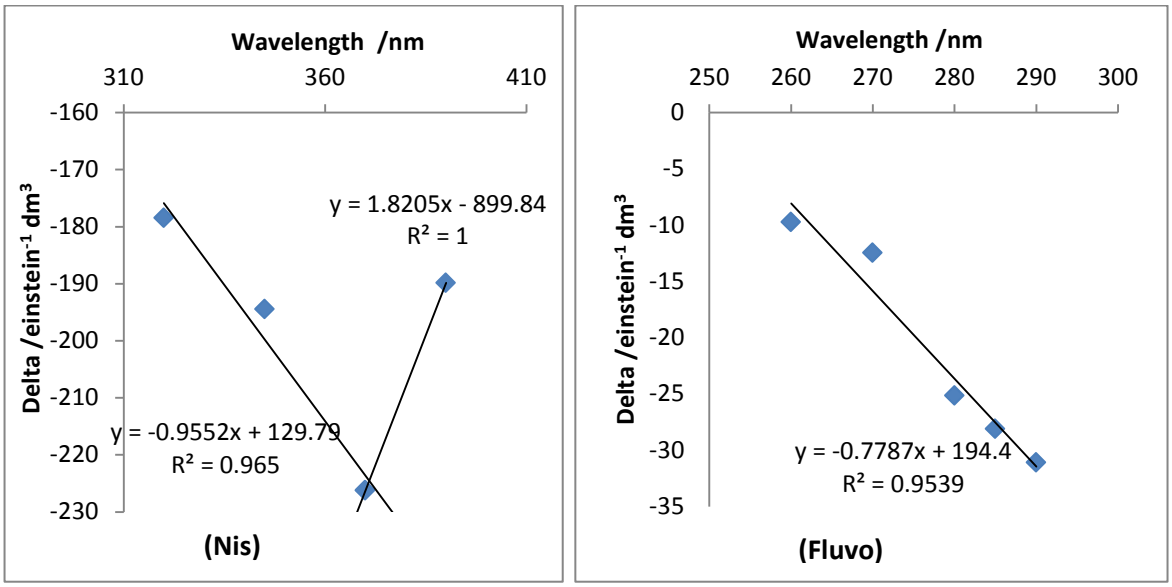

Figure 5: Linear correlation between $\delta_{\lambda_{irr}}$ and irradiation wavelength. $\beta_{\lambda_{irr}}$ and $\delta_{\lambda_{irr}}$ are expressed in einst^{-1}.dm^{3}.

Therefore, $\delta_{\lambda_{irr}}$ can be determined for any irradiation wavelength using the above correlation equations without the need to conduct an irradiation experiment.

A comparison of $\delta_{\lambda_{irr}}$ values determined using the correlation equations with wavelength (figure 5) and/or experimentally (table 2) ($\delta^{\lambda_{irr}}_{Mod.,Exp.}$) with the $\delta_{\lambda_{irr}}$ values calculated using its

mathematical expression (eq.6) ($\delta_{Cal..}^{\lambda_{irr}}$) derived from eq.2**,** shows a good correlation between the sets of values (figure 6).

$$\delta_{Cal..}^{\lambda_{irr}} = \left(\varepsilon_B^{\lambda_{obs}} - \varepsilon_A^{\lambda_{obs}}\right) \times l_{\lambda_{obs}} \times \Phi_{A\to B}^{\lambda_{irr}} \times \varepsilon_A^{\lambda_{irr}} \times l_{\lambda_{irr}} \times F_{\lambda_{irr}}(0) \times C_0 \quad (eq.6)$$

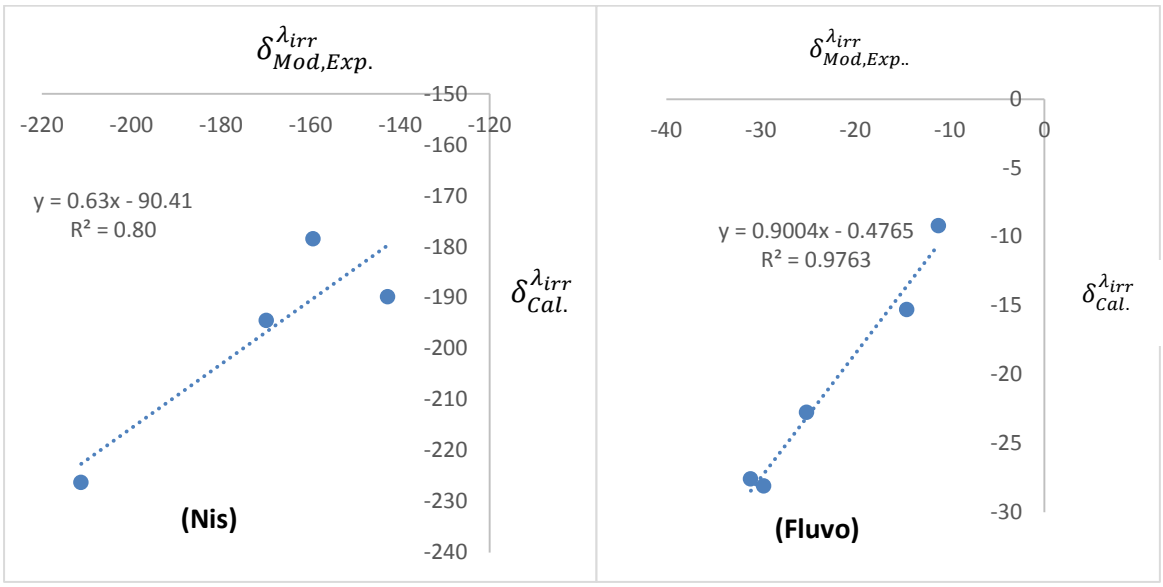

Figure 6: Correlation between $\delta_{Cal.}^{\lambda_{irr}}$ and $\delta_{Mod.,Exp.}^{\lambda_{irr}}$ for Nis and Fluvo.

These results confirm the validity of the above studied drugs to act as actinometers for any monochromatic irradiation experiment by substituting the values of $\delta_{\lambda_{irr}}$ and $\nu_0^{\lambda_{irr}/\lambda_{obs}}$ into eq. 3b;

$$P_{\lambda_{irr}}^{unk.} = \frac{\nu_0^{\lambda_{irr}/\lambda_{obs}}}{\delta_{\lambda_{irr}}} (eq.3b)$$

The gradient, $\delta_{\lambda_{irr}}$, represents the pseudo-initial velocity of a photoreaction at a given $l_{\lambda_{irr,actual}}$ and $C_{actual}(0)$ that that is independent of the radiant power. As for $\beta_{\lambda_{irr}}$, $\delta_{\lambda_{irr}}$

can be used to compare the initial velocities of different photoreaction experiments using the same or a different molecule. Similar to $\beta_{\lambda_{irr}}$, the value of $\delta_{\lambda_{irr}}$ must first be amended before it can be compared, if the initial concentration and/or irradiation path lengths are different.

2.5. Acinometry method

In order to measure the radiant power of an unknown light-source, a monochromatic irradiation is performed on one of the above drug solutions. The actinometer is selected so that the monochromatic irradiation of unknown radiant power lies within the spectral absorbance range of the actinometer. The experimental kinetic trace hence obtained for the actinometer's photoreaction is fitted to the Φ-order model equation and the reaction overall rate-constant value determined. Subsequently, the actual radiant power of the source can be determined by either of two methods as follows;

2.5.1. Method 1

(1) The value of $\beta_{\lambda_{irr}}$ is determined from the correlation equation with wavelength, as detailed above with the appropriate adjustments if $l_{\lambda_{irr}}$ and C (0) are different from the ones used above.

(2) The radiant power value is determined using eq. 3a.

2.5.2. Method 2

(1) The value of $\nu_0^{\lambda_{irr}/\lambda_{obs}}$ is determined either from (i) eq. 5, which is the derivative of the semi-empirical integrated rate-law equation; (ii) from the gradient of the first experimental points of the kinetic trace; or (iii) from the correlation equation with irradiation wavelength with the appropriate adjustments if the experimental conditions are different from the ones used above.

(2) The value of $\delta_{\lambda_{irr}}$ is determined, with the appropriate adjustments, either from (i) the correlation equation with wavelength or (ii) from $\delta_{\lambda_{irr}}$ analytical expression as defined in eq. 2.

(3) The radiant power value can then be determined using eq. 3b.

3. Discussion

Using the Φ-order kinetics, four new actinometers have been proposed and validated, namely; nisoldipine (320-400 nm), nifedipine (280-400 nm), montelukast (258 – 380 nm) and fluvoxamine (260 – 290 nm). These drugs together with a previously proposed actinometer, 1,2-bis[2-methylbenzo[b] thiophen-3,3,4,4,5,5-hexafluoro-1-cyclopentene, DAE, (405 – 570 nm) region (Maafi, 2010) cover the UV and visible regions of the spectrum where most drugs absorb. They, thus offer a large choice of actinometers that would cover any monochromatic irradiation within the 250-570 nm spectral range.

A detailed and quick to implement procedure for conducting actinometry was also proposed and can be performed in different ways that can also be used for confirmatory purposes. The procedure is extensible to high radiant power light-sources that are sometimes necessary for irradiation experiments conducted within absorption wavelength bands where the reaction is characterised by weak efficiencies as for λ_{irr} < 250 nm in the case of Monte. The actinometric strategies developed in these studies are complementary as UVB, UVA and visible ranges, spanning the wide 250 – 570 nm spectral region, can be readily covered by these drugs. In addition, these approaches are certainly not limited to the aforementioned species but can easily be extended to many other photo-absorbing molecules obeying similar types of mechanisms (i.e. unimolecular or photoreversible reactions).

The method proposed in this work can be considered as a good alternative to existing approaches and especially for the ICH recommended quinine hydrochloride actinometer (ICH, 1996).

References

Baertschi S.W., Alsante K.M., Tonnesen H.H. A critical assessment of the ICH guideline on photostability testing of new drug substances and products (Q1B): recommendation for revision. Journal of Pharmaceutical Sciences. 2010; 99 (7): 2934-2940.

Baertschi S.W. Commentary on the quinine actinometry system described in the ICH draft guideline on photostability testing of new drug substances and products. Drug stability. 1997; 1: 193-195.

De Azevedo Filho C.A., De Filgueiras Gomes D., De Melo Guedes J.P., Batista R. M. F., Santos B.S. Considerations on the quinine actinometry calibration method used in photostability testing of pharmaceuticals. Journal of Pharmaceutical and Biomedical Analysis. 2011; 54: 886-888.

ICH, Guidance for industry Q1B photostability testing of new drug substances and products, Fed. Regist. 1996; 62: 27115-27112.

Kuhn H. J., Braslavsky S.E., Schmidt R. Chemical Actinometry (IUPAC Technical Report). Pure Applied Chemistry. 2004; 76 (12): 2105-2146.

Maafi M., The potential of AB(1Φ) systems for direct actinometry. Diarylethenes as successful actimometers for the visible range. Phys. Chem. Chem. Phys. 2010; 12: 13248–13254.

Moore D. Determining the kinetics and mechanism of a photochemical reaction. In Piechocki J.T., Thoma K. Pharmaceutical photostability and photostabilisation technology. New York: Informa Healthcare; 2007. p. 79-86.

Chapter IX: General discussion & conclusions

1. General discussion

As the number of photoactive drugs is becoming increasingly important, the value of testing drugs for photoactivity and phototoxicity both *in vitro* and *in vivo* is significant. As a result, in 1998, The International Conference on harmonisation of photostability testing of new active substances and medicinal products (ICH Q1B) issued guidelines for the EU, Japan and USA on how to conduct photostability tests *in vitro*. In 2002, further guidelines were issued on phototoxicity and photosafety testing by the European Agency for the Evaluation of Medicinal Products (EMEA). This was followed, in 2009, by the ICH guideline M3(R2) on the non-clinical safety studies for the conduct of human clinical trials and marketing authorisation for pharmaceuticals, which highlighted the need for an initial assessment of phototoxic potential based on a drug's photochemical properties and pharmacological/chemical class and, depending on these results, subsequent non-clinical drug distribution studies and experimental evaluation on phototoxic potential before Phase III trials. In 2013, an ICH Harmonised Tripartite Guideline was issued on the photosafety Evaluation of Pharmaceuticals (S10) to provide further detailed recommendations on how the latter studies should be conducted.

The studies presented in this thesis, as well as numerous literature reports, show the potential photoactive and toxic effect of various drugs, and provide further support for the above guidelines. It has also been recognised that not only natural day light but also indoor artificial lighting increasingly emit wavelengths capable of inducing phototoxic skin reactions (Ferguson, 2006). Therefore, not only UVA radiation but also UVB, UVC and visible

radiations, depending on the drug's absorption spectrum, may photoactivate drugs *in vitro* and/or *in vivo*.

As shown in previous chapters, the Φ-order kinetic studies, provide a new, simple and accurate tool to evaluate and quantify the photostability of drugs. These studies, also provide additional support to the photostability and photosafety guidelines, that would benefit from widely applicable and photo-specific kinetic tools for the quantificaltion and prediction of drugs photolability. This would, in turn, inform on potential photoprotective means and provide a quantification tool to assess their photo-protective effects. This is, as mentioned in the guidelines, particularly important for topically applied and systemic drugs distributing to bodily exposed areas such as the eyes and skin. Further, in light of the increasingly recognised incidence of phototoxic reactions, even at normal daily irradiation doses, the need for such studies has long been awaited since they not only allow a quantifiable evaluation of photodegradation risks and identification of the causative radiation at an early stage, thereby avoiding human exposure to such effects; but they also provide tools to overcome the problem if a drug is identified as phototoxic.

It is worth noticing that the Φ-order kinetic studies, in this thesis, were conducted on drug concentration solutions in the micro-molar (ugs/ml) range with radiant power ranging from 7200 – 36000 $J.hr^{-1}.m^{-2}$. Photodegradation studies of drugs in solutions are relevant for liquid as well as solid dosage forms. This is due to the facts that (i) even for solid dosage forms, at a drug development and formulation levels, drugs may be prepared in solutions

and; (ii) following systemic absorption of a solid dosage form, the drug is distributed into a liquid environment within the circulation and cells. Furthermore, the drug concentrations reaching the systemic circulation and body tissues is much lower than the originally administered drug concentration due to bioavailability and tissue distribution reasons. Such low drug concentrations are in line with the photosafety testing (S10) maximum substrate concentration set at 100 ug/ml, in addition to testing recommendations on several dilutions (ICH(S10), 2013). Thus, photostability tests in solution and at low concentrations, as the ones conducted in this study, are of relevance as they closely mimic *in vivo* environmental conditions.

In terms of irradiance, the S10 document also recommends using a dose of approximately 5J/cm^2 UVA for the *in vitro* 3T3 Neutral Red Uptake phototoxicity test (3T3 NRU PT) to reflect natural irradiation conditions comparable to those obtained during prolonged outdoor activities on summer days around noon time, in temperate zones and at sea levels (ICH(S10), 2013). The doses used in our studies (0.72 and 3.6 J/cm2) were slightly lower but sufficient to effectively cause significant photodegradation of the studied drugs. These doses are also very likely to mimic average daily irradiation doses to which we are exposed throughout the year as well as irradiation doses potentially reaching drug molecules within our tissues and circulation.

Nevertheless, in order to verify the validity of lower concentration, lower intensity studies and their correspondence with higher concentration, higher intensity conditions, as is

normally the case under *in vitro* conditions; some simulation studies were conducted using various plausible scenarios that encompassed a wide range of concentrations and radiation intensities, making the hypothetical assumption that the absorbance linearity range is maintained with increasing concentrations (this in fact takes into account the worst case scenarios where absorbance is extremely high), (figure 1).

For all cases, a proportional relationship between the rate constant and intensity was observed. On the other hand, the rate-constant decreased in an exponential manner with increasing concentration. The rate-constant equation predicts these findings since *k* and *P* are proportionally related while the effect of concentration on rate-constant is implicitly conveyed in the absorbance terms of the exponential photokinetic factor (figure 2).

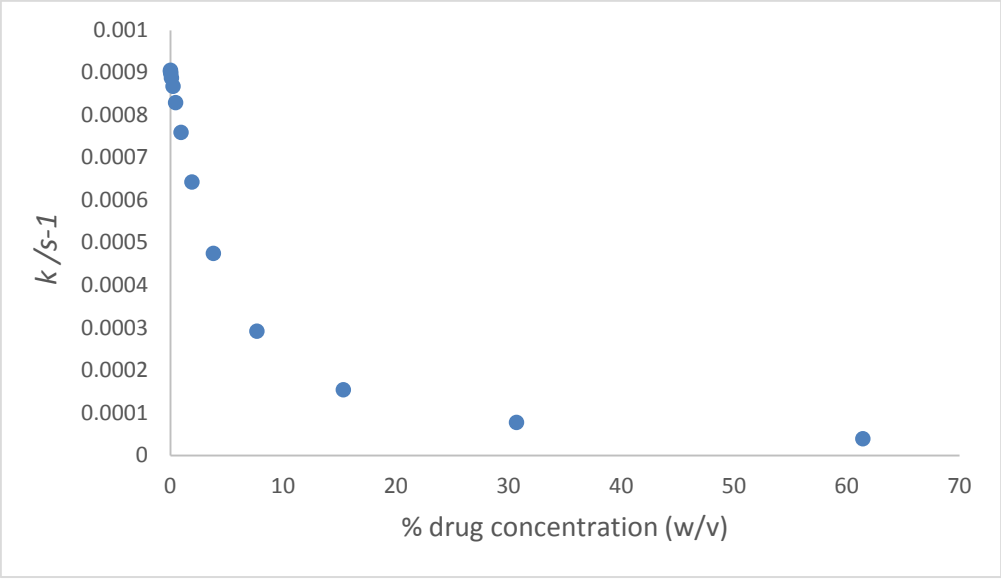

Figure 1: Correlations between rate-constants and initial drug concentrations for extrapolative scenarios for Nis photodegradation reactions as determined by using the rate-constant equation corresponding to Φ-order kinetics and theoretical initial drug concentrations assuming the absence of matrix effects.

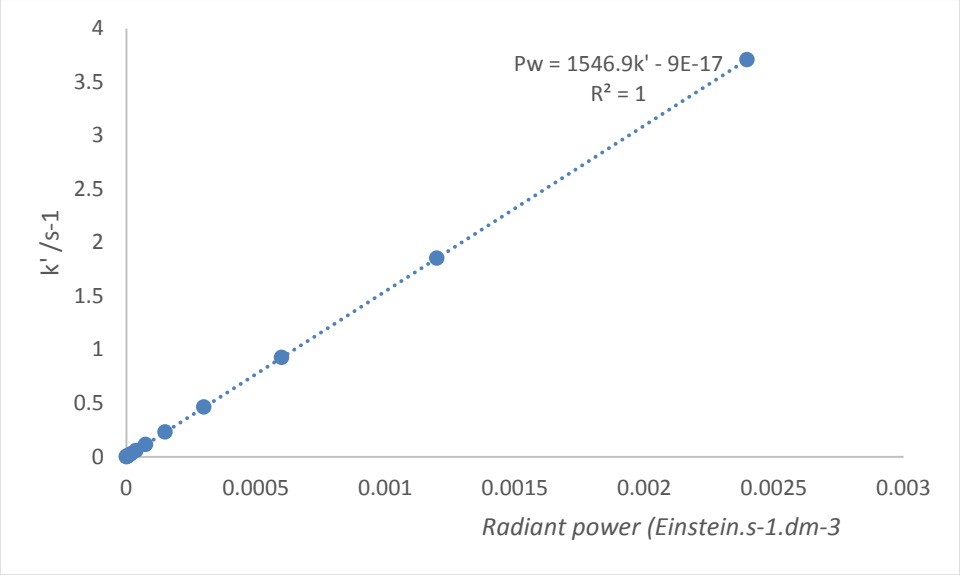

Figure 2: Correlations between extrapolative hypothetical radiant power intensities and rate constants for Nis photodegradation reactions in solution as determined by using the rate-constant equation corresponding to Φ-order kinetics and increasing radiant power values.

As such, increasing the absorbance through an increase in concentration would lead to an exponential reduction in the rate of photodegradation up to the limit of linearity range of the drug; after which further increase in concentration leads to modest increases in absorbance and therefore a reduced effect on photodegradation rate. Therefore, while the drug concentration is within the linearity range of the drug (as is the case in our experimental studies), increasing the concentration will exponentially retard photodegradation. However, if the drug concentration is increased beyond the limit of linearity; as for the concentrations encountered at a manufacturing level, in liquid oral and parenteral dosage forms and during extemporaneous reformulation of solid and liquid dosage forms; then the halting effect of concentration on photodegradation rate will be almost equal to the effect of the concentrations at the upper limits of the linearity range.

Therefore, conducting photostability studies using high drugs concentrations or simply concentrations of the dosage form itself may provide false negative results since the maximum photodegradation retarding effect of concentration would have been reached and this could somewhat counteract or mask the effect of low to moderate radiation intensities on photodegradation. Thus, despite being photostable on the shelf, the same drug could prove to be phototoxic in vivo due to the low concentrations encountered in the body.

The simulation scenarios were used to verify how low intensity/concentration studies would compare to high concentration/intensity in vitro drug exposure cases, especially in terms of photodegradation rate. A simple and very practical equation that relates different intensities to different photokinetic factors (due to different absorbances and thus concentrations), with different photodegradation rate-constants; was derived from the Φ-kinetics (eq.1). This equation can also be worked out from the Φ-order rate-constant equation for different conditions; as;

$$k' = \frac{P'}{P} \times \frac{F'}{F} \times k \qquad (eq.1)$$

Where P and P' are the radiant power of the low intensity and high intensity used, respectively; F and F', the photokinetic factors corresponding to low concentration and high concentration studies respectively and k and k', the overall rate-constants of low concentration/intensity study and high concentration/intensity study respectively. It is worth noting that once the limit of the linearity range is reached, the photokinetic factor for higher concentrations will almost be equal to that of the limit of linearity concentration; i.e.

increasing the concentration retards photodegradation only up to approximately the limit of linearity range, after which it would have already achieved its maximum effect. This euqtion (eq.1) could find important uses in the extrapolation and prediction of photodegradation rates and thus shelf-life anticipation.

Thus, using this equation, it is possible to extrapolate the studies presented here to larger scale conditions. This offers the benefit of using low concentrations and intensities, thereby reducing costs and time, to determine photordegradation rates for any drug concentration under any intensity using one simple experiment following which the results can be extrapolated using eq.1. Furthermore, the same experiment also constitutes a solid platform for the prediction of the drugs behaviour in vivo, since similar conditions are used.

Therefore, the photo-irradiation experiments and analytical protocols presented in this thesis represent a solid testing platform for conducting and informing photostability and photosafety studies, photokinetic data analysis as well as extrapolative predictive photoreaction studies.

2. Limitations and future studies

While the work presented in this thesis offers a long-awaited method for the study and analysis of photoreactions kinetics, it also opens new research perspectives in the field of photochemistry.

Thanks to the NIM-based methodology, it becomes possible to develop further kinetic models for molecules and drugs photo-degrading via different mechanistic routes from the ones described in this thesis. A stepwise approach to the study of other photoreaction mechanisms could gradually lead to the construction of an array of photoreactions' kinetic models eventually covering most eventualities, which would assist the development of photo-protective strategies. This process should be conducted in conjunction with practical photo-stability experiments on molecules whose reaction mechanism is under investigation. When information on drugs' photoreaction mechanism is lacking, the use of advanced analytical separation methods such as Liquid Chromatography Mass spectrometry (LC-MS) would be valuable for the determination of photoproducts and the elucidation/confirmation of reaction mechanisms. Furthermore, flash photolysis studies would provide a deeper insight into photoreaction mechanisms and excited state species which would help draw an accurate picture of the reactions involved and the effects of different variables such as solvents and excipients. When such tools are combined with a quantitative data treatment method such as Φ-kinetics, it becomes possible to draw accurate conclusions on the photostability of compounds and form informed choices over protective means and shelf-life.

The dependence of quantum yield of photoreactions on irradiation wavelength has been repeatedly demonstrated in these studies. This finding ought, in its own right, to be investigated further within the same mechanisms as well as new ones. The variation of this important parameter with wavelength should carefully be explored as it was, in every case, possible to establish a mathematical relationship between quantum yield and wavelength.

Furthermore, these studies offer a solid framework that can inform both photostability and photosafety testing of pharmaceuticals. Moreover, photostability studies on cell lines using Φ-order kinetics to treat and compare data could also offer a new strategy for the evaluation and prediction of drugs' phototoxicity *in vivo* and the effects of various photo-protective means such as cyclodextrins and inert photo-absorbers. As such, these studies would not only constitute a platform for the evaluation of the inherent photostability of a drug prior to administration but could also provide substantial information on possible phototoxcity *in vivo*. These initial findings would be followed with photo-protection studies using the same kinetic models to evaluate the most beneficial strategy to counteract any identified photo-instability and/or phototoxicity issues.

3. Conclusions

This work addressed the lack of accurate photokinetic models that describe the kinetics of photochemical reactions. A two-step methodology for the development of new kinetic models has been developed consisting of (i) a model development stage based on optimised closed-form integrated rate-laws and NIM simulation cases and (ii) a model validation stage that aims at confirming the validity of the developed model within defined limits of applicability using further NIM simulation kinetic cases.

The above methodology was employed for the development of three semi-empirical photokinetic integrated rate-laws for three types of photoreaction mechanisms, namely unimolecular AB(1Φ), photoreversible AB(2Φ) and consecutive AB_4(4Φ)photoreaction types.

The validity of the above models was further confirmed experimentally using NIF and NIS as model candidates for AB(1Φ) reaction types, Monte and Fluvo as drug candidates for AB(2Φ) reactions and Ribo as an example of AB_4(4Φ) reaction mechanisms.

The models accurately described the kinetic evolution of the drugs' photoreactions in solutions. The usefulness of the kinetic models also encompassed the elucidation of the kinetic parameters describing the studies photoreaction mechanisms as well as the quantitative study of the effects of initial concentration and some additives on photoreaction kinetics.

Furthermore, a new kinetic parameter that can be used universally to describe the rate of photoreactions, namely the beta factor or pseudo rate-constant, was also revealed and proved to be a useful tool for the study and comparison of photoreaction rates regardless of the intensity of monochromatic light used, a parameter that is most often impossible to accurately replicate between different laboratories.

The above models can be used to describe the kinetics of any molecule obeying the above photoreaction mechanisms. The kinetic parameters underlying these photoreactions can also be determined and used for shelf-life determination, as is routinely done in thermal studies, for comparative and photoprotection purposes using the proposed kinetic elucidation methods. In addition, the newly proposed NIM-based model development methodology offers new perspectives for the development of the kinetic integrated rate-laws underlying other photoreaction mechanisms.

Finally, these studies represent simple, accurate and universally reproducible experiments for conducting photostability studies as well as analysing the resulting kinetic data. They provide quantitative as well as qualitative information of the photostabilty of molecules and may also be used for the quantitative study of the effects of additives and variables as well as for predictive purposes by extrapolation.